Three-dimensional *in vitro* recapitulation of neuroblastoma: from model to drug screening platform

Phurit Bovornchutichai

St Cross College
University of Oxford

A thesis submitted for the degree of Doctor of Philosophy

Trinity 2018

Abstract

Neuroblastoma is one of the most common yet fatal paediatric cancer. Nevertheless, few drug treatments are available in the market. One of the difficulties is the drug responses reported in 2-D *in vitro* tests does not always accurately reflect those observed in 3-D *in vivo* models. As the process consumes time, money and animal lives, a 3-D *in vitro* drug testing bioreactor recapitulating neuroblastoma tumours are needed to screen out any unsuccessful drug candidates before they enter *in vivo* tests.

In this thesis, a 3-D *in vitro* model comprised neural stem cells (NSCs) or neuroblastoma cells (SH-SY5Ys) and human umbilical vein endothelial cells (HUVECs) were initially optimised and developed in the laminin-rich hydrogel matrix to recapitulate neuroblastoma tumours. Next, a modified polydimethylsiloxane bioreactor (TissueFlex®) was developed to extend the viability of the 3-D *in vitro* model by enhancing the mass transport of nutrients and oxygen. The bioreactor was continuously perfused with a supplemented endothelial basal medium (EGM-2) co-treated with cisplatin, retinoic acid (RA), both cisplatin and RA, or EGM-2 as a control for three weeks. Cell morphology, cell viability and expressions of markers (TuJ1, Nestin and CD31) were measured weekly. Results were compared to parallel cultures of 2-D monolayer and 3DFlo® automatic cell culture systems.

Our results show that hydrogel fragmentation allowed the formation of concentrated laminin and cellular networks along the gel granule boundaries with neurite extensions observed. Besides, cell surface marker expressions suggested an optimal NSC-HUVEC seeding density ratio of 3:1, cultured in 100% EGM-2 medium. The incorporation of perfusion culture to the model gave rise to significant increases in the number of cells and the expression of Nestin compared to static culture. After 3 weeks, only 2-D cultures showed a significant decrease in marker expressions upon treatment with cisplatin or cisplatin and RA in combination. Also, drug treatments were significantly less effective in 3-D bioreactors than in 2-D cultures. This suggests that the 3-D interactions between cells and hydrogel have created a microenvironment that recapitulates phenomena present in neuroblastoma and provides resistance to cancer therapeutics.

Our 3-D *in vitro* model and perfusion bioreactor have implications for a more efficient drug discovery process by closing the gap between cell culture and physiological tissue investigations. These can be applied towards personalised medicine, where a patient's biopsy specimen can be tested in the system against a series of drugs to identify ones giving rise to optimal therapeutic outcomes.

Three-dimensional *in vitro* recapitulation of neuroblastoma: from model to drug screening platform



Phurit Bovornchutichai

St Cross College

University of Oxford

A thesis submitted for the degree of

Doctor of Philosophy

Trinity 2018

Statement of originality

I hereby declare that this submission is my own work and to the best of my knowledge, it contains no materials previously published or written by another person or substantial proportions of material which have been accepted for the award of any other degree of diploma at the University of Oxford or any other educational institution, except where due acknowledgement is made in the thesis.

Any contribution made to the research by others, with whom I have worked at the University of Oxford or elsewhere, is explicitly acknowledged in the thesis.

I also declare that the intellectual content of this thesis is a product of my own work, except to the extent that assistance from others in the project's design and conception or in style, presentation and linguistic expression is acknowledged.

Phurit Bovornchutichai
St Cross College
October 2018

Abstract

Neuroblastoma is one of the most common yet fatal paediatric cancer. Nevertheless, few drug treatments are available in the market. One of the difficulties is the drug responses reported in 2-D *in vitro* tests does not always accurately reflect those observed in 3-D *in vivo* models. As the process consumes time, money and animal lives, a 3-D *in vitro* drug testing bioreactor recapitulating neuroblastoma tumours are needed to screen out any unsuccessful drug candidates before they enter *in vivo* tests.

In this thesis, a 3-D *in vitro* model comprised neural stem cells (NSCs) or neuroblastoma cells (SH-SY5Ys) and human umbilical vein endothelial cells (HUVECs) were initially optimised and developed in the laminin-rich hydrogel matrix to recapitulate neuroblastoma tumours. Next, a modified polydimethylsiloxane bioreactor (TissueFlex®) was developed to extend the viability of the 3-D *in vitro* model by enhancing the mass transport of nutrients and oxygen. The bioreactor was continuously perfused with a supplemented endothelial basal medium (EGM-2) co-treated with cisplatin, retinoic acid (RA), both cisplatin and RA, or EGM-2 as a control for three weeks. Cell morphology, cell viability and expressions of markers (TuJ1, Nestin and CD31) were measured weekly. Results were compared to parallel cultures of 2-D monolayer and 3DFlo® automatic cell culture systems.

Our results show that hydrogel fragmentation allowed the formation of concentrated laminin and cellular networks along the gel granule boundaries with neurite extensions observed. Besides, cell surface marker expressions suggested an optimal NSC-HUVEC seeding density ratio of 3:1, cultured in 100% EGM-2 medium. The incorporation of perfusion culture to the model gave rise to significant increases in the number of cells and the expression of Nestin compared to static culture. After 3 weeks, only 2-D cultures showed a significant decrease in marker expressions upon treatment with cisplatin or cisplatin and RA in combination. Also, drug treatments were significantly less effective in 3-D bioreactors than in 2-D cultures. This suggests that the 3-D interactions between cells and hydrogel have created a microenvironment that recapitulates phenomena present in neuroblastoma and provides resistance to cancer therapeutics.

Our 3-D *in vitro* model and perfusion bioreactor have implications for a more efficient drug discovery process by closing the gap between cell culture and physiological tissue investigations. These can be applied towards personalised medicine, where a patient's biopsy specimen can be tested in the system against a series of drugs to identify ones giving rise to optimal therapeutic outcomes.

List of publications and presentations

Peer reviewed journal articles

1. Wan, X., **Bovornchutichai, P.**, Cui, Z., O'Neill, E. and Ye, H. (2017). Morphological analysis of human umbilical vein endothelial cells co-cultured with ovarian cancer cells in 3-D: An oncogenic angiogenesis assay. PLoS ONE, 12(7).

2. Owen, J., McEwan, C., Nesbitt, H., **Bovornchutichai, P.**, Averre, R., Borden, M., McHale, A., Callan, J. and Stride, E. (2016). Reducing tumour hypoxia via oral administration of oxygen nanobubbles. PLoS ONE, 11(12).

Oral presentations

1. **Bovornchutichai, P.**, George, J., O'Neill, E. and Ye, H: "Three-dimensional hydrogel-based perfused drug screening platforms". *Samaggi Academic Conference and Careers Fair.* London, United Kingdom ($10^{th} - 11^{th}$ February 2018). (**Awarded best medical science abstract under the theme "innovation towards sustainability"**).

2. **Bovornchutichai, P.**, George, J., O'Neill, E. and Ye, H: "Recapitulating neuroblastoma: from model to drug screening platform". *Anglo-Thai Society Educational Award ceremony.* London, United Kingdom (17^{th} November 2017). (**Awarded highly-commended in engineering and technology**).

3. **Bovornchutichai, P.**, George, J., Wan, X., O'Neill, E. and Ye, H: "Three-dimensional *in vitro* neural-endothelial cells co-culture model: the recapitulation of neuroblastoma microenvironment for long-term drug testing". *Centre of Doctoral Training in Healthcare Innovation Symposium.* Oxford, United Kingdom (23^{rd} June 2017).

4. **Bovornchutichai, P.**, George, J., Wan, X., O'Neill, E. and Ye, H: "Recapitulating neuroblastoma: from model to drug screening platform". *Health Challenge Thailand.* London, United Kingdom (20^{th} May 2017). (**Awarded best presentation**).

5. **Bovornchutichai, P.**, George, J., Wan, X., O'Neill, E. and Ye, H: "Development of a three-dimensional neural cancer model *in vitro*". *MEIBioEng.* Oxford, United Kingdom ($5^{th} - 6^{th}$ September 2016).

Poster presentations

1. **Bovornchutichai, P.**, George, J., O'Neill, E. and Ye, H: "Three-dimensional hydrogel-based perfused drug screening platforms". *Theodore von Kármán Discussion Conference on Bioinspired and Biomimetic Hydrogels.* Bergisch Gladbach, Germany ($15^{th} - 18^{th}$ April 2018).

2. **Bovornchutichai, P.**, George, J., Wan, X., O'Neill, E. and Ye, H: "Three-dimensional *in vitro* neural-endothelial cells co-culture model: the recapitulation of neuroblastoma microenvironment for long-term drug testing". *TERMIS-EU.* Davos, Switzerland ($26^{th} - 30^{th}$ June 2017).

3. Wan, X., **Bovornchutichai, P.**, Cui, Z., O'Neill, E. and Ye, H: "Morphological analysis of human umbilical vein endothelial cells co-cultured with ovarian cancer cells in 3-D for oncogenic angiogenesis assay". *BioEngenuity Keynotes.* Oxford, United Kingdom (10^{th} November 2016).

4. Wan, X., **Bovornchutichai, P.**, Cui, Z., O'Neill, E. and Ye, H: "Morphological analysis of human umbilical vein endothelial cells co-cultured with ovarian cancer cells in 3-D for oncogenic angiogenesis assay". *Oxford Biomedical Imaging Festival.* Oxford, United Kingdom (18^{th} October 2016).

5. **Bovornchutichai, P.**, George, J., Wan, X., O'Neill, E. and Ye, H: "Development of a three-dimensional neural cancer model *in vitro*". *ChemEng Day.* Oxford, United Kingdom (5^{th} October 2016).

6. **Bovornchutichai, P.**, George, J., Wan, X., O'Neill, E. and Ye, H: "Three-dimensional *in vitro* neural cancer model". *Centre of Doctoral Training in Healthcare Innovation Symposium.* Oxford, United Kingdom (6^{th} May 2016).

Dedication

This thesis is dedicated to
Pakaporn Bovornchutichai, Thanat Bovornchutichai and Poomcharn Bovornchutichai
for the unconditional love and for always making me feel I am at home even though we were 5,971 miles apart. Thank you for trusting me to step out of Bangkok and always supporting me to pursue my dream.

Acknowledgements

This thesis would not be completed without the support of many individuals. Firstly, I would like to thank my supervisors, Professor Cathy Ye and Professor Eric O'Neill. I express my sincere gratitude. They both offered invaluable advice and guidance to keep me stay on track and become an independent researcher. With their encouragement and support, I acquired perseverance to pass through those tough times on this long journey.

I would like to extend my thank to the rest of the Oxford Tissue Engineering Group for their friendship and advice. In particular: Robin Nyland, Catriona Inverarity, Thomas Chui, Bo Zhang, Sharlayne Waller, Fabio Bianchi, Erfan Soliman, Carla Fuenteslópez, Miren Tamayo Elizalde, Di Shen, Meghan Lim, Tong Chen, Jason Liu, Richard Yu, Alex Wu and Gloria Lam. I enjoyed every single minute that we interact with each other, both inside and outside of the laboratory. I am so delighted to form these close and long-lasting bonds with you all. In addition, I would like to thank Dr Julian George, Dr Akinlolu Odeleye, Dr Linh Nyugen, Dr Naresh Kasoju and Dr Xiao Wan for sharing their knowledge and skills to help me excel in completing this DPhil thesis. I have learnt a lot from all the discussion we had for the past 3 years.

To the members of the the Institute of Biomedical Engineering (IBME): notably the workshop technicians, Jim Fisk and David Salisbury, thank you both so much for their help with the modifications of the bioreactor. In addition, I would like to thank Liza Brandon, Jo Armitage, Dr Michelle Kumin, Gabor Kiss and Caroline Brown for putting a smile on my face every time I met them and for their administrative support.

To my friends from the final cohort of the Centre of Doctoral Training (CDT) in Healthcare Innovation, thank you so much for your friendship and encouragement to push me through the MATLAB modules. Surprisingly, I will always remember IBME's brownies and tap water. Also to my friends at St Cross College, around Oxford and back home in Thailand, thank you so much for making this four-year experience a memorable one for me.

Finally, I would like to thank different funding bodies that supported my DPhil. These included: The Anandamahidol Foundation, the UK Research and Innovation (Digital Economy Programme grant number EP/G036861/1) and China Regenerative Medicine International Limited (CRMI).

Contents

List of Figures **xvii**

List of Tables **xxi**

List of Abbreviations **xxiii**

1 Introduction **1**
1.1 Motivation . . . 1
1.1.1 Cancer and drug development . . . 1
1.1.2 Cancer models . . . 3
1.1.3 Drug testing . . . 4
1.2 Aim and objectives . . . 5
1.3 Thesis structure . . . 6

2 Literature review **9**
2.1 Brain tumour microenvironment . . . 10
2.1.1 Cancer stem cells . . . 11
2.1.2 Vascular niche . . . 13
2.1.3 Hypoxic niche . . . 15
2.1.4 Invasive niche . . . 16
2.1.5 The reciprocal neurovascular relationship . . . 18
2.1.6 Neuroblastoma and its treatments . . . 19
2.1.7 Cancer resistance to therapeutics . . . 22
2.2 Three-dimensional *in vitro* cancer model . . . 26
2.2.1 Existing *in vitro* cancer models: 2-D vs 3-D . . . 26
2.2.2 Cells in neural cancer models . . . 28
2.2.3 Matrices for neural cancer models . . . 31
2.2.4 Types of 3-D *in vitro* cancer models . . . 35
2.3 Three-dimensional *in vitro* co-culture model . . . 39
2.3.1 Applications of 3-D *in vitro* co-culture models . . . 39
2.3.2 Supporting cells in co-culture models . . . 41
2.3.3 Matrices and co-culture conditions . . . 42
2.3.4 Effects of co-culture . . . 43

2.4 Perfusion bioreactor culture 43
2.4.1 Limitations of existing bioreactor systems 44
2.4.2 Considerations for bioreactor design 46
2.4.3 Scaling down: microbioreactor systems 48
2.4.4 Human biopsy culture as a biological avatar 50
2.5 Conclusion 53

3 Optimisation of hydrogel properties for 3-D *in vitro* neuroblastoma model 55
3.1 Introduction 56
3.2 Materials and methods 57
3.2.1 Cell culture 57
3.2.2 Hydrogel scaffold preparation 58
3.2.3 Monoculture model development 59
3.2.4 Microrheology studies 62
3.2.5 Dry gel morphological studies 62
3.2.6 Cell viability analysis 63
3.2.7 Cell immunostaining 63
3.2.8 Image analyses 64
3.2.9 Statistical analysis 65
3.3 Results and discussion 66
3.3.1 Selection of hydrogel for NSC-HUVEC model 66
3.3.2 Optimisation of hydrogel stiffness 71
3.3.3 Hydrogel fragmentation model 74
3.3.4 Characterisation of hydrogel morphology 75
3.3.5 Investigation of mixing techniques of cell-hydrogel suspensions 77
3.3.6 Effects of laminin on 3-D cell-hydrogel arrangements 79
3.4 Conclusion 81

4 Three-dimensional *in vitro* neural stem-endothelial cells co-culture model 83
4.1 Introduction 83
4.2 Materials and methods 85
4.2.1 Co-culture model development 85
4.2.2 Cell immunostaining 87
4.2.3 Image analyses 88
4.2.4 Statistical analysis 91
4.3 Results and discussion 92
4.3.1 Seeding NSCs from cryopreservation 92

4.3.2 Optimisation of co-culture media and seeding ratios 94
4.3.3 Investigation of neurovascular interactions 97
4.3.4 Characterisation of 3-D *in vitro* co-culture model 99
4.4 Conclusion 102

5 Perfused bioreactor recapitulating a neuroblastoma microenvironment 103
5.1 Introduction 104
5.2 Materials and methods 105
5.2.1 Cell culture 105
5.2.2 Bioreactor design 105
5.2.3 Flow rate calibration 106
5.2.4 Hydrogel scaffold preparation 108
5.2.5 Neuroblastoma model 108
5.2.6 Perfusion culture setup 108
5.2.7 Static 3-D culture 111
5.2.8 pH measurement 111
5.2.9 Waste metabolite analyses 111
5.2.10 Cell viability 113
5.2.11 Cell immunostaining 113
5.2.12 Image analyses 113
5.2.13 Statistical analysis 113
5.3 Results and discussion 113
5.3.1 Cell characterisation in perfused bioreactor and static culture systems 114
5.3.2 Evaluation of cell viability in perfused bioreactor and static culture systems 119
5.3.3 Analyses of metabolites in perfused bioreactor and static culture systems 120
5.3.4 Analyses of pH in perfused bioreactor and static culture systems 123
5.4 Conclusion 125

6 Evaluation of 3-D neuroblastoma model responses to chemotherapeutics 129
6.1 Introduction 129
6.2 Materials and methods 131
6.2.1 Treatment preparation 131
6.2.2 Co-culture model development 132
6.2.3 Culture systems set up 134

6.2.4 Cell immunostaining 138
6.2.5 Image analyses 138
6.2.6 Statistics 139
6.3 Results and discussion 139
6.3.1 Optimisation of cell seeding density 139
6.3.2 Optimisation of co-culture media 143
6.3.3 Evaluation of the neuroblastoma model's responses to cancer therapeutics 145
6.4 Conclusion 155

7 Conclusion and future perspectives **157**
7.1 Introduction 157
7.2 Thesis contribution 158
7.3 Thesis limitations 159
7.4 Future perspectives 161
7.4.1 Angiogenesis and pan-cancer therapy approach 161
7.4.2 Stromal components in 3-D cancer models 162
7.4.3 Genetic editing in 3-D cancer models 163
7.4.4 Combination therapy in 3-D *in vitro* drug screening platforms 164
7.4.5 Scaling up: microbioreactor systems 164
7.5 Concluding remarks 166

Appendices

A 3-D image visualisation and analyses **169**

References **175**

List of Figures

1.1 Cancer drug discovery process 2

2.1 Proliferation and differentiation of brain stem cells under normal and cancerous states 11
2.2 Angiogenic switch hypothesis 13
2.3 The relationship between hypoxic and vascular niche 15
2.4 Schematic illustration of a tumour microenvironment 17
2.5 Chemical structure of cisplatin 21
2.6 Chemical structures of all-trans-retinoic acid, 13-cis-retinoic acid and 9-cis-retinoic acid 23
2.7 The mechanism for the resistance of hypoxic cells to radiation . . . 23
2.8 The relationship between oxygen enhancement ratio and oxygen partial pressure 24
2.9 Morphologies of SH-SY5Y cells before and after differentiation . . . 30
2.10 The formation of HyStem® hydrogel by Michael-type addition reaction 33
2.11 Cell organisation and gradients in tumour spheroids 35
2.12 Schematic representation of different 2-D and 3-D tissue models . . 38
2.13 Set up of the TissueFlex® microbioreactor 49

3.1 Hydrogel scaffold preparation 58
3.2 Human umbilical vein endothelial cell monocultures in different 3-D hydrogel systems 68
3.3 Neural stem cell monocultures in different 3-D hydrogel systems . . 69
3.4 Effects of the hydrogel percentage (w/v in dH_2O) on neural stem cell viability 71
3.5 Comparisons between fragmented and unfragmented HyStem® hydrogel systems 74
3.6 Scanning electron microscope images of unfragmented and fragmented HyStem® 76
3.7 Comparisons between manual mix and vortex-centrifuge mixing techniques 78

3.8 Schematic illustration of the stabilised network formed by cells, laminin and gel granules 80
3.9 Z-stack image of a HUVEC 3-D fragmented HyStem® model stained for anti-laminin and CD31 markers 81

4.1 Schematic representation of 3-D *in vitro* neuroblastoma model . . . 87
4.2 Block diagram outlining the processes of background correction and image segmentation 89
4.3 Image analysis procedures used for 2-D images 90
4.4 Neural stem cells cultured in 3-D HyStem® after seeded from cryopreservation 93
4.5 Optimisation of co-culture medium and seeding ratios 95
4.6 Evaluation of neurovascular interactions between NSCs and HUVECs 98
4.7 Characterisation of the 3-D *in vitro* NSC-HUVEC model 100

5.1 The PDMS bioreactor for 3-D neuroblastoma model perfusion culture 107
5.2 Standard curve relating the flow rate to the volume of medium collected 108
5.3 The neuroblastoma model inside the cell culture insert 109
5.4 The 3-D perfusion culture system 110
5.5 Comparisons between co-culture morphologies under static and perfusion culture systems 115
5.6 Quantification of marker-expressing cells under static and perfusion culture systems 117
5.7 Comparisons of cell viabilities between static and perfusion cultures 119
5.8 Analyses of glucose concentration in static and perfusion cultures . 121
5.9 Analyses of VEGF and BDNF concentrations in static and perfusion cultures 122
5.10 pH measurements in perfused bioreactor and static culture systems 124

6.1 3-D printed hydrogel granule extrusion tool 134
6.2 3-D printed hydrogel granule and cell mixing tool 135
6.3 Casting and lifting of gel discs 136
6.4 Schematic representation of the 3DFlo® automatic cell culture system 137
6.5 Summary of different cell culture systems and treatments to evaluate 3-D *in vitro* neuroblastoma responses 138
6.6 Effects of cell seeding density on 3-D co-culture morphologies 141

6.7 Effects of cell seeding density on marker expressions 142
6.8 Effects of different media on SH-SY5Y-HUVEC co-cultures 144
6.9 Drug treatments in 2-D monolayer cultures 147
6.10 Drug treatments in 3-D TissueFlex® 148
6.11 Drug treatments in 3DFlo® 149

7.1 3-D *in vitro* model in cancer drug discovery process 166

A.1 Initial settings of 3-D image deconvolution 170
A.2 Overlaying of cell's surface markers 171
A.3 Thresholding of cell's surface markers 172
A.4 Quantification of cell surface markers 173
A.5 Computer-generated representations of three different cell surface markers 174

List of Tables

1.1 Treatment schedule of conventional anti-cancer drugs used in clinics 5

2.1 Advantages and disadvantages of 2-D and 3-D cell culture systems . 27
2.2 Advantages and disadvantages of different 3-D culture models . . . 38
2.3 Examples of 3-D *in vitro* co-culture systems 40

3.1 Average number of live cells/model in 2-D and 3-D monoculture systems after day 3 and day 7 70

4.1 Comparison of supplements between NBM and EGM-2 media . . . 96

6.1 The number of SH-SY5Y and HUVEC cells at different total cell seeding densities 133

List of Abbreviations

°C	Degrees Celsius
Δ	Change
μg*, *μL*, *μm	Microgram, microlitre, micrometre
%	Percentage
π	Pi
ω	Angular frequency
2-D, 3-D	Two- or three-dimensional
5-FU	5-Fluorouracil
6-OHDA	6-Hydroxydopamine
Akt	Protein kinase B
ANOVA	Analysis of variance
Bax	BCL-2-associated X protein
BCL-2	B-cell lymphoma 2
Akt	Protein kinase B
BDNF	Brain-derived neurotrophic factor
Calcein-AM	Calcein-acetoxymethyl
cAMP	Cyclic adenosine monophosphate
CASZ1	Castor zinc finger protein 1
CD	Cluster of differentiation
Cisplatin	Cis-diammine-dichloro-platinum
cm	Centimetre
CO_2	Carbon dioxide
CRISPR	Clustered regularly interspaced short palindromic repeats
dH_2O	Degassed water
DMSO	Dimethyl sulfoxide

DNA . . . . . Deoxyribonucleic acid

DWS . . . . . Diffusing wave spectroscopy

EBM-2 . . . . Endothelial basal medium-2

ECM . . . . . Extracellular matrix

EC50 . . . . . Median effective concentration

EGF . . . . . Epidermal growth factor

EGM-2 . . . . Endothelial cell growth medium-2

ELISA . . . . . Enzyme-linked immunosorbent assay

EMT . . . . . Epithelial–mesenchymal transition

EthD-1 . . . . Ethdium homodimer-1

EZH2 . . . . . Enhancer of zeste homolog 2

FAK . . . . . Focal adhesion kinase

FBS . . . . . Fetal bovine serum

FGF . . . . . Fibroblast growth factor

g . . . . . Standard gravity

$G^\star$ . . . . . Complex modulus

G' . . . . . Storage modulus

G'' . . . . . Loss modulus

GA-1000 . . . Gentamicin sulfate/Amphotericin

Gy . . . . . Gray

$\mathbf{H}^+$ . . . . . Hydrogen cation (Proton)

$\mathbf{HCO}^{3-}$ . . . . Hydrogen carbonate

HEPES . . . . 4-(2-hydroxyethyl)-1-piperazineethanesulfonic acid

HIF . . . . . Hypoxia-inducible factor

hESC . . . . . Human embryonic stem cell

HPC . . . . . Haematopoietic stem and progenitor cell

hPSC . . . . . Human pluripotent stem cell

HUVEC . . . . Human umbilical vein endothelial cell

i . . . . . Imaginary number

ID . . . . . Inhibitor of DNA binding proteins

IGF-1 . . . . . Insulin-like growth factor-1

k_B . . . . . Boltzmann constant

kg, kD . . . . . Kilogram, kilodalton

LD50 . . . . . Median lethal dose

LDH . . . . . Lactate dehydrogenase

LMO1 . . . . . LIM domain only 1

MAP . . . . . Microtubule-associated protein

MAPK . . . . Mitogen-activated protein kinase

mg, mL, mm . Milligram, millilitre, milligram

MMP . . . . . Matrix metalloproteinase

MnSOD . . . . Mitochondrial antioxidant manganese superoxide dismutase

mRNA . . . . Messenger ribonucleic acid

$NaHCO_3$ . . . Sodium bicarbonate

NaOH . . . . . Sodium hydroxide

NC3Rs . . . . The national centre for the replacement, refinement and reduction of animals in research

NBM . . . . . Neurobasal medium

NeuN . . . . . Neuronal specific nuclear protein

NF-κB . . . . . Nuclear factor-κB

ng, nm . . . . . Nanogram, nanometre

NGF . . . . . Nerve growth factor

NMA . . . . . N-myc amplification

NRG . . . . . Neuregulin

NSE . . . . . Neuron-specific enolase

NSC . . . . . Neural stem cell

OD . . . . . Optical density

p . . . . . P-value (Probability value)

Pa . . . . . Pascal

PBS . . . . . Phosphate-buffered saline

PCL . . . . . Polycaprolactone

PDMS . . . . . Polydimethylsiloxane

PDO . . . . . Patient-derived organoids

PDX . . . . . Patient-derived xenografts
PEG-DA . . . Polyethene glycol diacrylate
pg . . . . . Picogram
P-gp . . . . . P-glycoprotein
pH . . . . . Potential of hydrogen
PI3K . . . . . Phosphatidylinositol 3-kinase
PLO . . . . . Poly-L-ornithine
PSF . . . . . Point spread function
PTFE . . . . . Polytetrafluoroethylene
PVC . . . . . Polyvinyl chloride
R . . . . . Radius (tracer particle)
rad . . . . . Radian
R3-IGF-1 . . . Long arginine 3-insulin-like growth factor-1
RA . . . . . Retinoic acid (All-trans-retinoic acid)
RASSF1A . . Ras association domain family 1
rpm . . . . . Rounds per minute
RPMI . . . . . Roswell Park Memorial Institute medium
s . . . . . Second
SAP97 . . . . . Synaptic associated protein-97
SD . . . . . Standard deviation
SDF1α . . . . . Stromal cell-derived factor α
SEM . . . . . Scanning electron microscope
T . . . . . Temperature
TGF-β . . . . . Transforming growth factor-β
TMB . . . . . 3,3',5,5'-Tetramethylbenzidine
TNF-α . . . . . Tumour necrosis factor-α
tPA . . . . . Tissue plasminogen activator
TrkB . . . . . Tropomyosin receptor kinase B
V . . . . . Volts
VEGF(R) . . . Vascular endothelial growth factor (receptor)
VitD3 . . . . . Vitamin D3 (Cholecalciferol)
vs . . . . . Versus
w/v . . . . . Percentage weight per volume

1 Introduction

Table of contents

1.1 Motivation 1
1.1.1 Cancer and drug development 1
1.1.2 Cancer models 3
1.1.3 Drug testing 4
1.2 Aim and objectives 5
1.3 Thesis structure 6

1.1 Motivation

1.1.1 Cancer and drug development

Cancer is defined as the group of cells that proliferates uncontrollably and has the potential to invade to distant sites throughout the body. The spread of cancer disrupts the regulation mechanisms of normal growth in the body, which may also destroys the surrounding normal tissues (Grandér, 1998). In 2018, global statistics showed that there were 9.6 million deaths and 18.1 million new cases reported. Amongst that the brain and nervous system cancers accounted for 1.6% of the new cases and 2.5% of the deaths (Bray, Ferlay, et al., 2018).

According to the World Health Organisation, there are around 150 types of brain and nervous system cancers (Louis et al., 2016). Among that, neuroblastoma

is the second most common paediatric brain and nervous system cancer. The disease often originates in the nerve tissue of adrenal glands then grows along the spinal cord (Ohtaki et al., 2011). Neuroblastoma accounts for almost 10% of all paediatric cancer cases. Strikingly, 90% of patients are less than five years old. Despite intensive treatments of tumour resection and adjuvant chemotherapy, 60% of the patients are still presented with metastatic disease and poor clinical outcomes (Manchanda and Manchanda, 2009).

Billions of dollars have been invested annually in drug discovery and development process from basic research (studies in tissue culture plates and animals) to clinical trials (studies in human participants). The drug discovery and development process involve tests in these following steps: *in vitro* 2-D monolayer cultures, *in vivo* tests in animals, followed by tests in human participants. However, the process itself takes up is lengthy and can take up to 20 years for a single drug to be approved to use in clinics (see Figure 1.1). To break the process down, testing *in vitro* and in animal models take $1-3$ years (average $=$ 18 months); clinical trials, the longest and the most expensive step, takes $2-10$ years (average $=5$ years) and the approval by the ethic committee take $2-7$ years (average $=2$ years).

Furthermore, up to 92% of drug candidates that passed pre-clinical stages fail in the clinical trials and cannot make it to the bedside (Pampaloni et al., 2007). The weak correlation between the current pre-clinical models and *in vivo* tissues partially caused the high failure rate of drugs. A robust and more predictive platform capable

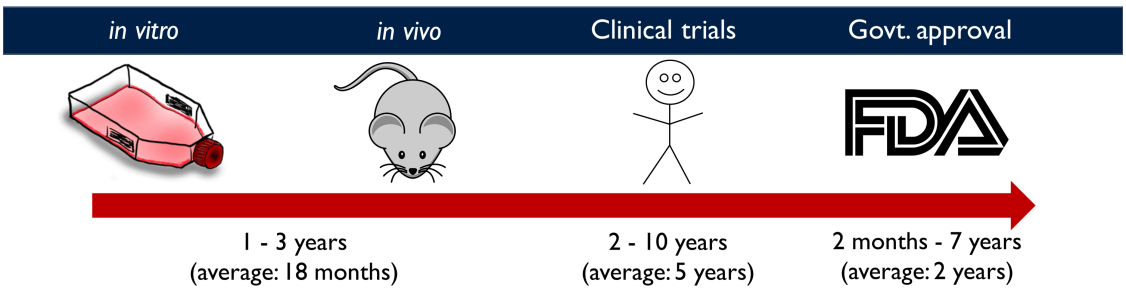


Figure 1.1: Cancer drug discovery process Drugs are initially tested on the 2-D monolayer culture systems before tested in animals, then in human participants. The process takes a considerable amount of time- up to 20 years for a single drug to be approved.

of screening and identifying drug candidates in pre-clinical studies is needed. This can be in the form of a bioreactor or a microfluidic device that allows the culture of human cells or tissues, under different interventions, for an extended period. The developed platform can increase the predictive power of drugs in high throughput screening while can also save animal lives sacrificed, money and time wasted with unsuccessful drug candidates in clinical trials (Mitra et al., 2013).

1.1.2 Cancer models

As human biological systems are extremely complex in nature, they cannot be recreated easily in either two-dimensional (2-D) monolayer cultures (static dish culture systems) or animal models (living, non-human animals). More realistic models are needed to mimic different phenomena occurring within the tumour (Hutmacher et al., 2009). Three-dimensional (3-D) *in vitro* cell cultures or the culturing of cells within a 3-D artificial environment can potentially close the gap between 2-D cell cultures and physiological tissues.

Despite the need to recreate a tumour in 3-D environment, the human tumour microenvironment is very complicated for any existing cancer models to recapitulate. This is because of the heterogeneity of the tumour that comprises various cell types, growth factors and extracellular matrix components. In addition, the complex interactions among these components make the tumour even more challenging to recreate in a 3-D environment. Hence, it is desirable to develop with a minimal functional cancer model containing primary aspects of tumour biology. However, the model should enable real-time imaging, detection and analysis of cells in culture (Villasante and Vunjak-Novakovic, 2015).

Although 3-D cancer models appear to recapitulate solid tumours more accurately than the 2-D monolayer cultures meanwhile minimise the ethical complications observed *in vivo* animal tests, 3-D *in vitro* systems cannot entirely replace the existing animal models in clinical trials. Instead, they can be used complementarily to provide a more effective and faster drug screening process (Szot et al., 2011). The 3-D *in vitro* testing systems can come in between the 2-D monolayer and

in vivo animal tests to primarily screen out any unsuccessful anti-cancer drug candidates from the drug discovery process.

In fact, the NC3Rs or the national centre for the replacement, refinement and reduction of animals in research has taken procedures to minimise the unnecessary harm to animal models (Prescott and Lidster, 2017). One example is the introduction of a new *in vivo* assay to assess platelet aggregation responses, which measures platelet function in real time using radiolabelled platelets and imaging. This method reduces the number of mice paralysed and killed from direct injection of thrombogenic substances (Moore and Emerson, 2012). The development of the 3-D *in vitro* model can contribute to the reduction of animal models sacrificed during *in vivo* tests by ensuring that only potent drug candidates in 3-D cultures are investigated.

1.1.3 Drug testing

Drug testing in humans may involves the use of a biopsy specimen in lieu of cell lines. Biopsy samples are extracted from patients, cultured and tested for drug responses to determine efficacy (Hickman et al., 2014). Due to its native source from individual patients, results obtained from biopsy culture testing are very patient-specific. At present, a biopsy specimen can be maintained *ex vivo* without losing its structure or viability for only $3-7$ days (Estes et al., 2016; Schmid et al., 2012; Vaira et al., 2010; Van der Kuip et al., 2006).

Drug testing using a biopsy specimen can only provide us with limited information regarding the efficacy and side effects of the drug over a period of 7 days. The treatment schedule of several common anti-cancer drugs used in clinics is shown in Table 1.1. The table shows that most conventional drugs used in clinics are administered once every $2-3$ weeks. This implies that the period of one week is not enough to observe the entire pharmacology of medications from drug administration to drug clearance from the body. Besides, there is also a possibility of tumour recurrence occurring after 7 days of drug administration, which cannot

Table 1.1: Treatment schedule of conventional anti-cancer drugs used in clinics

Drug name	Treatment schedule	Reference
Paclitaxel	Once every 3 weeks	Arrieta et al. (2010)
Bevacizumab	Once every 14 to 21 days	Benesch et al. (2008)
Doxorubicin	Once every 21 to 28 days	Muggia et al. (1997)
Cisplatin	From daily to monthly	Arrieta et al. (2010)

be observed in the current drug testing systems. Hence, there is a need to maintain the viability of the cells for an extended period.

This thesis addresses the approach of extending cell viability *in vitro*. The project initiates from the reconstruction of neuroblastoma using cell lines, growth factors and artificial extracellular matrices (ECM). To further the accuracy in recapitulating the tumour, we also consider its surrounding microenvironment such as: the mass transport of nutrients and oxygen into the cells. A bioreactor, which is an engineered device or system that carries out biological and chemical reactions, can be used to introduce the continuous mixing and flow of fluids in the culture vessel. Perfusion culture inside a bioreactor provides aspects of circulating the flow of oxygen and nutrients observed in the human body, which reflects the consistent recruitment of these necessities by the cancer cells within the solid tumours. Once the 3-D dynamic culture system accurately recapitulates the tumour microenvironment, it is possible that the cancer model can be retained inside the perfusion bioreactor for a longer time than when they are cultured in a static culture (Ferrarini et al., 2013). Therefore, bioreactor systems have a potential to allow determination of long-term drug responses, leading to the delivery of appropriate treatments to patients.

1.2 Aim and objectives

The research conducted in this thesis aims to create a 3-D hydrogel-perfused culture platform that maintains the integrity and characteristics of a neuroblastoma model for long-term drug testing. The duration of drug testing is anticipated

to be at least 21 days, which would comply with the treatment schedule of anti-cancer drugs listed in Table 1.1.

The culture platform developed in this thesis has a potential to be used as a platform to maintain a biopsy specimen extracted from patients. Potential applications of this research include a high-throughput drug-screening platform for anti-cancer drugs and personalised cancer therapeutics.

The aim of the thesis is subdivided into several objectives. The first objective dedicates to the development and characterisation of a 3-D *in vitro* hydrogel neuroblastoma co-culture model. The model provides the primary characteristics of neuroblastoma including: cancer cells, endothelial cells, growth factors and ECM, while ensures that the model is easily reproducible.

The second objective involves the design of a perfused bioreactor culture system, which extends the viability of the model from a conventional static culture up to at least 21 days. The work also comprises the measurement of metabolite levels including: glucose, vascular endothelial growth factor (VEGF) and brain-derived neurotrophic factor (BDNF) in both static and perfusion culture systems. The changes in these metabolite levels over the culture period could justify any differences observed in the cell viability, morphology and marker expressions between the two culture systems.

The last objectives of this project involve the investigation of the neuroblastoma model cultured inside three different established culture systems including: 2-D static monolayer culture, 3-D TissueFlex® perfused bioreactor and the 3DFlo® automatic cell culture machine. Different anti-cancer drugs are tested on the models up to 21 days to observe long-term drug responses. The microenvironment recapitulated in this work will provide an accurate determination of drugs or a combination of drugs chosen to treat each specific patient and give rise to optimal therapeutic outcomes.

1.3 Thesis structure

This thesis consists of seven chapters. Chapter 2 provides the review of literature regarding the brain tumour microenvironment, drug treatments for neuroblastoma,

3-D *in vitro* cancer models and perfusion bioreactor cultures. This starts with the relationship between neuronal cells and endothelial cells and gives an outline of the reciprocal neurovascular relationship. The chapter then describes the disease of neuroblastoma and its treatments. The concept of personalised medicine is also covered in this section. After that, the chapter describes different types of 3-D *in vitro* cancer and co-culture models. The last section of the literature review introduces different perfused bioreactor systems and provides any limitations and considerations in designing the essential microenvironment.

Chapter 3 involves the optimisation of hydrogels for their applications in 3-D cancer models, specifically a neuroblastoma co-culture model. Different factors are taken into consideration in designing the model to mimic neuroblastoma tumours. One of the important factors is the laminin-hydrogel matrix, which provides a microenvironment supporting the growth of cells encapsulated within it.

Chapter 4 describes the development of a 3-D *in vitro* neural stem-endothelial cells co-culture model based on the results acquired from the previous chapter. The co-cultures of neural stem cells (NSCs) and human umbilical vein endothelial cells (HUVECs) cell lines are optimised and characterised by immunostaining, cell viability assay and image analyses.

Chapter 5 involves the expansion of the model through perfusion culture, which mimics the physiological system of the human body. A microbioreactor is designed to facilitate the 3-D culture over the period of 21 days. Different endpoints are assessed weekly to compare the integrity and characteristics of the cancer model between static and perfusion cultures.

Chapter 6 initially describes several optimisation experiments are then conducted to recreate the distinct structures formed by each cell type (tubule-like structures in HUVECs and neurite outgrowth in SH-SY5Ys). Later, the work shifts toward the applications of 3-D neuroblastoma model culture inside the microbioreactor. The work compares the effects of drug treatments on the neuroblastoma model, as single agents and as a combination therapy, inside three different culture systems (2-D monolayer culture, 3-D TissueFlex® and 3DFlo®) for 21 days.

Chapter 7, to conclude this thesis, summarises the entire project; integrating the findings from Chapter $3-6$ with the previous findings in the literature review (see Chapter 2). This chapter also discusses several, but not limited to the potential future directions of this project.

2

Literature review

Table of contents

2.1 Brain tumour microenvironment 10
2.1.1 Cancer stem cells 11
2.1.2 Vascular niche 13
2.1.3 Hypoxic niche 15
2.1.4 Invasive niche 16
2.1.5 The reciprocal neurovascular relationship 18
2.1.6 Neuroblastoma and its treatments 19
2.1.7 Cancer resistance to therapeutics 22
2.2 Three-dimensional *in vitro* cancer model 26
2.2.1 Existing *in vitro* cancer models: 2-D vs 3-D 26
2.2.2 Cells in neural cancer models 28
2.2.3 Matrices for neural cancer models 31
2.2.4 Types of 3-D *in vitro* cancer models 35
2.3 Three-dimensional *in vitro* co-culture model 39
2.3.1 Applications of 3-D *in vitro* co-culture models 39
2.3.2 Supporting cells in co-culture models 41
2.3.3 Matrices and co-culture conditions 42
2.3.4 Effects of co-culture 43
2.4 Perfusion bioreactor culture 43
2.4.1 Limitations of existing bioreactor systems 44
2.4.2 Considerations for bioreactor design 46
2.4.3 Scaling down: microbioreactor systems 48
2.4.4 Human biopsy culture as a biological avatar 50
2.5 Conclusion 53

2.1 Brain tumour microenvironment

The brain is the central organ of the human nervous system. It comprises neurons that make up nerve tissues. The human brain also contains supporting cells such as: glial cells and blood vessels that help to create the complex microenvironment.

In normal tissues, the three-dimensional (3-D) interactions between cells and the extracellular matrix (ECM) and between cells themselves have established a communication network that retains their specificity and homeostasis. Any disruptions made to this healthy microenvironment as a result of either genetic or epigenetic processes can result in neoplastic transformation or an abnormal and excessive growth of tissue cells (Pampaloni et al., 2007).

It is becoming evident that the interactions between cells and stroma are essential for tumour growth and progression. Alemany-Ribes and Semino (2014) reported that the development of vascular structures was observed in collagen-based co-cultures of cancer cells, endothelial cells and fibroblasts. This observation is explained by the migration of pro-angiogenic factors and the formation of capillaries by endothelial cells, due to interactions between different cell types.

In fact, tumour growth and metastasis (the invasion of cancerous cells to distant sites) are results of the tumour microenvironment formed by different vital players such as: normal cells, immune cells, exosomes, secreted factors, oxygen gradients, physical signals, ECM and stem cells (Szot et al., 2011; Villasante and Vunjak-Novakovic, 2015). Each cell type making up the microenvironment is also different in its behaviour; cells can be in the state of proliferation, differentiation, quiescent or necrosis. These all depend on their location inside a tumour and its neighbouring environment. Besides, the non-uniform microenvironmental factors such as: pH, oxygen and glucose gradients add complexities to native tumours (Zhang et al., 2005).

2.1.1 Cancer stem cells

Over the last decade, there is increasing evidence supporting the model of cancer stem cell hypothesis. It is believed that a small population of cells, which shares similar biological properties to healthy stem cells, drives the initiation and the propagation of tumour malignancy (Rich and Eyler, 2008; Clarke, 2004). Cancer stem cells are characterised by its distinct invasiveness, metastatic potential and resistance to cancer therapeutics (Kievit et al., 2014).

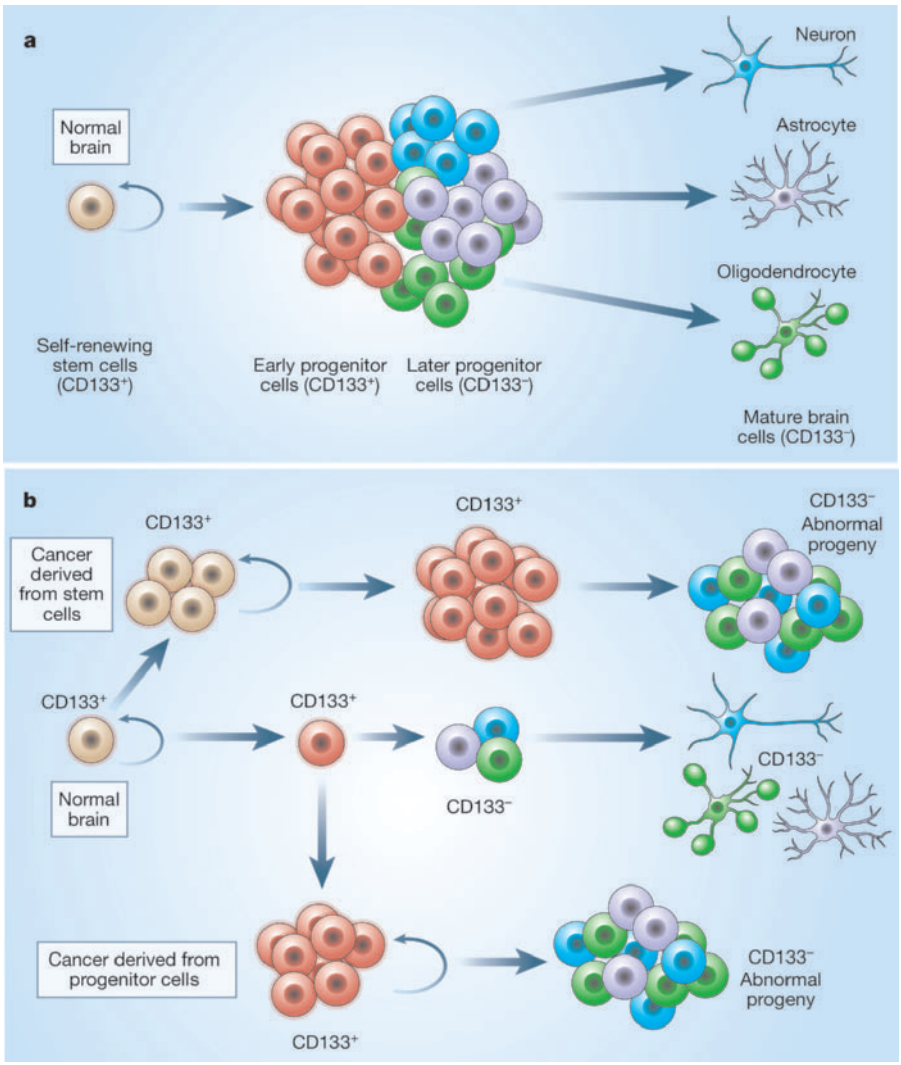


Figure 2.1: Proliferation and differentiation of brain stem cells under normal and cancerous states (A) Late progenitor cells in the normal brain differentiate into neurons, astrocytes or oligodendrocytes; (B) Late progenitors derived from cancer stem cells can also lead to an abnormal progeny due to mutations that cause unlimited self-renewing potentials. Image reproduced from Clarke (2004).

Cancer stem cells express the CD133 marker. Under normal circumstances, normal $CD133^+$ cells are capable to renew themselves, producing $CD133^+$ early progenitor cells and $CD133^-$ late progenitor cells respectively (see Figure 2.1A). Late progenitor cells eventually differentiate into $CD133^-$ neurons, astrocytes or oligodendrocytes (Clarke, 2004).

On the other hand, in cancer cells, the messenger ribonucleic acid (mRNA) expression of CD133 increases upon tumour recurrence. This increase is due to the loss of usual constraints, which causes an abnormal expansion of $CD133^+$ stem cells and unprecedented self-renewal ability of early $CD133^+$ progenitor cells (see Figure 2.1B). Cancer can be derived from both stem cells and progenitor cells. With an overexpressed level of CD133, these cells uncontrollably proliferate and ultimately differentiate to form a $CD133^-$ abnormal progeny (Clarke, 2004).

Cancer stem cells commonly reside near the vasculature (Lathia et al., 2011). Several studies observed that the extension of blood vessels in tumours were due to the stem cell factor expressed by neurons and infiltrating glioma cells *in vivo* (Sun et al., 2006; Rich and Eyler, 2008). The increase in the stem cell factor expression correlated with higher grade gliomas and the decrease in patient survival (Sun et al., 2006).

These changes imply that cancer stem cells provide the support for tumour vasculature while the vascular niche provides cancer stem cells with the support for tumour formation. Furthermore, specific factors secreted by stem cells influence the differentiation status of neighbouring cells, causing the cells to reprogram and to alter their growth and their responses to cancer therapeutics (Rizvanov et al., 2010).

However, until today, there are no perfect markers for brain tumour stem cells that match to the stem cell phenotype. As the search for an improved marker progresses, it is becoming clear that universal immunophenotype markers may not be the solution as brain tumours are heterogeneous diseases (Rich and Eyler, 2008; Mitra et al., 2013; Li, Sun, et al., 2013). As cancer stem cells are enriched in different microenvironments or niches within the tumour (Lathia et al., 2011), each niche will be thoroughly discussed in the following sections.

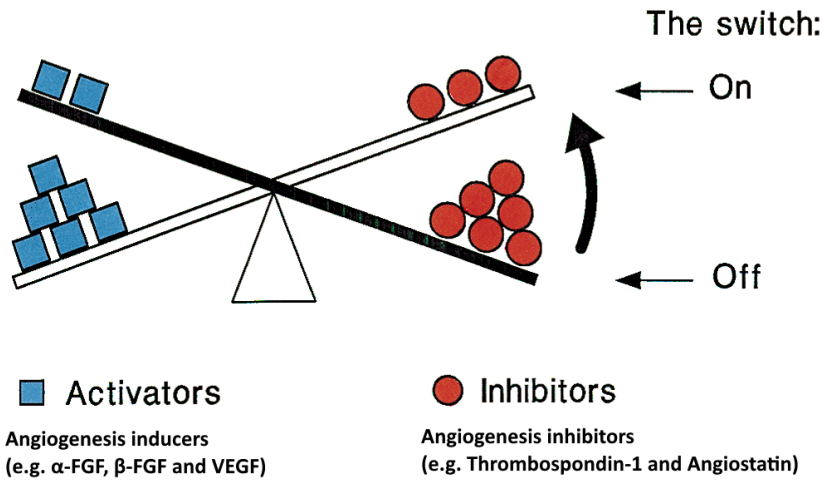


Figure 2.2: Angiogenic switch hypothesis The balance between pro- and anti-angiogenic factors in the tissue microenvironment induce and monitor angiogenesis. Image reproduced from Hanahan and Folkman (1996).

2.1.2 Vascular niche

Angiogenesis, the growth of new vessels from the existing ones, occurs when there is a demand for oxygen and nutrients in the tissue. This phenomenon is different from vasculogenesis, which is defined as when new vessels are formed by the migration of angioblasts as a response to local cues. The migration of angioblasts terminates at the sites of ischaemia, where they differentiate to form vessels. As either stem or progenitor cells in tissues can form endothelial cells, they both play a role in the growth and improvement of vascularisation (Clarke, 2004; Kievit et al., 2014).

Notch signalling pathway is known to mediate the cellular interactions within the stem cell niche and also contributes to vascular development (Kievit et al., 2014). Vascular endothelial growth factor (VEGF) acts through VEGF receptor 2 (VEGFR-2), which results in the proliferation of endothelial cells. VEGF then induces the notch signalling to counteract by downregulating the expression of VEGFR-2, completing the feedback loop (Chen, Htay, et al., 2009).

The observation is in agreement with the angiogenic switch hypothesis that the balance between pro- and anti-angiogenic factors in the microenvironment induce and monitor angiogenesis (see Figure 2.2). The switch may be kept off when there is an absence of angiogenesis inducers such as: α-FGF, β-FGF and VEGF. Else,

the presence of these angiogenesis inducers may be regulated by the higher levels of angiogenic inhibitors such as: thrombospondin-1 and angiostatin. The balance of the switch can be affected by the increase or decrease of these growth factor concentrations due to the induction of a tumour microenvironment or the loss of a tumour suppressor gene. This leads to tumour vasculature; the uncontrollable proliferation of endothelial cells that generates the stress to move cells apart and eventually forms a disorganised structure (Hanahan and Folkman, 1996).

Under normal circumstances, endothelial cells secrete factors to regulate the function of neural stem cells (NSCs) residing in the vascular niche. This vascular niche is only limited to the hippocampus and subventricular zones, where the rate of proliferation is low (Calabrese et al., 2007). On the contrary, the vascular niche in brain tumours is abnormal. With an abundance of $Nestin^{+}$ cells distributing throughout the brain, the rate of cell proliferation increases as the number of capillaries increases.

The niche itself serves as a protection for the stem cells. Apart from promoting survival signals in cancer stem cells, endothelial cells are capable of guarding cancer and stem cells from the radiation damage as well (Calabrese et al., 2007). This implies that a tumour vascular niche is partly responsible for the development of resistance against anti-cancer therapeutics such as chemotherapy and radiotherapy. Also, the brain tumour stem cells construct their microenvironment through the elaboration of angiogenic factors and in return, these cells depend on their niche for growth (Rich and Eyler, 2008).

Chen, Htay, et al. (2009) reported the increasing number of human umbilical vein endothelial cells (HUVECs) sprouts in co-cultures with VEGF-secreting glioma cells. The same study observed neovascularisation even there was no direct contact between both cell types; only the secretion of growth factors by cancer cells was required to induce endothelial cells to express ligands and their corresponding receptors. Besides, Khodarev et al. (2003) reported an increase in net-like structures in U87 human glioblastoma cell line and HUVECs co-cultures regardless of whether both cells were in contact.

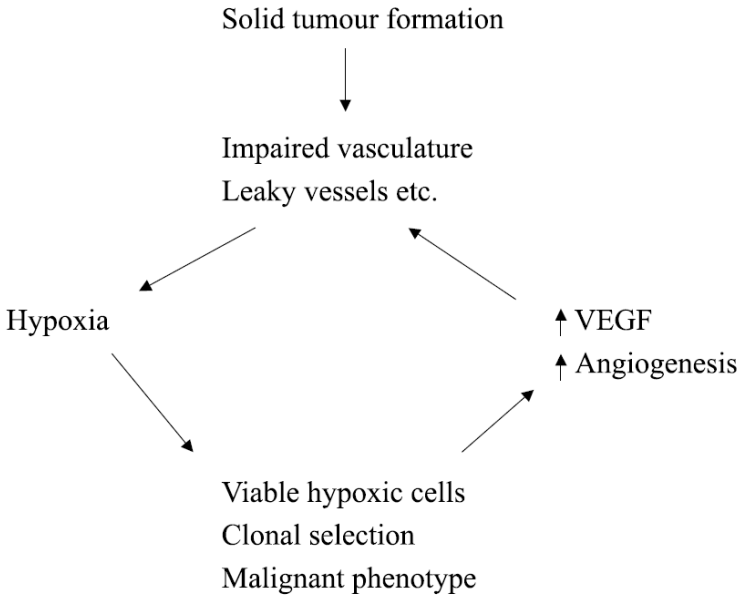


Figure 2.3: The relationship between hypoxic and vascular niche The microenviroment inside solid tumours is characterised by the leaky vasculature, which leads to the formation of a hypoxic niche within the innermost region. This hypoxic environment promotes the transcription of VEGF and angiogenesis. Image reproduced from Shannon et al. (2003).

2.1.3 Hypoxic niche

A cancer cell mass cannot grow beyond 200 μm in diameter without a blood supply. In a nodular tumour, the effective diffusion distance of nutrients was around $100 - 150$ μm (Tannock, 1989). Insufficient blood supply results in limited amounts of nutrients and oxygen delivered to cancer cells, which eventually leads to hypoxic conditions and necrosis of the innermost cells within a tumour (Szot et al., 2011; Zhang et al., 2005).

Hypoxia arises from an imbalance between oxygen delivery and oxygen consumption (Vaupel and Harrison, 2004). It is defined as the status that the oxygen level in tissues is around $5 - 10$ mmHg, which is much below the physiological levels of cells, i.e. $40 - 60$ mmHg. This unique characteristic of cancer distributes heterogeneously throughout the mass of tumours (Span and Bussink, 2015).

The hypoxic environment maintains and promotes accumulation of stem cells within a tumour (Lathia et al., 2011). Stem cells, both normal and cancerous,

reside within low-oxygen regions while exhibiting growth dependence on blood vessels (Mohyeldin et al., 2010; Shen et al., 2004).

A hypoxic region is characterised by a low potential of hydrogen (pH) and a high interstitial pressure, which causes the upregulation of hypoxia-inducible factor-1α (HIF-1α) (Chen, Htay, et al., 2009; Lathia et al., 2011). Hypoxia protects HIF-1α from degradation and eventually forms a hostile environment, promoting the transcription of proteins such as VEGF in the angiogenic factor cascade (Szot et al., 2011). The relationship between hypoxic and vascular niches is outlined in Figure 2.3.

Several studies showed that culturing cells in a hypoxic environment or under oxidation stress increase cancer and stem cells viabilities while promote sprout formations in HUVECs (Brown, Khodarev, et al., 2004; Rizvanov et al., 2010; Chen, Htay, et al., 2009). Hypoxic conditions can eventually lead to necrosis, which is the pathophysiology of malignant tumours. Cell population residing adjacent to necrotic regions are more resilient to radiotherapy and chemotherapy, impeding clinical outcomes (Nyga et al., 2011; Chen, Htay, et al., 2009).

2.1.4 Invasive niche

Metastasis accounts for 90% of cancer deaths, yet its mechanism is still poorly understood (Christofori, 2006). Lathia et al. (2011) speculated the existence of this niche and observed the *in vivo* invasion in cancer stem cell models to be similar to those found in human tumours.

As pro-angiogenic factors can be synthesised at any specific locations on demand, matrix metalloproteinases (MMPs) are required to regulate and remodel the surrounding ECM. Ultimately, this leads to the degradation of the basement membrane and metastasis through cascades like mitogen-activated protein kinase (MAPK) and focal adhesion kinase (FAK) signalling pathway (Alemany-Ribes and Semino, 2014; Nyga et al., 2011). Metastatic cells then enter the circulatory and lymphatic system; which later end up growing at distant parts of the body. As 90% of cancers originate from epithelial cells, they eventually lose their phenotype and result in the disruption of basal-apical polarity. The loss of cellular phenotype

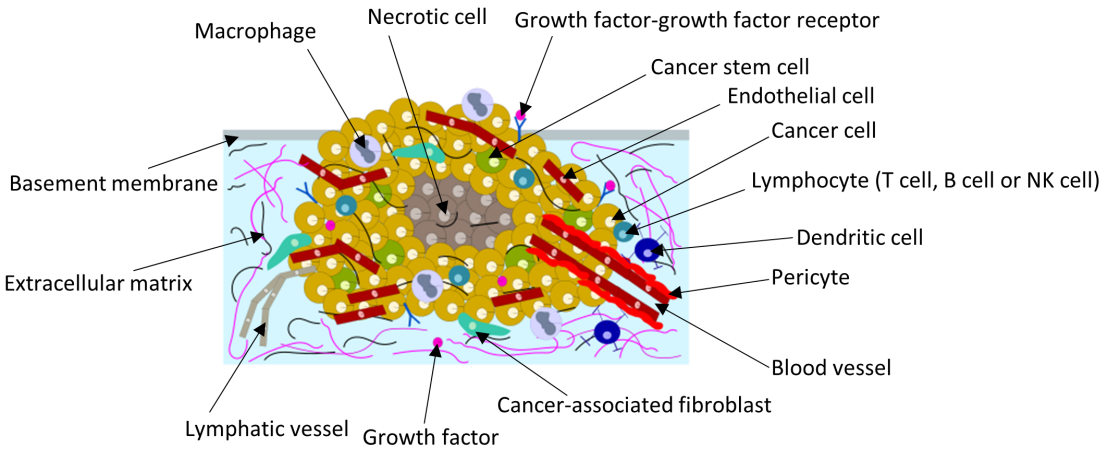


Figure 2.4: Schematic illustration of a tumour microenvironment Different microenvironmental niches are formed from the interactions of cancer cells with themselves as well as with other supporting cells, signalling molecules and stroma. These complex interactions contribute to tumour progression and metastasis to distal sites. Image modified from Xu, Farach-Carson, et al. (2014).

also causes the downregulation of focal adhesions and remodelling of the actin cytoskeleton. Finally, these cellular structures and functional changes result in a mesenchymal phenotype, also called epithelial-to-mesenchymal transition (EMT) (Alemany-Ribes and Semino, 2014; Mohyeldin et al., 2010).

The EMT phenomena and the generation of cadherin switch are consistent with the changes in mRNA expressions in cancer cells. The early expression of CD44 transmembrane protein promotes the downstream expression of CD133 through SNAI1, SNAI2, and Twist2 pathway and induces metastasis (Kievit et al., 2014).

It is evident that the microenvironment of the tumours are not homogeneous. Different niches, i.e. hypoxic regions, vascular niche, and invasive niche co-exist within the same tumour. Figure 2.4 illustrates the heterogeneity of a tumour and the microenvironment on which it depends. Identification of each niche within a tumour is still challenging as its composition is rapidly evolving and the experimental reagents are also lacking (Lathia et al., 2011).

2.1.5 The reciprocal neurovascular relationship

Endothelial cells contribute to the enhancement of neurogenesis and the regulation of stem cell renewal (Shen et al., 2004). Neurogenesis occurs in the subventricular zone and the subgranular zone of the brain. Neural stem and progenitor cells lie within the proximity to blood vessels with both proliferating neural and endothelial cells found in clusters. Both cell types respond to changing microenvironments by producing growth factors and receptors, which relate to the process of neurogenesis, involving the active recruitment and remodelling of vasculature (Nern and Momma, 2006; Park et al., 2003; Palmer et al., 2000).

Several studies reported the crosstalk between neuronal and endothelial cells. For example, a study by Shen et al. (2004) showed that NSCs extracted from mouse cerebral cortex grew more substantially and expressed an increase in progenitor markers when co-cultured with endothelial cells; compared to other cells such as CTX. On top of that, a study by Li, Ford, et al. (2006) reported stable phenotypes and developed vascular structures when both NSCs and endothelial cells were co-cultured; regardless whether the cells were in contact. Another study by Leventhal et al. (1999) also observed the enhancement of neuronal migration in neurovascular co-cultures.

Neurovascular niche is mediated by endothelial factors such as VEGF and brain-derived neurotrophic factor (BDNF). These growth factors stimulate the growth of NSCs and capillaries as well as enhance their outgrowth, differentiation and survival (Carmeliet, 2003). VEGF is upregulated in this capillary-abundant area by HIF-1 when there is a shortage of oxygen. Several *in vitro* and *in vivo* studies showed that VEGF along with its receptors were expressed in mouse embryonic cortical neurons and cultured NSCs (Ogunshola et al., 2002; Jin et al., 2002; Maurer et al., 2003). BDNF was secreted by endothelial cells in their microvascular network to recruit neuronal cells and increase their viability in the central nervous system (CNS) (Nakahashi et al., 2000; Leventhal et al., 1999).

Both VEGF and BDNF inhibit stem cell differentiation while facilitating their self-renewal potentials. In return, NSCs also play a primary role in regulating the niche by providing signals, e.g. The induction of endothelial cells by nitric

oxide to secrete these endothelial factors. The signalling activates receptors such as: VEGFR-2 and tropomyosin receptor kinase B (TrkB) (Li, Ford, et al., 2006).

2.1.6 Neuroblastoma and its treatments

In order to design a 3-D model of a particular type of cancer and recapitulate its microenvironment, it is important to understand the nature of the disease first. Although the model itself can help to further our understanding of neuroblastoma, the knowledge of the pathological conditions, treatments and resistance to these treatments are initially needed for the model to be developed accurately.

Neuroblastoma pathological conditions, signs and symptoms

Neuroblastoma can be diagnosed by either surgical biopsies or fine needle aspirates. Classifications of the primary tumour growth include, but not limited to imaging modalities such as ultrasound, computed tomography and magnetic resonance imaging. Urine samples may also be collected to determine the level of urinary catecholamine metabolites, where increased concentrations of these metabolites can be expected in cancer patients (Schleiermacher et al., 2003).

Poor prognosis markers for a high-risk stage 4s neuroblastoma comprise partial responses to chemotherapy, bone metastases ($>$ 100 tumour cells/10^5 normal nucleated bone marrow cells), overexpressed biological markers such as serum lactate dehydrogenase (LDH) of at least 143 ng/mL, ferritin or neuron-specific enolase (NSE), as well as overexpressed histopatholgical and genetic markers including N-myc amplification (NMA), tumour diploidy and chromosome 1p deletion. These poor prognosis markers are not limited to low telomerase activity, low expression of nerve growth factors and their corresponding receptors and the gain of chromosome 17q material (Matthay et al., 1999; Schleiermacher et al., 2003).

Patients with good outcomes, i.e. received little or no treatment are still prone to hepatomegaly (enlargement of the liver), which leads to respiratory, renal, gastrointestinal impairment or coagulation disorders. Ultimately, they would require a medical intervention (Schleiermacher et al., 2003).

Neuroblastoma treatments

Since there is no "gold standard" treatment for neuroblastoma currently available in the clinic, the benefits of treatments must be weighed against any possible short- and long-term side effects.

The first line of treatment for stage 4s neuroblastoma is a CE regimen, which comprises the combination of carboplatin (6.6 mg/kg/day, days $1-3$) and etoposide (5 mg/kg/day, days $1-3$) repeated every 21 days. This therapeutic course commences when the absolute neutrophil count is 500,000 per mL or higher (Schleiermacher et al., 2003). Other chemotherapeutic regimens include all-trans-retinoic acid (tretinoin) and 13-cis-retinoic acid (isotretinoin) applied after bone marrow transplantation; cisplatin (60 mg/m^2 of body-surface area for 6 hours on day 0), doxorubicin (30 mg/m^2 of body-surface area on day 2), etoposide (100 mg/m^2 of body-surface area on days 2 and 5) as well as cyclophosphamide (1000 mg/m^2 of body-surface area on days 3 and 4) for 5 cycles at 28-day intervals (Matthay et al., 1999).

Apart from chemotherapy, other modes of therapy are also applied to treat neuroblastoma and gross residual diseases. These include radiotherapy (hepatic irradiation at a total dose of 4.5 Gy, administered at 1.5 Gy/day for three consecutive days) and surgical resection (performed after a period of observation or after the first treatment schemes). However, surgical resection is still controversial due to the significant side effects that occur in small patients (Schleiermacher et al., 2003).

Purged bone marrow transplantation is another treatment modality for neuroblastoma with a significant improvement in an event-free survival among patients, compared to those only received intensive chemotherapy. However, a combination therapy of intensive chemotherapy and radiotherapy eventually resulted in a significantly higher event-free survival than transplantation (Matthay et al., 1999).

Side effects of neuroblastoma treatments are primarily haematological (around 71% of cases) with neutropenia (abnormal neutrophil levels in blood) and anaemia (iron deficiency) are often observed after courses of therapy (Schleiermacher et al., 2003; Matthay et al., 1999). Another main side effect noted is sepsis, which accounts for 17% of cases (Matthay et al., 1999). The incidence of interstitial pneumonitis

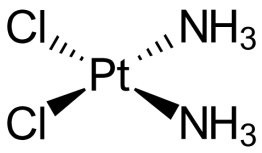


Figure 2.5: Chemical structure of cisplatin Image modified from Shaloam and Tchounwou (2014).

(chronic lung inflammation) and veno-occlusive disease (obstruction of small veins in the liver) are observed more in bone marrow transplantation cases than in chemotherapeutic cases. Side effects due to treatments with 13-cis-retinoic acid include elevations in aminotransferase levels, infection, hypercalcemia and effects in renal, gastrointestinal and skin (lips inflammation, dryness and rash) systems. Haematuria, proteinuria, hypertension and elevation of the serum creatinine level were reported in cases undergone bone marrow transplantation and received 13-cis-retinoic acid (Matthay et al., 1999).

Cisplatin

Cisplatin or cis-diammine-dichloro-platinum is a chemotherapeutic agent commonly used to treat head and neck, testicular, ovarian and lung carcinomas (see Figure 2.5) (Shalinsky et al., 1996). It is activated by a series of spontaneous aquation reactions, which in turn exerts its anti-tumour effect by adding methyl or alkyl group in the guanine N7 and O6 nucleophilic centres in the DNA. Consequently, the drug activates signalling transduction pathways such as p53 and MAPK, which induces apoptosis and kills rapidly dividing cells (Siddik, 2003).

As the drug is not selective towards tumour cells, the treatment often causes adverse effects such as neuro-, renal, oto- and gastrointestinal toxicities. The drug efficacy is limited by cumulative neurotoxicities, myelosuppression (bone marrow suppression), renal and ototoxicities, vomiting as well as resistance from cancer cells (Aebi et al., 1997; Shalinsky et al., 1996).

Retinoic acid

Retinoids, derivatives of vitamin A, are proven to exhibit anti-tumoural activity and cause growth inhibition by inducing differentiation and apoptotic pathways in cancer cells. All-trans-retinoic acid is delivered to the nucleus, activates the retinoic acid receptor (RAR) and binds to retinoic acid response elements that drive transcriptional regulation of the target genes (Pettersson et al., 2001).

In human cells, all-trans-retinoic acid can further metabolise into 13-cis- and 9-cis-retinoic acids (see Figure 2.6). These retinoic acids selectively bind and activate RAR and retinoid X receptor (RXR) to form heterodimers and modulate cellular differentiation and growth (Aebi et al., 1997; Shalinsky et al., 1996).

All-trans-retinoic acid and 13-cis-retinoic acid decrease proliferation and induce differentiation of neuroblastoma cells (Matthay et al., 1999). On the other hand, 9-cis-retinoic acid suppresses differentiation, possibly to induce and increase the cell's susceptibility to undergoing apoptosis by another drug with a different mechanism such as cisplatin. The combination of drug actions may lead to a decreased tumour viability and growth rate (Aebi et al., 1997).

Retinoic acid also affects non-tumoural cells such as HUVECs, in which it inhibits stromal cell-induced angiogenesis. It is hypothesised that retinoic acid downregulates the binding protein for FGF mRNA. Reduced angiogenesis in the tumour microenvironment can cause a bystander effect; which induces apoptosis in the surrounding cells (Liaudet-Coopman et al., 1997).

Hence, all-trans-retinoic acid has both direct and indirect effect in the regulation and determination of cell fate.

2.1.7 Cancer resistance to therapeutics

As discussed in Section 2.2.1, therapeutic outcomes from 3-D *in vitro* models were not as successful as observed in two-dimensional (2-D) monolayer cultures. 3-D models provide critical aspects of a native tumour and it is the recapitulated tumour microenvironment that plays a vital role both in acquiring and maintaining resistance. Mechanisms include: the maintenance of the survival signalling pathways,

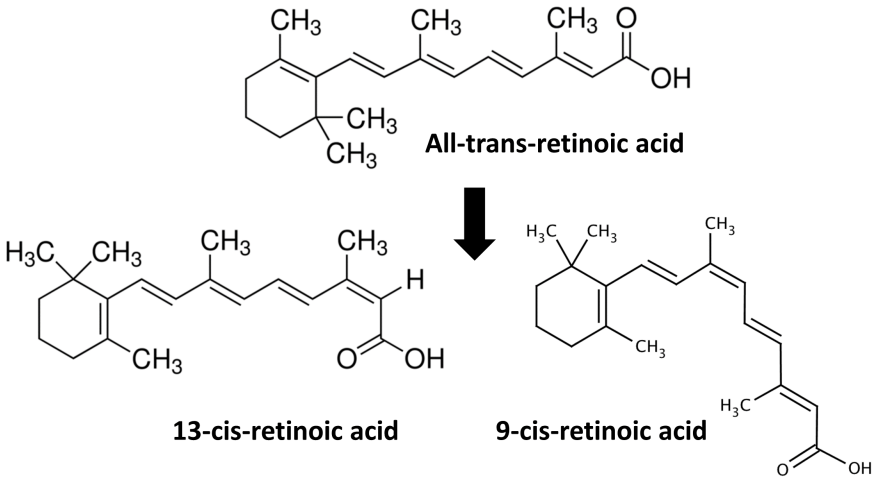


Figure 2.6: Chemical structures of all-trans-retinoic acid, 13-cis-retinoic acid and 9-cis-retinoic acid Human body metabolises all-trans-retinoic acid into 13-cis- and 9-cis-retinoic acids. These isomers all play a role in neuroblastoma treatment. Image modified from Reynolds et al. (2003).

modification of responses to drugs by apoptosis inhibition and alterations of drug targets (Holohan et al., 2013).

Hypoxia

Hypoxia, a niche created by the heterogeneous tumour microenvironment, is the primary concern for cancer therapeutics. Hypoxia can reduce the efficiency of treatments regardless of the modalities. It is hypothesised that oxygen, in radiotherapy, acts at a physiochemical level to fix the cellular damage from radiation. The damage is a result of the high affinity of an oxygen molecule that has for

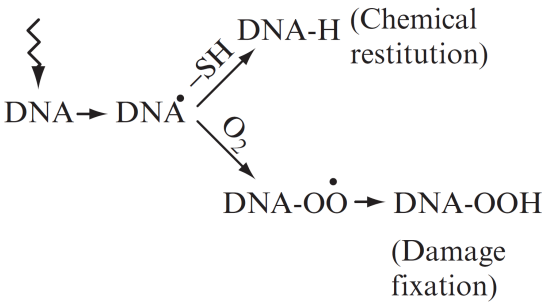


Figure 2.7: The mechanism for the resistance of hypoxic cells to radiation The radical fixes the DNA damage and causes DNA strands to break. Under hypoxic conditions, a sulfhydryl can donate a hydrogen atom to the radical and recover the DNA from damage. Image reproduced from Brown (2007).

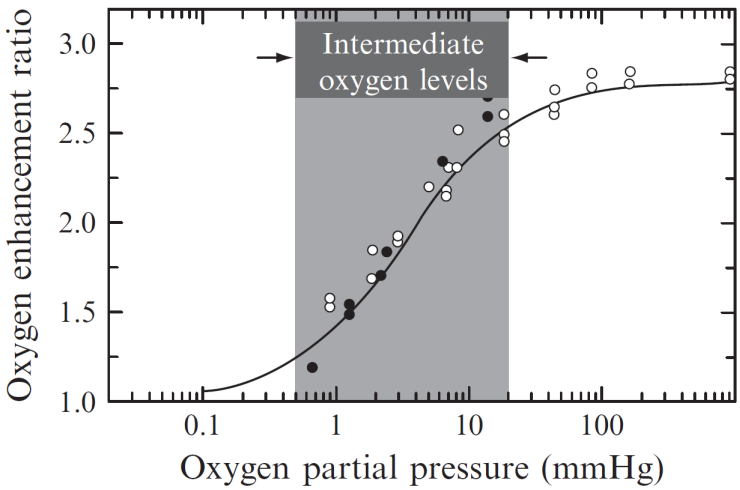


Figure 2.8: The relationship between the oxygen enhancement ratio and oxygen partial pressure Cells start to obtain radiation resistance during intermediate oxygen levels (between $0.2 - 20$ mmHg) and achieve a full radiation resistance from 0.2 mmHg. Image reproduced from Brown (2007).

the unpaired electron on free radicals produced by the radiation (Brown and Wilson, 2004; Brown, 2007).

In radiotherapy, DNA is the target of cell killing by radiation and produces free radicals in the molecules. Figure 2.7 shows this resistance mechanism that oxygen binds covalently to the radical, generating a peroxyl radical. The radical fixes the DNA damage, leading to the breaking of DNA strands and base damage. On the other hand, in the state of hypoxia, cellular non-protein sulfhydryl can donate a hydrogen atom to the radical and restore the DNA to its undamaged form (Brown and Wilson, 2004; Brown, 2007).

The oxygen enhancement ratio expresses the effect of oxygen on cell viability by radiation. This is defined as the ratio of radiation doses under hypoxic to aerobic conditions that give the same level of cell survival: for example, an oxygen enhancement ratio of 2.5 suggests that it may requires 1000 cGy of radiation to kill 50% of cells under hypoxic conditions, while it may only requires 400 cGy of radiation to kill the same proportion of cells if the cells are in aerobic conditions. Figure 2.8 shows that cells start to obtain radiation resistance during intermediate oxygen levels (between $0.2 - 20$ mmHg) and achieve a full radiation resistance below 0.2 mmHg.

Hypoxia is also responsible for the reduction of efficiency of chemotherapy. Firstly, hypoxic cells are not exposed to these anticancer drugs merely because they are distant from blood vessels.

Secondly, chemotherapeutics are more likely to target cells residing at the proximity of blood vessels, which appears to be highly proliferated. However, cellular proliferation decreases as a function of distance from blood vessels due to mass transport limitations, diffusive gradients and microenvironmental stresses. This results in the survival of hypoxic cells inside a tumour (Zhang et al., 2005; Lazzari et al., 2017).

Thirdly, hypoxia selects for cells that evade p53-mediated apoptosis, the main cell death mechanism for many anti-cancer agents.

Fourthly, some anticancer drugs such as bleomycin face the same issue as radiotherapy; they need oxygen to activate the cytotoxicity of the DNA.

Lastly, it can be as simple as hypoxia upregulates genes involved in developing drug resistance (Brown and Wilson, 2004; Brown, 2007).

The mechanisms of drug resistance originate deep down from the molecular level. These can be intrinsic, in which there are resistance-mediating factors pre-exist in tumour cells. Mechanisms can also be acquired; the resistance is developed during treatment by mutations and other adaptive responses. Resistance can also arise from the selection of a resistant minor population of cells that is present in an original tumour.

Other mechanisms

Other mechanisms of drug resistance at the cellular and molecular level can be subdivided into upstream mechanisms such as enhancing drug efflux, reducing drug uptake, inactivating or altering drug targets, repairing DNA damage. Also, drug resistance mechanisms can occur downstream, for example: developing a bypass track, deregulating apoptosis and autophagy (Gottesman, 2002; Holohan et al., 2013; Crystal et al., 2014).

2.2 Three-dimensional *in vitro* cancer model

Two-dimensional monolayer cell culture systems are commonly used as *in vitro* cell based methods for the evaluation of drugs, toxins and other chemicals. The popularity of 2-D monolayer culture is a result of its simplified procedures and relatively low cost, while enhanced the accountability of animal tests (Wu, Huang, et al., 2008; Brafman, 2013).

Nevertheless, there is still a gap in the knowledge between 2-D *in vitro* and *in vivo* models, which prevents the accurate determination of the therapeutic efficiency (Jaganathan et al., 2014). In other words, traditional 2-D monolayer cultures often produce results that are not representative of *in vivo* responses.

2.2.1 Existing *in vitro* cancer models: 2-D vs 3-D

Many aspects of 2-D cultures limit the accuracy of *in vitro* tests. Firstly, the interactions between cells and the ECM, which are essential for cell signalling pathways, are absent. Because of these non-physiological culture conditions, cells are forced to adapt to sheet-like morphology under monolayer culture to maximise the uptake of oxygen and nutrients (Alemany-Ribes and Semino, 2014; Hutmacher et al., 2009).

Secondly, metabolic and genetic changes are induced after weeks of culture. As the passage number increases, only cells undergoing rapid cell division are selected, which limits the utility of cells to model the disease (Rich and Eyler, 2008; Hutmacher et al., 2009; Alemany-Ribes and Semino, 2014).

Lastly, metastatic cells are poorly adhered to the culture surface because they cannot form tight focal adhesions. Therefore, they are not easily cultured in cell culture dishes. With these limitations discussed, 2-D monolayer cultures fail to reproduce tumour-specific characteristics accurately.

Growing cells in scaffolds give rise to 3-D models. The reduced proliferation rate, enhanced tumorigenicity and overexpressed pro-angiogenic growth factors are observed in 3-D cultures, but not in 2-D counterparts (Chen, Xiao, et al., 2012). Furthermore, the properties of the 3-D matrix have an effect on cell motility

Table 2.1: Advantages and disadvantages of 2-D and 3-D cell culture systems

	2-D models	**3-D models**
Advantages	• Simple protocols • Low cost	• 3-D interactions of between cells • Cells-ECM interactions present • Better representation of *in vivo* systems
Disadvantages	• Only 2-D interactions between neighbouring cells • Cells-ECM interactions absent • Cells have sheet-like morphologies to maximise oxygen and nutrients uptake • Induction of metabolic and genetic changes over time	• Relatively difficult protocols • More expensive to establish

in culture (Hutmacher et al., 2009). In several studies, 3-D cultures reproduced tissue organisation as well as expressed genes related to focal adhesion and cancer pathways, which were downregulated in 2-D cultures (Yamada and Cukierman, 2007; Villasante and Vunjak-Novakovic, 2015).

Previous studies reported the enhanced uptake of nanoparticles in 3-D models but not in 2-D. However, the anti-proliferative effects of drugs were significantly lower in 3-D models. It could be explained that ECM was greatly synthesised in 3-D models and acted as a barrier to drug diffusion into tumours (Meng, 2006; Chen, Htay, et al., 2009).

Although 3-D models closely resemble the phenotype and genotype of native tumours, appropriate seeding density, medium composition and ECM properties need to be identified to stimulate appropriate cellular responses within the microenvi-

ronment. 3-D cancer models also require the incorporation of other complex aspects such as: additional cell types, growth factors and different tumour microenvironment niches to provide heterogeneity and create a more functional cancer model (Villasante and Vunjak-Novakovic, 2015; Szot et al., 2011). The advantages and disadvantages of both 2-D and 3-D cell culture systems are summarised in Table 2.1.

2.2.2 Cells in neural cancer models

Cancer cell lines are often selected as a choice for modelling neural cancer. In contrast to primary neurons, cell lines are much cheaper, easier to culture and easier to transfect. Cancer cell lines also provide unlimited proliferation with minimal batch variations while disregard ethical issues raised in primary human neural cultures. The main limitation of using primary neural cultures in a neural cancer model is the incapability of mature neurons to proliferate (Smith et al., 2013).

Conversely, there are also several limitations in using cell lines to construct a neural cancer model. Firstly, cell lines show a variety of physiological differences depending on which cell types they are derived from. Secondly, passaging cell lines over time induces multiple genetic changes influencing its biological behaviours and therefore, cannot reflect the primary tumour physiology (Van der Kuip et al., 2006). Thirdly, many of these cell lines are being manipulated in culture conditions to display neuronal phenotype (Smith et al., 2013). Because they are more likely to assimilate the properties of neurons *in vivo*, the use of primary neural cultures is preferable than cell lines in cancer modelling.

Human pluripotent stem cells-derived neurons

As stem cells are difficult to expand and maintain, only a few such neural stem cells have been cultured and propagated *in vitro* successfully (Brafman, 2013).

Shi et al. (2012) developed a protocol to derive neurons from human pluripotent stem cells (hPSCs). Initially, hPSCs were programmed to differentiate to cortical progenitor cells, which was followed by a series of neural induction to generate cortical projection neurons. These neurons can potentially be raised *in vitro* to

undergo synaptogenesis, fire action potentials and form neural circuits. These phenomena were also observed in long-term co-cultures between rat astrocytes and hPSC-derived neurons, in which hPSC-derived neurons required much longer time to mature functionally compared to those derived from rats (Odawara, Saitoh, et al., 2014). Another study showed that the plasticity of hPSC-derived neurons could potentially be analysed to understand human neuronal circuits and brain functions (Odawara, Katoh, et al., 2015).

Human umbilical vein endothelial cells (HUVECs)

It is uncommon to consider mature endothelial cells for therapeutic applications due to its limited vasculature potential. Endothelial progenitor cells, e.g. HUVECs are receiving more attention due to its relatively higher proliferative potential compared to endothelial cells isolated from veins or arteries (Levenberg, 2005). The use of HUVECs in a neural cancer model is minimal, especially as a 3-D *in vitro* model. However, HUVECs were reported in many other co-culture cancer models as they introduced angiogenesis; one of the critical hallmarks of cancer, into the model.

In one study, human embryonic stem cells derived endothelial cells (hESC-derived endothelial cells) in a 3-D *in vivo* model promoted the formation of a vascular network, which interacted closely with the surrounding tissues (Levenberg, 2005). Another study reported the formation of the similar vascular network in 3-D collagen co-culture model with HT29 colorectal cancer cells. However, the presence of cancer cells caused the endothelial cells to aggregate and form a cobblestone pattern. The branching of tubule-like structures was significantly longer but not as sophisticated as when they were cultured along with stromal cells (Magdeldin et al., 2017). These examples illustrate the existence of a vascular niche through vascular network formation within the 3-D model, despite the unknown of its structural function compared to HUVECs encapsulated in a cancer model as single cells.

SH-SY5Y cells

SH-SY5Y is a neuroblastoma cell line that is cultured and used extensively in neural research. It is derived by subcloning from the parental metastatic bone tumour

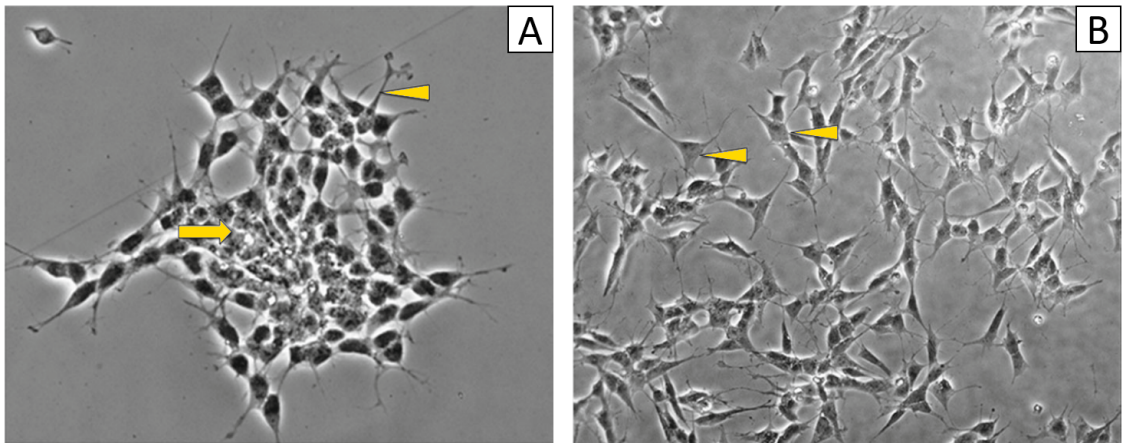


Figure 2.9: Morphologies of SH-SY5Y cells before and after differentiation (A) Undifferentiated SH-SY5Y cells are characterised by clustered cell growth, clumps of round cells (yellow arrow) and short neurite projections (yellow arrowhead); (B) Differentiated SH-SY5Y cells are more pyramidal in shape (yellow arrowhead), less clustered and display extensive neurite projections. Image modified from (Smith et al., 2013).

cell line, SK-N-SH by June Biedler in the 1970s. SH-SY5Y cells share common characteristics with dopaminergic neurons and hence, they are used extensively as a cell model for studies regarding neuronal behaviour and responses to neurotoxins (Xie, Hu, et al., 2010).

There are three main characteristics of SH-SY5Y cells. Firstly, the cultures contain both viable adherent and floating cells. Nevertheless, some studies discarded the floating cells during media changes and excluded those cells for the experiments (Smith et al., 2013). Secondly, the parental differentiated SK-N-SH cells contain both neuroblast-like and epithelial-like morphologies. These two phenotypes may correspond to either N or S types. Thirdly, SH-SY5Y cells can differentiate to form a more neuron-like structure, which is characterised by neuronal markers. Consequently, it is evident that SH-SY5Y cells have distinct characteristics depending on their differentiation status (Smith et al., 2013).

Undifferentiated SH-SY5Y cells are characterised by their continuous proliferation capacity, expression of immature neuronal markers and the lack of mature neuronal markers. The cell morphologies were characterised by the presence of clustered cell growth, clumps of round cells and short neurite projections (see Figure 2.9A). A neuroblast-like morphology determines undifferentiated cells with

polarised cell bodies. Several types of markers are expressed by undifferentiated SH-SY5Y cells, including proliferative markers such as proliferative cell nuclear antigen, immature neuronal markers such as Nestin and differentiation inhibiting basic helix-loop-helix transcription factors ID1, ID2 and ID3 (Smith et al., 2013).

Differentiated neurons are more pyramidal in shape, less clustered and display extensive neurite projections (see Figure 2.9B). Differentiated cells can be characterised by a series of specific events including the formation and extension of neurite processes, the increase in electrical excitability of the plasma membrane, the formation of synaptophysin-positive functional synapses, and the inductions of neuron-specific enzymes, neurotransmitters and neurotransmitter receptors. Differentiated neurons are morphologically similar to their primary counterparts, as such, they have expressed a number of mature neuronal markers including TuJ1 (Class III β-tubulin), synaptophysin, microtubule-associated protein-2 (MAP2), neuron-specific enolase (NSE), synaptic associated protein-97 (SAP97) and neuronal specific nuclear protein (NeuN) (Smith et al., 2013).

Depending on the differentiation induction methods such as retinoic acid (RA), phorbol esters and dibutyryl cyclic adenomonophosphate (cAMP), mature neurons can become polarised or display randomly distributed processes. These may induce a decrease in the rate of proliferation and an increase in the activity of NSE.

2.2.3 Matrices for neural cancer models

The ECM composes of a complex mixture of proteins, proteoglycans and polysaccharides undergoing a series of assembly, remodelling and degradation (Brafman, 2013). The ECM governs the tumour progression through biochemical and mechanical cues, integrating into intracellular signalling pathways (Alemany-Ribes and Semino, 2014). These cues allow the attachment between cells and basement membrane, the access to oxygen and nutrients, as well as the removal of waste products. As a consequence, gene expressions, cell fate decisions and cell phenotypes are determined and regulated (Hutmacher et al., 2009; Brafman, 2013; Jaganathan et al., 2014).

Currently, hydrogels extracted from animals are commonly used as a choice for cancer model to mimic features of the tumours (Nyga et al., 2011). Modifications made to the ECM mimicking scaffold change the fibre architecture, the cohesiveness and the pore size of the scaffold (Nyga et al., 2011; Wang, Forsythe, et al., 2012). Consequently, these affect the cell morphology, proliferation and migration (Wang, Forsythe, et al., 2012; Alemany-Ribes and Semino, 2014).

Matrigel®

Matrigel® is a commercialised hydrogel derived from the basement membrane of mouse sarcoma cells (Engelbreth-Holm-Swarm) (Arnaoutova and Kleinman, 2010). It composes of various ECM components including laminin, entactin, collagen IV, nidogen and heparan sulfate proteoglycans. Growth factors such as transforming growth factor-β (TGF-β), basic fibroblast growth factor (bFGF), insulin-like growth factor-1 (IGF-1) and tissue plasminogen activator (tPA) are also incorporated in Matrigel® (Nyga et al., 2011; Thonhoff et al., 2008).

Because of its high levels of laminin and growth factors, Matrigel® is commonly used in creating an angiogenesis model with vascular endothelial cells, such as HUVECs and promote these cells to form tubule-like structures. Matrigel® is also used in neuronal culture, in which the stimulation of neurite outgrowth, the differentiation and migration of NSCs are observed when seeded on top of the gel (Katakowski et al., 2005; Flanagan et al., 2006). However, when human NSCs cultured on Matrigel®, they primarily differentiate into astrocytes. One or more components of Matrigel® may induce cytotoxicity on human NSC-derived neurons and prevent neuronal differentiation (Thonhoff et al., 2008).

Furthermore, Matrigel® contains undefined substances, endogenous growth factors and signals, which do not represent the structure and composition of human tumour microenvironment (Jaganathan et al., 2014). It also suffers batch-to-batch variability and consequently, brings up a concern regarding the misinterpretation of a cancer model constructed from the matrix (Xu, Farach-Carson, et al., 2014).

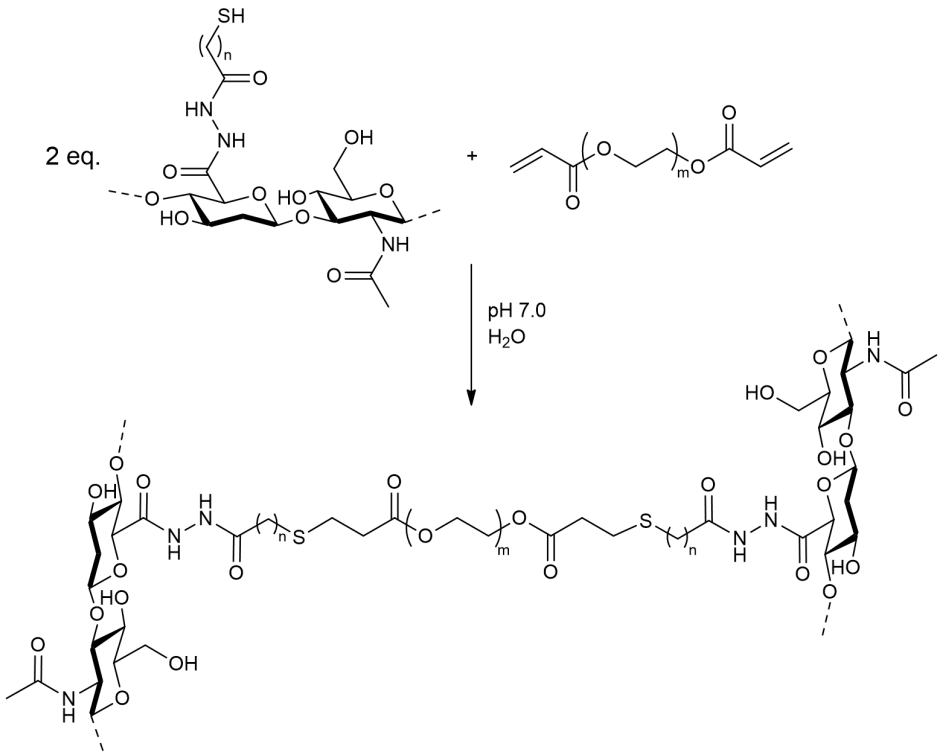


Figure 2.10: The formation of HyStem® hydrogel by Michael-type addition reaction The reaction involves the addition of a thiol group acts as a nucleophile to an $\alpha,\beta-$unsaturated carbonyl PEG-DA at the $\beta-$carbon. Image courtesy of Pattarakiat Seankongsuk.

HyStem®

HyStem® is a commercialised hyaluronan hydrogel. It is optimal for culturing brain stem cells, where their surrounding ECM is rich in hyaluronic acid (Nyga et al., 2011; Xu, Farach-Carson, et al., 2014). Hyaluronic acid is the simplest glycosaminoglycan that provides the ECM hydration, lubrication and compression strength. Unlike animal-derived ECM products, HyStem® mainly comprises two chemically and immunogenically defined components: thiol-modified hyaluronan (HyStem® macromer, Glycosil®) and polyethene glycol diacrylate crosslinker (PEG-DA, Extralink 1®) (Mehra et al., 2016). Gelation of HyStem® hydrogel is done by reacting a thiol-modified hyaluronic acid with a multifunctional electrophile such as PEG-DA in a Michael-type addition reaction as shown in Figure 2.10 (Xu, Jha, et al., 2012). In this reaction, a thiol group acts as a nucleophile to an $\alpha,\beta-$unsaturated carbonyl PEG-DA at the $\beta-$carbon.

Although the hydrogel does not support cell attachment, the ECM proteins of the seeded cells can provide differentiation and attachment signals instead (Shu et al., 2004). The hydrogel was reported to facilitate metastasis (Toole and Hascall, 2002), induce inflammatory cytokine production and trigger angiogenesis (Franzmann et al., 2003). The fate of seeded cells is dependent upon the hydrogel rigidity, which can be varied to match the stiffness of native tumours (Ghosh et al., 2007).

Collagen

Collagen is a native ECM produced in cells in the stromal environment with type I collagen as the critical ECM protein in most tissues (Xu, Farach-Carson, et al., 2014; Abou Neel et al., 2006). Several studies selected collagen as their choice of the matrix for their cancer model. Miller et al. (1985) discovered a greater anti-cancer drug resistance in cancer spheroids constructed from collagen gels compared to tissue culture on plastic flasks. Another study by Chen, Xiao, et al. (2012) reported the successful expansion and propagation of MCF-7 cells in collagen. The microenvironment induced the cells resistance to anti-growth signals, evasion of apoptosis and extension of proliferation time from 5 days in a 2-D culture to 13 days in a 3-D culture. The same study also showed that collagen gels drastically upregulated pro-angiogenic factors, EMT markers, cancer stem cell phenotypes and HIFs *in vitro*. These were consistent with *in vivo* conditions that the growth factors and the MMPs were upregulated in malignant tumours, thus promoted vascularisation (Chen, Xiao, et al., 2012).

Nevertheless, the main limitation of collagen is the lack of other essential proteins (Nyga et al., 2011). Since it is produced more widely than different commercialised matrices such as Matrigel®, collagen is affected by factors including sources of tissue, immunogenicity, assembly conditions and crosslinking density (Xu, Farach-Carson, et al., 2014; Willerth and Sakiyama-Elbert, 2007). Apart from its batch-to-batch variations, the intrinsic features of their precursors cause modifications of the matrix to be difficult (Hutmacher et al., 2009).

2.2.4 Types of 3-D *in vitro* cancer models

Three different approaches were investigated in the development of 3-D *in vitro* models. Each approach has their own advantages and disadvantages.

Spheroids

The development of different 3-D cancer models has increased over the past decade, in hopes to accurately model solid tumours. One of these advances is the tumour spheroid model, which represents the intermediate complexity between *in vivo* solid tumours and 2-D monolayer cultures (Zhang et al., 2005). Spheroids are defined as aggregates of cells formed by either self-assembly or forced interactions between cells (Zhuang et al., 2018).

Many studies reported that 3-D *in vitro* tumour spheroid models were more resistant to anti-cancer drugs than 2-D monolayer models (Knuchel et al., 1989; Oloumi et al., 2000). The resistance may be due to the recapitulation of different microenvironmental niches in 3-D spheroids with layers of proliferating, quiescent and necrotic cancer cells locating at the outer, middle and inner parts of the model respectively (see Figure 2.11). Other aspects of tumour recapitulation included specific gene expressions, deposition of native ECM components and 3-D

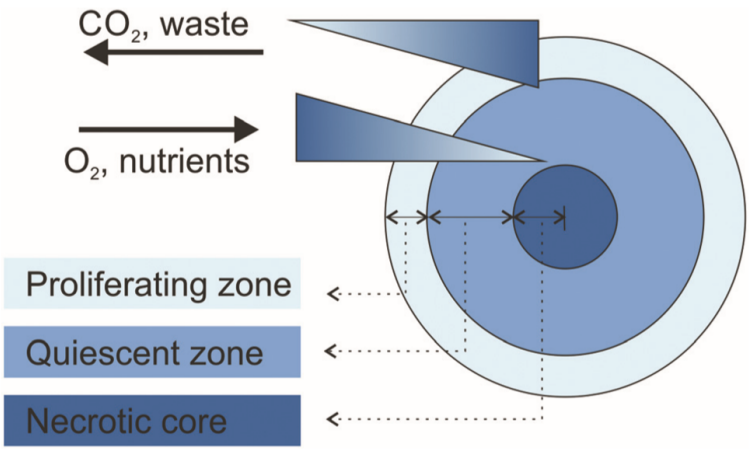


Figure 2.11: Cell organisation and gradients in tumour spheroids The microenvironment of tumour spheroids are subdivided into layers of proliferating, quiescent and necrotic cells. These layers establish gradients of oxygen, carbon dioxide, nutrients and waste. Image modified from Lazzari et al. (2017).

communication among cells and between cells and ECM (Lazzari et al., 2017). Examples of spheroid models reported are colorectal (Wan, Li, et al., 2016) and breast cancers (Imamura et al., 2015)

A study by Kumar et al. (2008) reported the differences in the protein expressions observed between 3-D neuroblastoma spheroids and their 2-D monolayer counterparts. These included the increased expressions in 3-D spheroids of glycolytic proteins (transketolase, triosephosphate isomerase, pyruvate kinase M1/M2, alpha-enolase and phosphoglycerate mutase-1), heat shock proteins, cytoskeletal proteins (adenylyl cyclase-associated protein-1, tubulin B-2, actin, translationally controlled tumour protein and cofilin), anti-apoptotic and neural cell growth promoting proteins (phosphoserine aminotransferase, thioredoxin, retinoic acid binding protein and peptidyl-prolyl cis/trans isomerase A). These proteins contributed to different hallmarks of cancer such as glycolytic phenotype and the Warburg effect, sustained angiogenesis, inhibited apoptosis, reorganised cytoskeleton and modulated tumour microenvironment.

However, the manipulation of tumour spheroid cultures is limited by the lack of a barrier between tumour cells and medium. This barrier is represented by endothelial cells and stromal cells in native tumours. Also, the size of cell spheroids is difficult to control (Zhang et al., 2005).

Organoids

Organoids are defined as a 3-D *in vitro* miniaturised version of an organ, comprising a few number of cells cultured on top of the Matrigel® ECM. Organoids capture greater fundamental features of native tumours than spheroids due to its larger size and the incorporation of a bed of Matrigel® that allows stem cells to organise themselves and spatially differentiate. This phenomenon is absent in spheroid models. The layer of hydrogel generally produces a more stable culture that preserves the integrity and characteristics of cells for a longer time (Zhuang et al., 2018). Many cancer organoids were reported including ductal pancreatic cancer (Huang et al., 2016), colorectal cancer and neuroblastoma (Wan, Ball, et al., 2017).

Nevertheless, organoids are limited by mass transport limitations due to their size. The formation of necrotic regions can be advantageous in recapitulating the microenvironment but should be supplemented by angiogenesis to mimic the recruitment of blood vessels to support cell growth. Furthermore, the use of Matrigel® with an unknown composition and a high batch-to-batch variability in the model makes it difficult to validate the results consistently (Fong et al., 2016; Zhuang et al., 2018).

Scaffold-based models

A tissue-engineered strategy of microencapsulation is introduced to overcome these issues raised in the spheroid and organoid cultures. The size of microcapsules can be controlled and created with a wide range of diameters ranging from $200 - 1500$ μm. Apart from being a biocompatible material, they also have a semi-permeable membrane that allows the transport of nutrients, oxygen, drugs and wastes while prevents the penetration of other substances with higher molecular weights.

Another advantage of microencapsulation is the variety of biomaterials available to choose from. These materials are readily reproducible and generally, have a spatial control over the ECM organisation with tunable mechanical and degradation properties (Zhuang et al., 2018).

Compared to 2-D monolayer and spheroid models, 3-D primary oral cancer model encapsulated in collagen-alginate displayed a significantly higher metabolic activity and a significantly higher rate of cell proliferation. The sensitivity of cancer cells to cisplatin in a high cell density 3-D collagen-alginate model showed no statistical difference when compared to the sensitivity of primary cells under the same treatment. This indicates the similarity of drug responses for cells within 3-D scaffold based model and for those within native tumours (Hsieh et al., 2015).

However, the permeability and transport mechanisms through the membrane of microcapsules, e.g. alginate-poly-L-lysine cannot be entirely assimilated to the layer of endothelial cells (Zhang et al., 2005). These models also neglect other

Table 2.2: Advantages and disadvantages of different 3-D culture models

	Advantages	**Disadvantages**
Spheroids	• Niches are divided into different layers • Easy and cheap to develop	• Lack barrier between cells and medium • Lack ECM components • Difficult to control size
Organoids	• More accurate recapitulation of tumours than spheroids • Matrigel® as an ECM • More stable culture than spheroids	• Mass transport limitations • Hard to validate results in Matrigel® models
Scaffold-based models	• Tunable model size • Wide range of biomaterials with tunable properties • Readily reproducible • Semi-permeable membrane	• Membrane may not accurately mimic the layer of endothelial cells • Lack other essential aspects of tumorigenesis

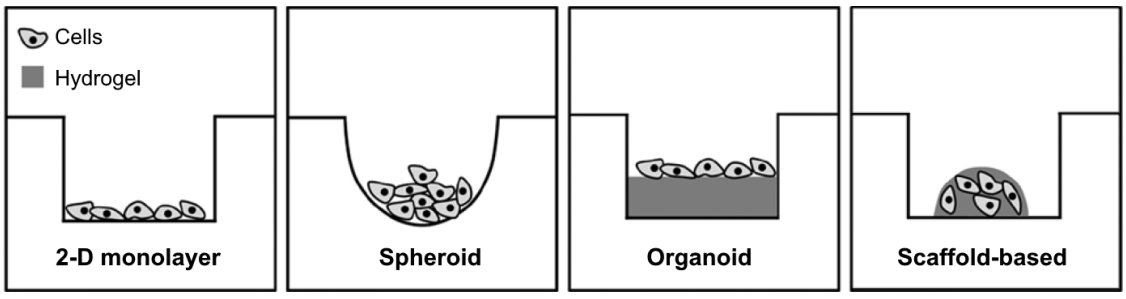


Figure 2.12: Schematic representation of different 2-D and 3-D tissue models The complexity of the model increases as the 3-D interactions among cells, integration of hydrogel as the ECM and tunability of the hydrogel properties increases. Image modified from Zeeberg et al. (2016).

essential aspects of tumorigenesis including angiogenesis, immune systems and fluid dynamics (Lazzari et al., 2017).

Comparison of different types of 3-D tissue models

The summary of the advantages and disadvantages for each 3-D models are shown in Table 2.2, with the schematic representation shown in Figure 2.12. Despite a variety of 3-D *in vitro* models developed, it is inaccurate to represent the tumour microenvironment unless there is an incorporation of elements accounting for cell-stromal interactions and blood perfusions (Imamura et al., 2015).

2.3 Three-dimensional *in vitro* co-culture model

Co-culture systems have been adopted to investigate the interactions between different types of cells in culture. There is an increasing interest in the use of co-cultures in 3-D *in vitro* models as they may have potential to represent human *in vivo*-like models than the current animal models (Goers et al., 2014). Examples of some 3-D *in vitro* co-culture systems are shown in Table 2.3.

2.3.1 Applications of 3-D *in vitro* co-culture models

Co-culture models are investigated for various purposes. One application is the further understanding of normal physiological biology by looking at the interactions between different cell types. Examples included: the co-culture of endometrial epithelial and stromal biopsies to investigate implantation and establishment of uterine receptivity (Arnold et al., 2001); or the co-culture model of mesenchymal stem cells (MSCs) and haematopoietic stem and progenitor cells (HPCs) that resulted in the recapitulation of two different niches co-exhibiting in the same model Leisten et al. (2012). The formation of niches observed is beneficial to future studies investigating the underlying mechanisms of stem cell interactions.

Another application for 3-D co-culture models is the modelling of diseases. As this thesis primarily focuses on cancer, the following examples given are different types of cancers recapitulated using 3-D *in vitro* systems. A study by Fang

Table 2.3: Examples of 3-D *in vitro* co-culture systems

Type	Main cell	Supporting cell	ECM	Main cell culture medium	Co-culture medium	Reference
Normal	Endometrial epithelial cells	Stromal cells	Matrigel®	High glucose DMEM-H	Phenol red M1999 and F12	[1]
Normal	NG108-15	Schwann cells	PCL microfibres	DMEM	DMEM and F12	[2]
Normal	MSCs	HPCs	Collagen	Mesenpan MSC medium	Mesenpan MSC medium	[3]
Disease	C4-2	WPMY-1	Alginate	High glucose DMEM	DMEM	[4]
Disease	SH-SY5Ys	MSCs	Poly-L-lysine, Matrigel®, Matrigel®, fibronectin, gelatin and collagen	DMEM	DMEM	[5]
Disease	U87, T98 and NT2	HUVECs	Cytodex® beads and fibrin gel	DMEM	EGM-2	[6]
Drug screening	MCF-7	HepG2	Alginate	DMEM	DMEM	[7]
Drug screening	UW288-3	NSCs	N/A	DMEM	DMEM + B27 + N2	[8]
Drug screening	DLBCLs	MLMVECs	Gelatin/HyStem-C	MLMVEC medium	MLMVEC medium	[9]

[1] Arnold et al. (2001), [2] Daud et al. (2012), [3] Leisten et al. (2012), [4] Fang et al. (2013), [5] Rizvanov et al. (2010)
[6] Chen, Htay, et al. (2009), [7] Xu, Farach-Carson, et al. (2014), [8] Ivanov et al. (2015), [9] Mannino et al. (2017)

et al. (2013) reported the interactions between C4-2 prostate cancer cells and WPMY-1 normal prostate stromal cells to be primarily responsible for both normal development and neoplastic formation. Another study by Chen, Htay, et al. (2009) recapitulated sustained angiogenesis, one of the hallmarks of cancer. The established cancer model did not just reinforce the relationship between key players such as: endothelial cells, VEGF and hypoxia in tumours, it also provided an opportunity to quantitatively analyse angiogenesis through cancer modelling and image analyses.

The 3-D *in vitro* co-culture systems can potentially be used in translational applications such as drug screening platforms and regenerative medicine. The co-culture model of UW288-3 medulloblastoma cells and NSCs was developed to determine screen neurodevelopmental toxicity from drugs treated (Ivanov et al., 2015). Another study by Hofmann et al. (2008) developed an osteoblast-HUVEC co-culture model, in which they discovered angiogenesis was the key phenomenon for early wound and fracture healing.

2.3.2 Supporting cells in co-culture models

In most co-culture models, there are main cell of interest and supporting cells that help to recapitulate the physiological conditions *in vivo* much accurately. Surprisingly, endothelial cells are one of the most common supporting cells in co-culture models. Endothelial cells were used in cancer models to mimic angiogenesis (Chen, Htay, et al., 2009), in modelling haematopoietic niche (Leisten et al., 2012), in a wound healing model (Hofmann et al., 2008) and in a perfused drug screening platform (Mannino et al., 2017).

Also, normal stromal cells were frequently used in co-culture models. Stromal cells play a paracrine role in directing functions of neighbouring cells such as epithelial cells (Arnold et al., 2001) and neurons (Daud et al., 2012).

Other types of cells such as hepatocytes were utilised in drug screening platforms to model drug efficacy in response to liver metabolism. This should give a more accurate prediction of drug dosage and any effects on both cancer and liver cells (Xu, Farach-Carson, et al., 2014).

It is important to mention that in several studies the medium used in co-culture experiments was different to when each cell line was cultured individually. Data shown in Table 2.3 implies that an optimisation experiment may be required before initiating any co-culture experiments. This would ensure that both cells cultured can thrive in the selected medium.

2.3.3 Matrices and co-culture conditions

Three-dimensional scaffolds, both natural and synthetic, serve as an ECM in 3-D *in vitro* models. A vast number of matrices were selected to develop 3-D co-culture models in different spatial arrangements. The simplest configuration is the on top culture or the co-culture of cells on pre-coated surfaces. One of the most common examples is Matrigel®, although sandwich cultures are also investigated recently to improve the 3-D interactions between cells and the hydrogel (Rizvanov et al., 2010; Wan, Bovornchutichai, et al., 2017).

Another common example is the cell encapsulation model. In many cases, cells were either encapsulated inside a microbead (Fang et al., 2013) or coated on its surface (Chen, Htay, et al., 2009). Other instances include the encapsulation of cells inside a hydrogel such as collagen (Leisten et al., 2012) and HyStem® (Mannino et al., 2017).

To mimic the human physiological systems, several studies have taken the advantage of 3-D scaffold structures and modified them to assimilate native tissues *in vivo*. Mannino et al. (2017) designed a cylindrical, endothelialised microchannel within the polydimethylsiloxane (PDMS) and gelatin/HyStem® constructs. The culture medium was perfused through that microchannel to mimic the flow of blood through the vessels into tumours. Another study designed a double alginate microsphere layer with poly-L-ornithine in between to separate normal and cancer cells. This model is helpful in furthering our understanding of the invasive niche and metastasis (Fang et al., 2013).

2.3.4 Effects of co-culture

As expected, the co-culture of main cells with supporting cells frequently gave rise to different results compared to those in monocultures. It is reported that the addition of schwann cells into the NG108-15 culture on top of polycaprolactone (PCL) microfibres resulted in an extended neurite outgrowth (Daud et al., 2012). This could be explained by the interplay between these different cell types that modulated the microenvironment to support each other. The co-culture of MSCs and HPCs within collagen secreted components such as fibronectin to support collagen I synthesis (Leisten et al., 2012). Meanwhile, a long-term co-culture of osteoblasts showed that the cells support the survival and neovasculature of co-cultured HUVECs (Hofmann et al., 2008).

Three-dimensional *in vitro* cultures explore different cell types, matrices and co-culture conditions to represent *in vivo* conditions; both normal and pathological. The relationships between different cells in the 3-D microenvironment elicit paracrine and endocrine responses. However, it is important to consider that the accuracy in recapitulating the model is counteracted by the complications in model characterisation and scaling up.

2.4 Perfusion bioreactor culture: the recapitulation of cancer microenvironment

Although the 3-D cancer model recapitulates different cellular components and architecture; other physiological parameters are also essential in influencing the integrity of the model and hence, the drug responses. Perfusion bioreactors are sterile, engineered cell culture constructs that provides a continuous supply of nutrients and waste removal (Wu, Huang, et al., 2008). They can also provide and monitor different culture factors such as pH, temperature and dissolved oxygen through cell culture chambers and incubators with pre-determined environmental settings. The perfusion of cell culture medium is commonly driven by a pump that simulates the circulatory system; allowing the transport of oxygen, nutrients and metabolites in

and out of cells (Lim et al., 2009). Furthermore, perfusion bioreactors recapitulate mechanical cues due to shear stress from blood circulation or interstitial flow *in vitro*, which are essential for stem cell and tissue development (Wan, Ball, et al., 2017).

Currently, there are numerous designs of perfusion bioreactors reported with various applications; for instance, a study by Xie, Hardouin, et al. (2006) designed the 3-stop tubes driving the peristaltic pump to expand MSCs. Another study by Hsieh et al. (2015) integrated pneumonic micropumps and microvalves into the bioreactor to assess its potential as a drug screening platform. In addition, the design of TissueFlex by Cui et al., 2007 facilitated a series of samples to be tested simultaneously under either peristaltic pumping or syringe pumping systems.

Even though the perfusion bioreactors provide a more accurate microenvironment resembling physiological tissues than static culture systems, there are several limitations that may arise when perfusion bioreactors are used in cell culture. These limitations are discussed below in the next section.

2.4.1 Limitations of existing bioreactor systems

The major drawbacks of many existing cell culture and bioreactor systems are the mass transport limitations and replenishment of medium. In addition, the balance between the scale of the culture vessel versus the complexity of the *in vitro* model needs to be optimised.

Mass transport

The availability of nutrients via intracellular mass transport must exceed metabolic thresholds required by the cultured tissues. Passive diffusion-driven mass transport is insufficient to support viable 3-D cell cultures beyond 200 μm gel thickness and 10^4 cells/mL seeding density (Cullen et al., 2007). The current limitation of spheroid or neurosphere models in a long-term culture is that passive diffusion cannot maintain the functions of cell organelles, especially in the centre where cells are undergoing necrosis (Wan, Li, et al., 2016). However, the deprivation of oxygen and nutrients arising within the core of a 3-D *in vitro* cancer model can be exploited

to mimic hypoxic and necrotic regions. In native tumours, cells residing at different depths from the surface give rise to variations in nutritional status and tumour microenvironment niches (Yamada and Cukierman, 2007).

Medium replacement

The conventional medium replacement process is intermittent and it is difficult to determine the cell culture conditions based on fluctuations of this microenvironment. This limitation increases the uncertainties in quantifying drug responses (Cui et al., 2007; Li and Cui, 2014).

Also, in between medium changes, the by-products of metabolism are released into the spent medium while the nutrients inside the same medium become depleted. The accumulation of metabolic wastes would eventually cause oxidative stress and rapid loss in cell viability (Cui et al., 2007; Li and Cui, 2014).

Complexity and scalability

Many of the current cancer models fail to mimic essential aspects of a tumour. These include the lack of specific end-point analyses and continuous monitoring of the system. In addition, most of these experiments can only be cultured for a short period. These limitations addressed indicate that not only the models can not reflect the complexity of native tumours, they also fail to represent any long-term drug effects on disease progression (Hirt et al., 2015).

However, the complexity of models is counteracted by the scalability of the system. Introducing different cell types and stroma in the model may represent tumour heterogeneity, but reproducing the entire model can be difficult, and costly if generated on a larger scale for commercialisation (Estrada et al., 2016).

Bioreactors are utilised to scale-up the culture system. They permit the expansion of cells such as mesenchymal stem cells (MSCs) without any loss of differentiation potential and produce a more uniform cellular distribution throughout the scaffold (King and Miller, 2007).

2.4.2 Considerations for bioreactor design

Perfusion bioreactors introduce the continuous flow of medium through the culture vessel, to minimise any diffusional limitation and uncertainties in the culture environment. The constant pumping of the culture medium through cells represents the miniaturised human circulatory system as well as provides the opportunities to introduce physiologically relevant biophysical and biomechanical forces into cultured cells (Xu, Farach-Carson, et al., 2014; Li and Cui, 2014). With different forces and factors mentioned, it implies that there are much more factors to consider when designing a perfusion bioreactor.

Hydrodynamic factors

Bioreactors have the potential to overcome mass transfer limitations associated with static cultures. Cell culture systems utilising bioreactors consider physiologically relevant biochemical and biophysical stimulations such as flow rate and shear stress.

Several studies reported the correlation between the performance of a bioreactor and its perfusion rate. Cullen et al. (2007) developed a microfluidic engineered 3-D neural culture platform that utilised forced convection to deliver nutrients and withdraw waste continuously. While maintaining the high nutrient concentration at a constant level, the cell viability and the distance from perfusion source, with an optimal perfusion rate of 11 μL/min (15.84 mL/day) (Cullen et al., 2007). Another study by Wu, Huang, et al. (2008) introduced pneumatic micropumps in their bioreactor. The pumps provided a uniform flow varying from 3.6 μL/hour to 439 μL/hour, depending on the pulsation frequency of the pumps to culture an oral cancer cell line (Wu, Huang, et al., 2008). These studies suggest that there is a range of optimal perfusion rate that should be achieved to match with the interstitial fluid flow in the body.

Morphologies and metastatic potentials of cancer cells are affected by the convective transport of the fluid as the cell migration patterns are observed along the streamlines (Thoma et al., 2014). Convective transport of oxygen and nutrients within the bioreactor is typically a result of the turbulent flow, which carries out

momentum, mass and heat transfer in the system. The formation of unstable eddies usually accompanies the flow, in which the smallest eddy size is defined as the Kolmogorov eddy size. Damages to cells and aggregates in the reactor can occur when the magnitude of the Kolmogorov eddy diameter is the same as the cells' and the aggregates' (Papoutsakis, 1991). Damages to cells and aggregates mostly occur at low agitation rates; when their sizes match the size of the eddies. Eddies decrease their sizes as the agitation rate increases.

Apart from the agitation rate, the hydrodynamic shear stress in the reactor also needs to be optimised; cells tend to clump together under low shear stress while they tend to rupture when the shear stress is too high. Shear stress increases as the impeller diameter or the vessel rotational speed increases. Shear stress also depends on the geometry, the location of the impeller and the location of probes installed inside the reactor as they all can disrupt the flow pattern (Thoma et al., 2014).

To achieve an adequate supply of nutrients and oxygen in large volumes of the bioreactors, especially in ones with high cell densities, gas bubbles are usually sparged into the reactor. However, sparging gas into the medium produces foam that reduces the capacity of the reactor. Furthermore, cells are more likely to attach themselves to the gas bubbles, which generate a high shear stress when these bubbles rupture (Hirt et al., 2015).

Culture vessel design

Vessel geometry and impeller design also affect oxygen mass transfer and shear stress in bioreactor systems. Vessel designs such as stirred suspension cultures facilitate high quantities of spheroid growth. However, this design produces variable sizes of spheroids and introduces the hydrodynamic shear force due to stirring, which induce cellular stress and limit the size of spheroids (Thoma et al., 2014). Rotating-wall culture system allows cells to culture in a suspended, dynamic flow environment. Unfortunately, the spheroids produced are mostly heterogeneous due to the mass transfer limitation of gas and nutrients throughout the vessel (Li and Cui, 2014).

Recent studies introduced forced convection cultures to eliminate the use of impeller in the system. In this bioreactor system, a fresh medium was fed into the culture vessel through syringes or external pumps. The pump continuously withdrew the waste medium to maintain high concentration of nutrients in the culture vessel. The convection currents allowed mixing through mass transport as well as momentum exchange between fresh and depleted media in the vessel (Cullen et al., 2007; Wan, Li, et al., 2016).

Oxygen and nutrient supply

As discussed in the earlier sections, perfusion culture overcomes diffusional limitation and provides better control of the microenvironment. Nutrients and oxygen supplies to the culture must be balanced by the hydrodynamic shear stress to avoid damages to cells. Oxygen diffuses from air into the medium before consumed by the cells. The level of dissolved oxygen in the medium relates to the oxygen uptake rate of cells, which determines the cell viabilities.

Although the oxygen supply to 3-D cancer models decreases with distance from the bulk-liquid interface, the low oxygen levels can be beneficial to mimic different niches within a heterogeneous microenvironment. Several studies reported a decrease in the rate of stem cell differentiation in contrast to an increase in the cells' proliferative potential under 5% dissolved oxygen level, compared with 20% level (Ezashi et al., 2005; Gibbons et al., 2006). Stem cells receive greater protection from chromosomal damage when cultured under lower oxygen levels. However, they are sensitive to oxidative damage when the oxygen level increases back up (Forsyth et al., 2006).

2.4.3 Scaling down: microbioreactor systems

Most conventional bioreactor systems are costly, require a large number of cells and challenging to set up large-scale parallel experiments (Wu, Urban, et al., 2006; Li and Cui, 2014). In addition, chemical gradients develop as the size of a bioreactor increases and hence makes it difficult to control the cell's microenvironment (Wu,

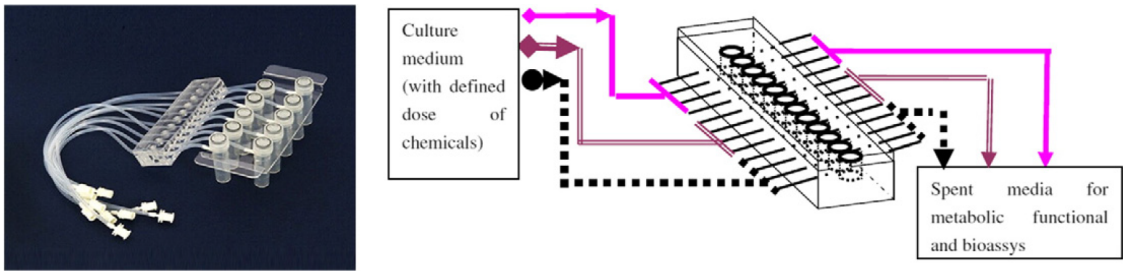


Figure 2.13: Set up of the TissueFlex® microbioreactor The bioreactor is fabricated from PDMS to form multiple microwells that can be tested in parallel. Peristaltic pump allows each well to be supplied continuously by the culture medium and the effluent to be collected. Image taken from Kaul et al. (2016).

Urban, et al., 2006). The size of the reactor, therefore, needs to be scaled down to comply with applications in high throughput screening (Cui et al., 2007). TissueFlex® is a multichannel perfusion culture system utilised in parallel long-term 3-D cultures and throughput drug screening tests. TissueFlex® consistently supplies a forced proactive flow of fresh medium, which dominates passive diffusion that only presents in static cultures (Li, Sun, et al., 2013).

TissueFlex® is fabricated from polydimethylsiloxane (PDMS), which is a biocompatible polymer used in various medical applications. PDMS bioreactors are gas permeable; they allow gas exchange between the incubator and the culture reactor. PDMS also exhibit other advantages over other materials including low toxicity, ease of handling and optical transparency. However, due to its hydrophobicity, PDMS is difficult to wet and is prone to protein serum adsorption. This issue of hydrophobicity can be prevented by treating the PDMS construct with a 3% Pluronic F68 solution (Cui et al., 2007; Wu, Huang, et al., 2008). The set up of the TissueFlex® microbioreactor is shown in Figure 2.13.

A previous study showed an improved cell viability and growth potential of NCI/ADR colorectal cancer spheroid cultured in a perfused TissueFlex®, compared to a static culture after 17 days of culture (Wan, Li, et al., 2016). The same bioreactor system also showed an enhanced SH-SY5Ys neurite outgrowth and higher cell metabolic activity (Wan, Ball, et al., 2017). Despite the advantages over static cultures, the limitation of this TissueFlex® culture system is the laminar

flow pattern inside the culture chamber. Laminar flow pattern introduces mass transport limitations at the boundary layers.

Photolithography and replica moulding techniques create another example of PDMS microbioreactors. Apart from perfusion culture, a membrane is incorporated as a scaffold for cell attachment between the layers of PDMS. The scaffold is particularly useful in modelling *in vivo* interactions across membranes. Compared to culture on dishes, 3-D perfusion culture shows a greater hepatocyte preservation potential with a formation of cellular aggregates along the membrane for at least 2 weeks (Ostrovidov et al., 2004).

In addition, Hsieh et al. (2015) introduced a microbioreactor with the similar design to TissueFlex®; nine cylindrical chambers with the same size as a standard 96-well plate. The difference of this bioreactor compared to TissueFlex® was the plug module, which allowed multiple closed systems for 2-D (0.2 mm depth), 3-D (0.2 mm depth), tumour and spheroid cultures (2 mm depth). This bioreactor was used to culture primary oral cancer model, in which the results of this experiment was discussed earlier in Section 2.2.4.

2.4.4 Human biopsy culture as a biological avatar

Three-dimensional *in vitro* models cultured in a perfusion system can advance into an efficient high throughput screening. However, cell lines in current models only represent a higher stage and a poorly differentiating cancer. The integration of primary cells derived from patients into the model are more likely to comprise cells undergoing proliferation and differentiation at different rates. Patient-derived primary cells are more appropriate than cell lines if the model is to be constructed to reflect the pathology of the disease as well as the variability of solid tumours observed in individual patients (Masters, 2000; Xu, Farach-Carson, et al., 2014).

Patient-derived xenografts

One may consider patient-derived xenografts (PDXs) to be used in a drug screening platform. These are created by engrafting and expanding patient-derived tumour

cells in immunocompromised rodent hosts. PDXs recapitulate major characteristics of native tumours such as the architecture, stromal components, as well as inter- and intra-tumoural heterogeneity much more accurately than cell-line based xenograft models. PDXs also enable the modelling of inter-patient variability and the prediction of drug responses and their mechanisms (Despina and Hannon, 2013; Fong et al., 2016). With each individual patient tumour sample is growing inside a specific rodent, one can observe their personalised progression of a tumour and plan their therapeutic regimen accordingly. Consequently, PDX models are also known as mouse avatars.

However, PDXs are difficult and costly to develop and expand (Choi, Lin, et al., 2014; Imamura et al., 2015). Personalised medicine may not be as effective as PDX models can suffer from prolonged and variable latency periods after engraftment. Varying from 2 to 12 months, this may be longer than the survival time of patients. Furthermore, tumour engraftment in rodents replaces the human stroma with the rodents' themselves, which may exert selective pressures for aggressive phenotypes. It is also unknown whether the cellular responses observed in a rodent stroma are the same as those found in a human stroma (Fong et al., 2016; Despina and Hannon, 2013).

Patient-derived organoids

As mentioned in the earlier section (Section 2.2.4), 3-D *in vitro* models especially organoids and scaffold-based models retain similar morphological and cytological features of their native tumours. These features also apply to patient-derived organoids (PDOs). Huang et al. (2016) demonstrated that a patient-derived ductal pancreatic tumour organoid maintained the differentiation status, histological organisation, morphologic heterogeneity and differentiation status of a primary tumour up to 16 days. Besides, different responses to an enhancer of zeste homolog 2 (EZH2) inhibition were observed from organoids derived from different patients, which matched those seen in each patient tumour.

The time taken to establish organoid cultures from the time of surgery is relatively short as well (around $21 - 45$ days), which limits the genetic drift and preserves the integrity and characteristics of the native biopsies (Huang et al., 2016). Due to the relative ease of handling and low cost compared to PDXs, PDOs serve as a more promising platform for high throughput drug screening and for studying tumour biology (Fong et al., 2016). However, the same limitations of 3-D cancer models still apply to PDOs. These include the use of Matrigel® as an ECM and the lack of stromal cells such as: immune and vascular cells (Choi, Lin, et al., 2014; Fong et al., 2016). These limitations can be overcome by utilising other established biocompatible hydrogels and co-culture of stromal cells such as MSCs or HUVECs in the model.

Considerations for 3-D *in vitro* patient-derived cancer model

The variability among different sites within a tumour and among different individuals eventually lead to a variety of responses to drug treatments. This variability increases the complication to define controls in the experiments as results obtained *ex vivo* cannot be reproduced *in vivo*. To achieve reliable results, many patient samples representing different sites of tumours are required and experiments need to be performed in replicates. Results from *ex vivo* experiments should be compared with results from *in vivo* and clinical trials under the same treatments and conditions (Hickman et al., 2014; Mitra et al., 2013).

There are also other factors needed to consider such as the availability of viable patients' cells and the presence of different tumour cells that contaminate, outcompete and disrupt the growth of cancer cells (Xu, Farach-Carson, et al., 2014; Masters, 2000; Mitra et al., 2013). The size of the culture is also essential. As discussed earlier, thick samples lead to issues in supplying nutrients and oxygen into the core. Hence, single cell cultures can be another option to consider.

Different techniques can be employed to dissociate cells from patient-derived tumour biopsies. Such techniques include enzymes that preserve cell viability and integrity due to its target specificity; chemical cations such as calcium ions (Ca^{2+})

and magnesium ions (Mg^{2+}) that maintain cell surface integrins and intercellular matrices; and mechanical dissociation techniques such as mincing, homogenisation, vortex, aspiration and filtration that can potentially reduce the cell viability (Ljung et al., 1989; Cunningham, 2009; Mitra et al., 2013).

It was reported that perfusion culture attenuated cell culture degradation and significantly increased survival of 3-D cancer models (Cullen et al., 2007). Perfusion culture also reduced research stress and risks of contamination while increased the ease to correlate tumour response to drug treatments. As bioreactors can be seen as a miniaturised patient's body or a human avatar, they can complement the 3-D *in vitro* models by providing a homogenous and a steady cell culture environment (Wu, Huang, et al., 2008).

2.5 Conclusion

Despite a long-term and intensive research on oncology, cancer remains as one of the incurable diseases known to humanity. This is due to the complex microenvironment these solid tumours possess and makes up the tumour heterogeneity. Different niches play different key roles in tumour initiation and progression, with signalling cascades driven by 3-D interactions between different cells as well as between cells and the ECM.

Recently, 3-D *in vitro* models are gaining increasing attention because of their vast advantages over conventional 2-D monolayer models. Different models have their advantages and disadvantages, although they shared a few limitations, namely the lack of stroma and vasculature components. The selection of cells and matrices for 3-D cell culture are also crucial in recreating essential characteristics of a native tumour while trying to compromise the model's simplicity and ease of use.

Perfusion bioreactors are introduced as a potential system to expand cells on a large scale as well as to preserve the integrity of cells and tissues for a more extended period than in static cultures. The system can be used to overcome the lack of blood flow present in 3-D *in vitro* models as the nutrients and oxygen will be continuously supplied to the cultured cells. This system grants an opportunity

for the system to be used in conjunction with the 3-D model to develop as an effective drug screening platform.

The recapitulation of solid tumours and its surrounding microenvironment using tissue engineering approaches will further our understanding of cancer and its responses to treatments.

3

Optimisation of hydrogel properties for 3-D *in vitro* neuroblastoma model

Table of contents

3.1 Introduction 56
3.2 Materials and methods 57
3.2.1 Cell culture 57
3.2.2 Hydrogel scaffold preparation 58
3.2.3 Monoculture model development 59
3.2.4 Microrheology studies 62
3.2.5 Dry gel morphological studies 62
3.2.6 Cell viability analysis 63
3.2.7 Cell immunostaining 63
3.2.8 Image analyses 64
3.2.9 Statistical analysis 65
3.3 Results and discussion 66
3.3.1 Selection of hydrogel for NSC-HUVEC model 66
3.3.2 Optimisation of hydrogel stiffness 71
3.3.3 Hydrogel fragmentation model 74
3.3.4 Characterisation of hydrogel morphology 75
3.3.5 Investigation of mixing techniques of cell-hydrogel suspensions 77
3.3.6 Effects of laminin on 3-D cell-hydrogel arrangements . . 79
3.4 Conclusion 81

3.1 Introduction

Three-dimensional (3-D) *in vitro* models are required to confirm whether results produced in two-dimensional (2-D) cultures are representative of *in vivo* responses. 3-D cultures take into account the spatial interactions between different cells and between cells and the extracellular matrix (ECM) that are essential for cell signalling pathways, which are absent in 2-D counterparts (Alemany-Ribes and Semino, 2014).

Hydrogel scaffolds are the first biomaterials designed for applications in the human body. These water-swollen materials are advantageous over other biomaterials due to its hydrophilicity, which allowed the material to absorb thousands of times of its dry weight. Hydrogels also can be easily modified physically and chemically to give rise desirable properties (Billiet et al., 2012). Different hydrogels were used to model cancer in 3-D, for example: collagen, Matrigel®, chitosan, alginate and HyStem®.

Since these different hydrogels differ in their physical and chemical properties, optimisation experiments need to be performed to select one that is the most suitable for particular applications. In this study, several hydrogel properties were optimised to develop a 3-D *in vitro* neuroblastoma model.

In Chapters 3 and 4, the 3-D hydrogel *in vitro* model are based on the co-culture of human pluripotent stem cell (hPSC)-derived NSCs and human umbilical vein endothelial cells (HUVECs). In this chapter, several hydrogel properties such as: the choice of hydrogel (which served as an ECM), hydrogel stiffness, hydrogel fragmentation, the cell-hydrogel dispersion technique and effects of laminin on the cell-hydrogel spatial arrangements were optimised to identify the suitable microenvironment for the co-culture. The model contains minimal yet specific aspects of the native tissue, but it enables real-time imaging, monitoring and analyses.

3.2 Materials and methods

This section first outlines the protocols for cell culture, hydrogel scaffold preparation and the development of a 3-D monoculture *in vitro* model.

Different characterisation methods are then described. In this study, hydrogels were characterised by microrheology and morphological studies. Cells were characterised for its viability and expression of cell surface markers through assays and image analysis. Finally, statistical analysis was conducted on the data collected.

3.2.1 Cell culture

The cell culture in this work involved two different types of cells: neural stem cells (NSCs) and human umbilical vein endothelial cells (HUVECs).

Neural stem cells

To mimic the cancer stem cells present in neuroblastoma and to minimise the metabolic and genetic changes presented in cell lines, hPSC-derived NSCs were used as the main cell type for the 3-D *in vitro* model. Cryopreserved hPSC-derived NSCs were purchased from Axol (Cambridge, UK). Cells were cultured in the neurobasal medium (NBM) (Lonza, UK) with 1% penicillin-streptomycin and 2% B-27 supplements (Gibco, UK). NSCs were thawed from cryopreservation on the seeding day. Cells were centrifuged at 1000 rpm for 5 minutes and cell pellets were re-suspended in 10 mL NBM supplemented medium.

Human umbilical vein endothelial cells

Human umbilical vein endothelial cells were used in this co-culture model to represent angiogenesis in solid tumours. HUVECs were purchased from Lonza, UK. Cells were cultured in endothelial cell growth medium (EGM-2) (Lonza, UK) comprised the basal medium (EBM-2) and BulletKit™ supplements (10 mL FBS, 0.2 mL hydrocortisone, 2 mL hFGF-β, 0.5 mL VEGF, 0.5 mL R3-IGF-1, 0.5 mL ascorbic acid, 0.5 mL hEGF, 0.5 mL GA-1000 and 0.5 mL heparin) (Lonza, UK). Cells were thawed and centrifuged at 1000 rpm for 5 minutes before re-suspended

in 3 mL EGM-2 medium. The cell suspension was then added to a pre-warmed flask containing 3 mL of the EGM-2 medium before incubated at 37°C, 5% CO_2. The medium was refreshed every $3 - 4$ days and cells were sub-cultured once they reached $80 - 90\%$ confluence.

3.2.2 Hydrogel scaffold preparation

To select the optimal hydrogel for the 3-D *in vitro* model, different hydrogels were prepared to be used as the ECM for the model. HyStem® was hypothesised to be the hydrogel of interest in developing a NSC-HUVEC co-culture model due to the abundance of hyaluronic acid in the brain ECM.

HyStem®

HyStem® hydrogel (Sigma-Aldrich, UK) was prepared by dissolving 1 mL of degassed water each into two bottles of HyStem® macromer and dissolving 1 mL of degassed water (dH_2O) into one bottle of Extralink 1®. The bottles were placed on a shaker for 1 hour to give a clear solution. Solutions in the bottles were mixed together, drawn up by a syringe and incubated at 37°C for 45 minutes to allow gelation.

In this study, fragmented hydrogel model was only investigated with HyStem® as it was the hydrogel of interest and was used as for screening other control scaffolds. Fragmentation of HyStem® was executed by pushing the set gel through a 40 μm sterile cell strainer repeatedly to ensure that the gel was completely

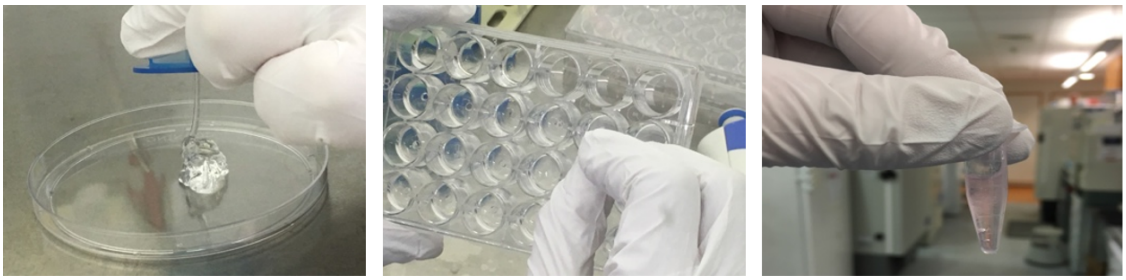


Figure 3.1: Hydrogel scaffold preparation Preparation of (A) fragmented HyStem®; (B) microwells; and (C) cell-hydrogel mixture.

fragmented (see Figure 3.1A). The fragmented gel was stored in a vial at 4°C before being used as a scaffold.

Matrigel®

Eppendorf tubes, pipette tips and culture plates were pre-chilled at 4°C before gel preparation. Matrigel® (Sigma-Aldrich, UK) with a protein concentration of 9.8 mg/mL was thawed in ice overnight before being used as a scaffold.

Collagen

Collagen type I, rat tail was purchased from IBIDI, Germany. The protocol of collagen gel preparation was adapted from IBIDI. The entire preparation process was performed in the cell culture hood on ice. 20 μL of 10X Roswell Park Memorial Institute (RPMI) medium (Sigma-Aldrich, UK) was mixed with 5 μL of NaOH (aq) (Sigma-Aldrich, UK), 81 μL of distilled water, 4 μL of $NaHCO_3$ (aq) (Sigma-Aldrich, UK), 50 μL of medium (NBM for NSCs and EGM-2 for HUVECs) and 90 μL of collagen in an Eppendorf tube. The tube was then vortexed to give a homogeneous solution.

3.2.3 Monoculture model development

The 3-D *in vitro* models of SH-SY5Y and HUVEC cells were developed in parallel using different hydrogels.

Cell seeding density calculations

As the formation of microenvironmental niches are important to recapitulate neurovascular interactions in 3-D, the phenomenon such as angiogenesis by HUVECs need to be considered. As suggested by Arnaoutova and Kleinman (2010) that the cell seeding density within the range of $45,000 - 70,000$ cell/cm^2 is required for an optimum and consistent tubule-like structure formation (50,000 cells/cm^2 seeding density was selected for this study). This cell seeding density was used for all 2-D culture experiments. As the seeding area in the microwell was around 0.2 cm^2, the original number of cells seeded in each microwell was 10,000 cells.

For 3-D cultures, the calculations for cell seeding density was based on the number of cells seeded in 2-D cultures. As there were 50,000 cells/cm^2 seeded in 2-D, the number was square-rooted and then cubed to approximate the number of cells seeded in 3-D. This gave rise the number of 10 million cells/mL. However, due to its high density, this cell seeding density will be used in the future chapters as the upper limit and a lower cell seeding density of 1 million cells/mL was used instead for most experiments in this thesis.

As the volume of each 3-D microwell is approximately 30 μL, this gave approximately 300,000 cells seeded in each 3-D model. This cell seeding density was successfully used in several studies concerning 3-D cell culture encapsulated within alginate (Godugu et al., 2013) and on top of Matrigel® hydrogel systems (Arnold et al., 2001).

Two-dimensional model

Cells were seeded as 2-D monolayers to serve as controls for the experiments. 500 μL of 1% laminin (Sigma-Aldrich, UK) in phosphate-buffered saline (PBS) (Sigma-Aldrich, UK) was added to each well as a pre-coating which promoted cell adhesion. The plates were incubated overnight at 37°C, 5% CO_2 before seeding. The cell seeding density was 45,000 cells/cm^2.

Three-dimensional model

Microwells preparation

For 3-D cultures, microwells were created inside each well of the 24-well plates to mimic the extracellular matrix (Figure 3.1B). 400 μL of autoclaved 10% agarose in PBS was added to each well. Once the gel set, a 4-mm diameter x 2 mm depth hole was created in the middle of each well using a sterile tube to form a microwell. The cell seeding density for 3-D cultures was 1 million cells/mL (unless stated otherwise).

HyStem®

In an Eppendorf tube, 100 μL of laminin, 400 μL of cell suspension and 500 μL of prepared HyStem® gel were added together, before vortexed and centrifuged at 1800 rpm for 3 minutes to remove any bubbles. The gel mixture was injected to fill up each microwell before covered with a nylon mesh to prevent the gel from floating outside the microwell. 1 mL of medium (NBM for NSCs and EGM-2 for HUVECs) was added to each well before incubated at 37°C, 5% CO_2.

Matrigel®

30 μL of pure Matrigel® was added to each microwell before incubated at 37°C, 5% CO_2 for 30 minutes. Once the gel set, 30 μL of cell suspension was seeded on top of the Matrigel® bed. 1 mL of medium (NBM for NSCs and EGM-2 for HUVECs) was added to each well before incubated at 37°C, 5% CO_2.

Compared to other hydrogel systems in this study, cells were cultured on top of Matrigel® instead of being encapsulated inside the gel. Matrigel® is a hydrogel which gels upon an increase in temperature, which makes it difficult to encapsulate the cells while the gel is still fluidised. In an attempt to encapsulate cells within Matrigel®, cells must be exposed to an abrupt change in temperature from 4°C until the gel polymerised at 37°C, which reduced the cell viability. Hence, cells were cultured on top of Matrigel® in this study.

Collagen

Initially prepared collagen gel mixture was mixed with 50 μL of cell suspension before vortexed and centrifuged at 1800 rpm for 3 minutes to remove any bubbles. The gel mixture was injected to fill up each microwell before covered with a nylon mesh to prevent the gel from floating outside the microwell. 1 mL of medium (NBM for NSCs and EGM-2 for HUVECs) was added to each well before incubated at 37°C, 5% CO_2.

3.2.4 Microrheology studies

Rheology tests were performed using diffusing wave spectroscopy (DWS) RheoLab (LS Instruments, Switzerland) optical rheometer to identify the stiffness of the hydrogel. Initially, 400 μL of three different concentrations of HyStem®(0.8%, 0.36%, and 0.056% w/v in dH_2O) were initially prepared. Each HyStem® concentration was mixed with 40 μL of 220-nm diameter polystyrene tracer particles (10% w/v in H_2O) before loaded into a cuvette. Each cuvette was exposed to a 685-nm laser at 37°C to measure the mean square displacement of tracer particles due to the Brownian motion.

The storage and loss moduli of the hydrogels were evaluated by applying the mean square displacement values to the generalised Stokes-Einstein equation. Given that $\langle \Delta r^2(i\omega) \rangle$ is the mean square displacement of tracer particles in the unit of nanometres (nm), the complex modulus, $G^\star$, describing the ratio of stress to strain of the viscoelastic material, e.g. hydrogel, is defined as:

$$G^\star(\omega) = \frac{k_B T}{\pi R i \omega \langle \Delta r^2(i\omega) \rangle} = G'(\omega) + iG''(\omega) \tag{3.1}$$

where k_B is Boltzmann constant (1.38×10^{-23} J/K), T is the temperature of the system (K), R is the radius of the tracer particle (nm), i is the imaginary number, G' is the storage modulus (the elastic portion) and G'' is the loss modulus (the viscous portion). All moduli have a unit of Pascal (Pa). The storage modulus, G', was then related to the stiffness of the hydrogel.

3.2.5 Dry gel morphological studies

Surface morphological studies were conducted to investigate the differences between the surface of the gel before and after fragmentation. Both unfragmented and fragmented HyStem® samples were initially prepared before freeze-dried to remove liquid from the gel. The protocol was optimised from previous studies (Chang and Patro, 2004; Haugh et al., 2010), with an initial shelf temperature of -40°C, a ramp to 0°C at a rate of 1°C/minute and a primary drying time of at least 15

hours at 0°C at 100 mTorr. Secondary drying was done at 4°C for a further 300 minutes at 100 mTorr. The samples were then coated with gold by sputtering (INCA X-Act X-ray system, Oxford Instruments, UK) before loaded into the scanning electron microscope (SEM).

The surface morphology of samples was observed by SEM (Carl Zeiss Evo LS15 VP-Scanning Electron Microscope, Carl Zeiss AG, Germany) at an accelerating voltage of 10 kV, at magnifications of 300X and 1000X.

Finally, analyses of the gel granular boundary size were evaluated by the ImageJ software. In this case, the diameter of each grain boundary was determined as an average measurement of the diameter at three different positions.

3.2.6 Cell viability analysis

The cell viability analysis was performed to determine the proportion of live deads in the samples. The medium was aspirated from each well, washed once with PBS before added 300 μL of 1% calcein acetoxymethyl or calcein-AM (Sigma-Aldrich, UK) (w/v) in PBS solution. After 45 minutes of incubation at 37°C, 5% CO_2, 300 μL of 0.4% ethidium homodimer-1 or ethD-1 (Sigma-Aldrich, UK) (w/v) in PBS solution was added further. Hydrogels were removed from each microwell into a covered dish after 10 minutes of incubation for imaging under the laser confocal microscope (Nikon Eclipse Ti, Nikon, Japan).

3.2.7 Cell immunostaining

Immunostaining assays were conducted to determine the changes in expression of different cell surface markers. All reagents were purchased from Sigma-Aldrich, UK. Cells were initially washed with PBS before fixed with 100 μL of 4% paraformaldehyde (w/v) in PBS. After 1 hour, samples were rinsed with 500 μL of wash buffer (0.2% bovine serum albumin and 0.2% Triton w/v in PBS) three times with 5 minutes interval between each wash, then 500 μL of blocking buffer (5% bovine serum albumin and 0.2% Triton w/v in PBS) was added to block any unspecific binding sites of samples. Cells were incubated with 100 μL of primary antibodies: 1:1000

(1 μg/mL) chicken Nestin; 1:2000 (0.5 μg/mL) mouse TuJ1 or 1:1000 (1 μg/mL) anti-laminin and 1:200 (5 μg/mL) rabbit CD31 added to each well overnight at 4°C. The dilution factors for antibodies were provided by results of the optimisation experiments from previous studies (Turaç et al., 2013; Orlova et al., 2014).

On the next day, samples were rinsed three times with a wash buffer before added 500 μL of secondary antibodies solution to each well. Samples were incubated in the dark at 4°C overnight before imaged under the laser confocal microscope (Nikon Eclipse Ti, Nikon, Japan).

3.2.8 Image analyses

Further image analyses were performed to quantify the results obtained earlier from cell viability and immunostaining assays. Three-dimensional z-stack images obtained from cell viability analysis and immunostaining were deconvoluted with AutoquantX3 software (see Figure A.1) to remove background signals before processed in Imaris x64 software to distinguish different coloured-interconnected voxels (see Figure A.2), representing different markers expressed on each cell's surface.

Since this method creates computer-generated representations of z-stack 3-D images, it is important to set the threshold to adjust the sensitivity of the algorithm so that the noise can be minimised. In each image, the threshold was selected from the kink formed by a steep change in the absolute intensity to ensure that most of the cells were overlaid and not the background signals (see Figure A.3).

The process of cell surface marker quantification was performed by an algorithm counting the number of 8-connected voxels (see Figure A.4). Ultimately, this creates a reconstructed 3-D images up to three different coloured surfaces, representing three different dyes stained in the sample (see Figure A.5). The process is the same for cell number quantification where cells expressing calcein-AM and ethD-1 were quantified based on the colour displayed on each cell's surface upon imaging (see Appendix A for more details on image analysis procedures).

3.2.9 Statistical analysis

All experiments were performed independently with three replicates, reported as mean (M) ± standard deviation (SD). GraphPad Prism 6.0© software was used to illustrate graphical results as well as to perform t-test and ANOVA with Tukey's post-hoc analysis to detect significant differences between culture groups. A significant value (α) of 0.05 was used to determine significance between groups.

3.3 Results and discussion

The work in this chapter regarded different optimisation experiments to develop a 3-D neuroblastoma co-culture model. This involved the selection of the hydrogel, the optimisation of hydrogel stiffness, the hydrogel fragmentation model and its morphological studies as well as the investigation of the mixing technique and the effects of laminin on the model.

3.3.1 Selection of hydrogel for NSC-HUVEC model

Main finding

HyStem® was the optimal choice of hydrogel for NSC-HUVEC model.

Different biophysical and biochemical properties of the hydrogel were initially investigated to determine one that would closely mimic the ECM of neuroblastoma tumours.

As different growth factors are present in different types of hydrogel-based scaffolds, it is essential to investigate the cellular and molecular responses for each of them. To overcome the lack of vasculature, the main limitation of existing cancer models, HUVECs were seeded together with NSCs as a co-culture neural cancer model. Both cell types were individually cultured in different hydrogel systems to identify those that gave rise to best cell viabilities. Cell encapsulations were performed in HyStem® and collagen hydrogel systems. On the other hand, cells were seeded as a monolayer culture configuration in Matrigel® as the gel set upon an increase in temperature.

The exposure of the encapsulated cells to the abrupt change in temperature from 4°C to 37°C, the temperature at which Matrigel® proteins polymerise, reduced the cell viability. It was also difficult to encapsulate cells while the gel was still fluidised; cells were likely to deposit to the bottom of the wells. Hence, it was preferable for cells to culture on top of the Matrigel® layer in the same manner as other previously reported studies (Arnold et al., 2001; Moghe et al., 1996; Arnaoutova and Kleinman,

2010). Also, Matrigel® is commonly used to demonstrate tubule-like structures formation when HUVECs were cultured on top of the hydrogel bed (Arnaoutova and Kleinman, 2010; Wan, Bovornchutichai, et al., 2017). The gel, therefore, served as a control for the experiments to model angiogenesis in 3-D *in vitro* models.

Morphological images in Figure 3.2A illustrate different cell morphologies observed for HUVECs. 3-D morphologies of HUVECs were rounded and segregated in small clusters throughout collagen while they were flattened in 2-D laminin, HyStem® and Matrigel®. HUVECs formed tubular structures in Matrigel®, characterised by the formation of long, thin projections of cell clusters from the centre of the hydrogel.

In HyStem®, the cells elongated across the nylon mesh, but dispersed more homogeneously across the gel than when cells were seeded on top of Matrigel®. It is speculated that the presence of endothelial growth factors in these hydrogels, especially Matrigel® and lesser in HyStem®, allowed cells to attach to themselves then migrated towards each other to form tubule and elongated structures.

Cell viabilities were calculated by counting the number of cells expressing calcein-AM to further support the morphological findings. Figure 3.2B shows the increase in the cell viabilities from day 3 to day 7 were observed in all culture systems, especially 3-D HyStem®, in which the increase was significant when compared to other 3-D systems such as Matrigel® and collagen.

Conversely, 3-D morphologies of NSCs in Figure 3.3A were almost identical in all hydrogels. Hence, cells were further stained with calcein-AM (green) and ethD-1 (red), representing live and dead cells in NSC monocultures to compare relative cell viabilities in each hydrogel system.

Figure 3.3B shows the increase of cell viabilities of NSCs from day 3 to day 7 for all culture systems. Similar to the HUVEC monocultures, the increase in NSCs viability for 3-D HyStem® was significant when compared to Matrigel® and collagen.

Table 3.1 shows the absolute number of average live cells in monocultures after 3 and 7 days of culture. Although it is more convenient to convert these cell viabilities value into relative percentages with respect to the original cell seeding numbers (Figures 3.2B and 3.3B), it is clearly seen from the absolute numbers

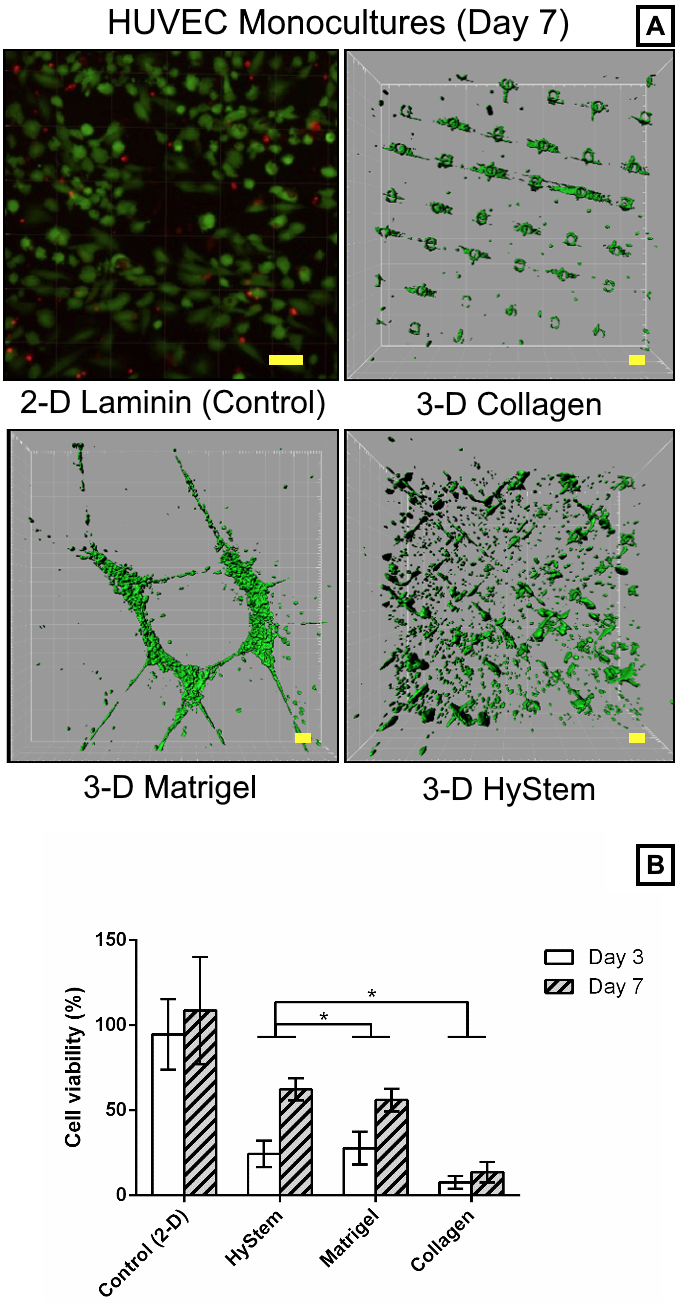


Figure 3.2: Human umbilical vein endothelial cell monocultures in different 3-D hydrogel systems HUVEC cell viability was higher in 3-D HyStem® and Matrigel® than in collagen hydrogel systems. (A) HUVECs morphologies are shown after 7 days of culture in different 3-D hydrogel systems. Morphologies of HUVECs varied among different hydrogel systems. Cell seeding density = 1 million cell/mL. Scale bar = 100 μm; (B) The bar graphs below display quantitative analyses of cell viability in HUVEC monocultures. Values are mean ± SD; n = 3 per group. Statistical analysis was performed by ANOVA with post-hoc analysis. $^{\star}p < 0.05$ vs 3-D HyStem®.

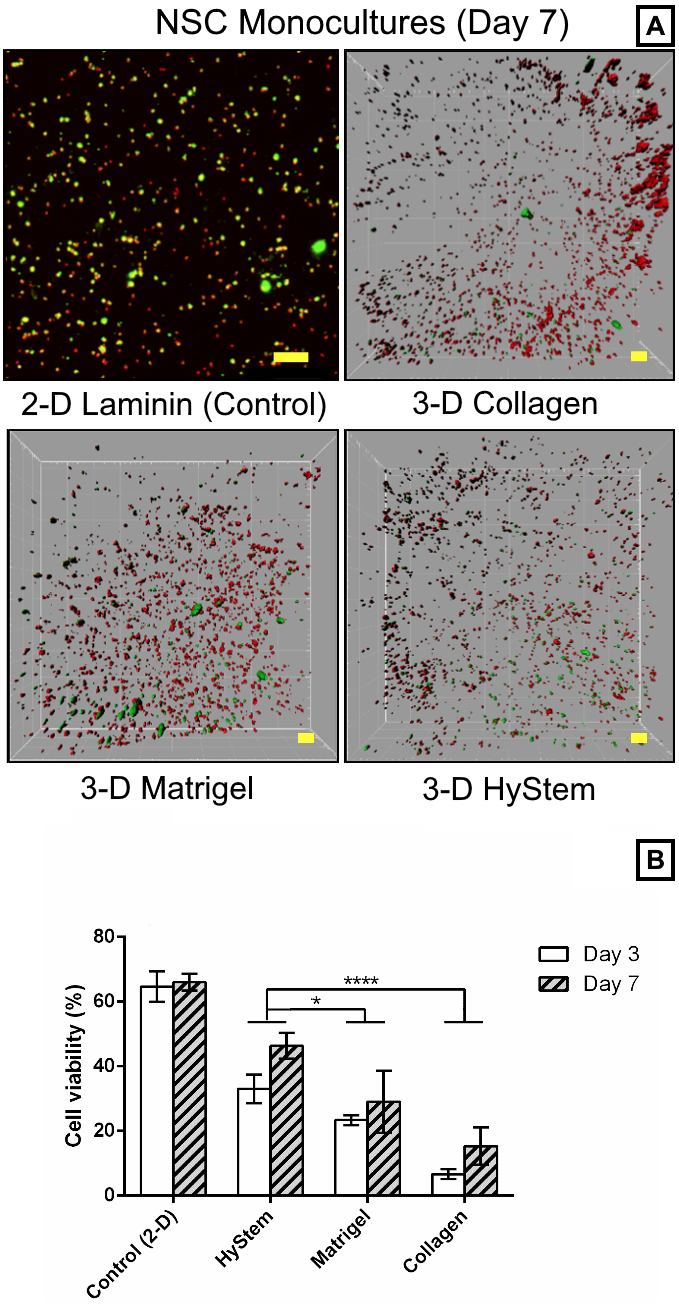


Figure 3.3: Neural stem cell monocultures in different 3-D hydrogel systems NSC cell viability in 3-D HyStem® system was the highest among all types of hydrogel tested. (A) NSCs morphologies are shown after 7 days of culture in different 3-D hydrogel systems. Morphologies of of NSCs remained the same throughout. Further staining by Calcein-AM (green) and EthD-1 (red) was performed on NSC monocultures as an additional indicator for the selection of hydrogel. Cell seeding density = 1 million cell/mL. Scale bar = 100 μm; (B) The bar graphs below display quantitative analyses of cell viability in NSC monocultures. Values are mean ± SD; n = 3 per group. Statistical analysis was performed by ANOVA with post-hoc analysis. $^{\star}p < 0.05$, $^{****}p < 0.0001$ vs 3-D HyStem®.

Table 3.1: Average number of live cells/model in 2-D and 3-D monoculture systems after day 3 and day 7

	HUVECs/NSCs	**HUVECs**		**NSCs**	
	Day 0	Day 3	Day 7	Day 3	Day 7
2-D Laminin (Control)	9,000	8,520	9,780	5,820	5,940
3-D HyStem©	300,000	73,000	187,000	99,000	139,000
3-D Matrigel©	300,000	83,000	168,000	70,000	87,000
3-D Collagen	300,000	23,000	41,000	20,000	46,000

that the viability of 3-D cultures was significantly lower than from day 0 for both NSCs and HUVECs. This could be due to the encapsulation of cells within the hydrogel implied that any dead cells were not removed from the hydrogel when changing the medium. These entrapped dead cells could release degrading enzymes that affect other surrounding viable cells (Ljung et al., 1989). Compared to 2-D monocultures, where dead cells detach from cell culture wells and remove along with the waste medium. Ultimately, this stimulates a decrease in cell viability much faster than in their 2-D monolayer culture counterparts.

Based on viability results, it is evident that HyStem® is the optimal choice of hydrogel among the three for both NSCs and HUVECs cultures. HyStem® is a hyaluronan-based hydrogel. Hyaluronic acid is an essential ECM component in various tissues including nerve tissues. Therefore, this makes HyStem® a suitable hydrogel to model nervous system diseases such as neuroblastoma. In fact, the hydrogel was previously used in retinal progenitor cell transplantation (Liu, Wang, et al., 2012) and *ex vivo* expansion of human corneal epithelial stem cells (Chen, Qu, et al., 2017).

In addition, the use of HyStem® is also reported in a co-culture cancer model with B-cell lymphomas and endothelial cells (Mannino et al., 2017). Although endothelial cells in this lab on a chip system were not in direct contact with HyStem®, results showed that endothelial cells were compatible to be used along with the hydrogel.

As a basement membrane extract, culturing HUVECs on Matrigel® reported to form tubule-like structures (Arnaoutova and Kleinman, 2010). However, compared

to native ECM, Matrigel® only composed of basement membrane components, which does not mimic the cellular surface membrane. Other components within the Matrigel® system is still unknown. Likewise, collagen gels still lack components of connective tissues and their extent of covalent crosslinking is also different (Yamada and Cukierman, 2007). Growth factors may need to be added into HyStem® in order to induce the migration of HUVECs into tubule-like structures; as same as when cells are cultured on Matrigel® bed.

3.3.2 Optimisation of hydrogel stiffness

Main finding

NSC viability was greater when cultured in stiffer HyStem® gel.

Hydrogels are viscoelastic materials as they exhibit both solid and liquid phases. According to the viscoelastic theory, viscoelastic materials such as hydrogels respond

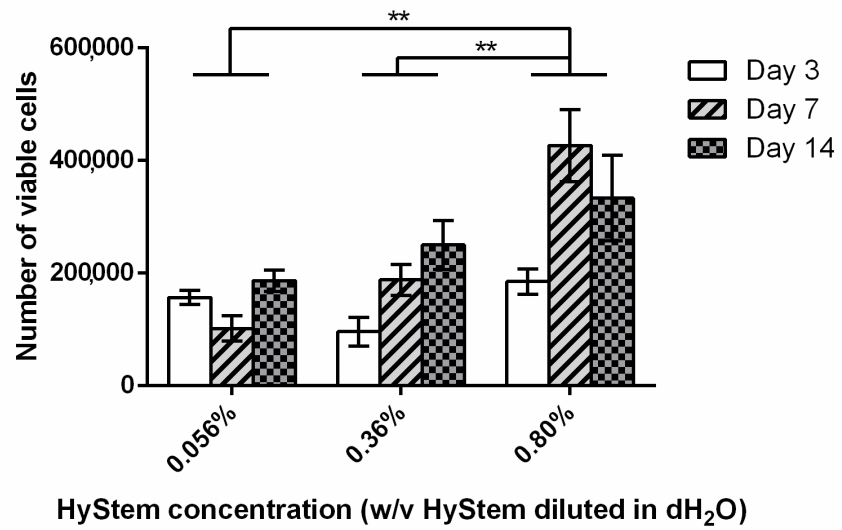


Figure 3.4: Effects of the hydrogel percentage (w/v in dH_2O) on neural stem cell viability NSCs viability was greater when cultured in a stiffer HyStem®. The bar graphs show the effects of different HyStem® concentration on NSC viability. NSCs were encapsulated and cultured in varying fragmented HyStem® concentrations (0.056%, 0.36% and 0.8% w/v diluted in dH_2O) for 3, 7 and 14 days. The cell viability of NSCs was assessed by staining with calcein-AM dye immediately after culture. Viable cells corresponded to those expressed calcein-AM. Values are mean ± SD; n = 3 per group. Statistical analysis was performed by ANOVA with post-hoc analysis. $^{**}p < 0.01$ vs 0.80% HyStem® concentration.

to stress as a function of how much energy is stored and lost (Christensen, 1982). As the stiffness of the ECM can affect both proliferation and differentiation capacities of cells, the hydrogel percentage (w/v in dH_2O) is another biophysical property optimised for NSCs culture.

The stiffness of HyStem® was tuned by varying the hydrogel percentage (w/v in dH_2O). In this study, the volume of dH_2O added to dissolve HyStem® macromer (Glycosil®) and Extralink 1® varied between 2 mL, 1 mL and 0.5 mL; each represented the different hydrogel percentages of 0.056%, 0.36% and 0.8% w/v HyStem® diluted in dH_2O respectively. The cell viability of NSCs was assessed by staining with calcein-AM dye after 3, 7 and 14 days of culture.

Figure 3.4 shows that the cell viability of NSCs were maintained in gels with higher levels of stiffness as the viability of NSCs in 0.8% w/v HyStem® was significantly greater than in 0.36% and 0.056% for all three-time points.

The stiffness of the hydrogel for each HyStem® concentration was measured using microrheology. Characterisation of hydrogel's viscoelastic properties by microrheology presents numerous advantages over by a conventional rheometer. These include the lack of contact between the rheology plates and the gel sample, which implies that the gel does not get physically damaged. Also, microrheology operates with a vast range of frequency sweep mode to measure a particle displacement to a nanometre resolution (Mansel et al., 2013).

Furthermore, microrheology is passive. It only relies on thermal energy to displace the tracer particles via Brownian motion within the sample. This means it operates under a very low thermal energy, which enhances the sensitivity of the measurement especially in the linear viscoelastic region (Mansel et al., 2013).

Based on microrheology results, the hydrogel percentage (w/v in dH_2O) of 0.056%, 0.36% and 0.8% correlated to the stiffness of 1.29, 5 and 326 Pa respectively. It is notable that the increases in the hydrogel percentage and in hydrogel stiffness do not establish a linear trend. This is because the stiffness measured was evaluated from the mean square displacement of tracer particles, then applied to the generalised Stokes-Einstein equation (Equation 3.1).

Microrheology results could be explained by the effect of gel hydration, which did not change the molar ratio between thiol groups (in Glycosil®) and acrylate groups (in Extralink 1®). However, gel hydration increased the distance between two adjacent crosslinking points and resulted in the decrease in the probability of thiol-acrylate bond formation as the hydration level increased (Putter, 2015).

The bulk stiffness of HyStem® in this experiment lies within the range of $10-500$ Pa, which is the range of bulk rigidities of neuroblastoma ECM from the tissue of origin to the point where optimal differentiation occurs. NSCs cultured in a stiffer ECM tend to form few large clusters with actin-rich neurite formation, while they were more evenly distributed with fewer clusters formed in a softer ECM (Lam et al., 2010; Watt and Huck, 2013).

The encapsulation of cells in HyStem® further decreased the stiffness of the hydrogel as the neurite outgrowth or even the presence of cells physically hindered any chemical reactions taking place between thiol-acrylate groups. In addition, NSCs also produced degradation enzymes, i.e. MMPs to promote outgrowth that resulted in the decrease in the hydrogel stiffness (Putter, 2015).

The changes in the hydrogel percentage (w/v in dH_2O) directly affect the concentration of sites bounded by integrin adhesion receptors. These presumably rely on the mechanotransduction signalling system. The cell surface integrin receptors and actin filaments would pull against the ECM to sense the stiffness. This alters intracellular signalling, enhances cell proliferation and promotes neoplasia (Yamada and Cukierman, 2007). Hydrogel stiffness results agree with a previous study, which showed an enhanced neuritogenesis as the ECM stiffness increased. In contrast, the downregulation of N-myc gene was reported, implying the suppression of cell proliferation (Lam et al., 2010).

3.3.3 Hydrogel fragmentation model

Main finding

Hydrogel fragmentation model increased the cell adhesion area.

As hydrogel scaffolds were designed to mimic the biophysical and biochemical properties of ECM, several properties of the hydrogel were investigated and optimised. This would identify the most suitable environment for NSCs to grow. One of the preliminary experiments performed involved the 3-D culturing of NSCs in HyStem® hydrogel for 7 days. However, it was observed under the laser confocal microscope that most of the cells were located less than 60 μm above the bottom of the wells (Figure 3.5A). This was most likely be due to the deposition of the cells to the bottom of the well during seeding as it took some time for gelation to occur and encapsulate the cells. Another explanation would be the disintegration

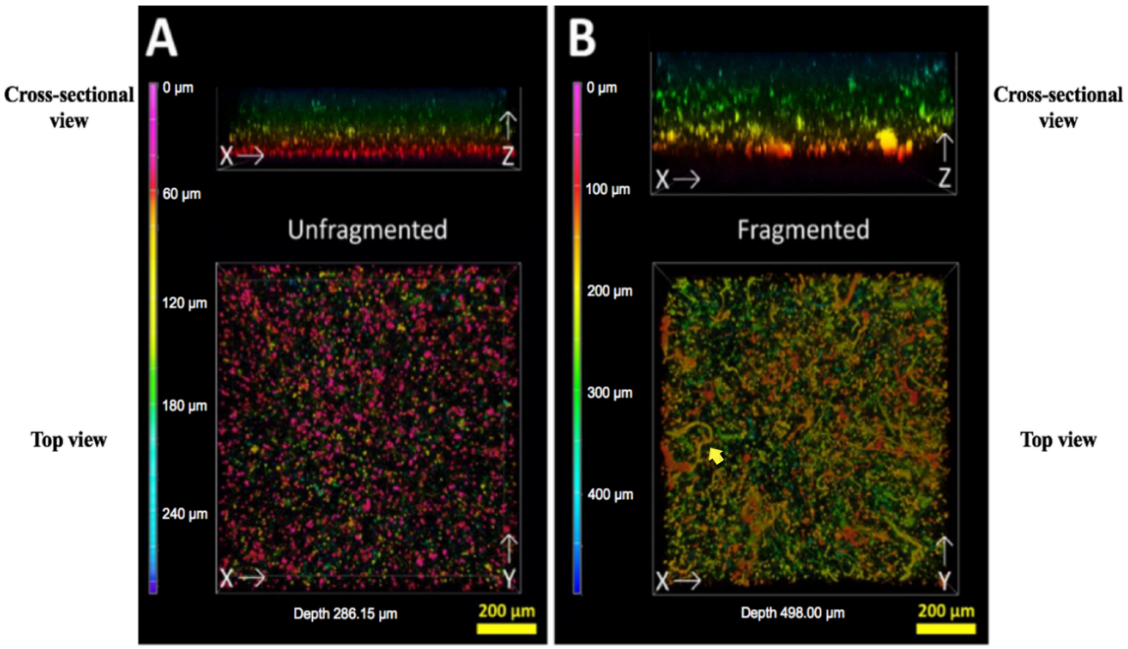


Figure 3.5: Comparisons between fragmented and unfragmented HyStem® hydrogel systems Fragmentation of HyStem® enhanced the adhesion area for each cell. Depth colour coding was used to highlight the depth of the cells within HyStem® after 14 days of culture. (A) Settling of cells due to gravity was observed during crosslinking of the unfragmented HyStem®; (B) Cells were well distributed throughout fragmented HyStem®. Neurite outgrowth was observed inside the gel (see yellow arrow). Cell seeding density = 10 million cells/mL. Scale bar = 200 μm.

of the hydrogel in culture, which left cells attached to the bottom of the well. To increase the adhesion area for each cell, hydrogels were fragmented by pushing them through a 40 μm cell strainer (see Figure 3.1A).

Results show that fragmented gels enhanced the area that NSCs could adhere to as the z-stack image in Figure 3.5B illustrates that NSCs remained intact to the fragmented hydrogel after 7 days of culture, i.e. the cell distribution spanned across 300 μm of the gel depth. Moreover, neurite outgrowth was observed in the fragmented gel (annotated on the figure with a yellow arrow), but not in the unfragmented gel.

Fragmentation of hydrogels increases the surface area to volume ratio. The higher surface area implies a greater number of physical attachment sites that cells can adhere to. It also means that an increasing number of cells are more likely to directly expose to culture medium and oxygen, compared to unfragmented counterparts where diffusional gradients are formed. Furthermore, the presence of gel granule boundaries provide spaces for cells to extend their protrusions and form specific structures within a 3-D culture system.

3.3.4 Characterisation of hydrogel morphology

Main finding

Fragmentation of HyStem® created interconnected grain boundaries allowing cells and growth factors to penetrate through.

As illustrated earlier in the previous sections, the stable network could be formed from fragmented HyStem®, laminin and cells. Focal adhesions and swelling of gel granules provided cells with both biological and physical attachments to the 3-D structure.

An additional experiment was performed to investigate the structure of fragmented HyStem® in more detail as well as to determine whether the cells could form any specific structures in this hydrogel network.

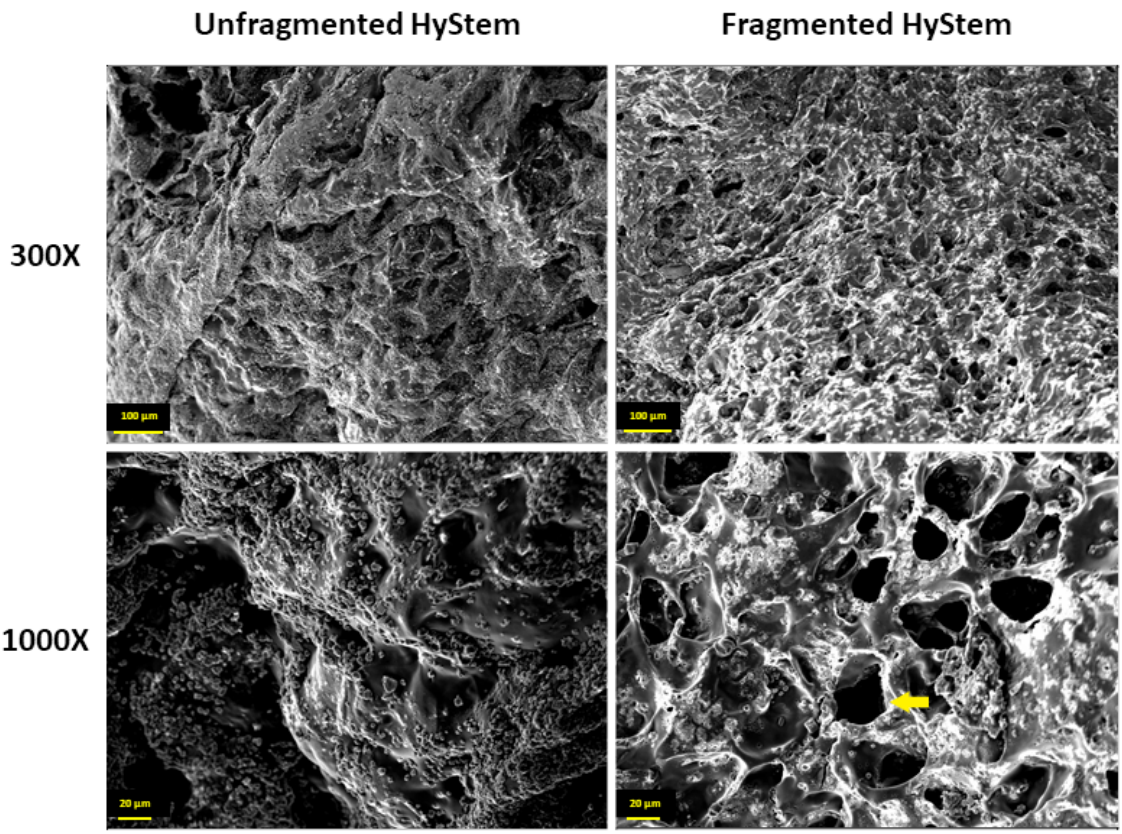


Figure 3.6: Scanning electron microscope images of unfragmented and fragmented HyStem® Fragmented HyStem® hydrogel created interconnected grain boundaries (see yellow arrow) to facilitate the motility of cells through the structure. The average boundary diameter is 29 ± 7.3 µm (mean ± SD, n = 20). The grain boundaries were not observed in unfragmented HyStem® samples. Scale bar = 100 μm for 300X images and 20 μm for 1000X images.

Both unfragmented and fragmented HyStem® were prepared, freeze-dried, sputtered with gold particles and imaged by SEM. Figure 3.6 shows the images of samples under 300X and 1000X. Interconnected grain boundaries were only observed in fragmented HyStem® samples, with the measured diameter ranged from $20 - 40$ μm and the average of 29 ± 7.3 μm (mean ± SD, n = 20). The diameters were measured by ImageJ software. This suggests that the upper limit of the hydrogel granule size may be controlled by the size of the mesh that fragmented the gel.

In addition, SEM results show that the average size of the pores is large enough for cells to penetrate through the hydrogel granules. The average size of SH-SY5Y cells is 12 μm, whereas the average size of HUVECs is around $14 - 15$ μm (Milo,

2013). This suggests that fragmented HyStem® also provides a suitable physical microenvironment for neurons and endothelial cells to grow within.

3.3.5 Investigation of mixing techniques of cell-hydrogel suspensions

Main finding

Vortex and centrifugation improved the distribution of cells throughout hydrogel scaffolds.

The conventional method of mixing cells within the hydrogel is to stir the mixture together until it is homogeneous manually. However, images produced from the z-stack distribution (see Figure 3.7A) demonstrate that cells were clustered in an area of the hydrogel (see yellow arrow). For the model to be used to investigate the initiation and propagation of different microenvironmental niches and 3-D spatial interactions, it is important that there is a repeatable starting point, i.e. a homogeneously dispersion of cells throughout the hydrogel. Investigations of cell migrations to specific areas within the gel in response to different stimuli such as growth factors, co-cultured cells or continuous perfusion of medium can be evaluated easier if cells were initially cultured as single cells without any aggregation. Furthermore, mixing cells in a hydrogel by manual stirring caused the formation of bubbles, which embedded within the gel and led to issues of obscuring cells during imaging.

Several procedures were conducted to resolve these issues. The cell suspension and hydrogel were mixed by vortexing for 20 seconds followed by centrifuging at 1800 rpm for 3 minutes. The slow rate of gel swelling was utilised to facilitate fluidisation of the gel granules. Gelation occurred around the cells as the fluid was absorbed and the granules started to swell.

The z-stack images in Figure 3.7B show that the cells were evenly distributed throughout the hydrogel. Histograms quantifying the number of cells in every 100 μm of the z-stack are displayed below each respective z-stack image. Results from

the histograms concluded that a more uniform distribution of cells was seen in the vortex-centrifuge mixing compared to the manual mixing technique. In addition, there were no bubbles observed in the vortex-centrifuge mixture, which made the imaging and image analyses of the hydrogel more convenient.

Although vortex mixing dispersed the cells throughout the hydrogel, the force applied to the cells might be strong enough to induce cellular damage. The damage

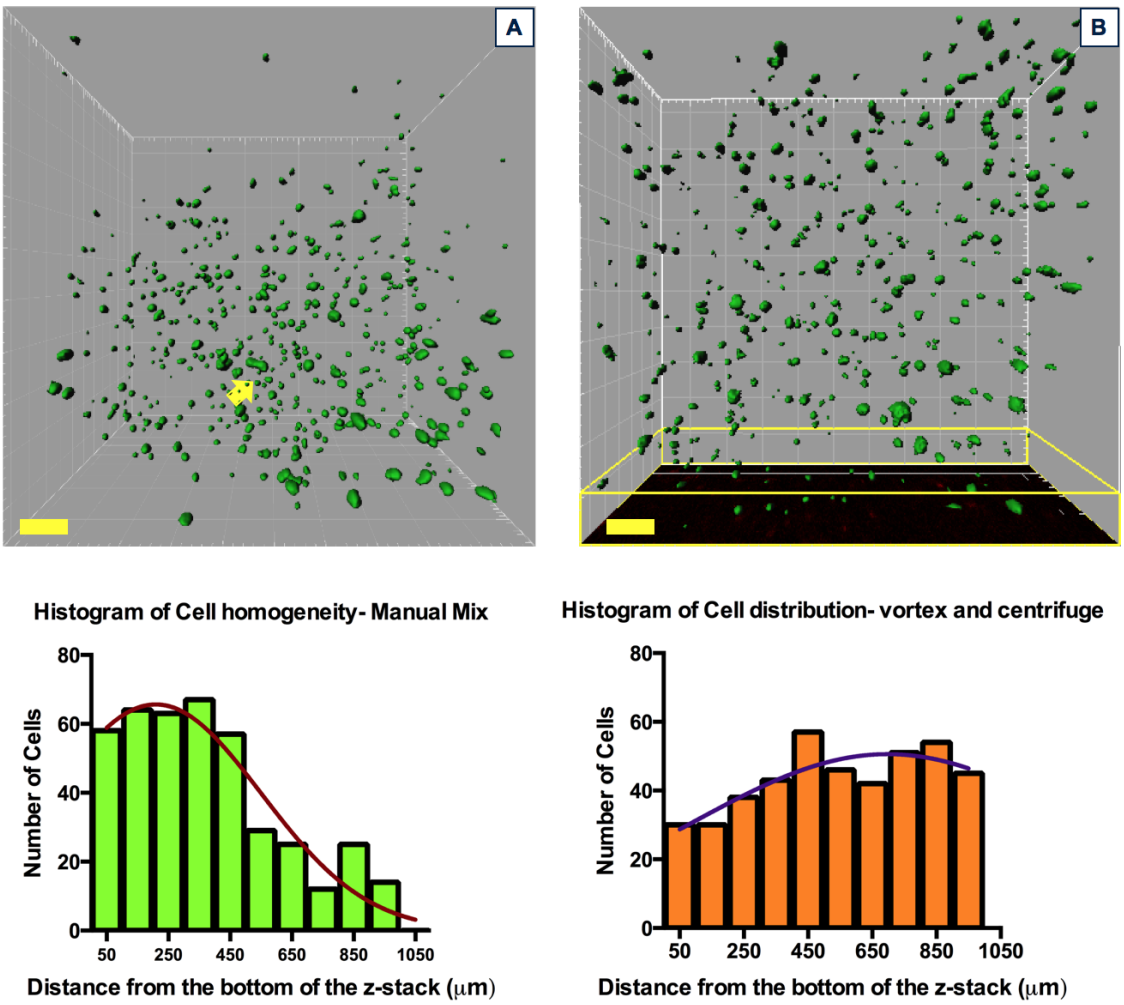


Figure 3.7: Comparisons between manual mix and vortex and centrifuge mixing techniques Vortex-centrifuge mixing improved the distribution of cells throughout the hydrogel. NSCs were seeded into HyStem® hydrogels and mixed together by two different techniques. (A) Manual stirred mixing, cells clustered together in the hydrogel (see yellow arrow); (B) Vortexed-centrifuged mixing, cells were uniformly dispersed throughout the hydrogel. Histograms below illustrate that cells were more homogeneously dispersed in hydrogels after vortex-centrifuge mixing. Cell seeding density = 1 million cells/mL. Scale bar = 150 μm.

was minimised by the addition of cell suspension rather than cell pellet to mix with the hydrogel. Hydrogels swelled and expanded once water or medium was added, resulted in the gel to act as a cushion for cells and reduced the physical impact caused by vortex mixing.

3.3.6 Effects of laminin on 3-D cell-hydrogel arrangements

It is hypothesised that the incorporation of laminin to the cell-hydrogel suspension allows these molecules of laminin to reside between the hydrogel granules. Initially hydrogels, cells and laminin molecules are dispersed as a fluidised granular suspension. The gel then absorbs water and swelled, which causes the entrapment of cells and the localisation of laminin between the gel granules.

The localisation of laminin along the gel granule boundaries leads to the attachment of cells to the laminin and formation of cellular focal adhesions to the laminin and to the excreted proteins (Figure 3.8A). Focal adhesion is formed from the binding and clustering of integrins to the ECM proteins, which link to actin filaments and trigger downstream signalling cascade to the nucleus. It is hypothesised that actin filaments are also reorganised, allowing cells to spread on the substrate.

These factors contribute to the structural stabilisation between hydrogel granules and neurite-forming networks (Figure 3.8B), which corresponds to the neurite outgrowth observed in the fragmented hydrogel model in Figure 3.5B. This suggests that NSCs are more likely to differentiate into neurons and extend their neurite outgrowth in fragmented gels than in unfragmented gels.

To illustrate the structural stabilisation of hydrogel granules and cells by laminin. 100 µL of laminin was added to the HUVEC-fragmented HyStem® mixture and cultured for 7 days in an EGM-2 medium. The z-stack morphology in Figure 3.9 shows the that laminin (stained blue) was evenly distributed throughout the hydrogel structure, implying the accessibility of laminin in the fluidised granular suspension. Laminin was also seen residing adjacent to the HUVECs (stained green), which expressed a CD31 marker (see arrow in Figure 3.9). These results support

the hypothesis addressed earlier that cells and gel granules attached to laminin along the gel granule boundaries to create a stabilised network.

Laminin is a glycoprotein predominately present in the ECM of the developing brain. It regulates cell adhesion, migration and proliferation by switching on mechanotransduction pathways. A study by Dwane et al. (2013) reported extensions of neurites after SH-SY5Y cells were cultured on laminin for 72 hours. The cells also expressed high levels of FAK, which was responsible for neuronal migration,

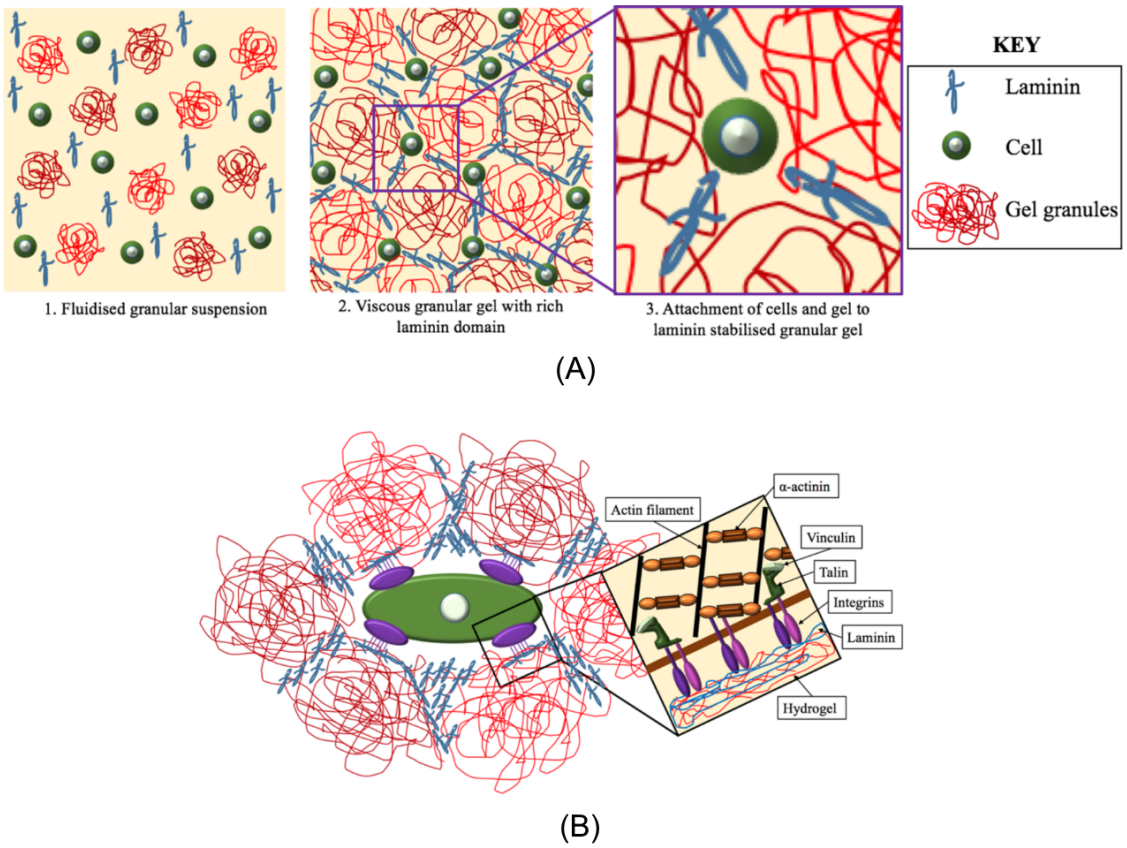


Figure 3.8: Schematic illustration of the stabilised network formed by cells, laminin and gel granules The swelling of gel granules and cellular attachment to laminin stabilised the network via focal adhesions. (A) Hydrogels, cells and laminin molecules are initially dispersed as a fluidised granular suspension. The gel then absorbs water and swelled, which causes the encapsulation of cells and the localisation of laminin between the gel granules. This enhances the adhesion area of the cells to the gel granules as well as attachment of cells to the laminin and to the excreted proteins, structurally stabilised the network; (B) Focal adhesion is formed from the binding and clustering of integrins to the ECM proteins, which link to actin filaments and trigger downstream signalling cascade to the nucleus. Actin filaments are hypothesised to be reorganised, allowing cells to spread on the substrate.

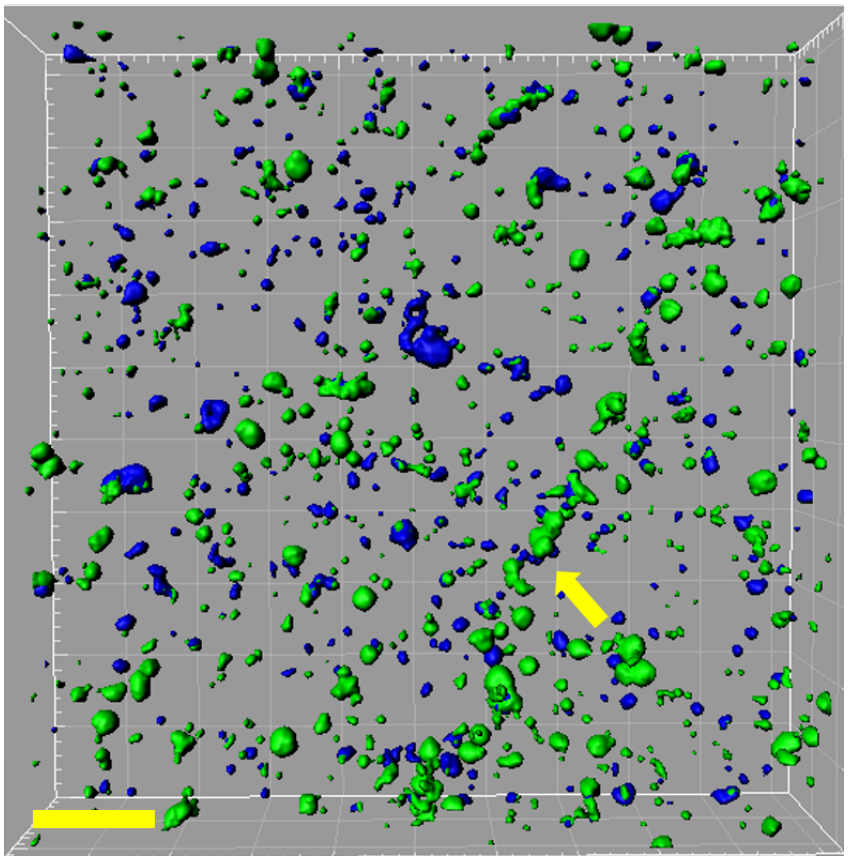


Figure 3.9: Z-stack image of a HUVEC 3-D fragmented HyStem® model stained for anti-laminin and CD31 markers Laminin was evenly distributed around the network of HUVEC-fragmented HyStem®, with rich laminin domains located adjacent to the cells (yellow arrow). The z-stack cell morphology illustrated the expression of anti-laminin (blue) and CD31 (green) antibodies after 7 days of culture in an EGM-2 medium. Cell seeding density = 1 million cells/mL. Scale bar = 150 μm.

axon guidance and neurite outgrowth in the developing CNS.

Besides, laminin also plays a vital role in angiogenesis. A study by Magdeldin et al. (2017) reported more significant interconnected vascular networks observed in HUVEC cultures on laminin. This implies the modulation of angiogenesis by laminin alongside with oxygen gradients.

3.4 Conclusion

The investigations of cell-hydrogel mixing techniques, gel fragmentation and hydrogel percentage (w/v in dH_2O) allowed modifications to the cell-ECM interactions. As these factors contribute to cell signalling and behaviour, the recapitulation of

tumour microenvironment is possible.

HyStem® hydrogel was selected as the hydrogel for NSC-HUVEC co-culture model as it gave rise to the best cellularity for both NSCs and HUVECs.

The hydrogel percentage (w/v in dH_2O) of the HyStem® was optimised to achieve a value of 0.80%. The stiffness of the gel corresponded to the stiffness of the ECM in neuroblastoma tumours.

Hydrogel fragmentation was investigated to overcome the issues of cell deposition upon culture. It also increased the physical attachment sites of cells along the gel granule boundaries, which may facilitated the formation of specific cellular structures and migration.

The mixing of cells and hydrogel were conducted by centrifugation and vortex to disperse the cells throughout 3-D hydrogels homogeneously and eliminate the presence of gas bubbles that would impair the imaging process. Ultimately, this gives a repeatable starting point for the 3-D cell culture.

Fragmentation of HyStem® and the incorporation of laminin provided both physical and biological attachment sites for cells, stabilising the structure. Hydrogel granules also facilitated neural outgrowth as they allowed the elongation of neurites around themselves.

This chapter introduced several key biophysical factors in recapitulating neuroblastoma tumours, which will be used in conjunction with other optimised factors in the next chapter to create a 3-D *in vitro* neural-endothelial co-culture model.

4

Three-dimensional *in vitro* neural stem-endothelial cells co-culture model

Table of contents

4.1 Introduction 83
4.2 Materials and methods 85
4.2.1 Co-culture model development 85
4.2.2 Cell immunostaining 87
4.2.3 Image analyses 88
4.2.4 Statistical analysis 91
4.3 Results and discussion 92
4.3.1 Seeding NSCs from cryopreservation 92
4.3.2 Optimisation of co-culture media and seeding ratios . . 94
4.3.3 Investigation of neurovascular interactions 97
4.3.4 Characterisation of 3-D *in vitro* co-culture model 99
4.4 Conclusion 102

4.1 Introduction

It is becoming evident that the tumour microenvironment is heterogeneous and comprises various niches such as: hypoxic regions, invasive regions and vascular-rich regions. These niches provide an optimal environment for cells exhibiting the tumour, especially cancer stem cell to self-renew, proliferate and more unlikely to differentiate. Ultimately, the microenvironment established to drive the tumour

towards malignancy (Clarke, 2004; Rich and Eyler, 2008).

Amongst all types of cells contributing to different niches, endothelial cells stand out as one that plays a prominent role in almost every single one of them. Firstly, a hypoxic niche is formed from the limitation of nutrients and oxygen to be supplied by blood to regions with greater depth from the surface, i.e. beyond 200 μm. This eventually leads to the formation of necrotic areas in the core, where cells residing adjacent are more resilient to therapies (Chen, Htay, et al., 2009).

Hypoxia-inducible factor (HIF) upregulates and proteins transcribe as part of an angiogenic factor cascade within this hypoxic region (Szot et al., 2011). Growth factors, for instance vascular endothelial growth factor (VEGF) produced in this process, stimulate the proliferation of endothelial cells to ensure that there is a sufficient supply of nutrients and oxygen throughout a tumour.

Secondly, endothelial cells are commonly used in invasive niche research involving blood-brain barriers due to the formation of tight junctions between cells. A study showed that VEGF-A along with transforming growth factor-β (TGF-β) and tumour necrosis factor-α (TNF-α) were secreted by primary tumour cells to induce the expression of inflammatory chemokines (Hiratsuka, Watanabe, Aburatani, et al., 2006). Such chemokines promoted cell migration from distal sites as well as increased the permeability of endothelial cells (Hiratsuka, Watanabe, Sakurai, et al., 2008; Wang, Luo, et al., 2014).

Lastly, the reciprocal relationship between the neural stem cell niche and the vascular niche was identified in two-dimensional (2-D) monolayer and animal models (Palmer et al., 2000; Park et al., 2003; Nern and Momma, 2006). Within a tumour, proliferating neural stem cells (NSCs) and endothelial cells are found in clusters adjacent to blood vessels. Several studies showed that mouse embryonic cortical neurons and cultured NSCs expressed VEGF and its receptors both *in vitro* and *in vivo* (Ogunshola et al., 2002; Jin et al., 2002; Maurer et al., 2003). This finding is in agreement with other studies that reported the enhancement of neuronal differentiation, migration and viability when co-cultured with endothelial cells.

Strikingly, the same trophic effect was not observed in other cells such as fibroblasts and astrocytes (Leventhal et al., 1999; Shen et al., 2004).

Although endothelial cells are commonly used in cancer models, a three-dimensional (3-D) *in vitro* co-culture model with NSCs has not been reported elsewhere. As a continuation from the last chapter, a 3-D hydrogel *in vitro* model of encapsulated human pluripotent stem cell (hPSC)-derived NSCs, and human umbilical vein endothelial cells (HUVECs) were further developed. Several factors such as: seeding densities, media ratios and interactions between NSCs and HUVECs were investigated to identify a suitable microenvironment for the co-culture. The 3-D recapitulation of the interactions between these two cell types that primarily involve the formation of niches in neuroblastoma will bring us closer to understanding the disease mechanisms and eventually overcoming the challenges faced in therapeutics.

4.2 Materials and methods

This section primarily describes the development of a 3-D *in vitro* NSC-HUVEC co-culture model and explains different methods for the characterisation of the developed 3-D *in vitro* co-culture model. This work was continued from the study in the previous chapter, in which the properties of hydrogel were optimised for the development of the 3-D *in vitro* co-culture model.

As a preparation, NSC (Axol, UK) and HUVEC cells (Lonza, UK) were cultured using the same protocols as previously described in Chapter 3 (see Section 3.2.1). The HyStem® hydrogel (Sigma-Aldrich, UK) was also prepared in the same manner as previously described in Chapter 3 (see Section 3.2.2).

4.2.1 Co-culture model development

The 3-D *in vitro* co-culture models of NSC and HUVEC cells were developed based on the findings in Chapter 3. Protocols for monoculture model development can be referred to Chapter 3 (see Section 3.2.3).

NSCs seeding from cryopreservation

NSCs were thawed from frozen, centrifuged and re-suspended in the neurobasal medium (NBM) (Lonza, UK) supplemented with 1% penicillin-streptomycin (Sigma-Aldrich, UK) and 2% B-27 (Sigma-Aldrich, UK). The suspension was then immediately seeded onto a culture plate or into a fragmented HyStem® hydrogel.

Two-dimensional model

For co-culture experiments, it was essential to consider the optimal environment suitable for culturing NSCs with HUVECs. Thus, the optimisation of cell seeding and media ratios were performed. The wells in a 24-well plate were initially pre-coated with 1% laminin (Sigma-Aldrich, UK) in phosphate-buffered saline (PBS) (Sigma-Aldrich, UK) in the same manner as in 2-D monoculture models (see Section 3.2.3). Both NSCs and HUVECs were trypsinised to obtain suspensions and plated in triplicates at the ratios of 100:0; 75:25; 50:50; 25:75; 0:100 percent respectively, with the total seeding density of 10,000 cells per well (50,000 cells/cm^2). For each well of different cell seeding ratios, it was treated with 1 mL of different ratios of the culture media; NBM (Lonza, UK) and EGM-2 (Lonza, UK) of the ratios: 100:0; 75:25; 50:50; and 0:100 percent.

Three-dimensional model

The 3-D *in vitro* neural cancer model was constructed based on the results obtained from the previous optimisation experiments. Microwells were initially prepared in the same manner as in 3-D monoculture models (see Section 3.2.3). Fragmented HyStem® hydrogel was prepared with only 0.5 mL degassed water added to both Glycosil® and Extralink 1®. 100 μL of laminin, 400 μL of NSC-HUVEC suspensions in 3:1 ratio and 500 μL of HyStem® were added together before vortexed then centrifuged at 1800 rpm for 3 minutes to obtain a cell-hydrogel mixture (see Figure 3.1C). The mixture was then injected to fill up each microwell and covered with a nylon mesh. Each well was treated with 1 mL of the EGM-2 medium before incubated at 37°C, 5% CO_2. The setup of the model is illustrated in Figure 4.1.

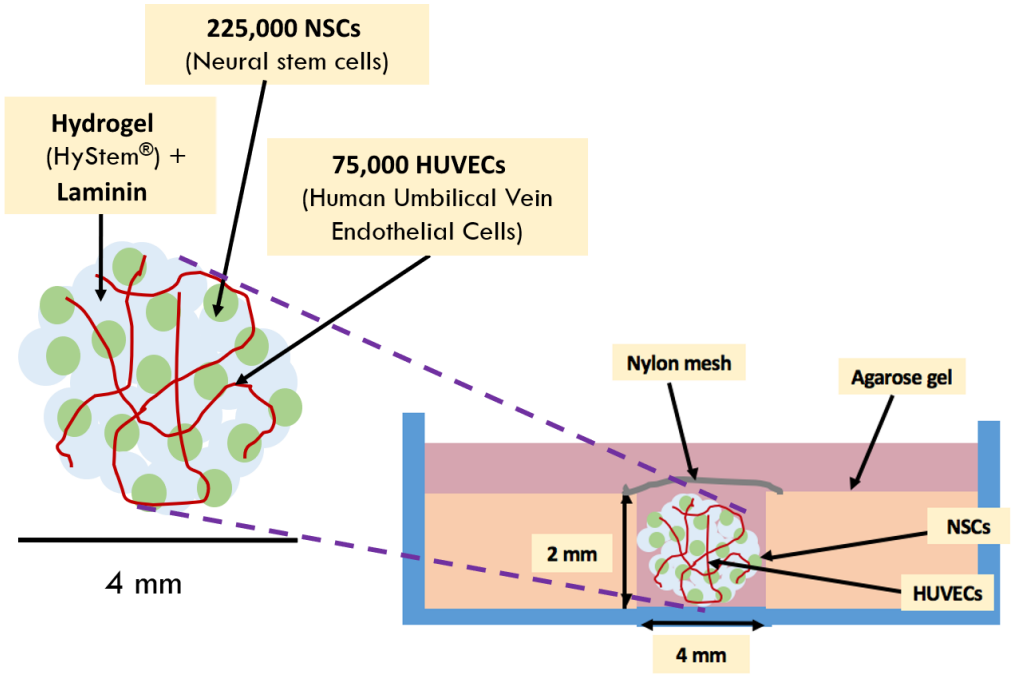


Figure 4.1: Schematic representation of 3-D *in vitro* neuroblastoma model. Cross-sectional view. NSCs were co-cultured with HUVECs, which were incorporated into the model to represent tumour angiogenesis. Cells were encapsulated within a fragmented HyStem® hydrogel and seeded into a 4 mm diameter × 2 mm depth agarose gel microwell inside a 24-well plate. A nylon mesh was put on top of the microwell to keep the model in place. Cell seeding density = 1 million cells/mL.

4.2.2 Cell immunostaining

Immunostaining assays were conducted to determine the changes in expression of different cell surface markers. All reagents were purchased from Sigma-Aldrich, UK. Cells were initially washed with PBS before fixed with 100 μL of 4% paraformaldehyde (w/v) in PBS. After 1 hour, samples were rinsed with 500 μL of wash buffer (0.2% bovine serum albumin and 0.2% Triton w/v in PBS) three times with 5 minutes interval between each wash, then 500 μL of blocking buffer (5% bovine serum albumin and 0.2% Triton w/v in PBS) was added to block any unspecific binding sites of samples. Cells were incubated with 100 μL of primary antibodies: 1:1000 (1 μg/mL) chicken Nestin or 1:1000 (1 μg/mL) anti-Ki67; 1:2000 (0.5 μg/mL) mouse TuJ1 and 1:200 (5 μg/mL) rabbit CD31 added to each well overnight at 4°C. The dilution factors for antibodies were provided by results of the optimisation experiments from previous studies (Turaç et al., 2013; Orlova et al., 2014).

On the next day, samples were rinsed three times with a wash buffer before added 500 μL of secondary antibodies solution to each well. Samples were incubated in the dark at 4°C overnight before imaged under the laser confocal microscope (Nikon Eclipse Ti, Nikon, Japan).

4.2.3 Image analyses

Image analyses of 3-D cultures were performed in the same manner as outlined previously in Chapter 3 (see Section 3.2.8 and Appendix A for more details on image analysis procedures).

2-D culture analyses were performed using MATLAB through processes that our laboratory has developed and analysed in OVCAR8-HUVEC co-cultures (Wan, Bovornchutichai, et al., 2017).

Figure 4.2 shows the block diagram outlining the processes of background correction and image segmentation. The 2-D images were initially taken from the microscope at 3,488 x 2,616 pixels. Their resolutions were then reduced by 25% to 872 x 654 pixels to reduce the computation resource required for image segmentation. Each image was initially pre-processed to correct an uneven illumination in the background using the polynomial correction technique. This is because, in some images, the cells were off-centre with respect to the light source of the microscope. As seen in Figure 4.3A, the illumination of these images tends to run from dark to bright. Therefore, the background was corrected using a polynomial fitting method.

Firstly, the background was separated from the cells using the entropy filtering method in which the entropy of each pixel was calculated from its 9-by-9 neighbourhood (Russ, 2011). These entropy values were then manually thresholded to create a binary mask containing the background and cells. A morphological close operation with a disc-shaped structuring element with a radius of 8 pixels was then used to fill the holes inside cells of a binary mask. The cells were then subtracted from the image using the binary mask and filled their spaces up with the pixel values from their boundaries. This extracted the background from the image before it was least-square fitted to a 4^{th}-degree polynomial. This gave an output of an

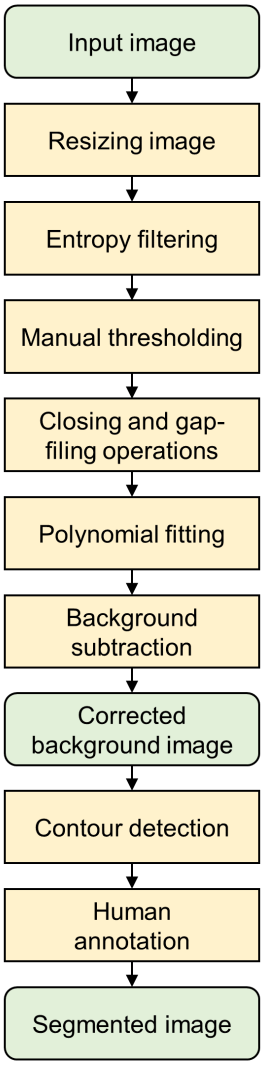


Figure 4.2: Flowchart outlining the processes of background correction and image segmentation The 2-D input image was initially resized to reduce the computational resource required for analyses. Then, it passed through an entropy filter, a manually-set threshold, close and fill operations. The background was extracted from the image and fitted to a 4^{th}-degree polynomial to give the corrected background image that made cell segmentation easier. Segmentation was performed using a combination of contour detection and semi-automated annotation. This gave rise images that distinguished different cell types from the background.

estimated background illumination, which was subtracted from the input image to provide the image with corrected background illumination. This pre-processing step created a sharper contrast between the cells and the background, which allowed the segmentation of cells to be more accurate (see Figures 4.3A and B).

Cell segmentation was performed using contour detection and hierarchical image

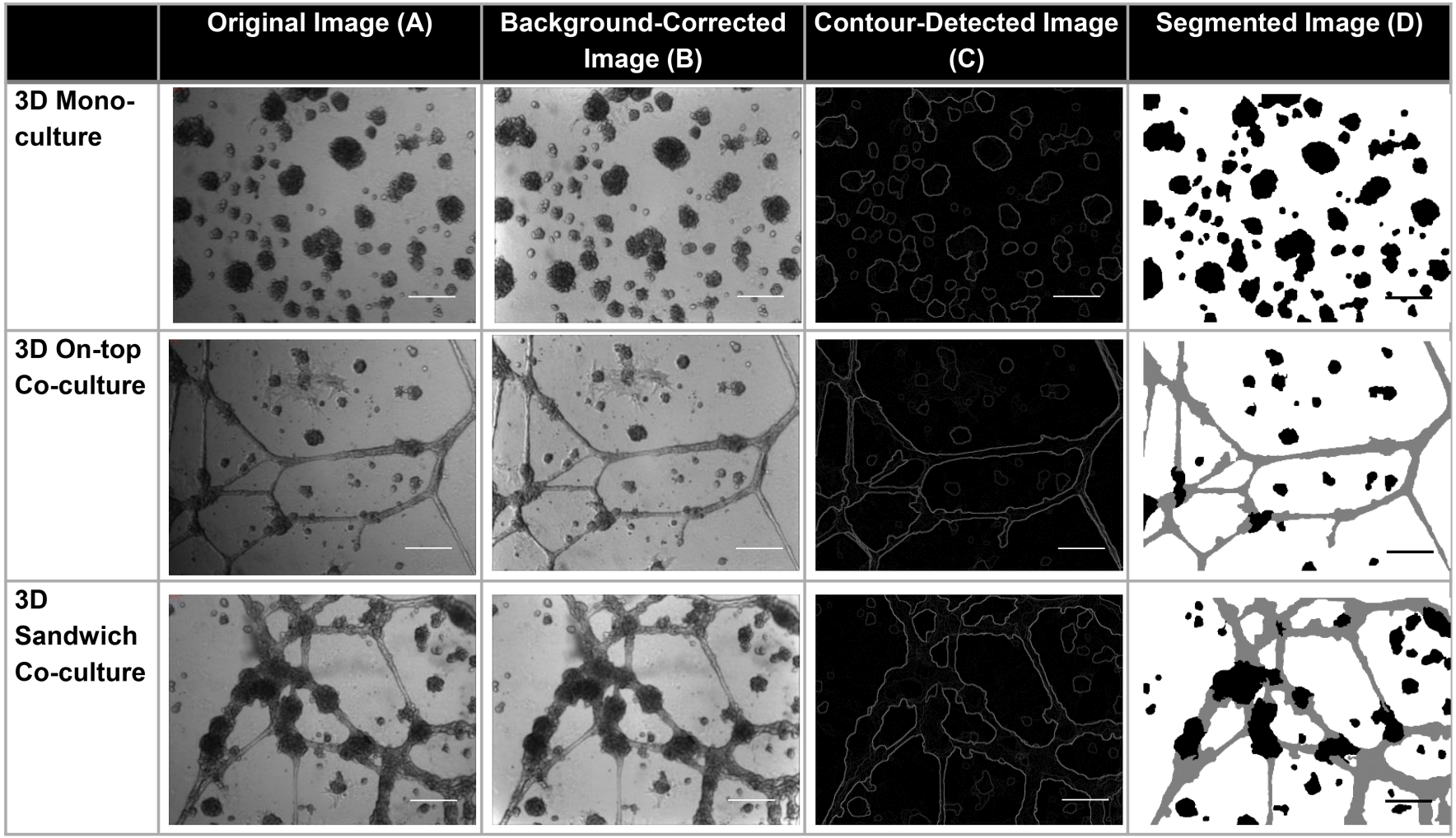


Figure 4.3: Image analysis procedures used for 2-D images (A) The original bright field images of 3-D mono-culture of OVCAR8 cells, on-top co-culture of OVCAR8 cells and HUVECs, and 3-D co-culture of OVCAR8 cells and HUVECs; (B) Background corrected images of each original image; (C) Different contour lines detected in each background corrected image; (D) Segmentation of spheroids (in black colour) and tubules (in grey colour) in each image. Scale bar = 100 μm.

segmentation technique (Arbeláez et al., 2011). This technique detects different contour intensities within the image. The contour intensities were then transformed into a hierarchy of regions (see Figure 4.3C). As most automated systems for tubule-structure segmentation mainly focused on monocultures (Delibasis et al., 2010; Barber et al., 2003) this method is useful for images with more than one irregular-shaped type of cells.

After detecting the cells' contours, the cells and the background were segmented from the image based on human-drawn annotations. The annotations were automatically propagated to nearby unlabelled regions resulting in user-specified segmentations. These were refined until high-quality segmentations of cells were yielded (see Figure 4.3D). Pixels classified as cells were summed up to give the total number of cells.

Nonetheless, the aim of image analyses in this study was not to create a software to automatically segment different cells from each other and the background, but rather to use them as a pipeline to assist the quantification of the respective cellular areas.

4.2.4 Statistical analysis

All experiments were performed independently with three replicates, reported as mean (M) ± standard deviation (SD). GraphPad Prism 6.0© software was used to illustrate graphical results as well as to perform t-test and ANOVA with Tukey's post-hoc analysis to detect significant differences between culture groups. A significant value (α) of 0.05 was used to determine significance between groups.

4.3 Results and discussion

In this section, several optimisation experiments were conducted, i.e. the investigation of seeding NSCs straight from cryopreservation into the model and the optimisation of co-culture medium and seeding ratios. Later, the work shifted to investigate the neurovascular interactions between NSCs and HUVECs before using all the data acquired to construct a 3-D *in vitro* NSC-HUVEC co-culture model.

4.3.1 Seeding NSCs from cryopreservation

Main finding

NSC seeding from cryopreservation was feasible.

The low viability of NSCs, as often up to 50% cell death, was observed when thawed from frozen. A further decrease in the viability of cells was observed when they were brought to culture on plates. The investigation was conducted to see whether it was possible to thaw and seed cells straight away from frozen into hydrogels and if this would maximise the number of viable cells in culture.

Figure 4.4 shows the z-stack distribution of NSCs throughout the hydrogel after 7 days of culture. The yellow arrow annotates one of the extended neurites observed within the gel.

The use of hPSC-derived NSCs in a cancer model provided us with the opportunity to mimic the cell-ECM interactions in native neuroblastoma accurately. However, the low cell viability remains to be the major limitation; even when the cells are cultured on a monolayer of laminin, the optimal substrate for NSCs culture (Flanagan et al., 2006). A study reported that only 55% cell viability was observed for adult human hepatocytes after cryopreservation (Rijntjes et al., 1986). As the NSCs are not as resilient as cancer cell lines, they were seeded straight away into 3-D hydrogels after thawed from cryopreservation to maximise the number of living cells in culture. The feasibility of this method was supported by a study by Kruyt et al. (2004), in which a significant amount of bone area or surface area

coverage of formation within the porous scaffold (14.0 ± 2.0%) was observed after 9 weeks compared to the devitalised scaffold control (0.2 ± 0.3%); when bone marrow stromal cells were seeded straight away into scaffolds and implanted into goats. Besides, the amount of bone area observed in cryopreserved cells was comparable to the one seen in cultured cells (11.5 ± 4.7%). The observation justified the establishment of cell seeding from cryopreservation as a valid technique for seeding into 3-D scaffolds and circumvented the need to grow in culture.

Another point to mention regarding this method, apart from the reduced viability of the cells, is the removal of dimethyl sulfoxide (DMSO) from the cryotubes before seeding cells into a hydrogel. DMSO is commonly used as a cryopreservation agent

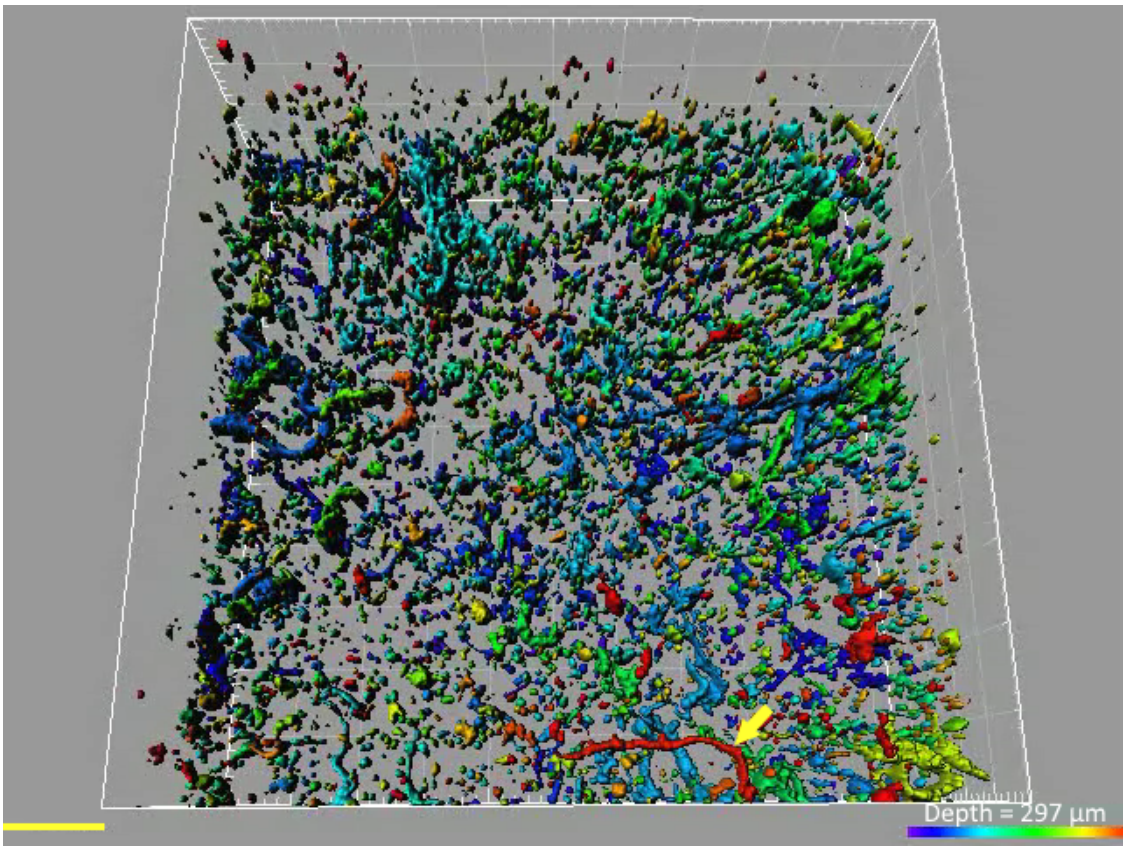


Figure 4.4: Neural stem cells cultured in 3-D HyStem® after seeded from cryopreservation NSCs viability was maintained after 7 days of culture when seeded instantly from cryopreservation in 3-D HyStem®. Neurite outgrowth was also observed in culture (see yellow arrow). NSCs were seeded at 10 million cells/mL in the HyStem® hydrogel. The gel was cultured for 7 days before imaged under a laser confocal microscope. Depth colour coding is used to highlight the depth of the cells within HyStem®. Scale bar = 150 μm.

to protect cells from the formation of ice crystals during freezing. However, it is also cytotoxic to the cells themselves. Therefore, the cryotubes were centrifuged once thawed, removed the supernatant and re-suspended the cell pellet in a fresh medium. This approach minimises the cell culture toxicities associated with the DMSO.

4.3.2 Optimisation of co-culture media and seeding ratios

Main finding

The NSC-HUVEC co-culture was optimal at 3:1 seeding density ratio, feeding with 100% EGM-2 medium.

HUVECs were incorporated into the model to introduce vasculature, which enhanced the diffusion of nutrients and oxygen from the surroundings into the hydrogel. As co-culture conditions affect both neurite outgrowth and angiogenesis, optimal cell seeding and media ratios need to be determined.

Figure 4.5 shows different seeding ratios of NSC-HUVEC co-cultures treated in different ratios of NBM:EGM-2 media. After 7 days of 2-D laminin monolayer culture, co-cultures were stained with TuJ1, Nestin and CD31 antibodies, representing mature neurons (blue), neural stem cells (red) and endothelial cells (green) respectively.

Morphological results illustrate that HUVECs formed tubule-like structures at any ratios of NBM:EGM-2 media, while an increase in neurite growth was observed when the ratio of NBM:EGM-2 media decreased. As the greatest proportion of neurite outgrowth was observed when NSCs were cultured under 100% EGM-2 medium, these results justified the choice of EGM-2 as the co-culture medium.

For seeding ratio, neurite extension was observed when the ratio of NSC: HUVECs increased whereas angiogenesis was observed surrounding NSCs for all 25:75, 50:50 and 75:25 ratios of NSC-HUVEC co-cultures. Since the main cell type in the model is NSC, it is preferable to maximise the neurite extension within the model, while allowing angiogenesis to take place simultanesouly. These findings

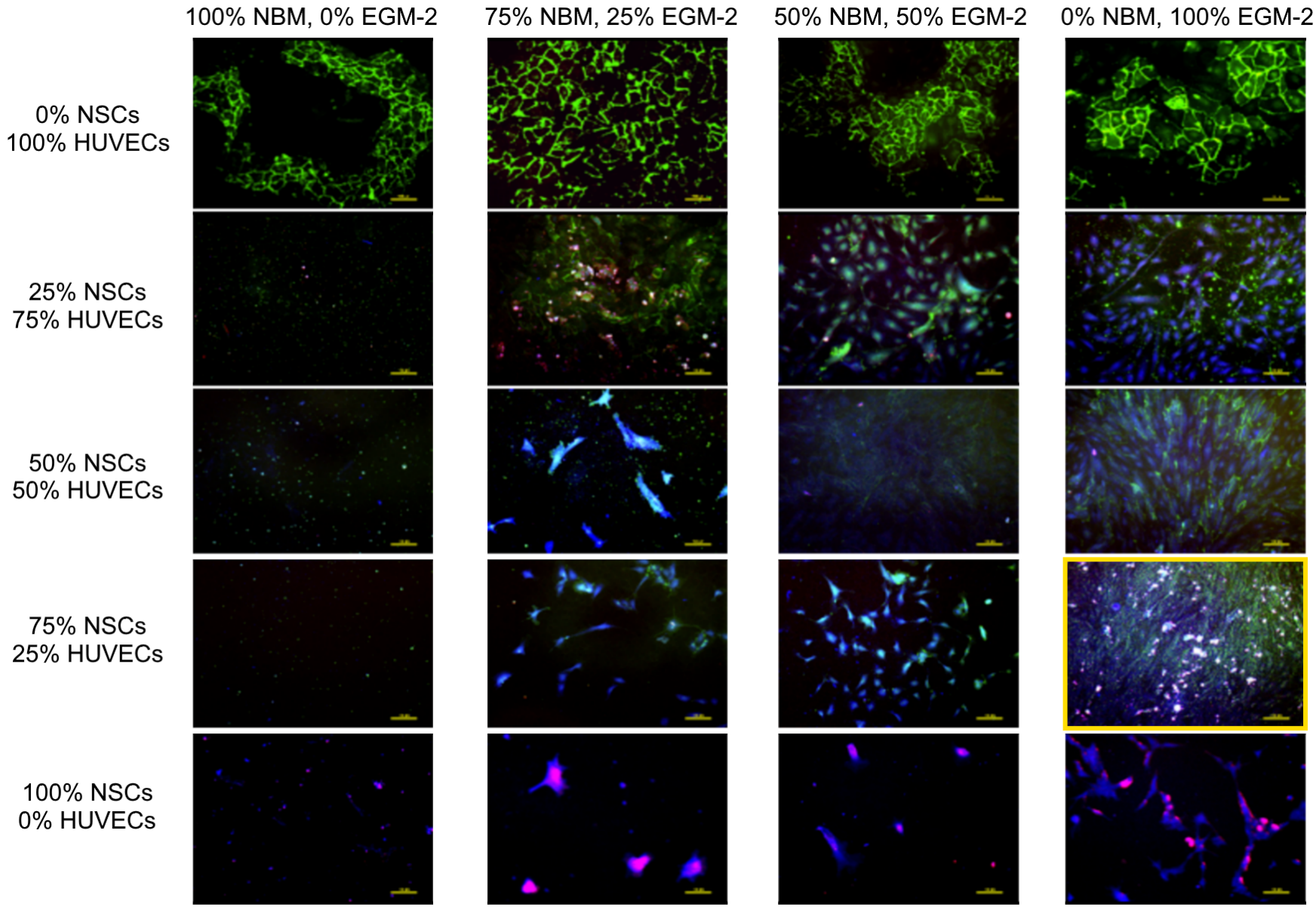


Figure 4.5: Optimisation of co-culture medium and seeding ratio Different cell morphologies were observed between different seeding ratios of NSCs and HUVECs cultured in different ratios of NBM and EGM-2 media. Co-cultures were stained after 7 days of 2-D laminin monolayer culture with TuJ1 (blue), Nestin (red) and CD31 (green) antibodies. The seeding ratio of 3:1 (NSCs:HUVECs) and 100% EGM-2 medium were selected for the 3-D co-culture model (yellow box). Cell seeding density = 45,000 cells/cm^2. Scale bar = 100 μm.

Table 4.1: Comparison of supplements between NBM and EGM-2 media

Supplement	Amount in 500 mL of NBM (ng)	Amount in 500 mL of EGM-2 (ng)
bFGF	2	20
hEGF	2	2.5
Ascorbic Acid	3,520	500
Hydrocortisone	–	40
Heparin	–	11,250

determined the choice of 75:25 or 3:1 seeding ratio of NSCs-HUVECs in the model (See yellow box, Figure 4.5).

The common composition of both NBM and EGM-2 media was investigated further to provide explanations to the results above. Common components in both media are listed in Table 4.1.

Table 4.1 demonstrates the higher concentrations of basic fibroblast growth factors (bFGF) and human epidermal growth factors (hEGF) in an EGM-2 medium than in a NBM medium. The receptors of both growth factors are co-expressed in stem-like cells in a subventricular zone of a mammalian forebrain and support their expansion (Gritti et al., 1999). Also, the high concentrations of other supplements such as: hydrocortisone (40 ng/500 mL medium) and heparin (11,250 ng/500 mL medium) were only included in the EGM-2 medium.

A study showed that hydrocortisone promoted NSC proliferation, including $MAP2^+$ neurons, in a dose dependent manner (Ninomiya et al., 2014), whereas a positive correlation between the concentration of heparin and the adhesion and proliferation of human adipose-derived stem cells was observed as well (Kim et al., 2013). The dose-dependent effect of heparin on NSCs is however, still unknown.

Nonetheless, ascorbic acid appears to be the only supplement that is presented in a higher concentration in NBM (3,520 ng/50 mL medium) than in EGM-2 medium (500 ng/500 mL medium). Ascorbic acid enhances differentiation of embryonic stem cells into neurons as it modulates genes responsible for cell adhesion and growth (Shin et al., 2004). However, it is possible that the concentrations of

ascorbic acid in both media are not significantly different enough or the effects of ascorbic acid on NSC-HUVEC co-cultures are not as strong as other supplements, which results in an extensive neurite outgrowth observed after treatment with high ratios of EGM-2 to NBM medium.

4.3.3 Investigation of neurovascular interactions

Main finding

The number of proliferating neurons increased significantly when cultured with HUVECs.

To further examine the interactions between NSCs and HUVECs observed in the seeding ratio experiments, NSCs and HUVECs were co-cultured in 3:1 ratio on top of a laminin monolayer (2-D culture) for 7 days. Cells were fixed and stained for TuJ1 (red) and Nestin (blue) after the culture period. NSCs were identified as cells co-expressing Nestin and TuJ1, whereas mature neurons were identified as cells expressing TuJ1 only. In parallel, the same co-culture experiment was performed but with TuJ1 (red) and Ki67 (blue) stains. This helped to identify further the proportion of NSCs-neuronal lineages undergoing cell division.

Morphological images shown in Figure 4.6A indicate red network extensions of neurites observed alongside spherical NSCs, coloured in purple (implying the co-staining of both TuJ1 and Nestin markers) in Nestin-TuJ1 stain group. This was also in accordance with Ki67-TuJ1 group, where neurite extensions expressed TuJ1 in red and other spherical-shaped cells co-expressing TuJ1 and Ki67 in purple were observed.

Results shown in Figure 4.6B quantify significant increases in the number of NSCs and mature neurons when co-cultured with HUVECs, compared to the NSCs monoculture control. This is further supported by analysis in Figure 4.6C where there was a significant increase in proliferating cells in co-culture compared to monoculture.

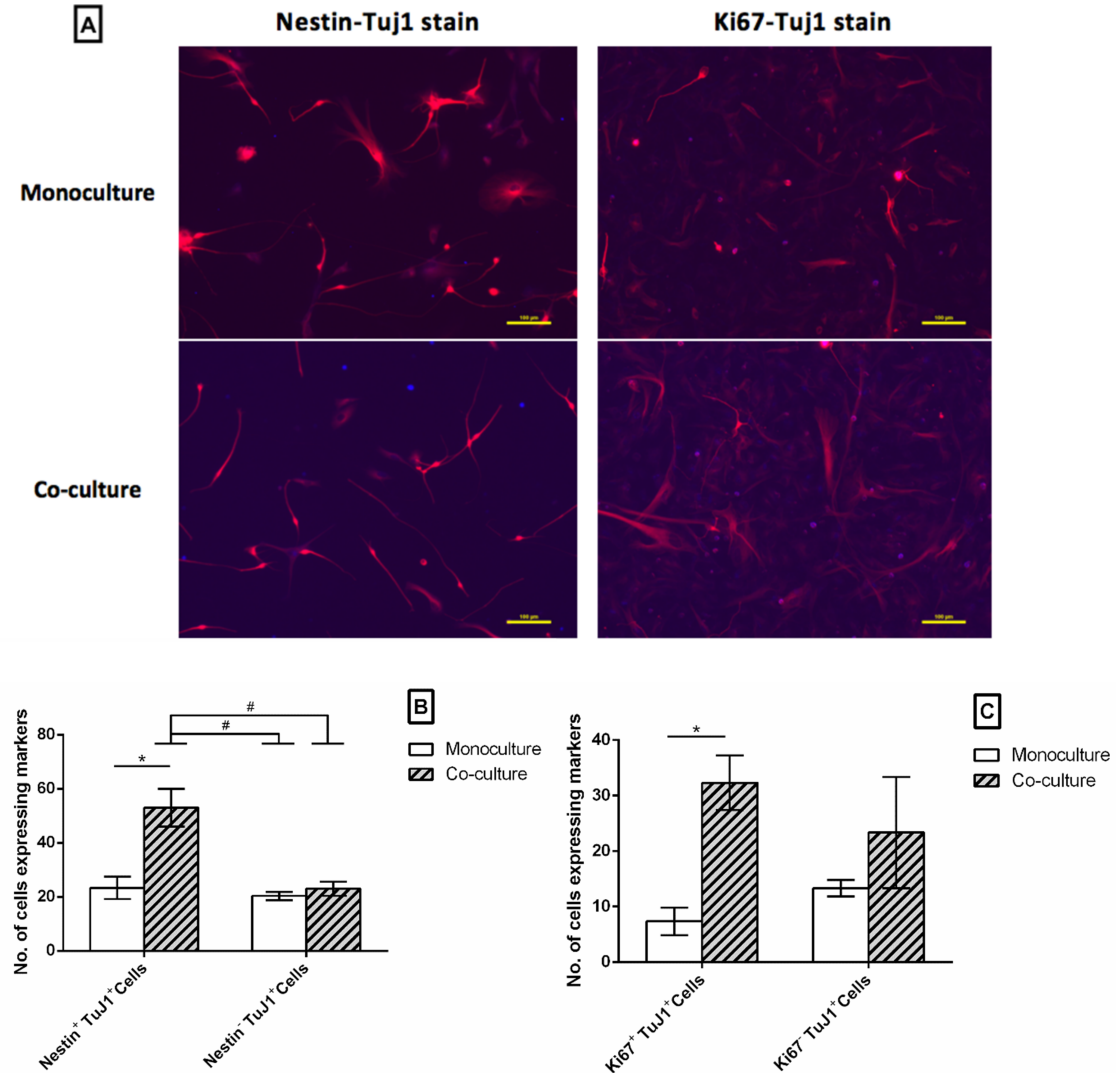


Figure 4.6: Evaluation of neurovascular interactions between NSCs and HUVECs Compared to NSC monocultures, co-cultures of NSCs and HUVECs exhibited significant increases in the number of NSCs and proliferating neurons. An NSC-HUVEC co-culture was performed in parallel with NSC monoculture, both on 2-D laminin monolayer for 7 days. Cell seeding densities = 33,750 cells/cm^2 NSCs and 11,250 cells/cm^2 HUVECs. (A) NSC morphologies from both monocultures and HUVEC co-cultures were stained with TuJ1 (red) and Nestin or Ki67 (blue). These represented neuronal lineages and NSCs (in Nestin-TuJ1 stain) or proliferating cells (in Nestin-Ki67 stain) respectively. Scale bar = 100 μm; (B) Further analyses were performed to quantify the number of cells co-expressing Nestin and TuJ1 as well as; (C) cells co-expressing Ki67 and TuJ1, cultured in parallel. Values are mean ± SD; n = 3 per group. Statistical analysis was performed by ANOVA with post-hoc analysis. $^{\star}p < 0.05$ vs Ki67$^+$TuJ1$^+$ expressing cells in monoculture. $^{\sharp}p < 0.05$ vs Ki67$^+$TuJ1$^+$ expressing cells in co-culture with HUVECs.

It is speculated that both HUVECs and NSCs could modulate their microenvironment by producing growth factors and receptors; which related to the process of neurogenesis involving the active recruitment and remodelling of vasculature (Nern and Momma, 2006; Palmer et al., 2000; Park et al., 2003). VEGF is one example of growth factors secreted by HUVECs and stimulates the growth of NSCs (Carmeliet, 2003). Perhaps, the incorporation of HUVECs into the model favour NSC proliferation than differentiation into mature lineages.

4.3.4 Characterisation of 3-D *in vitro* co-culture model

Main finding

The proliferation of HUVECs and differentiation of NSCs into neurons were observed after 14 days of culture.

Optimisation results in earlier sections provided us with the method of seeding of cells from cryopreservation, the technique of dispersing cells throughout the hydrogel, the selection of hydrogel for the 3-D neuroblastoma model, the effects of hydrogel crosslinking density and the fragmentation model as well as the seeding ratio of 3:1 (NSC:HUVEC) and EGM-2 as a co-culture medium. All the information obtained above was used to develop a 3-D *in vitro* co-culture model.

NSC-HUVEC co-cultures in fragmented HyStem® gel were prepared and cultured in a microwell (see Figure 4.1) before stained with TuJ1, Nestin and CD31 antibodies after 3, 7 and 14 days of culture. Cell morphologies and marker expressions were analysed through the laser confocal microscope (Nikon Eclipse Ti, Nikon, Japan) and image analyses software (AutoQuantX3 and Imarisx64).

Cell morphologies in Figure 4.7A display an increase in the number of CD31-expressing cells over 14 days. In addition, cells were observed to migrate towards the centre of the hydrogel after day 7. This may indicate cell signalling that form cell clusters to enhance their growth and form microenvironmental niches. 4X close-up shots in Figure 4.7A focus on the TuJ1-expressing cell or an NSC undergoing differentiation. It was evident that the cell were increasing in size after 7 days

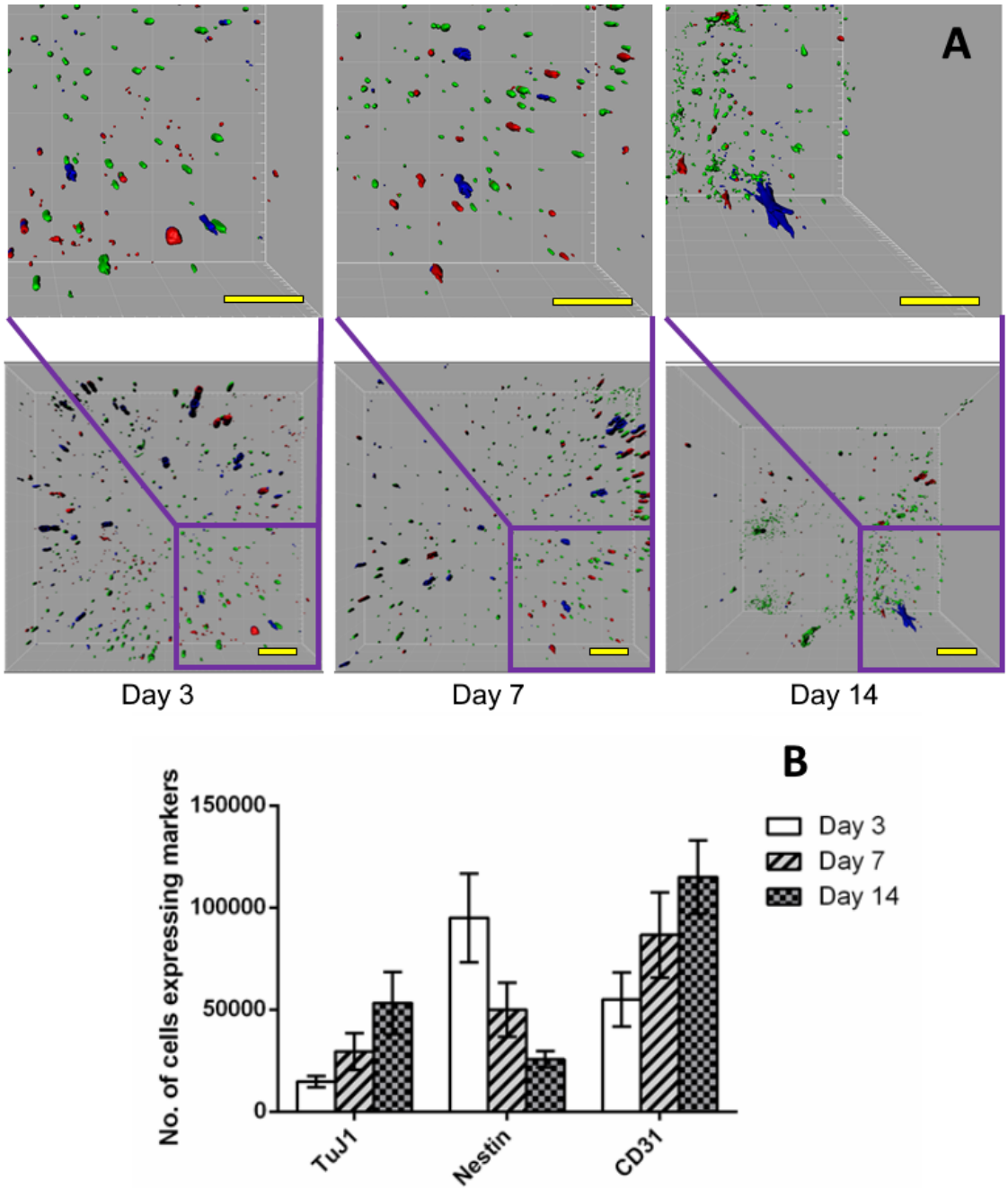


Figure 4.7: Characterisation of the 3-D *in vitro* NSC-HUVEC model A significant increase in the expression of CD31 and a significant decrease in the expression of Nestin were observed in an NSC-HUVEC 3-D co-culture model after 14 days of culture. NSCs and HUVECs were cultured in 3:1 ratio, embedded within 0.8% fragmented HyStem® as an encapsulated model. (A) Z-stack cell morphologies illustrate the expression of TuJ1 (blue), Nestin (red) and CD31 (green) antibodies after 3, 7 and 14 days of culture in an EGM-2 medium. 4X close-up shots are provided to clearly show the morphology of NSCs undergoing differentiation. Cell seeding density = 1 million cells/mL. Scale bar = 100 μm; (B) Bar graphs quantitatively represent the marker expressions at each time point. Values are mean ± SD; n = 3 per group. Statistical analysis was performed by ANOVA with post-hoc analysis.

and formed small projections after 14 days of culture. It is speculated that cells could migrate under an external stimuli or towards different, yet physiologically relevant cells that were co-cultured. A study by Chung et al. (2009) observed that MTLn3 cancer cells attracted endothelial cells towards themselves and induced these endothelial cells to form capillaries.

Figure 4.7B shows the relative expression of each marker in the model. The increases in TuJ1 and CD31 expressions were observed after 14 days of culture, whereas a decrease in Nestin expression was observed. The reduction in Nestin expression was due to the loss of proliferation potential of NSCs and the increase in the differentiation capacity of these stem cells into mature neurons ($TuJ1^+$ cells) over the culture period. In addition, HUVECs proliferated over 14 days, which led to the increase in CD31 expression. The results above were confirmed by z-stack morphological images shown below.

The biophysical properties of the hydrogel and the biochemical composition of the co-cultures are equally vital for cell fate determination. Therefore, it requires several optimisation experiments to develop the 3-D *in vitro* model. HyStem® was selected as the choice of hydrogel not just because of its high cell viabilities for both NSCs and HUVECs, but also because of its ease to manipulate its stiffness and induce fragmentation.

The incorporation of HUVECs introduced angiogenesis to the model, which aided the diffusion of nutrients and oxygen gradients. The interactions between NSCs and HUVECs were also evident. Growth factors secreted by NSCs might have paracrine effects on HUVECs and induced an increase in proliferation, migration and formation of tubule-like structures in the same manner that was observed in U87-HUVEC co-culture models in other studies; even though cells were not physically in direct contact (Chen, Htay, et al., 2009; Khodarev et al., 2003).

The 3-D interactions between NSCs and HUVECs in Figure 4.7 justify the symbiotic interactions between NSCs and HUVECs, which support each other to expand in culture space and environment. The 2-D co-cultures in Figures 4.5 and 4.6 confirm this hypothesis further, in which significant increases in the number of NSCs

and proliferating neurons were observed when co-cultured with HUVECs, compared to NSC monocultures. These findings demonstrate the potential of utilising this 3-D *in vitro* model to predict neuroblastoma *in vivo* responses.

4.4 Conclusion

In conclusion, this chapter discussed the development of a 3-D *in vitro* NSC-HUVEC co-culture hydrogel model. This was based upon optimisation of both biophysical properties from Chapter 3 and biochemical compositions from this chapter.

NSCs can be seeded straight from cryopreservation to maintain the number of viable cells. In co-culture with HUVECs, the cell seeding ratio was optimised at 3:1 (NSCs:HUVECs) cultured in 10% EGM-2 medium. Preliminary experiments in 2-D cultures showed the reciprocal neurovascular interactions between NSCs and HUVECs as there were significant increases in the number of stem cells and proliferating neurons in co-culture compared to the monoculture of SH-SY5Ys.

The 3-D crosstalk between NSC-HUVECs and cells-ECM determined cellular behaviours including motility, morphology as well as proliferation and differentiation capacities. The model did not just highlight the interactions between NSCs and HUVECs in 3-D but also provided a more specific yet ease-to-monitor recapitulation of the microenvironment of native tissues.

This co-culture crosstalk can be further extended to neuroblastoma cancer model development, which the interactions of cancer stem and HUVECs can be explored to further our understanding of the disease and sought for therapeutics that gives the optimal outcomes for the patients.

As our current 3-D *in vitro* NSC-HUVEC can be maintained for at least 14 days, another route to explore would be to further extend the cell viability by culturing inside a perfused bioreactor. Perfusion allows better transport of oxygen and nutrients to the model, which provides an opportunity to utilise the model as a 3-D *in vitro* drug screening platform and identify any effects of drug candidates in a matter of months, rather than weeks or days. Nevertheless, this 3-D *in vitro* co-culture model has potential in representing neuroblastoma drug responses observed *in vivo*.

5

Perfused bioreactor recapitulating a neuroblastoma microenvironment

Table of contents

5.1 Introduction 104
5.2 Materials and methods 105
5.2.1 Cell culture 105
5.2.2 Bioreactor design 105
5.2.3 Flow rate calibration 106
5.2.4 Hydrogel scaffold preparation 108
5.2.5 Neuroblastoma model 108
5.2.6 Perfusion culture setup 108
5.2.7 Static 3-D culture 111
5.2.8 pH measurement 111
5.2.9 Waste metabolite analyses 111
5.2.10 Cell viability 113
5.2.11 Cell immunostaining 113
5.2.12 Image analyses 113
5.2.13 Statistical analysis 113
5.3 Results and discussion 113
5.3.1 Cell characterisation in perfused bioreactor and static culture systems 114
5.3.2 Evaluation of cell viability in perfused bioreactor and static culture systems 119
5.3.3 Analyses of metabolites in perfused bioreactor and static culture systems 120
5.3.4 Analyses of pH in perfused bioreactor and static culture systems 123
5.4 Conclusion 125

5.1 Introduction

The three-dimensional (3-D) *in vitro* neural-endothelial cells co-culture model provides specific aspects of the native neuroblastoma, especially the 3-D neurovascular interactions. However, the microenvironment surrounding the tumour itself is still not accurately recapitulated. The lack of flow within the system limits the delivery of nutrients and dissolved oxygen from the medium into the inner parts of the model.

Here, the perfusion culture system is developed to provide a continuous and steady peristaltic flow of EGM-2 medium through the 3-D *in vitro* model. It is anticipated that perfusion culture would extend the cells' viability and maintain their integrity for much longer than static culture. Perfusion culture is also predicted to affect other surrounding factors contributing to the model's microenvironment such as metabolite levels and pH.

Due to the difficulties in the culturing process, the neuroblastoma cell line, SH-SY5Ys are used in this work and other subsequent experiments instead of neural stem cells (NSCs). SH-SY5Ys should still display the neurovascular interactions with the human umbilical vein endothelial cells (HUVECs) as previously observed with NSCs in the previous work (see Figure 4.6).

This chapter covers the development of the bioreactor and the perfusion culture system. The neuroblastoma model is cultured inside this developed system for 21 days. In parallel, the same model is also cultured under static conditions as a control. Endpoints of the experiment including cell morphologies, marker expressions and cell viabilities are assessed every 7 days. Waste medium samples are collected every other day for metabolite analyses and pH measurements.

5.2 Materials and methods

This section first outlines the cell culture protocol of SH-SY5Y cells before focuses on the design of the modified TissueFlex® bioreactor and the perfusion culture system. Methodologies of different experimental endpoints are described towards the end of the section.

5.2.1 Cell culture

Due to the difficulties in the culturing process of neural stem cells (NSCs), SH-SY5Ys neuroblastoma cell line was co-cultured with human umbilical vein endothelial cells to create a 3-D neuroblastoma model.

SH-SY5Y cells

SH-SY5Y neuroblastoma cells were purchased from ATCC, UK. Cells were cultured in Roswell Park Memorial Institute 1640 medium (RPMI) (Sigma-Aldrich, UK) with 10% FBS (Sigma-Aldrich, UK), 1% MEM Non-essential amino acid solution (Sigma-Aldrich, UK) and 1% penicillin-streptomycin (Sigma-Aldrich, UK). Cells were thawed and centrifuged at 1000 rpm for 5 minutes before re-suspended in 3 mL supplemented RPMI medium. The cell suspension was added to a pre-warmed flask containing 3 mL supplemented RPMI medium before incubated at 37°C, 5% CO_2. The medium was refreshed every 3-4 days and cells were sub-cultured once they reached 80-90% confluence.

Human umbilical vein endothelial cells (HUVECs)

HUVEC cells were cultured in the same manner as outlined previously in chapter 3 (see Section 3.2.1).

5.2.2 Bioreactor design

To facilitate the culture in 3-D, the mould for casting multiple parallel perfused bioreactors was designed and developed (see Figure 5.1). This design was a modification of TissueFlex® (Zyoxyel Ltd, UK) microbioreactors. Made changes

included the enlargement of the reactor size from a 96-well plate to a standard 24-well plate. Furthermore, the positions for the inlet and outlet ports were at different heights, i.e. the outlet port was in a higher position to allow the turbulent flow of the medium through the bioreactor and enhance the uptake of oxygen and nutrients by the cells. The designed single bioreactor could facilitate up to four parallel cultures.

A mixture of the PDMS polymer and the crosslinking reagent (Sylgard 184 silicone elastomer, DowCorning, UK) in a ratio of 10:1 was poured into the designed mould and incubated overnight at 60°C. Once cast, the PDMS bioreactor was removed from the mould, treated with 3% Pluronic F68 solution (Sigma-Aldrich, UK) for overnight then autoclaved before used in experiments.

5.2.3 Flow rate calibration

The flow rate of the medium through the bioreactor should reflect the flow of nutrients inside the neuroblastoma patient. The total volume of cerebrospinal fluid in children is 50 mL. The turnover of the entire volume is $3-4$ times per day, which sums up to around $150-200$ mL/day (Plunkett and Cross, 2014).

Since the volume of each 3-D neuroblastoma model is 150 μL, this corresponds to the cerebrospinal fluid turnover rate of around $450-600$ μL/day. However, the peristaltic perfusion system operates in rounds per minute (rpm), the system needs to be calibrated to identify the flow rate that matches the turnover rate.

The flow rate of the peristaltic pump was varied (0.5, 1, 2, 3, 4 and 5 rpm) and for each flow rate, the volume of the medium was collected after one hour to establish a calibration curve.

The calibration curve in Figure 5.2 shows that to achieve a turnover rate within a range of $450-600$ μL/day, the pump needs to be operated at 0.01 rpm. At this rate, the volume of medium collected after one hour was 23 μL, which was equivalent to around 500 μL per day.

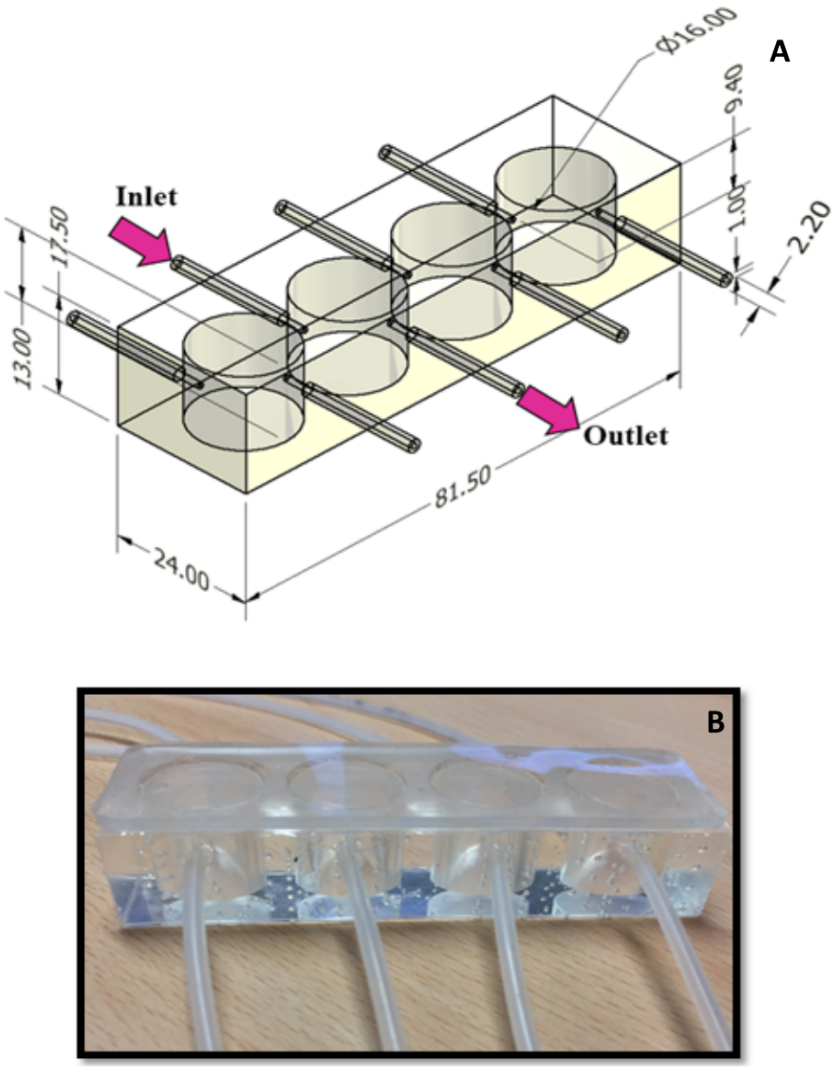


Figure 5.1: The PDMS bioreactor for 3-D neuroblastoma model perfusion culture (A) Schematic illustration of the PDMS bioreactor; (B) Photograph of the PDMS bioreactor. The design was modified from TissueFlex® to a 24-well plate format. Gas permeable PDMS was cast into the mould to create the bioreactor. Fresh medium was driven from an inlet to an outlet located at a higher position to ensure there were no dead spots during culture. Units are in mm.

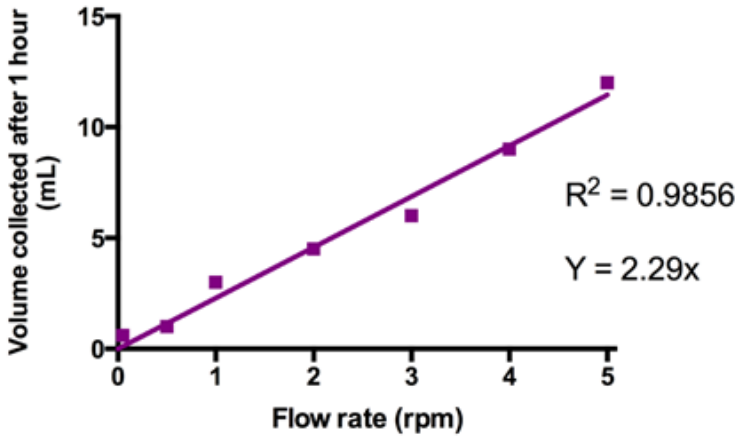


Figure 5.2: Standard curve relating the flow rate to the volume of medium collected The peristaltic pump was calibrated to determine the flow rate that matches the turnover rate of the cerebrospinal fluid in children ($450 - 600$ μL/day).

5.2.4 Hydrogel scaffold preparation

The HyStem® hydrogel was prepared and fragmented in the same manner as described previously in chapter 3 (see Section 3.2.2).

5.2.5 Neuroblastoma model

Inside a cell-culture hood, SH-SY5Ys and HUVECs in 3:1 ratio suspended in 400 μL of EGM-2 medium were added to 100 μL of laminin and 500 μL of fragmented HyStem® gel in an Eppendorf tube. This gave the total cell seeding density of 1 million cells/mL. The tube was vortexed and centrifuged at 1800 rpm for 3 minutes to remove any bubbles. 150 μL of the gel mixture was added inside a 24-well cell-culture insert with a polytetrafluoroethylene (PTFE) membrane attached to the bottom of the insert (Millicell, UK). In each well of the bioreactor, there was one cell insert placed inside and filled up with 1 mL of an EGM-2 medium. The reactor's lid was sealed up before started the experiment outside the cell culture hood. The setup of the model is illustrated in Figure 5.3.

5.2.6 Perfusion culture setup

Each bioreactor was perfused with an EGM-2 medium supplied from an ice-containing reservoir through silicone rubber tubings (transwall thickness 0.8 mm;

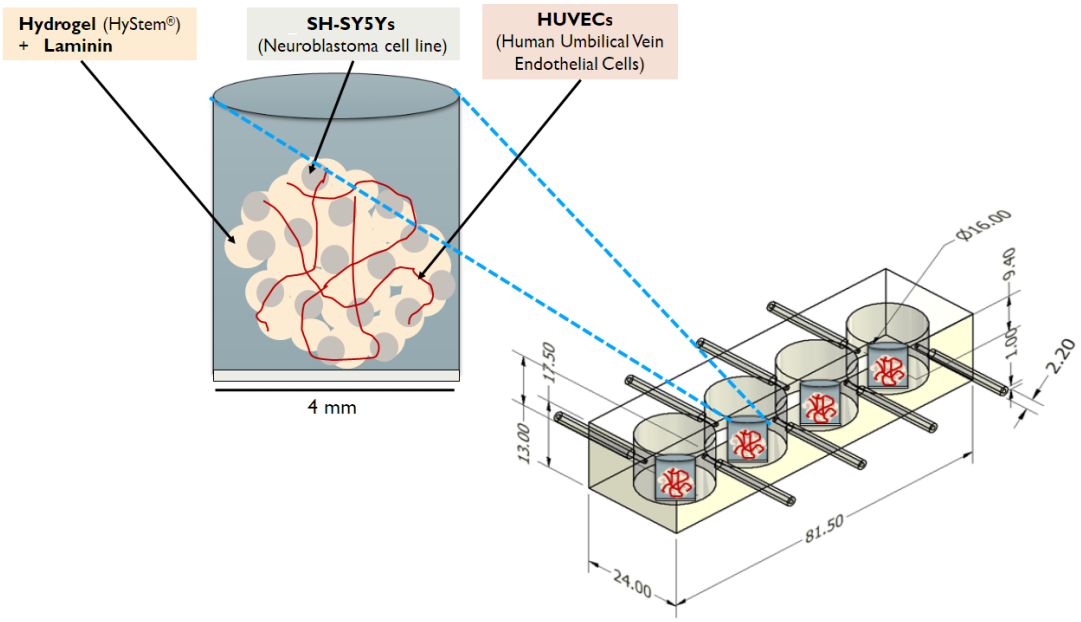


Figure 5.3: The neuroblastoma model inside the cell culture insert SH-SY5Y cells and HUVECs were cultured in fragmented HyStem® in a 3:1 ratio. The total volume of the cell-gel suspension was 150 μL. Gels were seeded inside a PTFE membrane cell insert then sealed with a PDMS cap to keep the cells in place. The entire set up was placed inside each well of the PDMS bioreactor.

inner diameter 0.8 mm; outer diameter 2.4 mm) (Silex, UK) and phthalate-free polyvinyl chloride (PVC) bridge pump tubings (inner diameter 0.64 mm; bridge distance 150 mm) (Gradko, UK). The ice inside the chilled reservoir was replaced every other day to keep the medium chilled throughout.

The PDMS bioreactor containing the neuroblastoma model was placed inside an incubator, maintained at 37°C with a constant pump of 5% CO_2 air. The airflow was provided by an external gas cylinder connected into the incubator. A multichannel peristaltic pump (Minipuls 3 M312, Gilson, USA) drove the medium perfusion in each channel at the rate of 0.01 rpm, which was calibrated earlier in Section 5.2.3. The waste medium from the bioreactor was collected every other day and stored in a -80°C freezer for metabolite and glucose assays.

To prevent any laminar flow within the reactor, the bioreactor was placed on top of an orbital shaker operating at 30 rpm to enhance mixing. Microfilters were placed at the ports of fresh medium and waste medium reservoirs to prevent the gas pressure built up within the system. In addition, a water-containing beaker

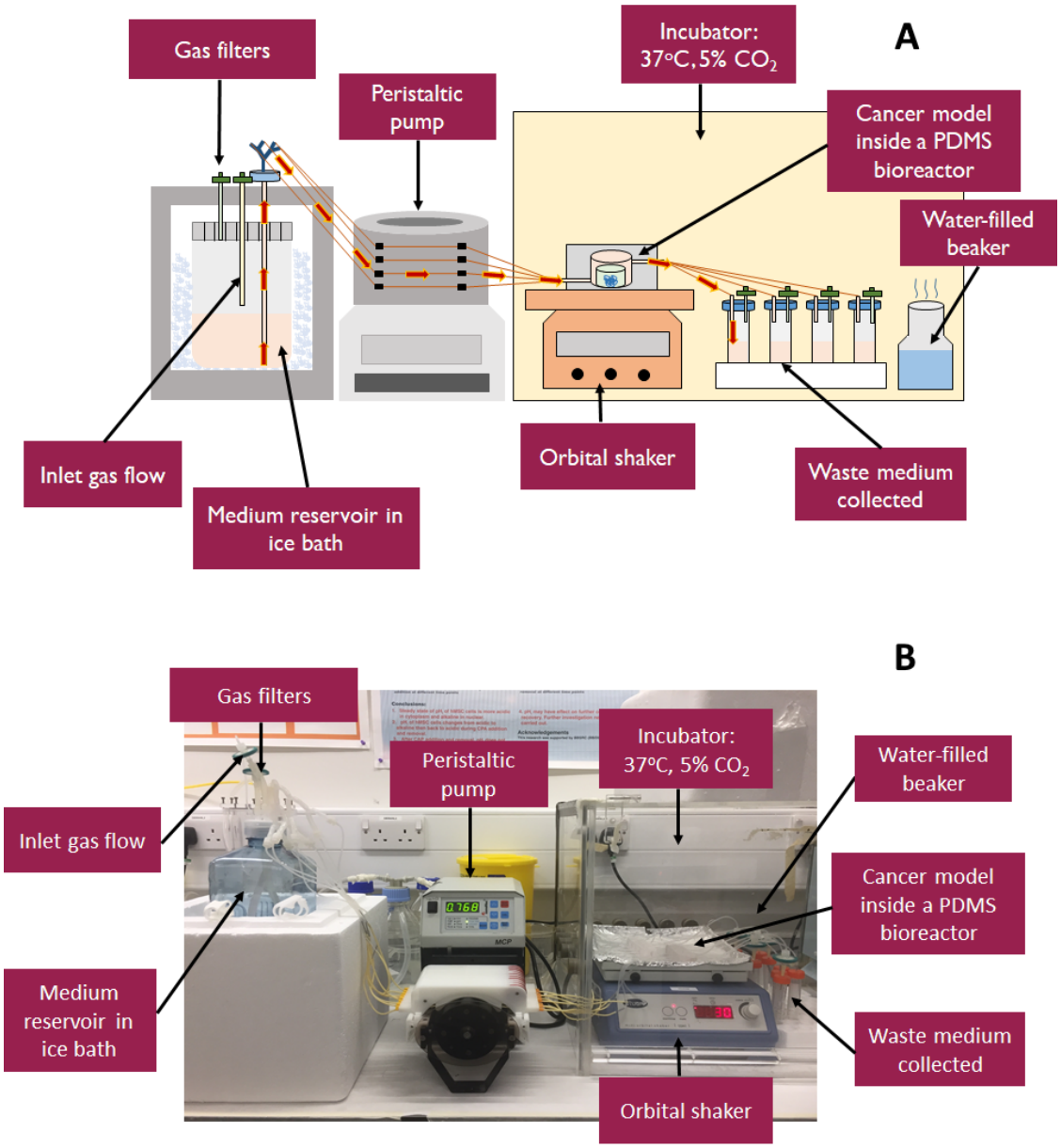


Figure 5.4: The 3-D perfusion culture system (A) Schematic illustration of the 3-D perfusion culture system; (B) Photograph of the actual perfusion culture system. Fresh medium was peristaltically pumped from a chilled reservoir into the PDMS bioreactor inside the incubator. The PDMS bioreactor was placed on top of an orbital shaker to enhance mixing of the medium. Gas filters were installed in fresh and waste medium reservoirs to prevent any pressure building up. A water-filled beaker was placed inside the incubator to maintain the vapour pressure equilibrium. The waste medium was collected every other day for metabolite analyses.

was placed inside the incubator to provide humidity in the system to avoid any disruption to the vapour pressure equilibrium within the bioreactor. The entire setup of the system is shown in Figure 5.4.

5.2.7 Static 3-D culture

For static controls, the cell inserts containing the neuroblastoma model were cultured inside the PDMS bioreactor without ports, within a tissue culture incubator at 37°C, 5% CO_2. Every other day, 1 mL of medium was replenished, which was equivalent to an outflow rate of 500 μL/day in perfusion culture. The waste medium was collected for an immediate pH measurement, then stored in a -80°C freezer for metabolite and glucose assays after the completion of the experiment.

5.2.8 pH measurement

Optical microsensor was chosen to measure pH of the waste medium as the system only requires small volumes (1 mL) to provide an accurate readout. Initially, the pH probes and optical microsensor (PreSens, Germany) were calibrated with pH standards (Sigma-Aldrich, UK) and compared readouts with a benchtop pH meter (Mettler Toledo, Hogentogler, USA). pH probes were placed at the bottom of each well; right beneath the cell culture insert containing the neuroblastoma model. Every two days, the pH of both static and perfusion cultures were measured using a pH optical microsensor (PreSens, Germany). The sensor was connected to the UNICORN 7.0 control software (GE Healthcare, UK), which read out the corresponding pH values. Each reading was recorded when the pH displayed on screen was stable for at least 10 seconds. For static cultures, the waste medium was collected and measured for its pH, before the culture medium was replenished.

5.2.9 Waste metabolite analyses

Waste media from both static and perfusion cultures were collected every two days to analyse the changes of three metabolite levels: glucose, VEGF and BDNF.

Glucose assay

Medium samples collected from both static and perfusion cultures were analysed for glucose concentration in duplicates using a glucose assay kit (Abcam, UK). The standards and samples were prepared, and the concentrations were measured following the manufacturer's protocol. In brief, a standard curve was initially prepared from 6 different glucose standard volumes (0, 6, 12, 18, 24 and 30 μL). Waste medium samples were thawed, diluted at 1:50 with glucose assay buffer and deproteinised by using a 10kD spin column (Abcam, UK). The spin column was centrifuged at 10,000 x g for 10 minutes before the filtrate was collected. After that, 50 μL of the reaction mix was prepared and added to 50 μL of each filtrate and control sample, incubated for 30 minutes at 37°C in the dark. Finally, absorbance was measured at OD570 nm and referred to the standard curve to determine the corresponding glucose concentration in each sample. Glucose concentrations were expressed as mM.

VEGF and BDNF ELISA assay

Medium samples collected from both static and perfusion cultures were also analysed for VEGF and BDNF levels in duplicates using an enzyme-linked immunosorbent assay (ELISA) kit (Abcam, UK). The standards and samples were prepared, and the concentrations were measured following the manufacturer's protocol. In brief, samples were thawed and diluted at 1:10 ratio. 50 μL of each sample or standard was added to appropriate wells before added 50 μL Antibody Cocktail to all wells, incubate at room temperature for 1 hour. After that, each well was aspirated and washed three times with 350 μL 1X wash buffer. 100 μL of 3,3',5,5'-Tetramethylbenzidine (TMB) Substrate was added to each well and incubated at 37°C in the dark for another 10 minutes. Finally, 100 μL Stop Solution was added before read OD at 450 nm. Both VEGF and BDNF levels were expressed as pg/mL.

5.2.10 Cell viability

To quantify the relative amount of living cells in culture, an analysis of the cell viability was performed. The medium was removed from each well, which was then washed once with PBS, and added with a solution of 500 μL of 1% calcein acetoxymethyl or calcein-AM (w/v)(Sigma-Aldrich, UK) in PBS solution was added. Three-dimensional models were removed from each bioreactor into a covered dish after 10 minutes of incubation for imaging under the laser confocal microscope (Nikon Eclipse Ti, UK).

5.2.11 Cell immunostaining

Each neuroblastoma model was fixed and stained at the end of the culture period to identify any markers for cellular proliferation and differentiation. The protocol was identical to the one outlined earlier in chapter 3 (see Section 3.2.7).

5.2.12 Image analyses

Image analyses of 3-D cultures were performed in the same manner as outlined previously in chapter 3 (see Section 3.2.8 and Appendix A for more details on image analysis procedures).

5.2.13 Statistical analysis

All experiments were performed independently with three replicates, reported as mean (M) ± standard deviation (SD). GraphPad Prism 6.0© software was used to illustrate graphical results as well as to perform t-test or ANOVA with Sidak's multiple comparison tests to detect significant differences between culture groups. A significant value (α) of 0.05 was used to determine significance between groups.

5.3 Results and discussion

To extend the viability of cells encapsulated within the HyStem® hydrogel, perfusion culture was introduced into the culture of 3-D *in vitro* neuroblastoma model. The perfusion culture system inside a PDMS bioreactor provided essential aspects of the

tumour microenvironment, i.e. circulatory system and enhancement of nutrients supply that could not be recapitulated in static cultures.

Encapsulated models of NSC-HUVEC co-cultures were cultured in a cell culture insert within a PDMS bioreactor (Figure 5.1) under a perfusion culture system (Figure 5.4). In parallel, samples were also cultured under static conditions inside a cell culture incubator. After 7, 14 and 21 days of culture, samples were stained with TuJ1 (blue), Nestin (red) and CD31 (green) antibodies. Cell morphologies and marker expressions were analysed through the laser confocal microscope and image analyses software. Furthermore, the waste medium was collected for pH measurement and metabolite analyses.

5.3.1 Cell characterisation in perfused bioreactor and static culture systems

Main findings

- SH-SY5Ys and HUVECs retained their single-cell morphologies throughout the culture period.
- SH-SY5Ys and HUVECs gradually migrated towards the centre of the hydrogel.
- The expressions for Nestin and CD31 increased significantly after 21 days.
- The expression for Nestin in perfusion culture was significantly higher than in static culture.

Analyses of cell morphologies

Figure 5.5 shows the 3-D z-stack images of neuroblastoma models after each respective endpoint. Both SH-SY5Ys and HUVECs cells retained their single cell morphologies throughout 21 days of culture. There were no specific structures formed from both cell types under static and perfusion cultures.

This observation was in a contradiction with previous results in Figure 3.2 where tubule-like structures were formed from HUVECs after only a short period

of culture under laminin coating in two-dimensional (2-D) monolayer cultures and on top of Matrigel®.

A study by Li et al. reported the formation of vascular tubes by brain-derived endothelial cells upon co-cultured with NSCs (Li, Ford, et al., 2006). Another research also indicated the co-culture between endothelial cells and NSCs formed epithelial sheets with junctional contacts *in vivo* (Shen et al., 2004). These results suggest that the formation of tubule-like structures by endothelial cells is expected in both 2-D and 3-D cultures as it is widely accepted as evidence for *in vitro* angiogenesis.

Conversely, many studies also reported unsuccessful observations of cellular structures in 3-D. Magdeldin et al. (2017) reported a significant interconnected tubule-like

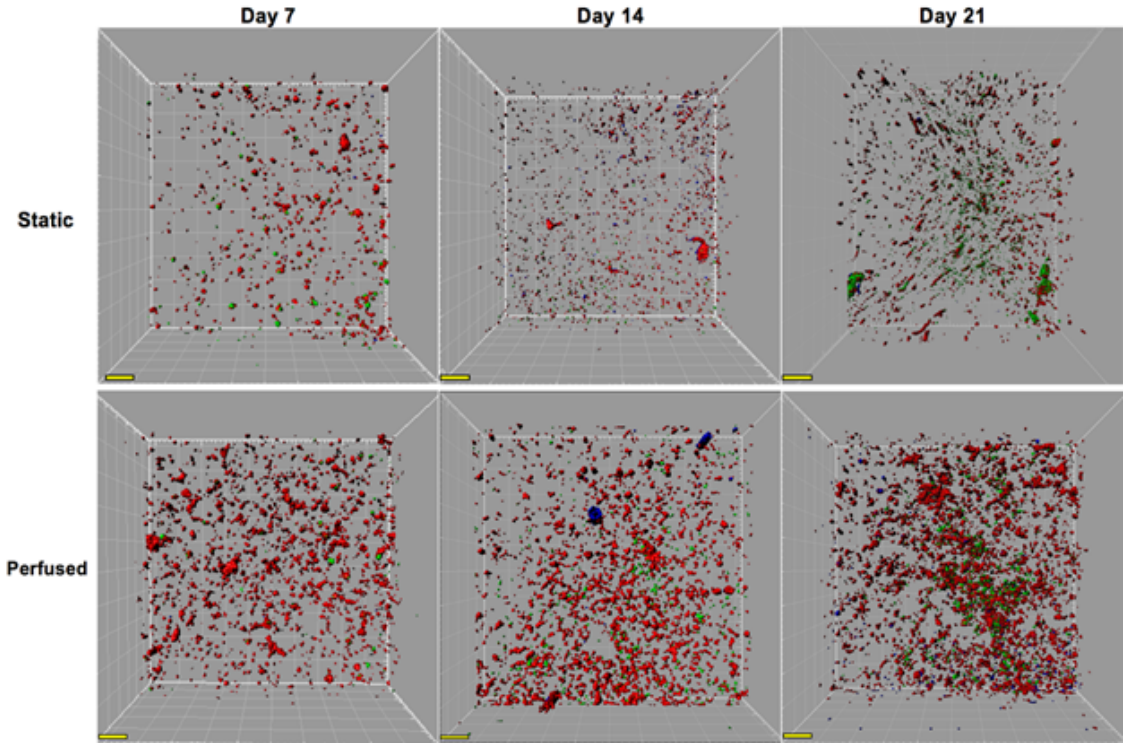


Figure 5.5: Comparisons between co-culture morphologies under static and perfusion culture systems SH-SY5Ys and HUVECs remained as single cells under both static and perfusion cultures and migrated towards the centre of the hydrogel after 21 days of culture. Z-stack cell morphologies taken with a laser confocal microscope of SH-SY5Ys and HUVECs illustrated the expression of TuJ1 (blue), Nestin (red) and CD31 (green) antibodies after 7, 14 and 21 days of culture in an EGM-2 medium under both static (top) and perfusion (bottom) conditions. Cell seeding density = 1 million cells/mL. Scale bar = 100 μm.

structures when laminin was incorporated into the 3-D collagen tumouroid compared to cultures without laminin. However, these highly branched networks were not observed in 3-D collagen-laminin tumouroid of HT29 and endothelial cells. The presence of cancer cells in the model led endothelial cells to instead aggregate into a cobblestone morphology.

In addition, the lack of neurite extension in the 3-D hydrogel was also reported in another study by Nakaji-Hirabayashi et al. (2009). Although the incorporation of BDNF significantly improved the survival of neurons and maintained its neural phenotypes, NSCs were observed as single cells when encapsulated inside a hyaluronan hydrogel (Nakaji-Hirabayashi et al., 2009).

The lack of tubule-like structures in this co-culture model may influence β-catenin signalling pathways, mode of cell division and notch activation as discussed in the literature (Shen et al., 2004). However, it is still questionable whether the tubule-like structures would serve any particular function in the model such as: facilitating the delivery of nutrients and gases in the medium and relating the integrity of these structures to angiogenesis *in vivo* (Li, Ford, et al., 2006; Thoma et al., 2014).

Analyses of cell distribution in hydrogel

As seen in day 7 samples in Figure 5.5, cells were initially dispersed throughout the hydrogel. However, cells migrated and predominantly resided towards the centre of the gel upon reaching day 21. This arrangement could be explained by the recruitment of endothelial cells from the centre of the hydrogel, where the supply of oxygen and nutrients from the medium was mostly required.

Within the central nervous system, the vascular niche secretes chemoattractant such as VEGF to attract more vessels to support the growth of inhabiting cells (Shen et al., 2004). On top of that, neurogenesis tends to occur nearby the blood vessels where the VEGF levels are the highest (Jin et al., 2002). The presence of neurons regulates the vessels' morphology and growth while the vessels provide oxygen and nutrients to the neurons in return. The vascular niche also guides nerves to respond to any microenvironmental changes (Park et al., 2003).

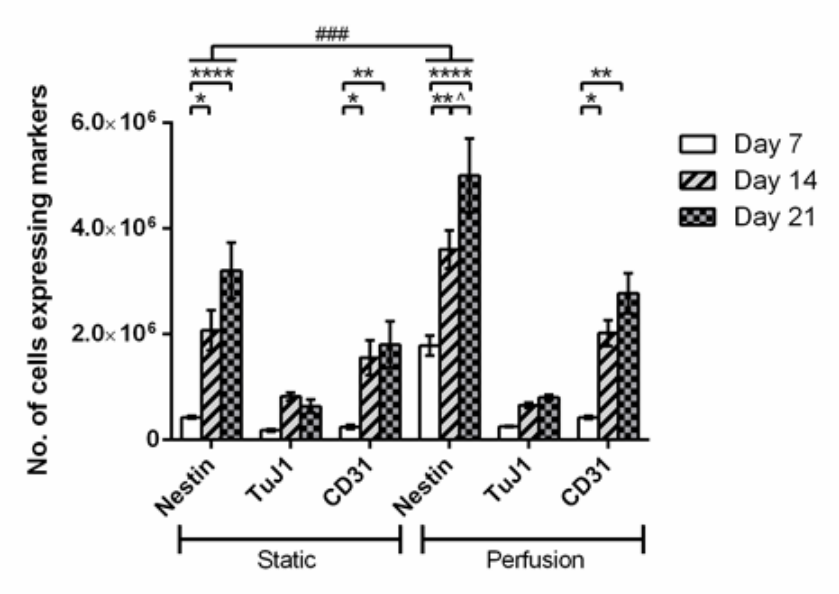


Figure 5.6: Quantification of marker-expressing cells under static and perfusion culture systems The expressions of Nestin and CD31 increased significantly after 21 days of culture. The overall expressions of Nestin under perfusion culture were significantly higher than ones cultured under static conditions. The bar graphs quantitatively represent the marker expressions at each time point. Values are mean ± SD; n = 3 per group. Statistical analysis was performed by two-way ANOVA with post-hoc analysis. $^{*}p < 0.05$, $^{**}p < 0.01$, $^{****}p < 0.0001$ vs cells expressing specific marker at day 7. $^{\wedge}p < 0.05$ vs cells expressing specific marker at day 14. $^{\#\#\#}p < 0.001$ vs cells cultured under static conditions.

Evaluation of marker expressions over the culture period

To extract quantitative data from 3-D z-stack images, the images of immunostained neuroblastoma models were analysed to show the relative expressions of each cell surface marker (see Figure 5.6). The expressions of Nestin, which represented undifferentiated SH-SY5Ys and CD31, which represented HUVECs increased significantly after 21 days under both static and perfusion cultures. The levels of TuJ1, which represented differentiated SH-SY5Ys, in both cases, remained stagnant after day 7. It is evident that cells were proliferating and retaining their stemness within the 3-D model.

The results could be explained by the interactions between HUVECs and SH-SY5Ys as there are many supporting evidence for reciprocal neurovascular interactions both *in vitro* and *in vivo* (Jin et al., 2002; Ogunshola et al., 2002; Maurer et al., 2003). Growth factors such as VEGF and BDNF are responsible for

the growth of NSCs and HUVECs as well as for the enhancement of these cells' outgrowth, differentiation and survival. They also inhibit stem cell differentiation while facilitate their self-renewal potentials (Carmeliet, 2003).

Evaluation of marker expressions between static and perfusion cultures

When comparing marker expressions between static and perfusion cultures, the expressions of Nestin in perfusion culture appeared to be significantly higher than in static. Several studies claimed that perfusion culture was advantageous over static cultures for numerous reasons such as enhancing delivery of oxygen and nutrients into cells, especially when they were encapsulated inside the hydrogel, through continuous flow and mixing (Cullen et al., 2007; Wan, Li, et al., 2016).

In addition, the replenishment of medium in static culture resulted in an instant change in the microenvironment, which induced oxidative stress and loss in cell viability. These changes made the investigation of cellular responses to drugs less accurate (Cui et al., 2007; Li and Cui, 2014).

The significant increase in the Nestin expressions over time, compared to TuJ1 can be explained by the use of PDMS in bioreactor design. Several studies reported that culturing cells inside a bioreactor cast from PDMS promoted proliferation of mesenchymal and embryonic stem cells and retained their stem cell potentials (Oh et al., 2005; Zhao and Ma, 2005).

5.3.2 Evaluation of cell viability in perfused bioreactor and static culture systems

Main finding

The number of live cells in perfusion culture was significantly higher than in static culture.

Although the increase in overall marker expressions indicated cellular growth, an additional stain with calcein-AM on separate samples was performed to confirm the cell viability. Upon counting the number of live cells in each sample, the number of cells in static culture increased significantly from day 7 to day 21 (see Figure 5.7). Meanwhile, the increase in the number of cells in perfusion culture over 21 days were not significant. However, the total number of cells in perfusion culture

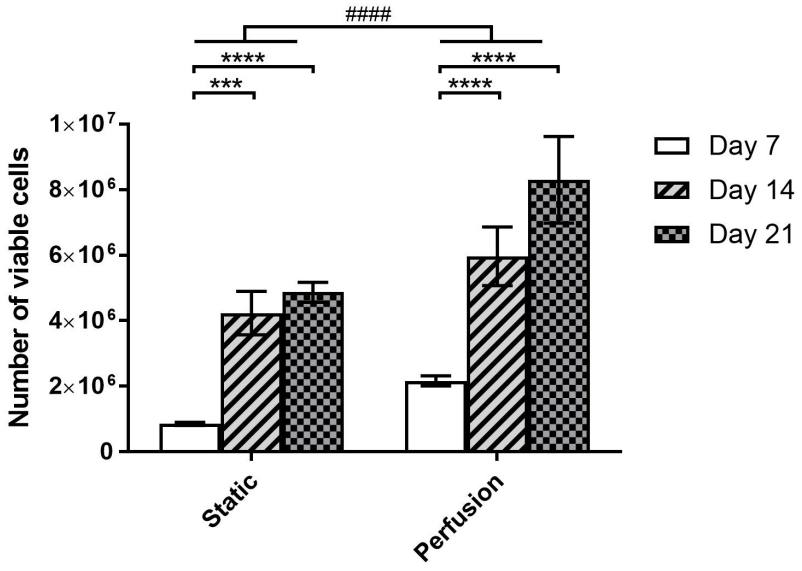


Figure 5.7: Comparisons of cell viabilities between static and perfusion cultures The number of viable cells increased significantly over 21 days under static conditions. However, the total number of viable cells cultured under perfusion was significantly higher than the one cultured under static conditions. Calcein-AM stained 3-D *in vitro* models after 7, 14 and 21 days of culture under both static and perfusion cultures. The bar graphs showed the number of viable cells encapsulated within the hydrogel. Values are mean ± SD; n = 3 per group. Statistical analysis was performed by two-way ANOVA with post-hoc analysis. ***$p < 0.001$, ****$p < 0.0001$ vs number of viable cells at day 7. $^{\#\#\#\#}p < 0.0001$ vs number of viable cells cultured under static conditions.

was significantly higher than in static counterparts since day 7 and maintained throughout the entire culture period.

The cell viability justified the findings regarding the increase in marker expressions over time, especially for static cultures. Overcoming the diffusional limitations while maintaining the stable culture microenvironment within the bioreactor was also the reason behind significant differences between the number of live cells in static and in perfusion cultures. This explanation is supported in a study where a significantly higher cell density of human mesenchymal stem cells was achieved under perfusion cultures, compared to cultures under static conditions for up to 40 days (Zhao and Ma, 2005). Similarly, another study reported a five-fold increase in embryonic stem cell density under perfusion culture compared to static counterparts after 6 days (Oh et al., 2005).

5.3.3 Analyses of metabolites in perfused bioreactor and static culture systems

Main findings

- Glucose concentration decreased sharply in the perfusion culture but remained stable in the static culture.
- The concentration of VEGF and BDNF were higher in perfusion than in static after 21 days.

In addition to immunostaining for markers and live cell number quantification, metabolite levels from cultures were also assessed. The waste media from both static and perfusion cultures were collected every other day for analyses. These levels were anticipated to reflect and provide further explanation to the results acquired in earlier experiments.

Analyses of glucose concentration

Figure 5.8 shows the changes in the glucose concentration in the waste medium for 21 days. The glucose level remained relatively stable at around 2.5 mM when

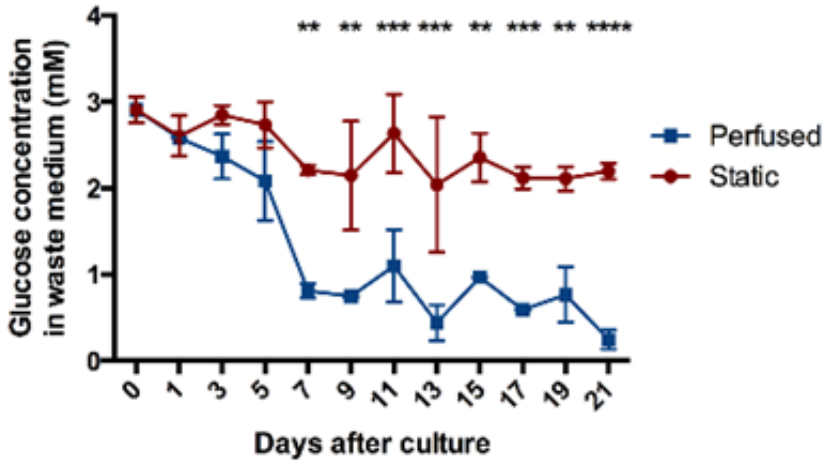


Figure 5.8: Analyses of glucose concentration in static and perfusion cultures A significant decrease in the glucose concentration was observed in perfusion culture after 21 days of culture. Waste media was collected from both static and perfusion cultures every 2 days and stored in -80°C freezer until the last medium sample from day 21 was collected. Results from a glucose assay show that the glucose concentration in perfusion culture decreased significantly after 7 days of culture, whereas the concentration in static culture remained at around 2.5 mM. Values are mean ± SD; n = 2 per group. Statistical analysis was performed by two-way ANOVA with post-hoc analysis. **p < 0.01, ***p < 0.001, ****p < 0.0001 vs glucose concentration under the static culture.

the 3-D model was cultured under static conditions. However, the glucose level dropped sharply after day 5 under perfusion culture.

The increase in the demand for glucose by the cells as they were rapidly expanding within the scaffold. This is in agreement with a study concluded that perfusion culture gave rise to a higher consumption rate of glucose as there was a higher cell density than in static counterparts (Xie, Hardouin, et al., 2006).

Analyses of VEGF and BDNF concentrations

The concentrations of waste metabolites secreted by cells such as VEGF and BDNF are shown in Figure 5.9. The level of VEGF in perfusion culture remained higher in static counterparts throughout 21 days. VEGF levels remained relatively stagnant at around 300 pg/mL under static culture conditions. However, under perfusion culture, the levels increased abruptly from approximately 500 pg/mL to 1000 pg/mL between day 7 and day 14 and retained at the high concentration until day 21.

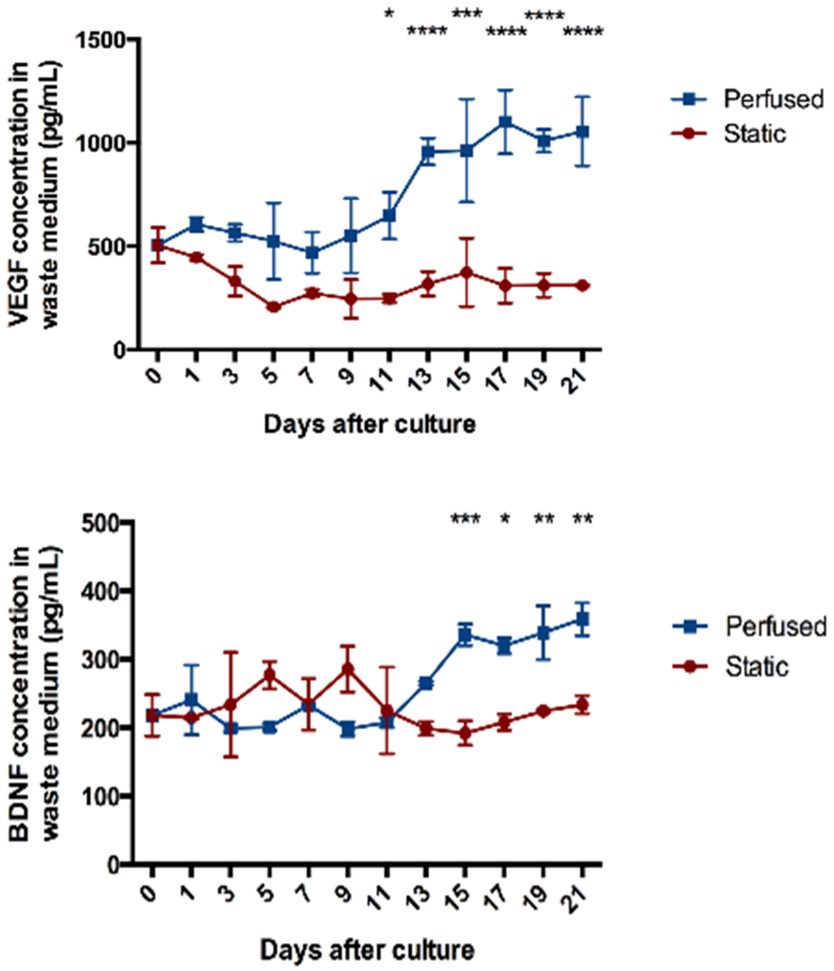


Figure 5.9: Analyses of VEGF and BDNF concentrations in static and perfusion cultures Significant increases in VEGF and BDNF concentrations were observed in perfusion culture after 21 days of culture. Waste media was collected from both static and perfusion cultures every 2 days and stored in -80°C freezer until the last medium sample from day 21 was collected. ELISA tests were performed to determine the concentrations of VEGF and BDNF over the culture period, where the protein concentrations increased significantly after 11 (VEGF) and 15 (BDNF) days of culture compared to static counterparts, respectively. Values are mean ± SD; n = 2 per group. Statistical analysis was performed by two-way ANOVA with post-hoc analysis. *p < 0.05, **p < 0.01, ***p < 0.001, ****p < 0.0001 vs VEGF or BDNF concentrations under static cultures.

On the other hand, the concentration of BDNF in the waste medium fluctuated around $200-300$ pg/mL for the first 11 days of culture, for both static and perfusion cultures. After day 11, the gap between the levels of BDNF in static and perfusion cultures started to increase when the BDNF concentration in perfusion increased.

The increase in the levels of VEGF and BDNF could be explained by the

increase in cell densities of SH-SY5Ys and HUVECs over time, which appeared to be significantly higher in the perfusion culture than in the static culture (see Figure 5.7). Hence, perfusion culture is preferable than static culture; the simulation of the human physiological system, the control and monitoring of environmental factors all contribute to providing a suitable microenvironment for these cells in hydrogel scaffolds- just like in native tumours. Ultimately, these factors stimulate the expansion of neurovascular niche; hence the secretion of growth factors and vice versa, as supported by previous studies both *in vitro* and *in vivo* (Leventhal et al., 1999; Jin et al., 2002; Li, Ford, et al., 2006).

5.3.4 Analyses of pH in perfused bioreactor and static culture systems

Main findings

- The pH inside the perfusion culture was more basic than inside the static culture.
- The pH rapidly decreased after two weeks of culture.

Evaluation of pH levels between static and perfusion cultures

Real-time measurements were made from the bioreactor every other day to track changes in the pH. For static cultures, the waste medium was collected every other day to measure its pH, before the culture medium was replenished. Figure 5.10 illustrates that the pH of the waste medium collected from the perfusion culture was more basic than the waste medium collected from the static culture.

Results show that there was a significant difference in the pH in static (mean = 7.755, SD = 0.177) and in perfusion cultures (mean = 7.535, SD = 0.259). These observations can be explained by the development of hypoxic regions by the cells at the centre of the neuroblastoma model. As shown in Figure 5.5, SH-SY5Ys and HUVECs migrated towards the centre of the model and underwent cellular respiration. With an increasing demand for oxygen in the core, yet oxygen cannot be transported adequately due to diffusional limitations, especially in static cultures

where bioreactor systems do not enhance oxygen uptake. Cells, therefore, undergo anaerobic respiration to produce lactate and carbon dioxide. As lactate builds up, it reduces the pH of the medium.

In addition, carbon dioxide produced by cellular respiration is highly soluble in water. It produces carbonic acid that ionises to H^+ and HCO_3^- ions. High carbon dioxide levels in the medium imply that there are more H^+ ions to decrease the pH of the medium.

In a perfusion culture system, oxygen is delivered to the core of the model easier due to enhanced mixing and the formation of eddies due to the induction of a turbulent flow inside the bioreactor. Therefore, perfusion culture is more efficient than static culture in keeping up with the increasing demands of nutrients and oxygen from cells. Cells tend to undergo aerobic respiration and produce less lactate to reduce the pH of the medium.

Evaluation of pH levels over the culture period

As shown in Figure 5.10, the pH of both static and perfusion cultures started to decrease after 2 weeks of culture. Since the pH levels correlate to the concentration

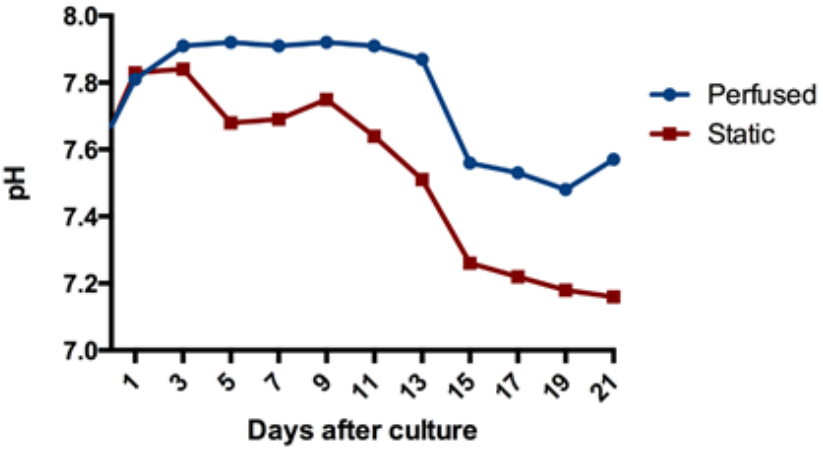


Figure 5.10: pH measurements in perfused bioreactor and static culture systems The pH inside perfusion and static cultures decreased gradually over time. The pH inside perfusion culture was more basic than one inside the static culture. pH measurements were performed for both perfusion and static samples with an optical probe and a sensor attached to the bottom of the PDMS bioreactors every two days. Values are mean ± SD; n = 3 per group. Statistical analysis was performed by paired two-tailed t-test.

of dissolved oxygen in the medium, the growth of cells encapsulated within the model increases the demand for oxygen especially at the core where necrotic regions are likely to be formed. The state of oxygen deprivation upregulates the expressions of hypoxia-inducible factors, which shifts the metabolism state from oxidative to glycolytic (Ebert et al., 1995). This, in turn, upregulates downstream glucose transporters, glycolytic enzymes and pyruvate dehydrogenase kinase 1 (PDK1). The pyruvate dehydrogenase is then phosphorylated and inactivated. Ultimately, this results in an increase in lactate production along with an increase in glucose consumption (Semenza, 2010).

Fermentative metabolism can occur even under aerobic conditions. In this case, pyruvate is converted for use in oxidative phosphorylation by lactate dehydrogenase (Pedersen, 1978). Overall, the production of lactate and fermentative metabolism cause the reduction in pH and even further under poorly perfused culture conditions, i.e. in static cultures (Parks et al., 2013).

The changes in the glucose metabolism within cancer cells is called the Warburg effect and it is one of the hallmarks of cancer. It is postulated that cancer cells reprogram themselves to take in large amounts of nutrients and produce energy to support their indefinite growth via high rate glycolysis and lactate fermentation (Warburg, 1956). The evaluation of lactate production over 21 days of culture would provide strong supporting evidence. However, the EGM-2 medium contains a considerable amount of foetal bovine serum (FBS), which includes a significant amount of lactate dehydrogenase. Hence, this increases the background signal and reduces the sensitivity of the lactate production assay (Decker and Lohmann-Matthes, 1988). Due to this limitation, the lactate production assay is not performed in this study.

5.4 Conclusion

This chapter concerned the development of a perfusion microbioreactor system that introduced the key components of the tumour microenvironment, i.e. continuous flow and gradient of oxygen and nutrients that were absent in a majority of 3-D *in*

vitro cancer models. Perfusion also added the hydrodynamic effect into cultures, which introduced shear stress to stimulate functions of cells and reduced diffusional limitation in promoting convective mass transfer.

The modification of the TissueFlex® bioreactor maximised mixing by locating the inlet and outlet ports at different heights and placing the bioreactor on top of a rocker. These ensured that the flow of cell culture medium inside the system was turbulent, and not laminar. The laminar flow would cause mass transfer limitations as the boundary layers developed between fluid and layers of cells.

The enhanced uptake of nutrients and oxygen by cells allowed them to extend their viability for a longer period compared to static cultures. This was illustrated in the cell morphology (see Figure 5.5) and cell viability (see Figure 5.7) results.

However, it is worth mention that calcein-AM has a potential to create false-positive results as they tend to have a very strong background signal upon staining in 3-D hydrogels. Other methods should be considered in evaluating cell viability such as nuclear staining (Hoechst 33342) alongside with ethD-1 staining (Patel, 1998).

Further metabolites and pH analyses showed that the induction of VEGF and BDNF mediated the neurovascular interactions between SH-SY5Ys and HUVECs. The interactions were further enhanced in perfusion cultures. In addition, the Warburg effect was observed in both static and perfusion cultures, as seen from the drastic decrease in pH and the increase in metabolic activities via glucose consumption.

The lack of neurite outgrowth from SH-SY5Ys and tubule-like structures from HUVECs in the 3-D model (see Figure 5.5) are still present as the main limitation to recapitulating neuroblastoma. The incorporation of laminin has shown to promote the growth of both neurons and endothelial cells. However, other growth factors such as VEGF and BDNF are also important in mediating the tumour microenvironment and considering incorporating into the model in the future work.

The 3-D *in vitro* neuroblastoma model under the perfusion culture system is useful in studying the effects of drugs in long-term. Numerous advantages of perfusion culture over conventional static culture make the system suitable to

recapitulate the tumour microenvironment inside humans. It can also be useful in studying different phenomena and niches such as the recruitment of endothelial cells or angiogenesis even further. Due to its ease of modification, the model and the perfusion system can be utilised in the development of miniaturised drug screening platform using either cell lines or patient-derived biopsy samples. This would further our understanding of tumour progression and drug responses.

6

Evaluation of 3-D neuroblastoma model responses to chemotherapeutics

Table of contents

6.1 Introduction 129
6.2 Materials and methods 131
6.2.1 Treatment preparation 131
6.2.2 Co-culture model development 132
6.2.3 Culture systems set up 134
6.2.4 Cell immunostaining 138
6.2.5 Image analyses 138
6.2.6 Statistics 139
6.3 Results and discussion 139
6.3.1 Optimisation of cell seeding density 139
6.3.2 Optimisation of co-culture media 143
6.3.3 Evaluation of the neuroblastoma model's responses to cancer therapeutics 145
6.4 Conclusion 155

6.1 Introduction

The development of a three-dimensional (3-D) *in vitro* neuroblastoma model and the perfusion bioreactor system enable many prominent features of tumours to be captured. As the perfusion culture system has proven to extend the viability

of the 3-D cancer model for at least 21 days, it has a potential to be used as a long-term drug screening platform.

In addition to the TissueFlex® bioreactor, an automatic perfused cell culture system, 3DFlo® is introduced as a comparable system. 3DFlo® system shares similarities and differences with the TissueFlex® that may give rise to different culture responses.

Anti-cancer drugs cisplatin and all-trans-retinoic acid (RA) are commonly used to treat neoplasms including neuroblastoma. They target cancer cells via different mechanisms, and drug responses, i.e. cisplatin targets rapidly proliferating cells and RA differentiates SH-SY5Ys to mature neurons, inhibiting its growth.

The drug responses of the 3-D *in vitro* neuroblastoma model are evaluated for 21 days. The experiments compare the effects of cisplatin and RA on cells, as well as their effects when both drugs are treated as single agents and in combination. Long-term cell responses are evaluated weekly for 3 weeks to observe any potential side effects such as tumour development of resistance to drug treatments and tumour recurrence. Furthermore, comparisons between different culture systems (2-D monolayer, 3-D TissueFlex® and 3DFlo®) are made to evaluate their potential as a personalised drug screening platform.

As addressed earlier in Chapter 5, both SH-SY5Ys and HUVECs in the model did not form any representative structures, i.e. neurite outgrowth and tubule-like formation. The lack of structures presented the current limitation of the 3-D *in vitro* neuroblastoma model. Perhaps, the creation of these structures in 3-D would give rise to a more accurate recapitulation of neuroblastoma.

Consequently, this chapter later explores different factors such as cell seeding density, medium composition and growth factors that could contribute to SH-SY5Ys neurite outgrowth and HUVEC tubule-like structures formation in 3-D fragmented HyStem®.

6.2 Materials and methods

The protocols for cell culture (SH-SY5Y and HUVEC cells) were identical to those described in Chapter 5 (Section 5.2.1) for SH-SY5Y cells and in Chapter 3 (Section 3.2.1) for HUVEC cells.

6.2.1 Treatment preparation

In this chapter, two drugs with different mechanisms: cisplatin and RA were prepared and treated on the 3-D neuroblastoma model. For the following experiments, cell lines (SH-SY5Ys and HUVECs) were purchased from Lonza, UK; RA was purchased from Sigma-Aldrich, UK; and cisplatin was received as a gift kindly provided by Martin Gill, Department of Oncology, University of Oxford, UK.

Culture medium optimisation

To investigate the medium composition that gave rise to SH-SY5Y neurite outgrowth and HUVEC tubule-like structures, cells were treated under different conditions in 2-D inside a 24-well plate for 7 days. Before culture, each well was pre-coated with 500 μL 1% laminin in phosphate-buffered saline (PBS) (Sigma-Aldrich, UK) overnight.

Treatments included: RPMI medium (supplemented with 10% FBS, 1% MEM Non-essential amino acid solution and 1% penicillin-streptomycin), supplemented RPMI medium with RA, EBM-2 medium, EBM-2 medium supplemented with RA, EGM-2 medium and EGM-2 medium supplemented with RA. For cultures under RA treatment, SH-SY5Y cells were pre-treated with EGM-2 supplemented with RA (10 μM/500 mL medium) 5 days before the experiment. The concentration of RA has been optimised by a previous study to differentiate the SH-SY5Y cells into neurons (Dwane et al., 2013).

Drug testing

Two different treatments were applied to the cultures: EGM-2 medium in control and RA-treated samples; and cisplatin (7 ng dissolved in 7 mL EGM-2) in cisplatin-treated and cisplatin-RA combination therapy samples.

Dosing of cisplatin in this chapter was based on a previous study (Norris et al., 2014), in which the combination therapy of cisplatin and 13-cis-retinoic acid was assessed on tumour-bearing mice. The concentration used in that study was 7 mg/kg, which approximated to 7 ng/100 μL per model. This conversion of 1 L of the 3-D hydrogel model weighs 1 kg was under the assumption that the 3-D model was entirely water-based.

Since the TissueFlex® bioreactor perfusion system replenished 500 μL of medium daily, 7 mL of EGM-2 medium was needed to culture each model for 14 days. This gave rise to the dosing of 7 ng of cisplatin dissolved in 7 mL of EGM-2 medium for 14-day experiments.

6.2.2 Co-culture model development

The 3-D *in vitro* neuroblastoma model was modified in this chapter. The size and shape of the previously developed model were inconsistent due to its small volume. On top of that, the volume of the model was lost during the experiments when an apparatus was in a physical contact with the fluidised hydrogel. Therefore, the model in this chapter was cast into a rigid disc so it can be dislocated in and out of the culture wells easily.

Two-dimensional model

The two-dimensional (2-D) co-culture model was developed in parallel as a control for the experiments. 500 μL 1% laminin in PBS was added to each well as a pre-coating. The plates were incubated overnight at 37°C, 5% CO_2 before seeding. The cell seeding density was extrapolated from 5 million cells/mL seeding density in 3-D cultures, which was 40,000 cells/cm^2 or 75,000 cells/well (in a 24-well plate). For SH-SY5Y-HUVEC co-cultures, cells were cultured in a 3:1 ratio, approximately 60,000 (exact number = 56,250) SH-SY5Ys and 20,000 (exact number = 18,750) HUVECs per well.

Table 6.1: The number of SH-SY5Y and HUVEC cells at different total cell seeding densities

Cell seeding density (Million cells/mL)	SH-SY5Ys /mL	HUVECs /mL	SH-SY5Ys /200 μL	HUVECs /200 μL
1	750,000	250,000	150,000	50,000
3	2,250,000	750,000	450,000	150,000
5	3,750,000	1,250,000	750,000	250,000
10	7,500,000	2,500,000	1,500,000	500,000

Three-dimensional model

The HyStem® hydrogel (Sigma-Aldrich, UK) was prepared by dissolving 1 mL of degassed water each into two bottles of HyStem® macromer (Glycosil®)and dissolving 1 mL of degassed water (dH_2O) into one bottle of Extralink 1®. The bottles were placed on a shaker for 1 hour to give a clear solution. Solutions in the bottles were then mixed together, drawn up by a syringe and incubated for 45 minutes to allow gelation. The gel was then pushed through a 3-D printed hydrogel granule extrusion tool, which comprised a 10 μm pore diameter nylon mesh (Figure 6.1).

This 3-D hydrogel extrusion tool is our laboratory's own invention. The design included the two-parts tool, with the 5 mm nylon diameter mesh placed and sealed in the upper recess by polydimethylsiloxane (PDMS). The mesh pore diameter used in this tool was much smaller than the one used in the earlier chapters (10 μm vs 40 μm).

From the research conducted in our laboratory, we have shown that extrusion through pore diameters of at least 10 μm resulted in gel granules with proportionate size (George et al., 2017). This implied that the smaller the pore diameter, the higher the surface area in contact with cellular integrins and laminin. Hence, a more stable network of cell-hydrogel established in the model.

SH-SY5Ys and HUVECs in 3:1 ratio was suspended in 400 μL of EGM-2 medium. The total cell seeding density in each experiment varies and was shown in Table 6.1. Note that the total volume of the model in this experiment was 200 μL.

In addition, cell suspension was supplemented with 100 ng/mL BDNF, 10 μg/mL VEGF, 10 μg/mL stromal cell-derived factor 1α (SDF1α), 200 μg/mL laminin and

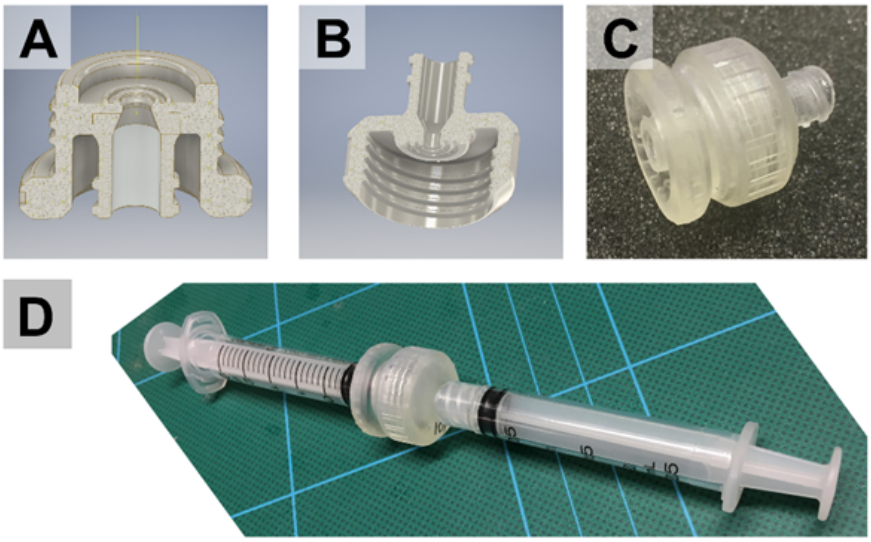


Figure 6.1: 3-D printed hydrogel granule extrusion tool Cross-sectional CAD model of (A) the lower and; (B) the upper parts of the extrusion tool. PDMS is added to create a seal with a 5 mm nylon diameter mesh placed into the upper recess; (C) The assembled printed part of the granule extrusion tool; (D) The tool is attached to syringes to pass hydrogel back and forth through the mesh. Image courtesy of Dr Julian George.

1.5% (by volume) Extralink 1® (All supplements listed were purchased from Sigma-Aldrich, UK). Equal volumes of supplemented cell suspension and fragmented HyStem were drawn into two different syringes and connected to their respective ports in the 3-D printed cell mixing tool (Figure 6.2). Both syringes were extruded at the same time, which allowed the mixing of the hydrogel granules and cell suspension to occur and collected in another syringe connected at the other side of the tool.

Next, 100 μL of the tube mixture was drawn up by the gel micropipette and cast into gel discs between modified glass slides (Figure 6.3). After incubated at 37°C for 10 minutes, set gel discs were removed from the glass slide and moved into culture wells.

6.2.3 Culture systems set up

In this chapter, the effects of different culture systems on the *in vitro* neuroblastoma model were investigated. The protocols for each culture system were described below.

2-D static culture

Cells were seeded as 2-D monolayers to serve as controls for the experiments. Each well was treated with 1 mL of treatment prepared in section 6.2.2, which was replenished every other day.

The waste medium was collected and stored in a -80°C freezer for the glucose assay after the completion of the experiment.

3-D static culture

The co-culture SH-SY5Y-HUVEC model was prepared with various cell seeding densities as shown in Table 6.1. 1 mL of EGM-2 was treated in each well and replenished every other day.

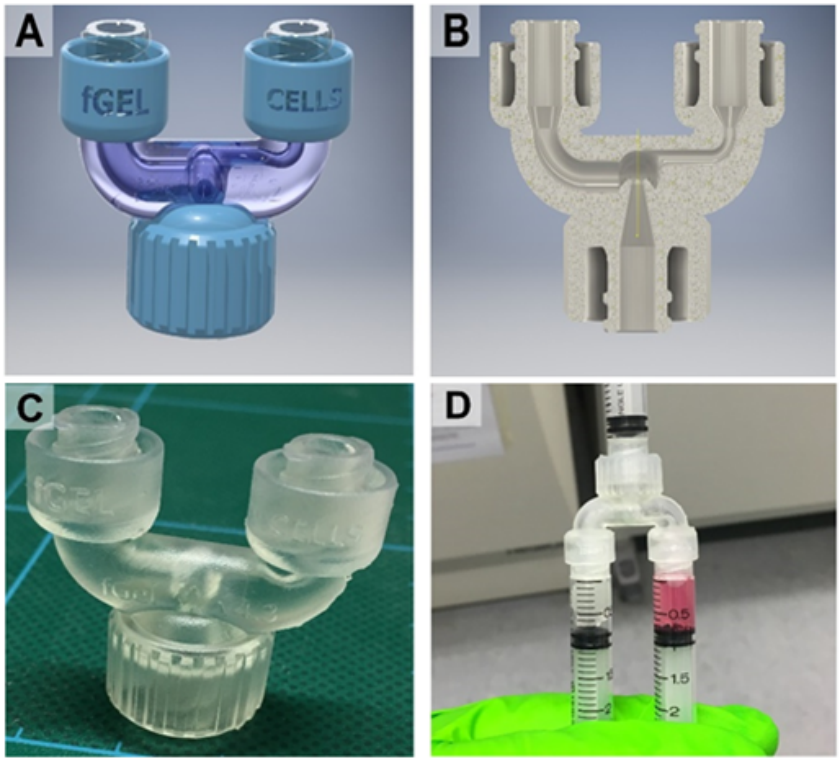


Figure 6.2: 3-D printed hydrogel granule and cell mixing tool (A) Rendered; and (B) cross-section CAD model of the mixing tool; (C) The printed mixing tool showing luer-lock fittings; (D) The mixing tool (inverted view) containing hydrogel granule and cell suspension inside syringes connected to 2 different ports, ready to be mixed into another syringe at the other side of the tool. Image courtesy of Dr Julian George.

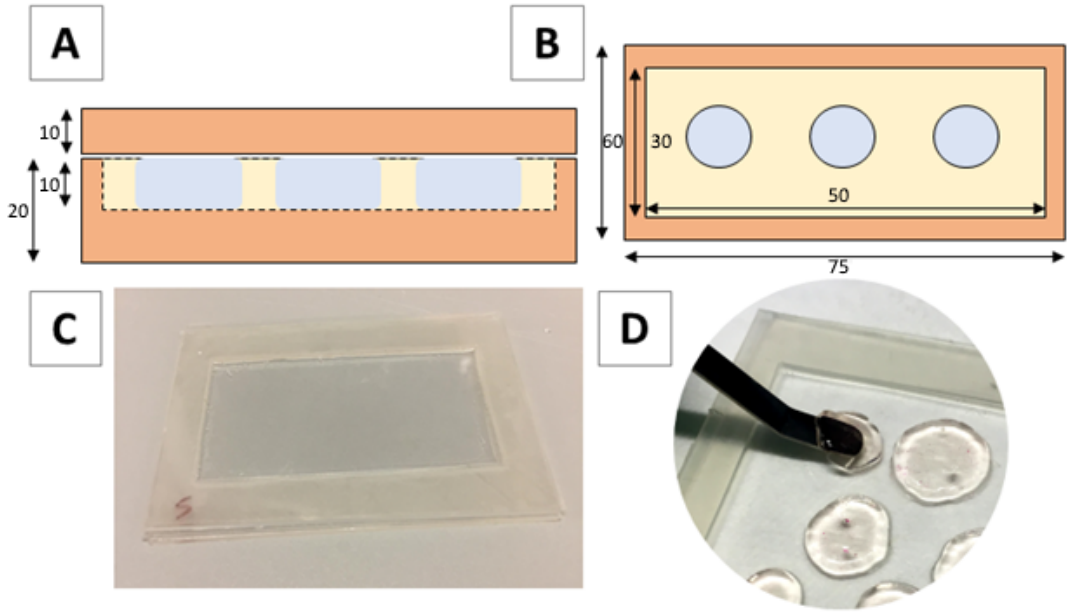


Figure 6.3: Casting and lifting of gel discs Once gel granules have been mixed with cells, they can be cast into gel discs between glass slides. (A) The cross-sectional view; (B) top view; and (C) photograph of the glass slides; (D) Set discs are easy to handle and can be moved around by a spatula. Units are in mm. Image (D) courtesy of Dr Julian George.

3-D perfused culture inside a modified TissueFlex®

The setup of the perfused culture inside a TissueFlex® bioreactor is like those in the previous experiments (see Section 5.2.6, Figure 5.3). In each well of the bioreactor, placed a model inside a cell insert and filled up with 1 mL of an EGM-2 medium. The reactor's lid was sealed up before started the experiment outside the cell culture hood.

Each bioreactor was perfused their specific treatment supplied from an ice-containing reservoir through silicon tubing. The ice inside the chilled reservoir was replaced every other day to keep the medium chilled throughout.

The PDMS bioreactor containing the neuroblastoma model was placed inside an incubator, maintained at 37°C with a constant pump of 5% CO_2 air. The airflow was provided by an external gas cylinder connected into the incubator. A multichannel peristaltic pump (Minipuls 3 M312, Gilson, USA) drove the medium perfusion in each channel at the rate of 0.01 rpm.

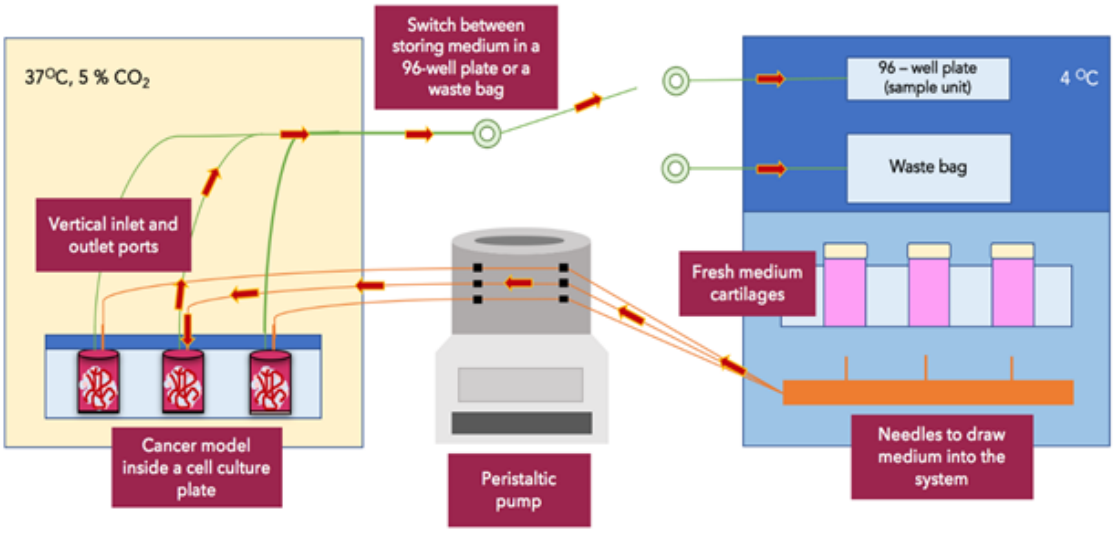


Figure 6.4: Schematic representation of the 3DFlo® automatic cell culture system Fresh medium or treatment was peristaltically pumped from the cartilages inside a mini-fridge into the cancer model inside the incubator. The waste medium was stored inside the mini-fridge and can be collected in real-time.

3-D perfused culture inside a 3DFlo® system

In this 3DFlo® cell culture system (Oxford MEStar, UK), three discs of a 3-D *in vitro* model were placed inside a cell insert then placed inside a 24 -well plate. The plate was sealed with a silicone lid, connected to 2 vertical ports before placed inside the 3DFlo® incubator. The incubator was maintained at 37°C with a constant pump of 5% CO_2 air.

The treatments prepared were loaded into 50 mL cartilages, then placed inside a mini-fridge. Once initiated, a multichannel peristaltic pump drove the medium perfusion in each channel at the rate of 0.01 rpm. A switch can be pressed to discard undesirable medium into a waste bag inside the mini-fridge as well. The setup of the 3DFlo® system is shown in Figure 6.4 .

Three different culture systems were investigated for drug responses in this work: 2-D monolayer, 3-D TissueFlex® and 3DFlo®. The summary of the treatments and cell culture systems were shown in Figure 6.5.

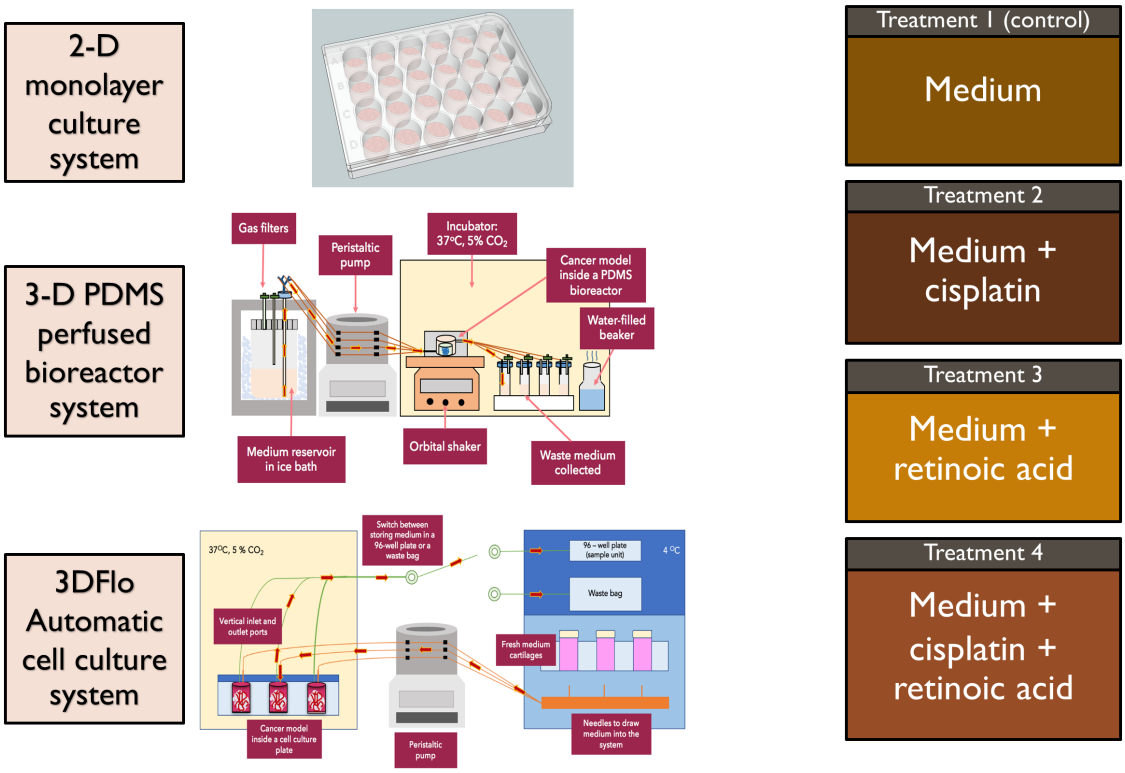


Figure 6.5: Summary of different cell culture systems and treatments to evaluate 3-D *in vitro* neuroblastoma responses The *in vitro* neuroblastoma model was cultured under the 2-D monolayer culture system, 3-D TissueFlex® bioreactor system or 3DFlo® cell culture system for 21 days. In each culture system, 3-D model samples were treated with EGM-2 medium, cisplatin, retinoic acid or the combination of cisplatin and retinoic acid.

6.2.4 Cell immunostaining

The protocols for cell immunostaining were identical to those outlined earlier in Section 3.2.7.

6.2.5 Image analyses

Image analyses of 3-D cultures were performed in the same manner as outlined previously in chapter 3 (see Section 3.2.8 and Appendix A for more details on image analysis procedures).

2-D cell area analyses were performed using MATLAB. Each image was split into different channels, representing different markers expressed on the cell's surface. The number of cell-expressing markers was quantified by counting the number

of interconnected pixels in each respective channel (see Section 4.2.3 for more details on the protocol).

6.2.6 Statistics

All experiments were performed independently with three replicates, unless stated otherwise. GraphPad Prism 6.0© software was used to illustrate graphical results as well as to perform t-test or two-way ANOVA and Sidak's multiple comparison tests to compare the means between different culture groups. Statistically significant difference between the means of two groups was considered if the significance value (α) was less than 0.05.

6.3 Results and discussion

In this section, several optimisation experiments were conducted to ensure that the effects observed in a NSC-HUVEC model were also evident in a SH-SY5Y-HUVEC model. Later, the *in vitro* neuroblastoma model was cultured under three different culture systems: 2-D monolayer culture, 3-D TissueFlex® and 3DFlo® automatic cell culture machine to compare the marker expressions and cell morphologies under different drug treatments (control EGM-2 medium, cisplatin, RA, and cisplatin + RA in combination) for 21 days.

6.3.1 Optimisation of cell seeding density

Main finding

The optimal cell seeding density for 3-D SH-SY5Y-HUVEC co-culture was 5 million cells/mL.

Since the development of the 3-D *in vitro* neuroblastoma model, the lack of SH-SY5Ys neurite outgrowth and HUVECs tubule-like structures remains to be a major hurdle to overcome. These structures were evident in 2-D cultures on laminin-coated wells (see Figures 4.5 and 4.6), but not in 3-D cultures. The only occasion neurite

outgrowth was seen, despite there was a few of them, was when NSCs were cultured in fragmented HyStem® at the seeding density of 10 million cells/mL (see Figure 4.4).

It is hypothesised that the lack of cell-cell contacts in 3-D space limits the formation of these specific structures. Hence, in this experiment, SH-SY5Ys and HUVECs were co-cultured in 3:1 ratio inside a fragmented HyStem® at different total cell densities of 1, 3, 5 and 10 million cells/mL for 7 days.

Morphological z-stack images in Figure 6.6 shows that cells expressing Nestin (blue) were forming small structures or clusters at the density of 1 million cells/mL. The number of these structures increased as the cell seeding density increased. Cells expressing TuJ1 (green) remained as single cells regardless of the cell seeding density. On the other hand, HUVECs started to migrate towards the centre of the cell and formed clusters with themselves as well as with SH-SY5Ys beyond the density of 5 million cells/mL. However, there were no outgrowth or elongated structures observed, even at the density of 10 million cells/mL.

A further quantitative analysis was conducted to evaluate the growth rate of cells at different seeding densities. Figure 6.7A shows that the number of cells after 7 days of culture increased as the original cell seeding density increased, as expected. However, the number of TuJ1 and CD31 expressed at samples seeded at 10 million cells/mL were less than those seeded at 5 million cells/mL. This observation is confirmed with the decrease in the total cell number after 7 days when cells were cultured at 10 million cells/mL, especially for SH-SY5Ys where the percentage decrease was significant (see Figure 6.7B). The percentage change in the number of SH-SY5Ys was only significant at the seeding density of 1 million cells/mL, whereas the change in the number of HUVECs was significant at the densities of 1, 3 and 5 million cells/mL.

Results suggest that the increase in the cell seeding density enhances the cell-cell interactions and cells are more likely to form structures. However, because of the heterogeneous nature of the cancer model. Necrotic cells at the core of the model and dead cells encapsulated within the hydrogel can exert a bystander effect and affect neighbouring cells (Liaudet-Coopman et al., 1997). The induction of apoptosis

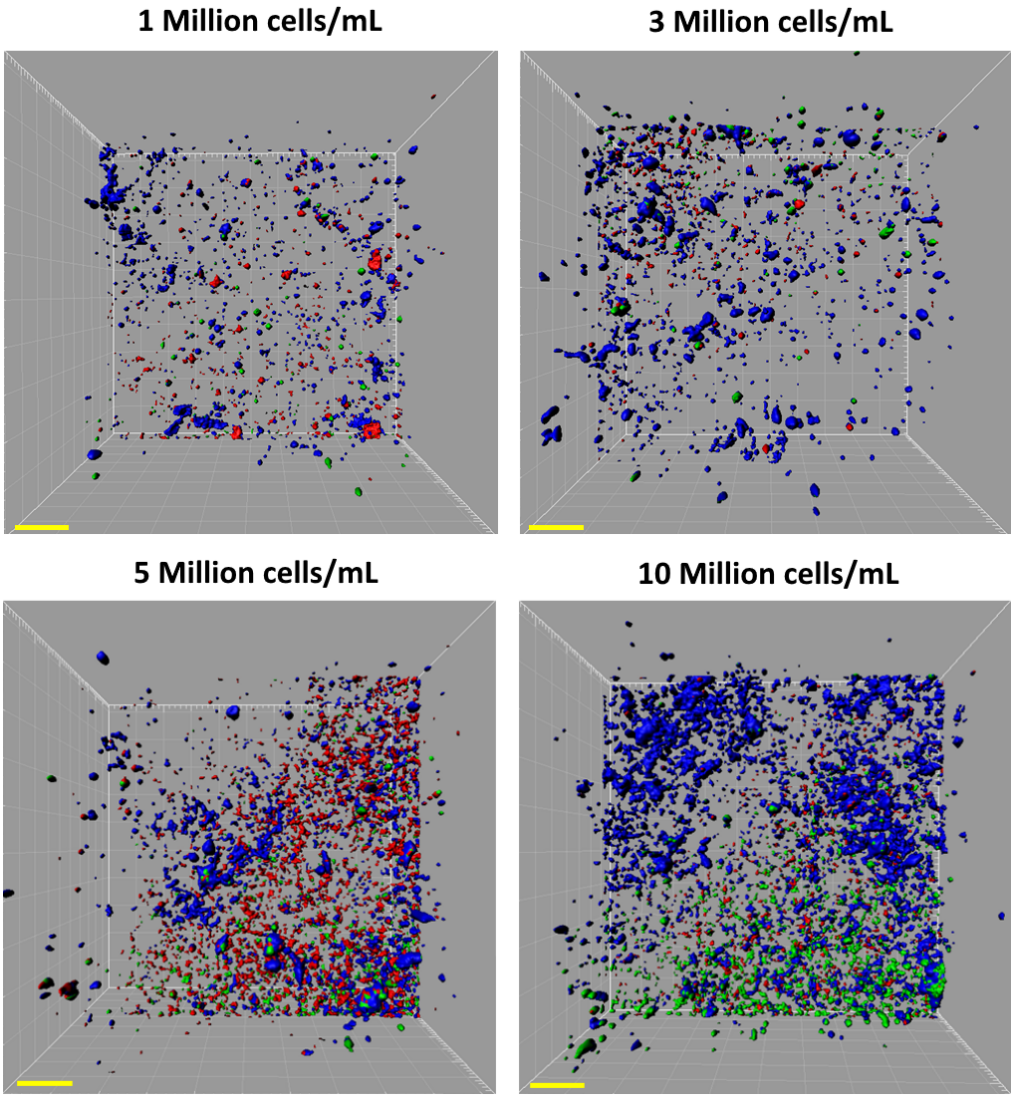


Figure 6.6: Effects of cell seeding density on 3-D co-culture morphologies Cell clusters and small structures were formed in SH-SY5Ys from the cell seeding density of 1 million cells/mL whereas they were formed in HUVECs after the density of 5 million cells/mL. Z-stack cell morphologies illustrated the expression of TuJ1 (green), Nestin (blue) and CD31 (red) antibodies after 7 days of culture in an EGM-2 medium. Scale bar = 100 μm.

occurs more readily at higher cell seeding density because there's an increasing demand for nutrients and oxygen. The optimum cell seeding density is determined to be at 5 million cells/mL to balance between the formation of structures by both SH-SY5Ys and HUVECs and the induction of cell death by neighbouring cells.

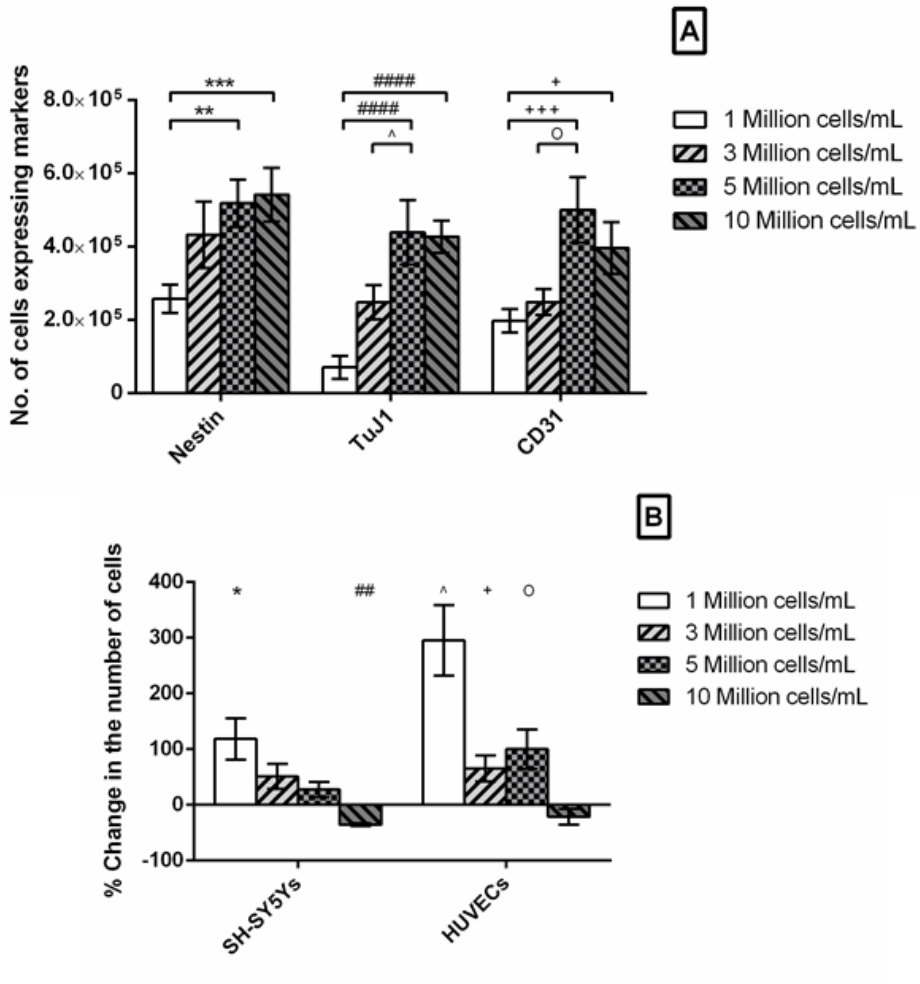


Figure 6.7: Effects of cell seeding density on marker expressions The expressions of TuJ1 and CD31 in cultures seeded at 10 million cells/mL were less than cultures seeded at 5 million cells/mL after 7 days of culture. (A) Bar graphs quantitatively represent the marker expressions at each total cell seeding density. Values are mean ± SD; n = 3 per group. Statistical analysis was performed by two-way ANOVA with post-hoc analysis. $^{**}p < 0.01$, $^{***}p < 0.001$ vs Nestin$^+$ cells at the density of 1 million cells/mL. $^{\#\#\#\#}p < 0.0001$ vs TuJ1$^+$ cells at the density of 1 million cells/mL. $^{\wedge}p < 0.05$ vs TuJ1$^+$ cells at the density of 3 million cells/mL. $^{+}p < 0.05$, $^{+++}p < 0.001$ vs CD31$^+$ cells at the density of 1 million cells/mL. $^{\circ}p < 0.05$ vs CD31$^+$ cells at the density of 1 million cells/mL; (B) The bar graphs show the percentage change in the cell number of both SH-SY5Ys and HUVECs between day 0 and day 7. Values are mean ± SD; n = 3 per group. Statistical analysis was performed by Student's t-test with post-hoc analysis. $^{+}p < 0.05$ vs the number of SH-SY5Ys originally seeded at 1 million cells/mL. $^{\wedge\wedge}p < 0.01$ vs the number of SH-SY5Ys originally seeded at 10 million cells/mL. $^{\wedge}p < 0.05$ vs the number of HUVECs originally seeded at 1 million cells/mL. $^{+}p < 0.05$ vs the number of HUVECs originally seeded at 3 million cells/mL. $^{\circ}p < 0.05$ the number of HUVECs originally seeded at 5 million cells/mL.

6.3.2 Optimisation of co-culture media

Main findings

- SH-SY5Ys differentiated in all tested medium, regardless of RA.
- HUVECs formed tubule-like structures in the RA-supplemented medium.
- HUVECs and SH-SY5Ys migrated to overlap on top of each other after 7 days of culture.

Another factor to consider for recreating neurite outgrowth and tubule-like structures are the compositions of the co-culture medium. It is speculated that the supplements of the EGM-2 medium may play a role in determining the morphology of SH-SY5Ys. Many studies reported the induction of SH-SY5Ys differentiation after treatment with RA for at least 5 days (Schneider et al., 2011; Cheung et al., 2009; Dwane et al., 2013) and hence the RA-supplemented RPMI medium was used as a control. Also, the effects of RA on HUVECs were investigated in this experiment.

SH-SY5Ys and HUVECs were cultured independently and in co-culture on top a laminin layer for 7 days. Upon the completion of the experiment, cells were stained with TuJ1 (green), Nestin (blue) and CD31 (red).

Two-dimensional cultures in Figure 6.8 show that SH-SY5Ys differentiated, as shown in the expression of TuJ1 markers, even in the absence of RA. However, in RPMI medium, mature neurons only formed a network of clusters without any extensions of axons or dendrites. The neurite outgrowth was evident in all other treatments, and even more in medium supplemented with RA. Cell morphologies also imply that the constituents of EBM-2 and EGM-2 medium induced differentiation of SH-SY5Ys into neurons. RA-treated SH-SY5Ys formed a layer of neurite outgrowth in parallel, which was enhanced further when they were co-cultured with HUVECs. This observation is in agreement with a study by Cheung et al. (2009) that reported neurite outgrowth in 2-D monolayer cultures on laminin coating, with the presence of RA, significantly increased the outgrowth even further. It was also shown that undifferentiated SK-N-SH cells, the sister

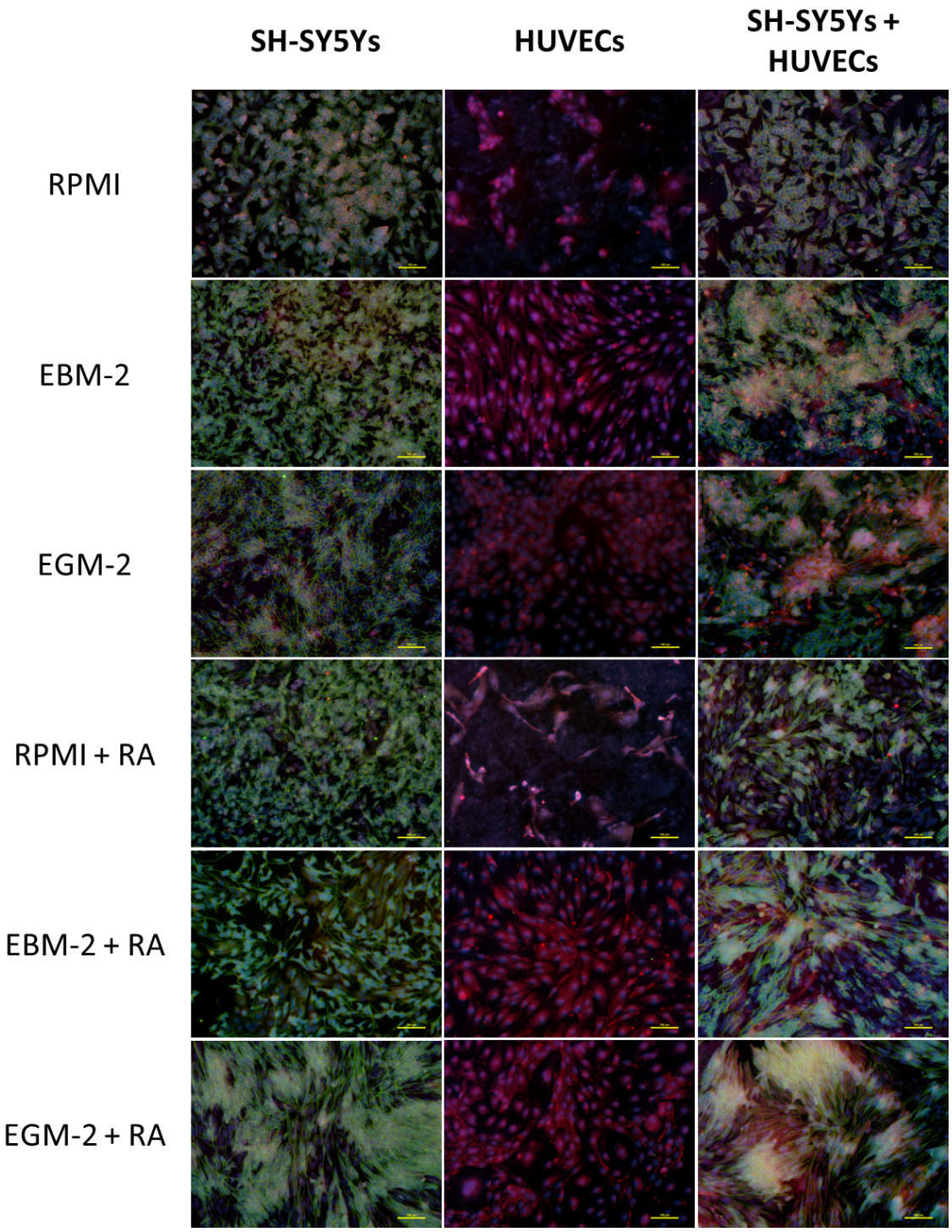


Figure 6.8: Effects of different media on SH-SY5Y-HUVEC co-cultures HUVECs formed tubule-like structures when cultured in EGM-2 or medium supplemented with RA. SH-SY5Ys formed neurite outgrowth in every culture medium but RPMI. The presence of RA enhanced the outgrowth further. SH-SY5Ys and HUVECs were cultured independently as well as in co-culture (3:1 ratio) on a layer of laminin. Cells were stained after 7 days of 2-D culture with TuJ1 (green), Nestin (blue) and CD31 (red). Total cell seeding density = 45,000 cells/cm^2. Scale bar = 100 µm.

cell line of SH-SY5Y cells, did not exhibit significant difference in their neuronal properties compared to RA-differentiated counterparts.

As for HUVECs, tubule-like structures were observed under the EGM-2 treatment, but also in treatments supplemented with RA. This suggests that RA plays a role in inducing angiogenesis, which is in contrast with a study by Liaudet-Coopman et al. (1997) that reported the inhibition of stromal cell-induced angiogenesis by RA.

Another observation worth mentioning is the overlapping of SH-SY5Ys on top of HUVECs in every co-culture samples, regardless of the treatment. As cells were initially homogeneously dispersed upon culture, this indicated the migration of cells in co-culture; HUVECs were recruited by SH-SY5Ys to support their growth as vasculature in the stromal layer. The underlying mechanisms of neurovascular interactions between two cell types require further investigations.

6.3.3 Evaluation of the neuroblastoma model's responses to cancer therapeutics

Main findings

- Cells expressing markers decreased after 2 weeks in 2-D culture, whereas they increased or maintained in 3-D perfusion systems.
- TissueFlex® and 3DFlo® systems shared similarities in the levels of marker expressions except for TuJ1.
- Treatment with cisplatin decreased marker expressions of Nestin and CD31 in 2-D cultures to around 50% (against controls) within 7 days, whereas these marker expressions increased after 7 days in 3-D cultures.
- Treatment with RA dramatically increased marker expressions in 2-D cultures. However, these marker expressions tend to decrease in 3-D cultures.
- Combination therapy gave rise to an enhanced decrease ($< 40\%$, compared to controls) in marker expressions only in 2-D and 3DFlo® cultures. However, in TissueFlex®, the marker expressions increased after 7 days.

As the co-culture model and the perfusion bioreactor are established in the previous work, the 3-D culture system was explored further as a potential drug screening platform. SH-SY5Ys and HUVECs were co-cultured on a 2-D layer of laminin inside a 24-well plate and in 3-D fragmented HyStem® cultured inside the TissueFlex® and 3DFlo® perfusion bioreactors for 21 days. Samples were collected weekly for cell viability and morphological analyses. Medium samples were collected every other day for glucose assay.

Cell morphologies and quantitative analyses of TuJ1 (green), Nestin (blue) and CD31 (red) after 7, 14 and 21 days of culture in 2-D monolayer, 3-D TissueFlex® and 3DFlo® are shown in Figures 6.9, 6.10 and 6.11, respectively.

Effects of culture systems on cell morphologies

Figure 6.9 shows that cells cultured on top of 2-D laminin layer formed structures at all treatments and was capable of maintaining them up to 21 days. This was especially the case for the control and RA treated groups, in which extensive SH-SY5Ys neurite outgrowth and HUVECs tubule-like structures were observed.

In contrast, SH-SY5Ys and HUVECs cultured in 3-D TissueFlex® (see Figure 6.10) were clustered with minimal extended structures observed. However, the cells appeared to migrate towards the centre of the gel and overlapped each other. This observation was like those reported earlier in Figure 6.6.

The morphology of cells cultured in 3DFlo® (see Figure 6.11) was less clustered, with cells remained homogeneously dispersed as single cells. However, it appeared that differentiated cells ($TuJ1^+$) migrated cells away from undifferentiated ($TuJ1^-$) SH-SY5Y cells. This was the case for all treatments, including those not exposed to RA-induced differentiation.

As seen in the results above, neurite outgrowth and tubule-like structures were not observed in any of the 3-D bioreactor systems, even with a high cell seeding density and upon treatment with RA. As RA induced the expression of TrkB in SH-SY5Y cells and made them responsive to BDNF, perhaps replacing the RA-supplemented medium with the BDNF-supplemented medium after 5 days of

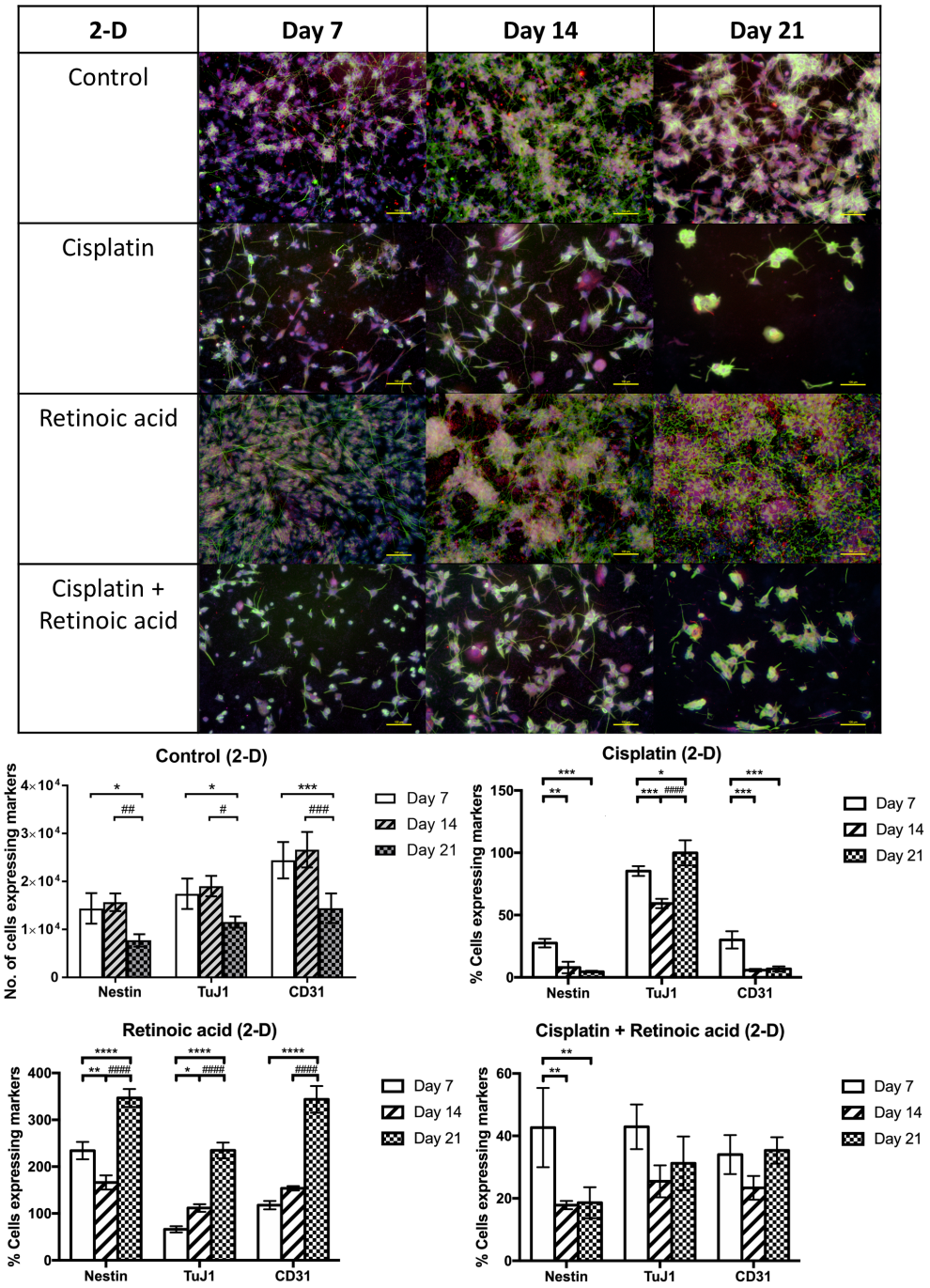


Figure 6.9: Drug treatments in 2-D monolayer cultures (Top) Cell morphologies of SH-SY5Ys and HUVECs cultured on top of laminin monolayer after 7, 14 and 21 days of culture. Cells were treated in EGM-2 (control), cisplatin, RA and a combination of cisplatin and RA. Cells were stained with expressing TuJ1 (green), Nestin (blue) and CD31 (red) antibodies. Images taken under a bright-field microscope. Scale bar = 100 μm. (Bottom) Bar graphs quantitatively represent the marker expressions of each treatment after 7, 14 and 21 days of culture (drug treatments were normalised by the control group). Cell seeding density = 45,000 cells/cm^2. Values are mean ± SD; n = 3 per group. Statistical analysis was performed by two-way ANOVA with post-hoc analysis. $^{*}p < 0.05$, $^{**}p < 0.01$, $^{***}p < 0.001$, $^{****}p < 0.0001$ vs cells expressing marker at day 7. $^{\sharp}p < 0.05$, $^{\sharp\sharp}p < 0.01$, $^{\sharp\sharp\sharp}p < 0.001$, $^{\sharp\sharp\sharp\sharp}p < 0.0001$ vs cells expressing marker at day 14.

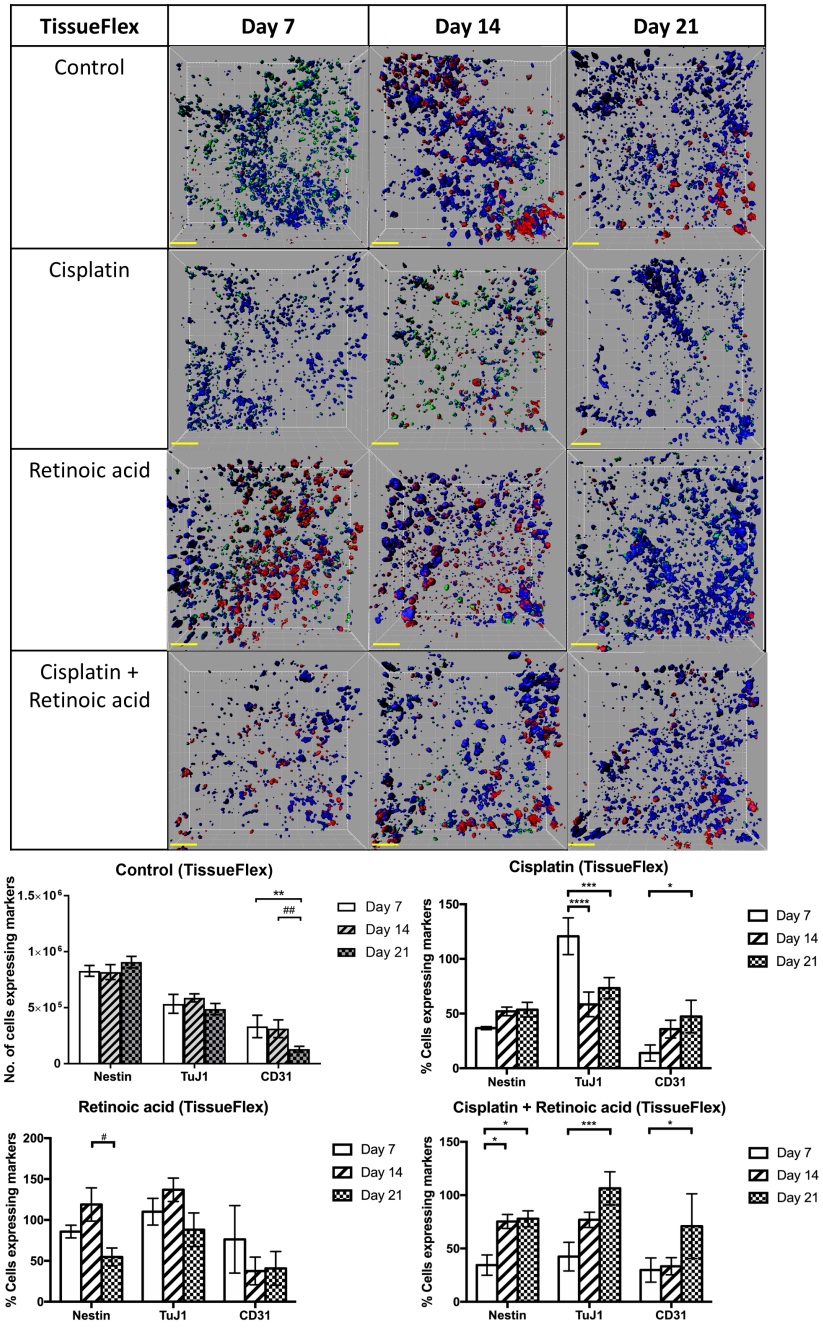


Figure 6.10: Drug treatments in 3-D TissueFlex® (Top) Z-stack 3-D cell morphologies of SH-SY5Ys and HUVECs cultured inside the TissueFlex® bioreactor after 7, 14 and 21 days of culture. Cells were treated in EGM-2 (control), cisplatin, RA and a combination of cisplatin and RA. Cells were stained with expressing TuJ1 (green), Nestin (blue) and CD31 (red) antibodies. Images taken under a laser confocal microscope. Cell seeding density = 5 million cells/mL. Scale bar = 100 μm. (Bottom) Bar graphs quantitatively represent the marker expressions of each treatment after 7, 14 and 21 days of culture (drug treatments were normalised by the control group). Values are mean $\pm$ SD; n = 3 per group. Statistical analysis was performed by two-way ANOVA with post-hoc analysis. $^{\star}p < 0.05$, $^{\star\star}p < 0.01$, $^{\star\star\star}p < 0.001$, $^{\star\star\star\star}p < 0.0001$ vs cells expressing marker at day 7. $^{\sharp}p < 0.05$, $^{\sharp\sharp}p < 0.01$ vs cells expressing marker at day 14.

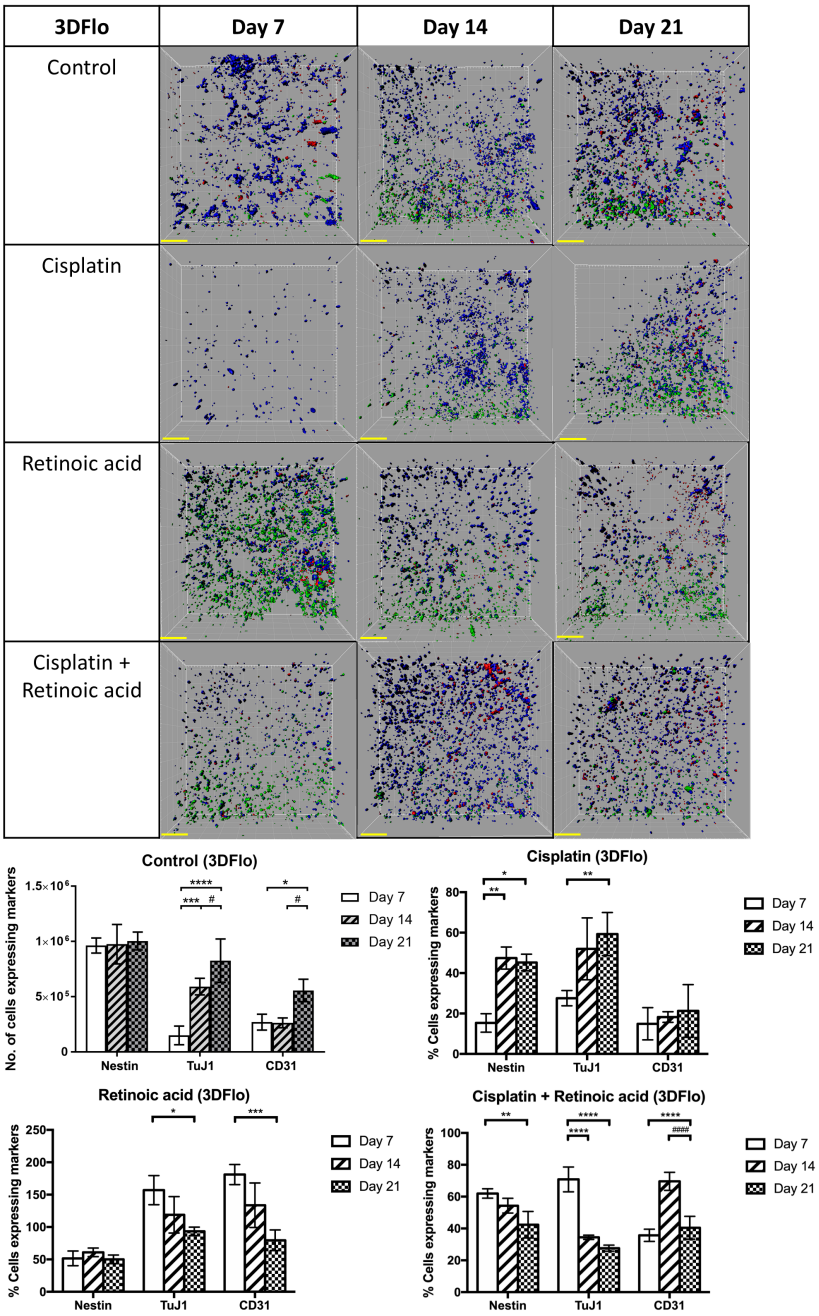


Figure 6.11: Drug treatments in 3DFlo® (Top) Z-stack 3-D cell morphologies of SH-SY5Ys and HUVECs cultured inside the 3DFlo® bioreactor after 7, 14 and 21 days of culture. Cells were treated in EGM-2 (control), cisplatin, RA and a combination of cisplatin and RA. Cells were stained with expressing TuJ1 (green), Nestin (blue) and CD31 (red) antibodies. Cell seeding density = 5 million cells/mL. Images taken under a laser confocal microscope. Scale bar = 100 μm. (Bottom) Bar graphs quantitatively represent the marker expressions of each treatment after 7, 14 and 21 days of culture (drug treatments were normalised by the control group). Values are mean ± SD; n = 3 per group. Statistical analysis was performed by two-way ANOVA with post-hoc analysis. $^{\star}p < 0.05$, $^{\star\star}p < 0.01$, $^{\star\star\star}p < 0.001$, $^{\star\star\star\star}p < 0.0001$ vs cells expressing marker at day 7. $^{\sharp}p < 0.05$, $^{\sharp\sharp\sharp\sharp}p < 0.0001$ vs cells expressing marker at day 14.

pretreatment may enhance the differentiating effects of RA further. This effect was evident in a study by Encinas et al. (2000) when SH-SY5Ys was supplemented with 50 ng/mL BDNF after 5 days of RA pre-treatment. This BDNF concentration was 167 times higher than the one measured previously at day 21 in perfused TissueFlex® bioreactor (see Figure 5.9).

Agholme et al. (2010) reported the combination of the ECM gel and BDNF to be the crucial factors in developing neurite outgrowth. Addition of other factors such as nerve growth factor (NGF), neuregulin (NRG), vitamin D3 (VitD3) or RA gave rise to at least an additive effect.

Regarding recreating HUVECs tubule-like structures in 3-D hydrogels, morphogenesis of endothelial cells is dependent on the hydrogel stiffness and the growth factor content. It is suggested that tubule-like structures favour developing in a soft hydrogel (200 Pa) containing VEGF165. Soft hydrogels allowed cells to branch out their capillaries and elongate, whereas VEGF increased the expression of MMPs, regulated contractile cell forces and increased angiogenesis (Bray, Binner, et al., 2015; Chwalek et al., 2014). This effect was enhanced further when growth factors such as bFGF and SDF1α were supplemented. The final concentration of each growth factor reported was 5 μg/mL, 5000 times higher than the VEGF concentration measured earlier in the perfused TissueFlex® system at day 21 (see Figure 5.9).

Effects of culture systems on marker expressions

Quantitative analyses of cell surface marker expressions show that 2-D cultures could not maintain the cell viability for more than 2 weeks, as the number of cells expressing each marker decreased from day 14 to day 21 in the control group (see Figure 6.9). On the other hand, the marker expressions of the control groups in 3-D TissueFlex® (see Figure 6.10) and 3DFlo® (see Figure 6.11) increased or maintained for the entire culture period. This suggested that 3-D hydrogel perfused culture systems provided a microenvironment more like native tumours than in 2-D cultures.

The levels of marker expressions in both TissueFlex® and 3DFlo® systems were similar, except for TuJ1. The clustering or formation of structures in

TissueFlex® may be responsible for this difference. Similarities in cell expressions and morphologies in both systems were possibly due to similar mechanisms that both TissueFlex® and 3DFlo® shared. These included the utilisation of the 3-D fragmented HyStem®, the peristaltic pump, the temperature-controlled and gas-controlled incubator.

Notable differences between these two perfused bioreactor systems included the utilisation of a gas permeable PDMS microbioreactor and the rocker to enhanced mixing in TissueFlex®, whereas cell inserts were cultured inside a typical 24-well plate with no enhanced mixing in 3DFlo®.

Conversely, 3DFlo® mini-fridge installation limited the temperature fluctuations of the medium reservoir and the waste medium collected. This was not the case for the TissueFlex® system, at which the medium reservoir was placed inside an icebox that needs to be replaced frequently (every other day) while the waste medium was collected at the room temperature. These fluctuations in temperature may degrade the levels of proteins or glucose desired to measure.

In addition, the location of medium ports in 3DFlo® was vertical, compared to the horizontal ports configuration in TissueFlex®. Medium inlet and outlet ports at high elevations were reported to generate significant 3-D convection. Convective transport substantially enhanced nutrient delivery and increased survival of neural cultures in 3-D (Cullen et al., 2007). On top of that, the automatic system of 3DFlo® minimised human intervention during culture, which reduced the risk of culture infections.

Effects of treatment on cultures

Figure 6.9 shows that treatment of cells in 2-D monolayer laminin with cisplatin decreased the expression of markers since day 7. The decrease of cells expressing TuJ1 was not as much as other markers due to the mechanism of cisplatin that targeted rapidly proliferating cells. Strikingly, the marker expressions in TissueFlex® (see Figure 6.10) and 3DFlo® (see Figure 6.11) increased throughout the culture period, with the exception of TuJ1 in TissueFlex® that the expression decreased after day 14.

It is hypothesised that cells acquired resistance to cisplatin in 3-D cultures. One explanation was the development of the hypoxic niche within the core of the 3-D model that reduced the efficacy of the drug through mass transfer limitations and selection of cells evading p53-mediated apoptosis (Brown and Wilson, 2004; Brown, 2007). At the molecular level, the resistance of cells to cisplatin could be due to the overexpression of BCL-2 protein in resistant cells. This inhibited apoptosis by forming a heterodimer with Bax, a homologous apoptosis-promoting protein (Aebi et al., 1997).

Treatment of cells with RA dramatically increased marker expressions in 2-D monolayer cultures (see Figure 6.9). However, the expressions of markers in 3-D perfusion culture systems decreased as the cultures approached day 21.

SH-SY5Ys neurite outgrowth can be observed after 5 days of RA treatment. This allows the cells to display mature excitability and action potential propagation (Sarkanen et al., 2007). Rapidly dividing cells or tumoural cells are largely dependent on glycolysis, whereas post-mitotic neurons rely on mitochondria to meet their bioenergetic demands. Supported by the Warburg effect, undifferentiated cells lose their bioenergetic reserve capacity due to the downregulation of mitochondrial function (Choi, Gerencser, et al., 2009).

Upon differentiation, cells alter their metabolic requirement from glycolysis to mitochondrial as mitochondria network distributes throughout the cell and neurites. Cells acquire a higher bioenergetic reserve capacity to utilise under increased stress. A higher bioenergetic reserve capacity also allows cells to repair protein and lipid damage by reactive oxygen species (ROS) (Schneider et al., 2011; Choi, Gerencser, et al., 2009). Furthermore, RA-induced differentiated SH-SY5Ys alters their survival signalling pathways in response to neurotoxins. The modulation of the Akt pathway by RA resulted in higher tolerance to 6-OHDA-induced oxidative stress (Cheung et al., 2009).

Another study showed that RA inhibited the growth rate of SH-SY5Y cells during the first $8 - 10$ days of treatment. However, the total number of cells increased as the period of incubation continued. Long-term treatments of RA also

led to the accumulation of S-type neurons over the N-type (Van der Kuip et al., 2006). This observation is in accordance to the decrease in marker expressions when treated in RA for more than 2 weeks.

Treatment with RA induced differentiation and decreased proliferation of cells. Apart from the differentiation of SH-SY5Ys into mature neurons, RA also affects non-tumoural cells such as HUVECs. It is speculated that RA downregulates the binding protein for FGF mRNA and causes inhibition of angiogenesis. Reduced angiogenesis in the tumour microenvironment can produce a bystander effect, which subsequently induces apoptosis to the surrounding cells (Villasante and Vunjak-Novakovic, 2015).

Effects of combination therapy on cultures

Combination therapy of cisplatin and RA gave rise to an enhanced decrease in marker expressions in 2-D cultures (see Figure 6.9) and 3DFlo® systems (see Figure 6.11). This implies the synergy between cisplatin in targeting rapidly proliferating cells and retinoic acid in differentiating cancer stem cells.

All-trans-retinoic acid and 13-cis-retinoic acid decrease proliferation and induce differentiation in neuroblastoma cells (Matthay et al., 1999). On the other hand, 9-cis-RA suppress differentiation, possibly to induce and increase the cell's susceptibility to undergoing apoptosis by another drug such as cisplatin, leading to a decreased tumour viability and growth rate (Shalinsky et al., 1996; Aebi et al., 1997).

Despite different mechanisms of action, 9-cis-RA, 13-cis-RA and all-trans-RA can all be used in combination therapy with cisplatin. Shalinsky et al. (1996) reported an enhanced cytotoxic activity and improved anti-tumour efficacy when 9-cis-RA was treated in combination with cisplatin. Different pathways targeted in each drug could explain this; RA suppressed the differentiation of carcinoma and increased the number of basal cells while cisplatin selectively targeted these proliferating tumour cells.

Conversely, any retinoids treated as a single agent was reported to be inefficient against any neoplasms, compared to a response rate of 30% reported in cisplatin (Shalinsky et al., 1996). Recently, another study showed that RA was ineffective

in increasing the survival time of the human ovarian carcinoma, IGROV-1 when treated as a single agent. The anti-tumour activity of the combination therapy is shown to be dependent on cisplatin sensitivity (Zhao, Au, et al., 2010).

Nevertheless, the synergistic interactions between cisplatin and RA were not as evident in 3-D TissueFlex® (see Figure 6.10), where the marker expressions of TuJ1, Nestin and CD31 increased over time. It is possible that cells develop resistance to both pathways induced by cisplatin and RA, or the treatment of drug combinations at the same concentrations when they're treated as single agents give rise to antagonistic outcomes instead.

To address this further, very minimal synergistic interactions were observed in the combination therapy of cisplatin and RA on BxPc-3 and T3M-4 human pancreatic adenocarcinoma cell lines. However, an increase in growth inhibition was observed when cells were pre-treated with RA, followed by cisplatin (Pettersson et al., 2001). The order of treatment may influence the cell's responses to drugs, especially when in practice drug combinations were mostly treated to patients one at a time (Shalinsky et al., 1996; Aebi et al., 1997).

Nevertheless, the efficacy of these drugs on cells could not be properly assessed without the therapeutic index of the drugs treated. Therapeutic index is defined as the the ratio between the median lethal dose (LD50- dose required to kill half of the cells in the population) and the median effective concentration (EC50- minimum drug concentration that produces a biological response in 50% of the cells *in vitro*) (Double and Bibby, 1989). The measurements of both LD50 and EC50 require the testing of cell responses to varying concentrations of both cisplatin and RA, in order to construct a dose-response curve.

In this study, cell viability assays such as a live/dead stain (calcein-AM and ethD-1) have been investigated but encountered issues regarding a high strong background signal from calcein-AM when the hydrogel discs were stained and imaged under the laser confocal microscope. Other methods of determining cellular responses to drugs including flow cytometry, protein assay or cell counting were discussed, but ultimately, were not performed in this study. The main limitation of

these methods was the difficulty to dissociate cells embedded inside the hydrogel discs after culture; the cells could not be removed for further assessments even after the attempt to re-fragment and typsinise the hydrogel discs.

6.4 Conclusion

This chapter started off with optimising different cell culture factors, which contributed to the formation of SH-SY5Ys neurite outgrowth and HUVECs tubule-like structures. Experimental results showed that prominent structures were formed when the initial cell seeding density in 3-D fragmented HyStem® was 5 million cells/mL. Neurite outgrowth and tubule-like structures were observed in 2-D cultures upon treatment with EBM-2, EGM-2 or RA-supplemented RPMI media. The addition of RA into the culture medium enhanced the neurite outgrowth even further.

However, these structures were not observed in a 3-D *in vitro* model. It is speculated that specific growth factors such as VEGF165, SDF1α and BDNF are required at higher concentrations to induce the neurite outgrowths and tubule-like structures in 3-D models.

Next, 3-D *in vitro* neuroblastoma models were assessed for drug responses in 2-D monolayer, 3-D TissueFlex® and 3DFlo® perfusion bioreactor systems. Results show that drug treatments were significantly less effective in both 3-D TissueFlex® and 3DFlo® bioreactors than in 2-D cultures. This is mainly due to the 3-D interactions between cells, hydrogel and bioreactor systems that create a microenvironmental niches. These niches recapitulate various phenomena present in neuroblastoma and play a prominent role in acquiring resistance to cancer therapeutics.

Treatment with RA is speculated to increase the therapeutic index of cisplatin by increasing its efficacy and decreasing its side effects. This served RA as a potential candidate to use in treatment in combination with cisplatin due to their different mechanisms of action and the lack of overlapping toxicity. Further investigations are required to identify the main reason why the synergistic effects of cisplatin-RA were not observed in 3-D cultures.

7

Conclusion and future perspectives

Table of contents

7.1 Introduction 157
7.2 Thesis contribution 158
7.3 Thesis limitations 159
7.4 Future perspectives 161
7.4.1 Angiogenesis and pan-cancer therapy approach 161
7.4.2 Stromal components in 3-D cancer models 162
7.4.3 Genetic editing in 3-D cancer models 163
7.4.4 Combination therapy in 3-D *in vitro* drug screening platforms 164
7.4.5 Scaling up: microbioreactor systems 164
7.5 Concluding remarks 166

7.1 Introduction

The work in this thesis concerned the development of a 3-D *in vitro* hydrogel-based perfused culture platform. The platform comprised a 3-D *in vitro* neuroblastoma model and a perfused microbioreactor. The developed system mimicked essential aspects of neuroblastoma tumours, i.e. cancer cells (SH-SY5Ys), endothelial cells (HUVECs), growth factors, extracellular matrix (HyStem®) and a continuous flow of nutrients and oxygen (3-D TissueFlex® and 3DFlo bioreactors®).

Firstly, the work in this thesis focussed on the development of the 3-D *in vitro* hydrogel neuroblastoma co-culture model. This involved the optimisation of hydrogel and co-culture properties.

Secondly, the perfused bioreactor system was designed based on the TissueFlex® microbioreactor system. The perfusion system allowed further extension of the cell viability and therefore, extended the period of drug testing from the conventional 2-D monolayer cultures.

Lastly, drug testing on the established 3-D hydrogel perfused bioreactor system was performed and compared with two other systems: 2-D monolayer culture and 3DFlo® automatic cell culture machine. The work demonstrated the potential for this 3-D perfused bioreactor system as an effective drug screening platform for treating neuroblastoma.

7.2 Thesis contribution

As stated earlier, the 3-D recapitulation of neuroblastoma and its microenvironment was a balance between practicality to scaling up and capturing clinically relevant aspects of the disease. The research conducted in each chapter of this thesis has answered some of the questions that more or less contributed to the scientific research community.

The first contribution in this thesis is the development of a novel 3-D *in vitro* hydrogel co-culture neuroblastoma model. This is the first cancer model that uses the HyStem® hydrogel and investigates hydrogel fragmentation. As to date, there is no 3-D neuroblastoma model reported elsewhere. This specific 3-D cancer model can be used in determining drug responses in relatively rare paediatric cancer cases.

Also, the model can be used to further our understanding of the disease by ultilising the model to investigate the interactions between different components or niches of the solid tumour. In fact, this 3-D hydrogel *in vitro* model can be extended to recapitulate other types of cancers, diseases or normal tissues by fine-tuning different hydrogel and co-culture properties to match those observed in the human physiological system.

The second contribution is the development of a novel 3-D polydimethylsiloxane (PDMS) perfused bioreactor. Based on the TissueFlex® microbioreactor, a turbulent flow is introduced inside the culture chamber to enhance the mixing of oxygen and nutrients. The bioreactor's PDMS construct retain a high gas permeability between the gases flowing inside the incubator and the cultured model. The bioreactor wells have the same size as those in a 24-well plate, which allow cancer models to be displaced easily for further analyses without any physical contact. This novel design of the PDMS bioreactor in a 24-well plate format and the perfusion culture system takes in account of the microenvironmental factors that could affect the cultured model.

Lastly, this thesis is the first to investigate the 3DFlo® automatic cell culture machine as a drug screening platform and utilise the system to compare its efficacy against our perfused bioreactor and the conventional 2-D monolayer culture. Furthermore, this thesis is also the first to preliminarily investigated the combination therapy potential of cisplatin and retinoic acid for treating neuroblastoma. Despite the results of marker expression changes over 3 weeks, the interactions between the drug mechanisms need further investigations.

The most significant contribution that this thesis made to the fields of tissue engineering, drug discovery and oncology is the overall development of the 3-D *in vitro* hydrogel model and the perfused bioreactor. Cells extended their viabilities from the conventional 2-D monolayer cultures in this recapitulated neuroblastoma microenvironment. In addition, the developed culture systems gave rise cellular responses to therapeutics that is more likely to reflect responses observed *in vivo* than in 2-D cultures. With further development, this 3-D hydrogel *in vitro* model and perfused bioreactor systems could potentially serve as an efficient drug screening platform.

7.3 Thesis limitations

There are several limitations that need to be addressed in this thesis. Firstly, due to the limited number of cells in the cryopreservation bank, the technique

of seeding neural stem cells (NSCs) from cryopreservation was not compared to the conventional technique of culturing cells on plates before seeding into the 3-D model. This would rather give a better indication of the feasibility in seeding cells right after thawed from cryopreservation.

The assessment of cell viability was challenging throughout this thesis. The penetration of dyes into the cells encapsulated inside the hydrogel was not an issue as cells were shown to be stained with dyes throughout the sample. To validate this further, a real-time diffusion test can be conducted by adding a dye into the hydrogel and look through the microscope to see how long it takes for the dye to completely diffuse throughout the gel. This would ensure that when live/dead stains are added, they would be in contact with all the cells in the model.

It is observed that calcein-AM gave out strong background signals after staining the hydrogel discs. Calcein-AM enters the cell and is cleaved by esterases present in the cytoplasm to give out green fluorescence (Sanfilippo et al., 2011). It is speculated the strong green signals may be a result of the release of esterases from cells with damaged membranes, but these esterases were partially entrapped within the hydrogel discs and produced the strong signals. A better method of measuring cell viability in 3-D hydrogels need to be utilised. One suggestion is the use of Hoechst 33342 alongside ethD-1 dyes. Hoechst 33342 stain would stain DNA in the nuclei of all cells whereas ethD-1 would only give red fluorescence to cells with compromised membranes as they bind to nucleic acids and enhances their fluorescence 40-fold (Sanfilippo et al., 2011). The difference between cells expressed Hoechst 33342 and ethD-1 stains would indicate the number of live cells in the sample.

Lastly, several areas can be conducted if not limited by the time-scale of DPhil such as the effects of growth factors (bFGF, SDF1α and BDNF) on the formation of tubule-like structures in HUVECs and neurite outgrowth in SH-SY5Ys; the recapitulation of other microenvironmental niches e.g. invasive and hypoxia niches; the assessment of cell viability and changes in glucose levels between 2-D monolayer, 3-D TissueFlex® and 3DFlo® culture systems, as well as the comparison between

the drug responses of the 3-D *in vitro* neuroblastoma model to patient-derived neuroblastoma biopsies.

7.4 Future perspectives

Following up from this thesis, there are various approaches this project can be taken further as described below.

7.4.1 Angiogenesis and pan-cancer therapy approach

As shown in Chapter 6 and many other studies, cancer cells develop resistance to drug candidates such as cisplatin and reduce their efficacy. Other neurotoxic anticancer drugs such as vincristine and methotrexate also need preliminary screening to prevent damage to cultured cells due to high dose. Most importantly, these drugs can affect any proliferating cells regardless of origin. Hence, a targeted drug delivery approach may come in hand to improve the selectivity of these drugs (Ivanov et al., 2015).

Another approach worth exploring is the indirect treatment of cancer by targeting its microenvironment instead. As its leaky vasculature characterises tumours, drug delivery to cancerous cells within the vascular niche can be made explicitly. Targeting angiogenic factors such as VEGF can be more advantageous than other chemotherapeutic drugs targeting cancer cells. This is because the drugs are not prone to any induction of resistance by the cancer cells as the therapeutic target is not these cancer cells directly. In addition, the angiogenesis inhibitors are delivered intravenously through the bloodstream, which is a pan-cancer therapy approach. This approach of cancer therapeutics can be applied alone or even in combination with other conventional therapies for synergistic outcomes (Khodarev et al., 2003).

An example of anti-angiogenic drugs is bevacizumab (Avastin), which is a neutralising antibody against VEGF. In glioma cells-HUVEC co-culture, HUVEC sprouting was suppressed by 75% when treated with bevacizumab (Chen, Htay, et al., 2009). Another glioma cells-HUVEC co-culture study also showed the

inhibition of vessel net-like structure after treatments with Herbimycin A and anti-VEGF antibody. The effect of which was not observed in HUVEC monocultures (Khodarev et al., 2003).

Analyses of treatment efficacy can be evaluated by looking at changes in CD31 expressions, changes in the cell viability or quantitatively by image analyses. Examples of quantitative analysis include the measurement of tubule branching points and tubule areas (Wan, Bovornchutichai, et al., 2017).

7.4.2 Stromal components in 3-D cancer models

The established 3-D *in vitro* neuroblastoma model and perfused bioreactors have overcome major limitations of the current 3-D cancer models, yet the system still neglects the presence of the immune system. This could be done by incorporating stromal cells such as mesenchymal stem cells (MSCs) into the culture. This is supported by a study showing that a tri-culture of cancer, endothelial and mesenchymal stem cells developed an enhanced resistance to chemotherapeutics compared to 2-D cultures (Bray, Binner, et al., 2015).

Another component worth exploring is the composition and interactions of tumour and stroma in the model. The 3-D organisation of tumour mass and stroma alters the diffusion profile of drugs through cell-cell and cell-matrix interactions (Xu, Farach-Carson, et al., 2014). The ratio between a tumour and stroma has been a prognostic factor for cancer: the higher stromal component, the higher risk of relapse and poor prognosis. Lower penetration is observed for drugs with high molecular weight in high-density tumours with more stroma content. Jaganathan et al. (2014) reported that the response of Doxorubicin and Doxil to treat CAF breast cancer cells and human pulmonary fibroblasts in 3-D co-culture were not drastically reduced when compared to 2-D monolayer culture. This implies that the addition or production of ECM plays a vital role in representing drug efficiency *in vitro*.

7.4.3 Genetic editing in 3-D cancer models

The 3-D *in vitro* neuroblastoma model can be further investigated at a genetic level to recapitulate native tumours more accurately. Clustered regularly interspaced short palindromic repeats (CRISPR)-Cas 9 system can be utilised to induce the loss-of-function to tumour suppressor genes and the gain-of-function to proto-oncogenes in NSCs. This will give rise to neural cancer stem cells as observed in human neuroblastoma.

The loss of heterozygosity in the short arm of chromosome 3 is one of the most common alterations in human cancer, in which within the segment 3p21.3 homes Ras association domain family 1 (RASSF1A) gene. The aberrant methylation of the RASSF1A promoter region results in the silencing of the tumour suppressor gene that is often detected in neuroblastoma, glioblastoma and medulloblastoma (Dammann et al., 2005). Besides, Liu, Yang, et al. (2011) reported the zinc-finger transcription factor CASZ1, locating at segment 1p36.22, to be the candidate tumour suppressor gene for neuroblastoma.

On the contrary, the overexpression of MYCN oncogene (located at 2p24.3) is reported to be the prognostic factor for neuroblastoma. As $50 - 100$ copies of gene amplifications observed in 25% of neuroblastoma cases, these amplifications correlate to the overexpression of trkB receptors as bad prognosis as well (Westermark et al., 2011; Manchanda and Manchanda, 2009). Furthermore, Wang, Diskin, et al. (2010) described a significant association of the LIM domain only 1 (LMO1) gene with developing neuroblastoma. Further alterations at this locus would lead to malignant progression.

Once edited, NSCs can be used in lieu of SH-SY5Ys to overcome the limitations of cancer cell lines, especially the selection of rapidly proliferating cells in late passages. 3-D genetically edited neuroblastoma model can be evaluated for cell responses to drugs and compared to the non-edited 3-D *in vitro* neuroblastoma model, 2-D monolayer model and 3-D biopsy cultures.

7.4.4 Combination therapy in 3-D *in vitro* drug screening platforms

It is important to mention that the concentrations of drugs used in combination therapy need to be evaluated for their interactions before administration. Some drugs such as retinoic acid (RA) can be used in combination with cisplatin without the need to reduce its concentration; RA-enhanced efficacy occurs without increasing the side effects of either cisplatin and RA itself (Formelli and Cleris, 2000).

Nevertheless, this is not the case for all drugs as some drug combinations can give rise to synergistic, additive or antagonistic effects at varying concentrations and drug ratios (Zhao, Au, et al., 2010). A study by Aebi et al. (1997) showed that the greatest degree of synergy occurred when RA and cisplatin were treated in the low concentration range, which seems to be beneficial for patients as the side effects due to high dosage are minimised.

Evaluation of drug interactions can be assessed by techniques such as combination index, isobologram analysis and Loewe additivity (Zhao, Au, et al., 2010; Novick, 2013).

7.4.5 Scaling up: microbioreactor systems

The goal of this project, given more time and resources, is to push TissueFlex® and 3DFlo® bioreactors into clinics as personalised drug screening platforms. The first step for scaling up requires the validation of results. This can be done by analysing protein expressions that is expected in neuroblastoma tumours and treatments such as NMA (related to a poor prognosis factor in neuroblastoma cases), cytochrome C oxidase and MnSOD (related to a decrease in ROS due to induction by RA) (Schneider et al., 2011), BCL-2 (related to drug resistance), NSE and ID1 (pertained to RA-induced differentiation) (Cheung et al., 2009). These can be measured using western blot and immunocytochemistry.

The next point to validate is the potential to apply the 3-D *in vitro* hydrogel model and the perfused microbioreactor into a personalised drug screening platform. The patients' responses towards the same drug can be different even when their

tumours share similarities in their genetic mutations. It is becoming evident that drug testing results on a small number of cell lines could not represent the diversity of the human population. The disparities in patient-dependent tumour variability and response to treatments are leading us towards personalised medicine (Mitra et al., 2013). To realise this target, a biopsy specimen can be applied to construct individualised testing models to screen out the most suitable treatment regimen for each patient.

The neuroblastoma biopsy specimen can be extracted from patients via various methods, such as enzymatic, chemical and mechanical techniques to produce cell suspensions. As the size of embedding cells within matrix affects experimental outcomes, a further investigation is needed to identify the tumour size that most represents the native tumour microenvironment in the perfused bioreactor. This presents a various choice of cultures: single cells, small aggregates or large aggregates; that will allow the observation of different phenomena such as individual cell migration/invasion, collective cell migration or a mixture of invasive and necrotic cells, respectively (Yamada and Cukierman, 2007).

Comparisons between neuroblastoma models and *ex vivo* samples under three-week perfusion culture should be performed. The end-point assays may include morphological analysis, cell viability and immunostaining for markers such as TuJ1, Nestin and CD31.

Even though the perfused bioreactor systems are validated to be used as personalised medicine, the main hurdle to overcome is the costs of the equipment, the operation and the throughput. Examples, in this case, would be the cost and the preparation of fragmented HyStem® and the peristaltic pump. In addition, the culture time of three weeks may appear to be either too short to observe any long-term side effects or too long for patients who need immediate medical intervention. Ultimately, the assay equipment, the ease of operation and the compatibility with existing culture systems must be weighed considerably against the cost and the quality of data acquired (Li and Cui, 2014).

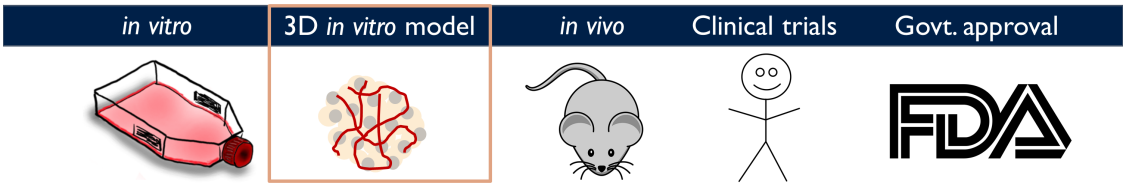


Figure 7.1: 3-D *in vitro* model in cancer drug discovery process Drugs are initially tested on the 2-D monolayer culture systems before tested in animals, then in human participants. The 3-D *in vitro* model has a potential to screen out unsuccessful candidates beforehand and shorten the length of the process.

7.5 Concluding remarks

Neuroblastoma remains one of the most fatal paediatric cancer due to the lack of effective therapeutic strategies. To investigate the efficacy of cancer drugs, each drug has to go through a series of screening tests on 2-D monolayer culture systems before tested in animals, then in human participants. This lengthy process can take up for 20 years for a single drug to be approved for use in clinics.

In addition, the inaccuracy of the 2-D *in vitro* tests further the complication of the drug screening process with a high failure rate up to 92%. The developed system of 3-D *in vitro* model and a perfused bioreactor has a potential to come in between the 2-D and 3-D *in vivo* models (see Figure 7.1). The system would screen out any unsuccessful candidates beforehand and shorten the length of the process.

3-D *in vitro* cancer models are advantageous tools for drug discovery and development, ranging from high throughput screening, drug delivery testing, metabolism and toxicity testing as well as target validation studies. Bioreactors can complement the models by allowing real-time and continuous genetic analyses and functional assessment of cells. This gives an opportunity to incorporate patient-derived biopsies into the system. Ultimately, the system helps to determine personalised therapeutic strategies and narrows the gap between cell culture and physiological tissue investigations.

Appendices

A

3-D image visualisation and analyses

For all 3-D images taken by the laser confocal microscope, there were mismatch of refraction indices between the 3-D hydrogel model and the water-based cell culture medium. This mismatch caused spherical aberration, which led to the spreading and distortion of the point spread function (PSF). The accuracy of PSF representation determines whether the extent of a successful image restoration (Model et al., 2010). In this case, the AutoquantX software was used to deconvolute, which was the process of using a mathematical algorithm to separate image information from artefacts. Ultimately, deconvolution improved the image resolution.

1. The 3-D image of the neuroblastoma model acquired from the laser confocal microscope was loaded into AutoquantX software (see Figure A.1A). After pressed on the 3-D deconvolution icon (see Figure A.1B), the display on the left-hand side was shown. Different inputs of z-spacing, wavelength channels, modality (see Figure A.1C), objective lens, numerical aperture, immersion medium, sample medium and distance from coverslip were required.

   For all 3-D images analysed in this thesis, the settings were fixed as follow: z-spacing = default from the input image; wavelength channels = 660 nm (blue), 525 nm (green) and 785 nm (red); modality = laser confocal microscope;

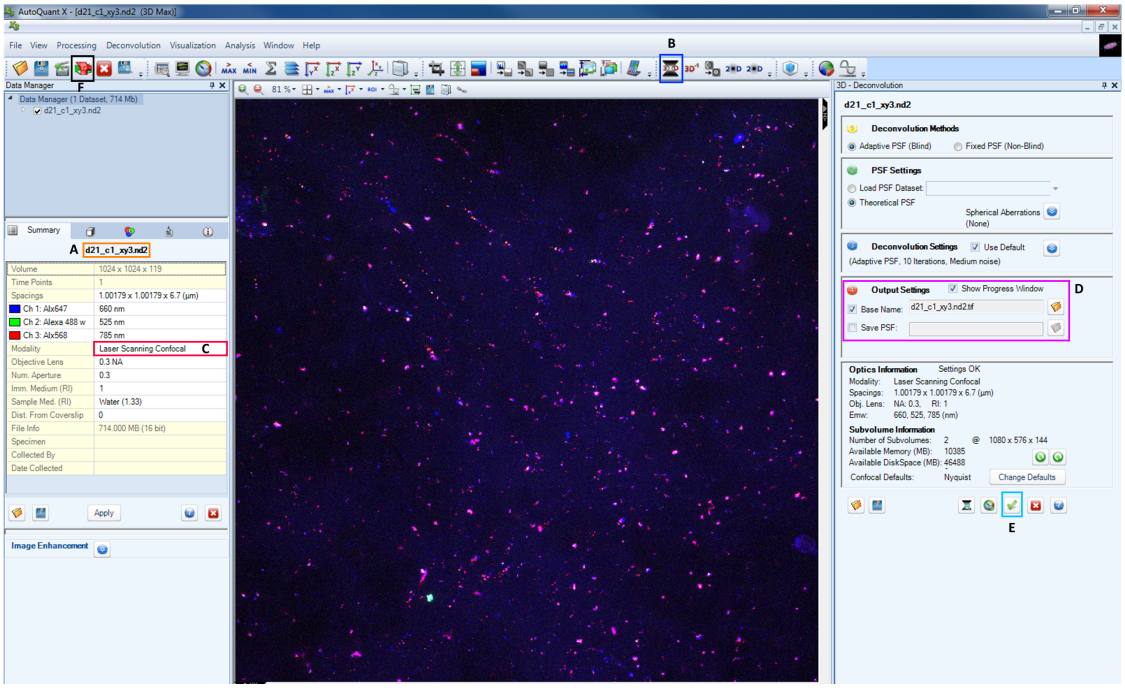


Figure A.1: Initial settings of 3-D image deconvolution Several inputs need to be checked before initiating the deconvolution process. (A) The original image file; (B) the 3-D deconvolution icon to start adjusting the parameters; (C) several inputs including the modality; (D) the location and name of the output image file; (E) the icon to start the deconvolution process and (F) the icon to export the output image to Imaris x64 software.

objective lens = 0.3NA; numerical aperture = 0.3; immersion medium = 1; sample medium = water (1.33) and distance from coverslip = 0.

After that, the location and name of the output image can be selected from the right-hand side of the screen (see Figure A.1D). The green tick button (see Figure A.1E) at the bottom-right of the screen was clicked to start the deconvolution process. The deconvolution process involved first-guessing at the initial image estimate by processing the input image through the inverse filter. The error was calculated between the initial image estimate and the input image. With the constraints provided by the previous image estimates, the deconvolution cycle was repeated until it reached the image estimate at the minimum error. Once completed, the output image was directly exported to Imaris x64 (see Figure A.1F) for further image analyses.

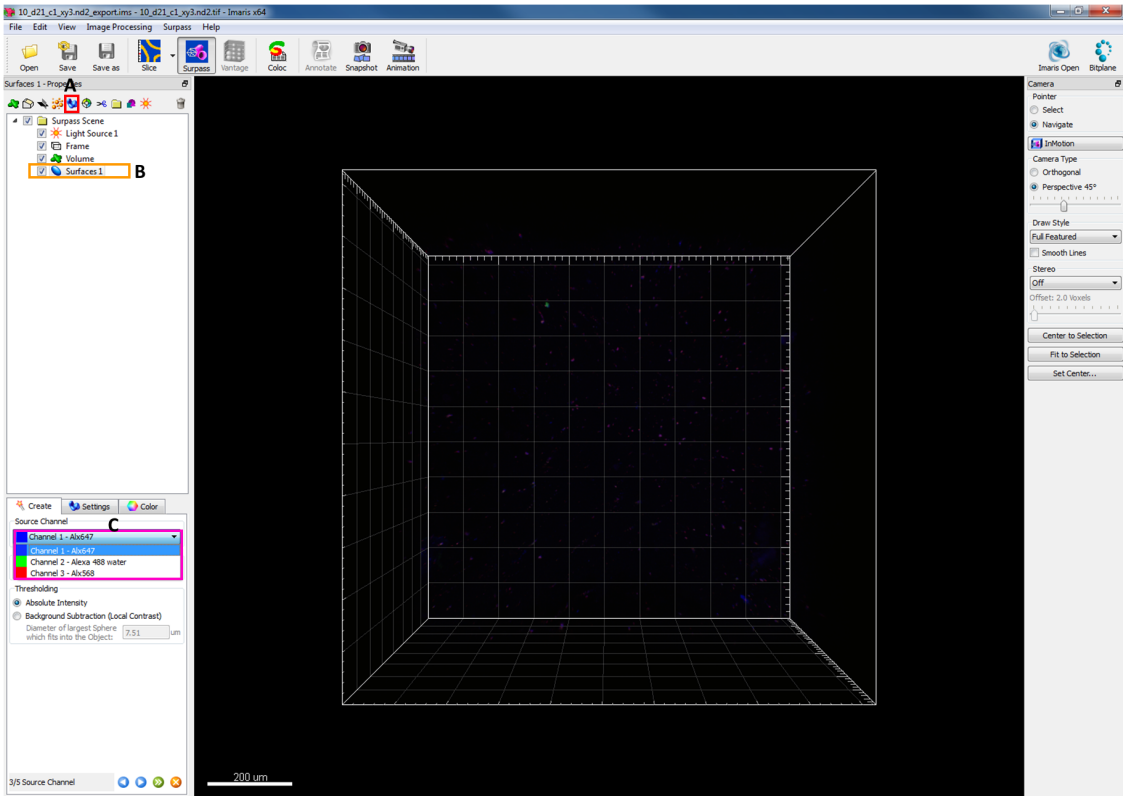


Figure A.2: Overlaying of cell surface markers (A) The icon to start the surface overlay on cells; (B) the first surface represented a selected channel shown in (C) under the surpass scene.

2. Imaris x64 software allowed the 3-D images to be clearly displayed and quantified. First, the surface icon (see Figure A.2A) was clicked to introduce the first surface (see Figure A.2B) under the surpass scene. Each surface represented only one of the selected channels (see Figure A.2C). The surface then formed an overlay to the cells that expressed surface markers that matched the selected channel.

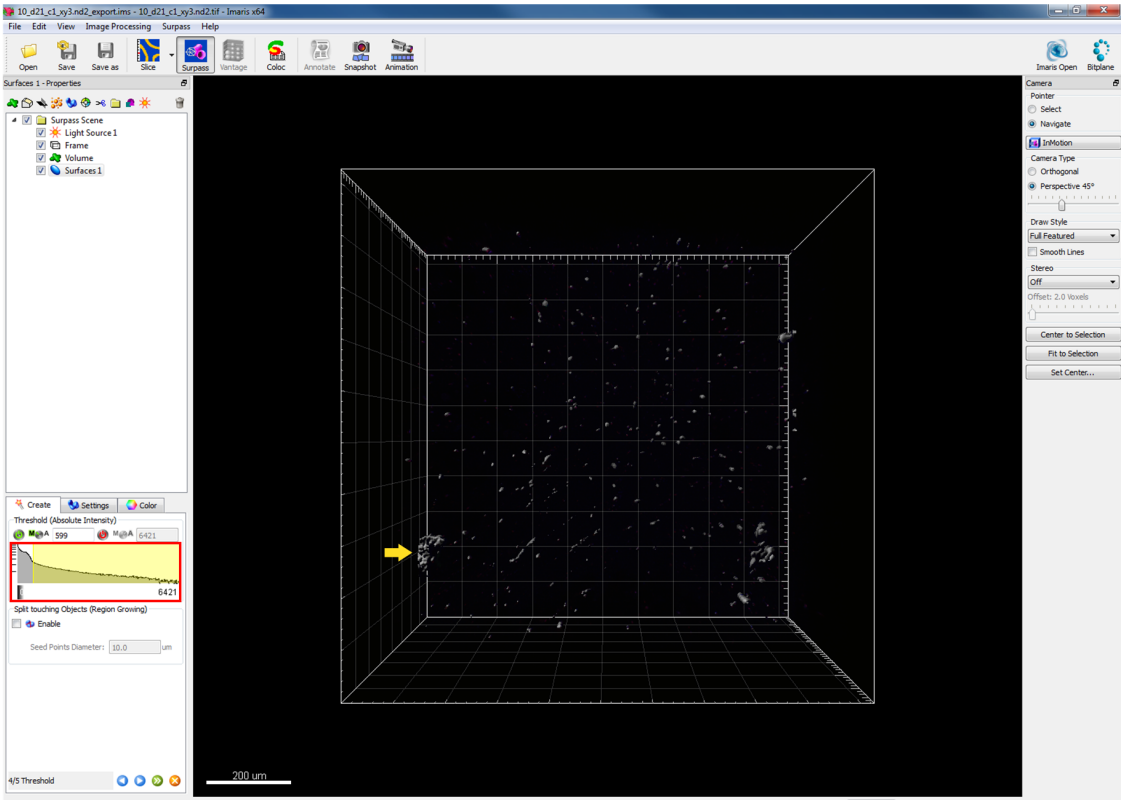


Figure A.3: Thresholding of cell surface markers The threshold for each 3-D image was selected as a point where there was a steep change in the absolute intensity (see red rectangle). The selected threshold ensured that only cells were selected (see yellow arrow) and not the background signals.

3. The surface created in each channel was determined by a threshold (see red rectangle in Figure A.3). The threshold in each image was selected from the kink formed by a steep change in the absolute intensity. High intensity regions implied that background signals were considered to form surfaces as well. Once the threshold was selected, the formation of surfaces around cells and their clusters can be seen in the z-stack image (see yellow arrow in Figure A.3).

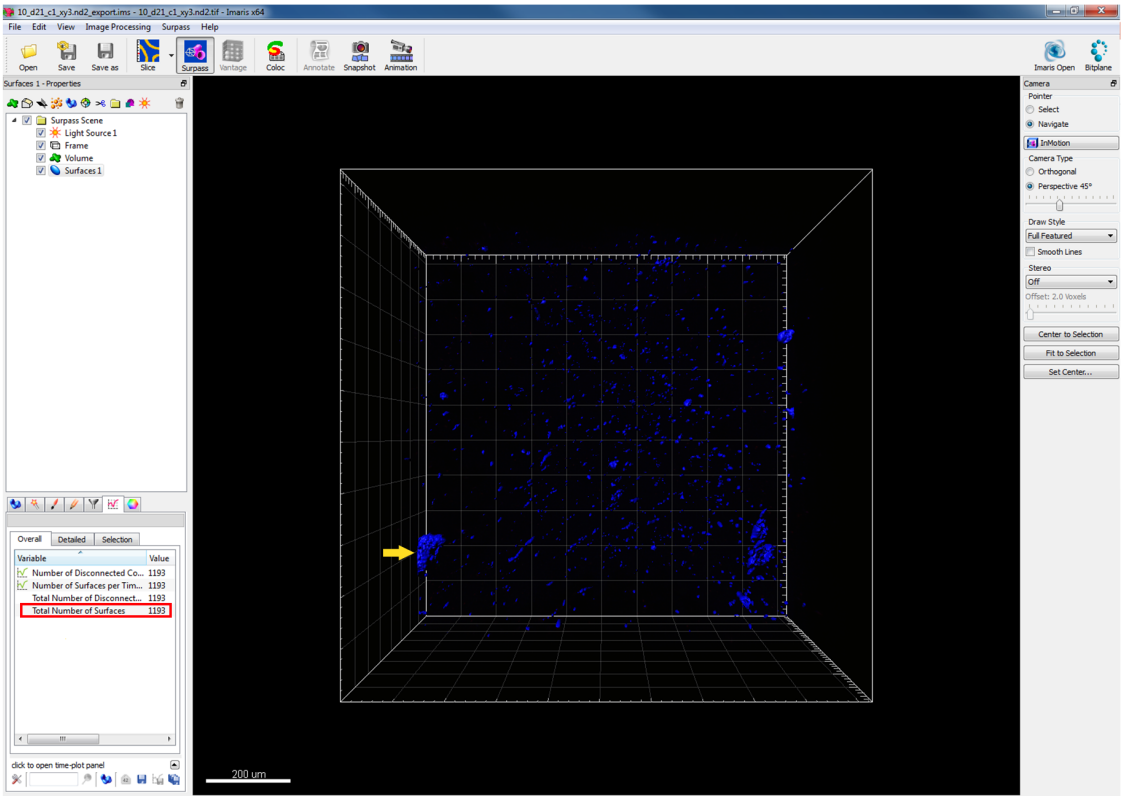


Figure A.4: Quantification of cell surface markers The number of cells expressing specific markers was determined by the total number of surfaces counted. Cell counting was performed by an algorithm counting the number of 8-connected voxels.

4. The total number of cells expressing specific markers was determined by an algorithm that counted the number of 8-connected voxels. As shown in a yellow arrow in Figure A.4, the number of cells expressing TuJ1 was shown in blue colour and the total number of TuJ1^{+} cells was represented by the total number of surfaces (see red rectangle in Figure A.4).

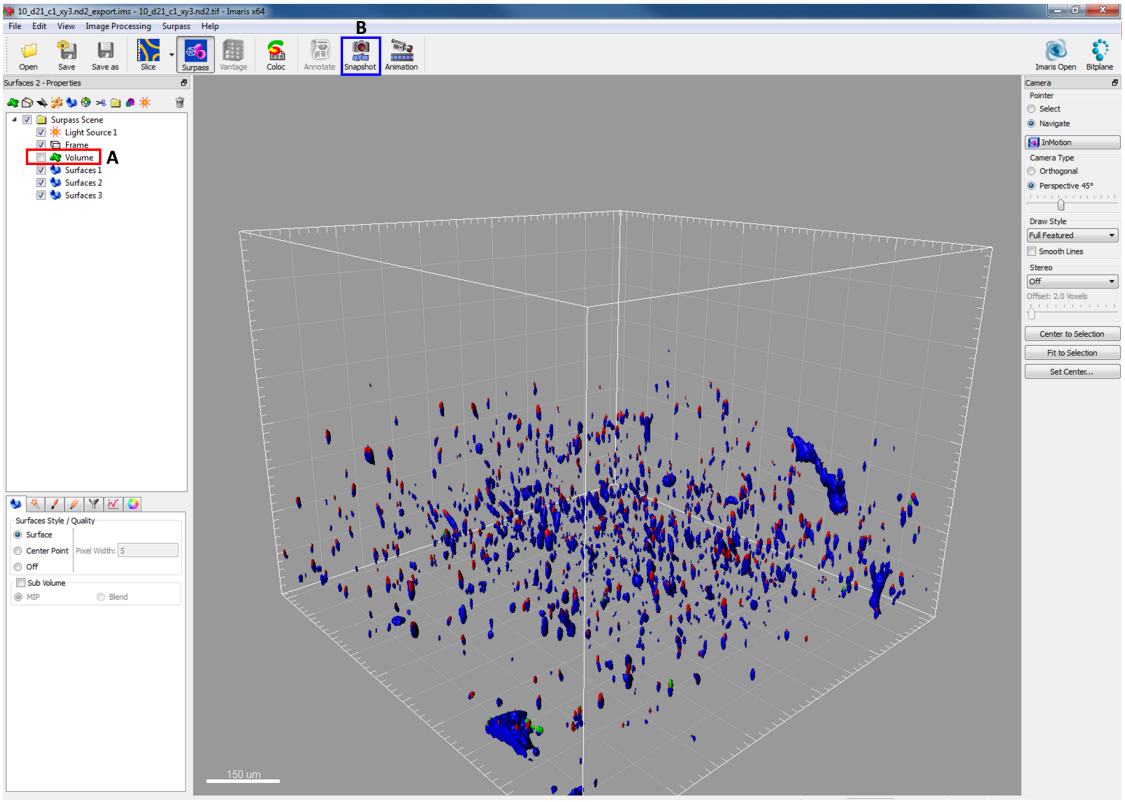


Figure A.5: Computer-generated representations of three different cell surface markers (A) The unclicked volume icon revealed the reconstructed 3-D image with all coloured surfaces; (B) the snapshot icon allowed the screenshots of the image to be saved.

5. The process of computer-generated representations by surface overlaying was repeated for all other channels of stained markers. Figure A.5 shows the z-stack 3-D image of three different coloured surfaces formed representing three different cell surface markers. Once then, the volume icon was unclicked (see Figure A.5A) to reveal the reconstructed 3-D image of the co-culture model. The orientation and the magnification of the model can be adjusted. Finally, the snapshot icon (see Figure A.5B) was clicked to save the image.

References

Abou Neel E. A., Cheema U., Knowles J. C., Brown R. A., and Nazhat S. N. (2006). "Use of multiple unconfined compression for control of collagen gel scaffold density and mechanical properties". In: *Soft Matter* 2.11, pp. 986–992.

Aebi S., Kröning R., Cenni B., Sharma A., Fink D., Los G., Weisman R., Howell S. B., and Christen R. D. (1997). "All-trans retinoic acid enhances cisplatin-induced apoptosis in human ovarian adenocarcinoma and in squamous head and neck cancer cells". In: *Clinical Cancer Research* 3.11, pp. 2033–2038.

Agholme L., Lindstrom T., Kagedal K., Marcusson J., and Hallbeck M. (2010). "An in vitro model for neuroscience: differentiation of SH-SY5Y cells into cells with morphological and biochemical characteristics of mature neurons". In: *Journal of Alzheimer's Disease* 20.4, pp. 1069–1082.

Alemany-Ribes M. and Semino C. E. (2014). "Bioengineering 3D environments for cancer models". In: *Advanced Drug Delivery Reviews* 79-80.1, pp. 40–49.

Arbeláez P., Maire M., Fowlkes C., and Malik J. (2011). "Contour detection and hierarchical image segmentation". In: *IEEE Transactions on Pattern Analysis and Machine Intelligence* 33.5, pp. 898–916.

Arnaoutova I. and Kleinman H. K. (2010). "In vitro angiogenesis: endothelial cell tube formation on gelled basement membrane extract". In: *Nature Protocols* 5.4, pp. 628–635.

Arnold J. T., Kaufman D. G., Seppälä M., and Lessey B. A. (2001). "Endometrial stromal cells regulate epithelial cell growth in vitro: a new co-culture model". In: *Human Reproduction* 16.5, pp. 836–845.

Arrieta O., González-De La Rosa C. H., Aréchaga-Ocampo E., Villanueva-Rodríguez G., Cerón-Lizárraga T. L., Martínez-Barrera L., Vázquez-Manríquez M. E., Ríos-Trejo M. Á., Álvarez-Avitia M. Á., Hernández-Pedro N., Rojas-Marín C., and De La Garza J. (2010). "Randomized phase II Trial of all-trans-retinoic acid with chemotherapy based on paclitaxel and cisplatin as first-line treatment in patients with advanced non-small-cell lung cancer". In: *Journal of Clinical Oncology* 28.21, pp. 3463–3471.

Barber P. R., Vojnovic B., Ameer-Beg S. M., Hodgkiss R. J., Tozer G. M., and Wilson J. (2003). "Semi-automated software for the three-dimensional delineation of complex vascular networks". In: *Journal of Microscopy* 211.1, pp. 54–62.

Benesch M., Windelberg M., Sauseng W., Witt V., Fleischhack G., Lackner H., Gadner H., Bode U., and Urban C. (2008). "Compassionate use of bevacizumab (Avastin) in children and young adults with refractory or recurrent solid tumors". In: *Annals of Oncology* 19.4, pp. 807–813.

Billiet T., Vandenhaute M., Schelfhout J., Van Vlierberghe S., and Dubruel P. (2012). "A review of trends and limitations in hydrogel-rapid prototyping for tissue engineering". In: *Biomaterials* 33.26, pp. 6020–6041.

Brafman D. A. (2013). "Constructing stem cell microenvironments using bioengineering approaches". In: *Physiological Genomics* 45.23, pp. 1123–1135.

Bray F., Ferlay J., and Soerjomataram I. (2018). "Global cancer statistics 2018 : GLOBOCAN estimates of incidence and mortality worldwide for 36 cancers in 185 countries". In: *CA: A Cancer Journal for Clinicians* 00.00, pp. 1–31.

Bray L. J., Binner M., Holzheu A., Friedrichs J., Freudenberg U., Hutmacher D. W., and Werner C. (2015). "Multi-parametric hydrogels support 3D in vitro bioengineered microenvironment models of tumour angiogenesis". In: *Biomaterials* 53.1, pp. 609–620.

Brown C. K., Khodarev N. N., Yu J., Moo-Young T., Labay E., Darga T. E., Posner M. C., Weichselbaum R. R., and Mauceri H. J. (2004). "Glioblastoma cells block radiation-induced programmed cell death of endothelial cells". In: *FEBS Letters* 565.1-3, pp. 167–170.

Brown J. M. (2007). "Tumor hypoxia in cancer therapy". In: *Methods in Enzymology.* Vol. 435. Chap. 15, pp. 295–321.

Brown J. M. and Wilson W. R. (2004). "Exploiting tumour hypoxia in cancer treatment". In: *Nature Reviews Cancer* 4.6, pp. 437–447.

Calabrese C., Poppleton H., Kocak M., Hogg T. L., Fuller C., Hamner B., Oh E. Y., Gaber M. W., Finklestein D., Allen M., Frank A., Bayazitov I. T., Zakharenko S. S., Gajjar A., Davidoff A., and Gilbertson R. J. (2007). "A perivascular niche for brain tumor stem cells". In: *Cancer Cell* 11.1, pp. 69–82.

Carmeliet P. (2003). "Blood vessels and nerves: common signals, pathways and diseases". In: *Nature Reviews Genetics* 4.1, pp. 710–720.

Chang B. and Patro S. Y. (2004). "Design of freeze-drying processes for pharmaceuticals: practical advice". In: *Lyophilization of Biopharmaceuticals*, pp. 113–138.

Chen D., Qu Y., Hua X., Zhang L., Liu Z., Pflugfelder S. C., and Li D. Q. (2017). "A hyaluronan hydrogel scaffold-based xeno-free culture system for ex vivo expansion of human corneal epithelial stem cells". In: *Eye* 31, p. 962.

Chen L., Xiao Z., Meng Y., Zhao Y., Han J., Su G., Chen B., and Dai J. (2012). "The enhancement of cancer stem cell properties of MCF-7 cells in 3D collagen scaffolds for modeling of cancer and anti-cancer drugs". In: *Biomaterials* 33.5, pp. 1437–1444.

Chen Z., Htay A., Santos W. D., Gillies G. T., Fillmore H. L., Sholley M. M., and Broaddus W. C. (2009). "In vitro angiogenesis by human umbilical vein endothelial cells (HUVEC) induced by three-dimensional co-culture with glioblastoma cells". In: *Journal of Neuro-Oncology* 92.2, pp. 121–128.

Cheung Y., Lau W. K. W., Yu M. S., Lai C. S. W., Yeung S. C., So K. F., and Chang R. C. C. (2009). "Effects of all-trans-retinoic acid on human SH-SY5Y neuroblastoma as in vitro model in neurotoxicity research". In: *NeuroToxicology* 30.1, pp. 127–135.

Choi S. W., Gerencser A. A., and Nicholls D. G. (2009). "Bioenergetic analysis of isolated cerebrocortical nerve terminals on a microgram scale: Spare respiratory capacity and stochastic mitochondrial failure". In: *Journal of Neurochemistry* 109.4, pp. 1179–1191.

Choi S. Y. C., Lin D., Gout P. W., Collins C. C., Xu Y., and Wang Y. (2014). "Lessons from patient-derived xenografts for better in vitro modeling of human cancer". In: *Advanced Drug Delivery Reviews* 79-80.1, pp. 222–237.

Christensen R. M. (1982). "Viscoelastic stress strain constitutive relations". In: *Theory of Viscoelasticity: An Introduction*. 2nd ed. Academic Press. Chap. 1, pp. 1–34.

Christofori G. (2006). "New signals from the invasive front". In: *Nature* 441.7092, pp. 444–450.

Chung S., Sudo R., MacK P. J., Wan C. R., Vickerman V., and Kamm R. D. (2009). "Cell migration into scaffolds under co-culture conditions in a microfluidic platform". In: *Lab on a Chip* 9.2, pp. 269–275.

Chwalek K., Tsurkan M. V., Freudenberg U., and Werner C. (2014). "Glycosaminoglycan-based hydrogels to modulate heterocellular communication in in vitro angiogenesis models". In: *Scientific Reports* 4.4414, pp. 1–8.

Clarke M. F. (2004). "At the root of brain cancer". In: *Nature* 432.7015, pp. 281–282.

Crystal A. S., Shaw A. T., Sequist L. V., Friboulet L., Niederst M. J., Lockerman E. L., Frias R. L., Gainor J. F., Amzallag A., Greninger P., Lee D., Kalsy A., Gomez-Caraballo M., Elamine L., Howe E., Hur W., Lifshits E., Robinson H. E., Katayama R., Faber A. C., Awad M. M., Ramaswamy S., Mino-Kenudson M., Iafrate A. J., Benes C. H., and Engelman J. A. (2014). "Patient-derived models of acquired resistance can identify effective drug combinations for cancer". In: *Science* 346.6216, pp. 1480–1486.

Cui Z. F., Xu X., Trainor N., Triffitt J. T., Urban J. P. G., and Tirlapur U. K. (2007). "Application of multiple parallel perfused microbioreactors and three-dimensional stem cell culture for toxicity testing". In: *Toxicology in Vitro* 21.7, pp. 1318–1324.

Cullen D. K., Vukasinovic J., Glezer A., and Laplaca M. C. (2007). "Microfluidic engineered high cell density three-dimensional neural cultures". In: *Journal of Neural Engineering* 4.2, pp. 159–172.

Cunningham R. E. (2009). "Tissue Disaggregation". In: *Immunocytochemical Methods and Protocols*. Vol. 588, pp. 327–330.

Dammann R., Schagdarsurengin U., Seidel C., Strunnikova M., Rastetter M., Baier K., and Pfeifer G. P. (2005). "The tumor suppressor RASSF1A in human carcinogenesis: An update". In: *Histology and Histopathology* 20.1, pp. 645–663.

Daud M. F. B., Pawar K. C., Claeyssens F., Ryan A. J., and Haycock J. W. (2012). "An aligned 3D neuronal-glial co-culture model for peripheral nerve studies". In: *Biomaterials* 33.25, pp. 5901–5913.

Decker T. and Lohmann-Matthes M. L. (1988). "A quick and simple method for the quantitation of lactate dehydrogenase release in measurements of cellular cytotoxicity and tumor necrosis factor (TNF) activity". In: *Journal of Immunological Methods* 115.1, pp. 61–69.

Delibasis K. K., Kechriniotis A. I., Tsonos C., and Assimakis N. (2010). "Automatic model-based tracing algorithm for vessel segmentation and diameter estimation". In: *Computer Methods and Programs in Biomedicine* 100.2, pp. 108–122.

Despina S. and Hannon G. J. (2013). "Patient derived tumor xenografts: transforming clinical samples into mouse models". In: *Cancer Research* 13.2, pp. 83–96.

Double J. A. and Bibby M. C. (1989). "Therapeutic index: A vital component in selection of anticancer agents for clinical trial". In: *JNCI: Journal of the National Cancer Institute* 81.13, pp. 988–994.

Dwane S., Durack E., and Kiely P. A. (2013). "Optimising parameters for the differentiation of SH-SY5Y cells to study cell adhesion and cell migration". In: *BMC Research Notes* 6.1, p. 366.

Ebert B. L., Firth J. D., and Ratcliffe P. J. (1995). "Hypoxia and mitochondrial inhibitors regulate expression of glucose transporter-1 via distinct cis-acting sequences". In: *The Journal of Biological Chemistry* 270.49, pp. 29083–29089.

Encinas M., Iglesias M., Liu Y., Wang H., Muhaisen A., Ceña V., Gallego C., and Comella J. X. (2000). "Sequential treatment of SH-SY5Y cells with retinoic acid and brain-derived neurotrophic factor gives rise to fully differentiated, neurotrophic factor-dependent, human neuron-like cells". In: *Journal of Neurochemistry* 75.3, pp. 991–1003.

Estes J. M., Oliver P. G., Straughn J. M. J., Zhou T., Wang W., Grizzle W. E., Alvarez R. D., Stockard C. R., LoBuglio A. F., and Buchsbaum D. J. (2016). "Efficacy of anti-death receptor 5 (DR5) antibody (TRA-8) against primary human ovarian carcinoma using a novel ex vivo tissue slice model". In: *Gynecologic Oncology* 105.2, pp. 291–298.

Estrada M. F., Rebelo S. P., Davies E. J., Pinto M. T., Pereira H., Santo V. E., Smalley M. J., Barry S. T., Gualda E. J., Alves P. M., Anderson E., and Brito C. (2016). "Modelling the tumour microenvironment in long-term microencapsulated 3D co-cultures recapitulates phenotypic features of disease progression". In: *Biomaterials* 78.1, pp. 50–61.

Ezashi T., Das P., and Roberts R. M. (2005). "Low O2 tensions and the prevention of differentiation of hES cells". In: *Proceedings of the National Academy of Sciences* 102.13, pp. 2–7.

Fang X., Sittadjody S., Gyabaah K., Opara E. C., and Balaji K. C. (2013). "Novel 3D co-culture model for epithelial-stromal cells interaction in prostate cancer". In: *PLoS ONE* 8.9, pp. 1–10.

Ferrarini M., Steimberg N., Ponzoni M., Belloni D., Berenzi A., Girlanda S., Caligaris-Cappio F., Mazzoleni G., and Ferrero E. (2013). "Ex-vivo dynamic 3-D culture of human tissues in the RCCS™ bioreactor allows the study of multiple myeloma biology and response to therapy". In: *PLoS ONE* 8.8, pp. 1–10.

Flanagan L. A., Rebaza L. M., Derzic S., Schwartz P. H., and Monuki E. S. (2006). "Regulation of human neural precursor cells by laminin and integrins". In: *Journal of Neuroscience Research* 83.5, pp. 845–856.

Fong E. L. S., Harrington D. A., Farach-Carson M. C., and Yu H. (2016). "Heralding a new paradigm in 3D tumor modeling". In: *Biomaterials* 108.1, pp. 197–213.

Formelli F. and Cleris L. (2000). "Therapeutic effects of the combination of fenretinide and all-trans-retinoic acid and of the two retinoids with cisplatin in a human ovarian carcinoma xenograft and in a cisplatin-resistant sub-line". In: *European Journal of Cancer* 36.18, pp. 2411–2419.

Forsyth N. R., Musio A., Vezzoni P., Simpson A. H. R. W., Noble B. S., and McWhir J. (2006). "Physiologic oxygen enhances human embryonic stem cell clonal recovery and reduces chromosomal abnormalities". In: *Cloning and Stem Cells* 8.1, pp. 16–23.

Franzmann E. J., Schroeder G. L., Goodwin W. J., Weed D. T., Fisher P., and Lokeshwar V. B. (2003). "Expression of tumor markers hyaluronic acid and hyaluronidase (HYAL1) in head and neck tumors". In: *International Journal of Cancer* 106.3, pp. 438–445.

George J. H., Waller S. T., and Ye H. (2017). "4.13 Use and manipulation of microporous membranes in mammalian cell cultures". In: *Comprehensive Membrane Science and Engineering, Second Edition*, pp. 272–292.

Ghosh K., Pan Z., Guan E., Ge S., Liu Y., Nakamura T., Ren X., Rafailovich M., and Clark R. A. F. (2007). "Cell adaptation to a physiologically relevant ECM mimic with different viscoelastic properties". In: *Biomaterials* 28.4, pp. 671–679.

Gibbons J., Hewitt E., and Gardner D. K. (2006). "Effects of oxygen tension on the establishment and lactate dehydrogenase activity of murine embryonic stem cells". In: *Cloning and Stem Cells* 8.2, pp. 117–122.

Godugu C., Patel A. R., Desai U., Andey T., Sams A., and Singh M. (2013). "AlgiMatrix based 3D cell culture system as an in-vitro tumor model for anticancer studies". In: *PLoS ONE* 8.1, e53708.

Goers L., Freemont P., and Polizzi K. M. (2014). "Co-culture systems and technologies: Taking synthetic biology to the next level". In: *Journal of the Royal Society, Interface* 11.96, pp. 1–13.

Gottesman M. M. (2002). "Mechanisms of cancer drug resistance". In: *Annual Review of Medicine* 53.1, pp. 615–627.

Grandér D. (1998). "How do mutated oncogenes and tumor suppressor genes cause cancer?" In: *Medical Oncology* 15.1, pp. 20–26.

Gritti A., Frölichsthal-Schoeller P., Galli R., Parati E. A., Cova L., Pagano S. F., Bjornson C. R., and Vescovi A. L. (1999). "Epidermal and fibroblast growth factors behave as mitogenic regulators for a single multipotent stem cell-like population from the subventricular region of the adult mouse forebrain". In: *The Journal of Neuroscience* 19.9, pp. 3287–3297.

Hanahan D. and Folkman J. (1996). "Patterns and emerging mechanisms of the angiogenic switch during tumorigenesis". In: *Cell* 86.3, pp. 353–364.

Haugh M. G., Murphy C. M., and O'Brien F. J. (2010). "Novel freeze-drying methods to produce a range of collagen–glycosaminoglycan scaffolds with tailored mean pore sizes". In: *Tissue Engineering Part C: Methods* 16.5, pp. 887–894.

Hickman J. A., Graeser R., De Hoogt R., Vidic S., Brito C., Gutekunst M., and Van der Kuip H. (2014). "Three-dimensional models of cancer for pharmacology and cancer cell biology: Capturing tumor complexity in vitro/ex vivo". In: *Biotechnology Journal* 9.9, pp. 1115–1128.

Hiratsuka S., Watanabe A., Aburatani H., and Maru Y. (2006). "Tumour-mediated upregulation of chemoattractants and recruitment of myeloid cells predetermines lung metastasis". In: *Nature Cell Biology* 8.12, pp. 1369–1375.

Hiratsuka S., Watanabe A., Sakurai Y., Akashi-Takamura S., Ishibashi S., Miyake K., Shibuya M., Akira S., Aburatani H., and Maru Y. (2008). "The S100A8-serum amyloid A3-TLR4 paracrine cascade establishes a pre-metastatic phase". In: *Nature Cell Biology* 10.11, pp. 1349–1355.

Hirt C., Papadimitropoulos A., Muraro M. G., Mele V., Panopoulos E., Cremonesi E., Ivanek R., Schultz-Thater E., Droeser R. A., Mengus C., Heberer M., Oertli D., Iezzi G., Zajac P., Eppenberger-Castori S., Tornillo L., Terracciano L., Martin I., and Spagnoli G. C. (2015). "Bioreactor-engineered cancer tissue-like structures mimic phenotypes, gene expression profiles and drug resistance patterns observed "in vivo"". In: *Biomaterials* 62.1, pp. 138–146.

Hofmann A., Ritz U., Verrier S., Eglin D., Alini M., Fuchs S., Kirkpatrick C. J., and Rommens P. M. (2008). "The effect of human osteoblasts on proliferation and neo-vessel formation of human umbilical vein endothelial cells in a long-term 3D co-culture on polyurethane scaffolds". In: *Biomaterials* 29.31, pp. 4217–4226.

Holohan C., Van Schaeybroeck S., Longley D., and Johnston P. (2013). "Cancer drug resistance: An evolving paradigm". In: *Nature Review Cancer* 13.1, pp. 714–726.

Hsieh C. H., Chen Y. D., Huang S. F., Wang H. M., and Wu M. H. (2015). "The effect of primary cancer cell culture models on the results of drug chemosensitivity assays: The application of perfusion microbioreactor system as cell culture vessel". In: *BioMed Research International* 2015.1, pp. 1–10.

Huang L., Holtzinger A., Jagan I., Begora M., Lohse I., Ngai N., Nostro C., Wang R., Muthuswamy L. B., Howard C., Arrowsmith C., Kalloger S. E., Renouf D. J., Ashton A., Gallinger S., Keller G., and Muthuswamy S. K. (2016). "Ductal pancreatic cancer modeling and drug screening using human pluripotent stem cell and patient-derived tumor organoids". In: *Nature Medicine* 21.11, pp. 1364–1371.

Hutmacher D. W., Horch R. E., Loessner D., Rizzi S., Sieh S., Reichert J. C., Clements J. A., Beier J. P., Arkudas A., Bleiziffer O., and Kneser U. (2009). "Translating tissue engineering technology platforms into cancer research". In: *Journal of Cellular and Molecular Medicine* 13.8, pp. 1417–1427.

Imamura Y., Mukohara T., Shimono Y., Funakoshi Y., Chayahara N., Toyoda M., Kiyota N., Takao S., Kono S., Nakatsura T., and Minami H. (2015). "Comparison of 2D- and 3D-culture models as drug-testing platforms in breast cancer". In: *Oncology Reports* 33.4, pp. 1837–1843.

Ivanov D. P., Parker T. L., Walker D. A., Alexander C., Ashford M. B., Gellert P. R., and Garnett M. C. (2015). "In vitro co-culture model of medulloblastoma and human neural stem cells for drug delivery assessment". In: *Journal of Biotechnology* 205.1, pp. 3–13.

Jaganathan H., Gage J., Leonard F., Srinivasan S., Souza G. R., Dave B., and Godin B. (2014). "Three-dimensional in vitro co-culture model of breast tumor using magnetic levitation". In: *Scientific Reports* 4.6468, pp. 1–9.

Jin K., Zhu Y., Sun Y., Mao X. O., Xie L., and Greenberg D. A. (2002). "Vascular endothelial growth factor (VEGF) stimulates neurogenesis in vitro and in vivo". In: *Proceedings of the National Academy of Sciences* 99.18, pp. 11946–11950.

Katakowski M., Zhang Z., DeCarvalho A. C., and Chopp M. (2005). "EphB2 induces proliferation and promotes a neuronal fate in adult subventricular neural precursor cells". In: *Neuroscience Letters* 385.3, pp. 204–209.

Kaul H., Ventikos Y., and Cui Z. (2016). "A computational analysis of the impact of mass transport and shear on three-dimensional stem cell cultures in perfused micro-bioreactors". In: *Chinese Journal of Chemical Engineering* 24.1, pp. 163–174.

Khodarev N. N., Yu J., Labay E., Darga T., Brown C. K., Mauceri H. J., Yassari R., Gupta N., and Weichselbaum R. R. (2003). "Tumour-endothelium interactions in co-culture: coordinated changes of gene expression profiles and phenotypic properties of endothelial cells." In: *Journal of cell science* 116.1, pp. 1013–1022.

Kievit F. M., Florczyk S. J., Leung M. C., Wang K., Wu J. D., Silber J. R., Ellenbogen R. G., Lee J. S. H., and Zhang M. (2014). "Proliferation and enrichment of CD133(+) glioblastoma cancer stem cells on 3D chitosan-alginate scaffolds". In: *Biomaterials* 35.33, pp. 9137–9143.

Kim M., Kim Y. H., and Tae G. (2013). "Human mesenchymal stem cell culture on heparin-based hydrogels and the modulation of interactions by gel elasticity and heparin amount". In: *Acta Biomaterialia* 9.8, pp. 7833–7844.

King J. A. and Miller W. M. (2007). "Bioreactor development for stem cell expansion and controlled differentiation". In: *Current Opinion in Chemical Biology* 11.4, pp. 394–398.

Knuchel R., Hofstadter F., Jenkins W. E. A., and Masters J. R. W. (1989). "Sensitivities of monolayers and spheroids of the human bladder cancer cell line MGH-U1 to the drugs used for intravesical chemotherapy". In: *Cancer Research* 49.6, pp. 1397–1401.

Kruyt M. C., Bruijn J. D. de, Yuan H., Blitterswijk C. A. van, Verbout A. J., Oner F. C., and Dhert W. J. A. (2004). "Optimization of bone tissue engineering in goats: a peroperative seeding method using cryopreserved cells and localized bone formation in calcium phosphate scaffolds". In: *Transplantation* 77.3, pp. 359–365.

Kumar H. R., Zhong X., Hoelz D. J., Rescorla F. J., Hickey R. J., Malkas L. H., and Sandoval J. A. (2008). "Three-dimensional neuroblastoma cell culture: proteomic analysis between monolayer and multicellular tumor spheroids". In: *Pediatric Surgery International* 24.11, pp. 1229–1234.

Lam W. A., Cao L., Umesh V., Keung A. J., Sen S., and Kumar S. (2010). "Extracellular matrix rigidity modulates neuroblastoma cell differentiation and N-myc expression". In: *Molecular Cancer* 9.35, pp. 1–7.

Lathia J. D., Heddleston J. M., Venere M., and Rich J. N. (2011). "Deadly teamwork: neural cancer stem cells and the tumor microenvironment". In: *Cell Stem Cell* 8.5, pp. 482–485.

Lazzari G., Couvreur P., and Mura S. (2017). "Multicellular tumor spheroids: a relevant 3D model for the in vitro preclinical investigation of polymer nanomedicines". In: *Polymer Chemistry* 8.34, pp. 4947–4969.

Leisten I., Kramann R., Ventura Ferreira M. S., Bovi M., Neuss S., Ziegler P., Wagner W., Knüchel R., and Schneider R. K. (2012). "3D co-culture of hematopoietic stem and progenitor cells and mesenchymal stem cells in collagen scaffolds as a model of the hematopoietic niche". In: *Biomaterials* 33.6, pp. 1736–1747.

Levenberg S. (2005). "Engineering blood vessels from stem cells: Recent advances and applications". In: *Current Opinion in Biotechnology* 16.5, pp. 516–523.

Leventhal C., Rafii S., Rafii D., Shahar A., and Goldman S. A. (1999). "Endothelial trophic support of neuronal production and recruitment from the adult mammalian subependyma". In: *Molecular and Cellular Neurosciences* 13.6, pp. 450–464.

Li Q., Ford M. C., Lavik E. B., and Madri J. A. (2006). "Modeling the neurovascular niche: VEGF- and BDNF-mediated cross-talk between neural stem cells and endothelial cells: An in vitro study". In: *Journal of Neuroscience Research* 84.11, pp. 1656–1668.

Li Z. and Cui Z. (2014). "Three-dimensional perfused cell culture". In: *Biotechnology Advances* 32.2, pp. 243–254.

Li Z., Sun H., Zhang J., Zhang H., Meng F., and Cui Z. (2013). "Development of in vitro 3D TissueFlex islet model for diabetic drug efficacy testing". In: *PLoS ONE* 8.8, pp. 1–10.

Liaudet-Coopman E. D., Berchem G. J., and Wellstein A. (1997). "In vivo inhibition of angiogenesis and induction of apoptosis by retinoic acid in squamous cell carcinoma". In: *Clinical Cancer Research* 3.2, pp. 179–184.

Lim K., Seonwoo H., Son H., Baik S., Kim J., Jeon S., Park J., Choung Y., Cho C., Choung P., and Chung J. H. (2009). "Biomechanical effects of fluid dynamics and mass transport on cell growth in perfusion bioreactors for tissue engineering". In: *Tissue Engineering and Regenerative Medicine* 6.14, pp. 1327–1328.

Liu Y., Wang R., Zarembinski T. I., Doty N., Jiang C., Regatieri C., Zhang X., and Young M. J. (2012). "The application of hyaluronic acid hydrogels to retinal progenitor cell transplantation". In: *Tissue Engineering Part A* 19.1-2, pp. 135–142.

Liu Z., Yang X., Li Z., McMahon C., Sizer C., Barenboim-Stapleton L., Bliskovsky V., Mock B., Ried T., London W. B., Maris J., Khan J., and Thiele C. J. (July 2011). "CASZ1, a candidate tumor-suppressor gene, suppresses neuroblastoma tumor growth through reprogramming gene expression". In: *Cell Death and Differentiation* 18.7, pp. 1174–1183.

Ljung B., Mayall B., Lottich C., Boyer C., Sylvester S. S., Leight G. S., Siegler H. F., and Smith H. S. (1989). "Cell dissociation techniques in human breast cancer - Variations in tumor cell viability and DNA ploidy". In: *Breast Cancer Research and Treatment* 159.13, pp. 153–159.

Louis D., Perry A., Reifenberger G., Deimling A. von, Figarella-Branger D., Cavenee W. K., Ohgaki H., Wiestler O. D., Kleihues P., and Ellison D. W. (2016).

"The 2016 World Health Organization classification of tumors of the central nervous system: A summary". In: *Acta Neuropathologica* 131.6, pp. 803–820.

Magdeldin T., López-Dávila V., Pape J., Cameron G. W. W., Emberton M., Loizidou M., and Cheema U. (2017). "Engineering a vascularised 3D in vitro model of cancer progression". In: *Scientific Reports* 7.1, pp. 440–445.

Manchanda A. and Manchanda U. (2009). "Neuroblastoma in an adult". In: *The Internet Journal of Internal Medicine* 9.1, pp. 1–5.

Mannino R. G., Santiago-Miranda A. N., Pradhan P., Qiu Y., Mejias J. C., Neelapu S. S., Roy K., and Lam W. A. (2017). "3D microvascular model recapitulates the diffuse large B-cell lymphoma tumor microenvironment in vitro". In: *Lab on a Chip* 17.3, pp. 407–414.

Mansel B. W., Keen S., Patty P. J., Hemar Y., and Williams M. A. K. (2013). "A practical review of microrheological techniques". In: *Rheology - New Concepts, Applications and Methods*, pp. 1–21.

Masters J. R. W. (2000). "Human cancer cell lines: fact and fantasy". In: *Nature Reviews Molecular Cell Biology* 1.3, pp. 233–236.

Matthay K. K., Villablanca J. G., Seeger R. C., Stram D. O., Harris R. E., Ramsay N. K., Swift P., Shimada H., Black C. T., Brodeur G. M., Gerbing R. B., and Reynolds C. P. (1999). "Treatment of high-risk neuroblastoma with intensive chemotherapy, radiotherapy, autologous bone marrow transplantation, and 13- cis -retinoic acid". In: *New England Journal of Medicine* 341.16, pp. 1165–1173.

Maurer M. H., Tripps W. K. C., Feldmann R. E., and Kuschinsky W. (2003). "Expression of vascular endothelial growth factor and its receptors in rat neural stem cells". In: *Neuroscience Letters* 344.3, pp. 165–168.

Mehra T. D., Ghosh K., Shu X. Z., Prestwich G. D., and Clark R. A. F. (2016). "Molecular stenting with a crosslinked hyaluronan derivative inhibits collagen gel contraction". In: *Journal of Investigative Dermatology* 126.10, pp. 2202–2209.

Meng W. (2006). "Evaluation of a nanoparticle drug delivery vehicle in medulloblastoma and organotypic brain cell cultures". PhD thesis, pp. 1–256.

Miller B. E., Miller F. R., and Heppner G. H. (1985). "Factors affecting growth and drug sensitivity of mouse mammary tumor lines in collagen gel cultures". In: *Cancer Research* 45.9, pp. 4200–4205.

Milo R. (2013). *Sizes of Various Cells*.

Mitra A., Mishra L., and Li S. (2013). "Technologies for deriving primary tumor cells for use in personalized cancer therapy". In: *Trends in Biotechnology* 509.7500, pp. 385–388.

Model M. A., Fang J., Yuvaraj P., Chen Y., and Zhang Newby B. M. (2010). "3D deconvolution of spherically aberrated images using commercial software". In: *Journal of Microscopy* 241.1, pp. 94–100.

Moghe P. V., Berthiaume F., Ezzell R. M., Toner M., Tompkins R. G., and Yarmush M. L. (1996). "Culture matrix configuration and composition in the maintenance of hepatocyte polarity and function". In: *Biomaterials* 17.3, pp. 373–385.

Mohyeldin A., Garzón-Muvdi T., and Quiñones-Hinojosa A. (2010). "Oxygen in stem cell biology: A critical component of the stem cell niche". In: *Cell Stem Cell* 7.2, pp. 150–161.

Moore C. and Emerson M. (2012). "Assessment of platelet aggregation responses in vivo in the mouse". In: *Platelets and Megakaryocytes: Volume 3, Additional Protocols and Perspectives*, pp. 21–28.

Muggia F. M., Hainsworth J. D., Jeffers S., Miller P., Groshen S., Tan M., Roman L., Uziely B., Muderspach L., Garcia A., Burnett A., Greco F. A., Morrow C. P., Paradiso L. J., and Liang L. J. (1997). "Phase II study of liposomal doxorubicin in refractory ovarian cancer: Antitumor activity and toxicity modification by liposomal encapsulation". In: *Journal of Clinical Oncology* 15.3, pp. 987–993.

Nakahashi T., Fujimura H., Altar C. A., Li J., Kambayashi J., Tandon N. N., and Sun B. (2000). "Vascular endothelial cells synthesize and secrete brain-derived neurotrophic factor". In: *FEBS Letters* 470.2, pp. 113–117.

Nakaji-Hirabayashi T., Kato K., and Iwata H. (2009). "Hyaluronic acid hydrogel loaded with genetically-engineered brain-derived neurotrophic factor as a neural cell carrier". In: *Biomaterials* 30.27, pp. 4581–4589.

Nern C. and Momma S. (2006). "The realized niche of adult neural stem cells". In: *Stem Cell Reviews* 6.2, pp. 233–240.

Ninomiya E., Hattori T., Toyoda M., Umezawa A., Hamazaki T., and Shintaku H. (2014). "Glucocorticoids promote neural progenitor cell proliferation derived from human induced pluripotent stem cells". In: *SpringerPlus* 3.527, pp. 1–8.

Norris R. E., Nguyen V. T., and Adamson P. C. (2014). "Evaluation of the Retinoids With Cisplatin and Vincristine in Xenograft Models of Neuroblastoma". In: *Journal of Pediatric Hematology/Oncology* 36.1.

Novick S. J. (2013). "A simple test for synergy for a small number of combinations". In: *Statistics in Medicine* 32.29, pp. 5145–5155.

Nyga A., Cheema U., and Loizidou M. (2011). "3D tumour models: Novel in vitro approaches to cancer studies". In: *Journal of Cell Communication and Signaling* 5.3, pp. 239–248.

Odawara A., Katoh H., Matsuda N., and Suzuki I. (2015). "Induction of long-term potentiation and depression phenomena in human induced pluripotent stem cell-derived cortical neurons". In: *Biochemical and Biophysical Research Communications* 469.4, pp. 856–862.

Odawara A., Saitoh Y., Alhebshi A. H., Gotoh M., and Suzuki I. (2014). "Long-term electrophysiological activity and pharmacological response of a human induced pluripotent stem cell-derived neuron and astrocyte co-culture". In: *Biochemical and Biophysical Research Communications* 443.4, pp. 1176–1181.

Ogunshola O. O., Antic A., Donoghue M. J., Fan S., Kim H., Stewart W. B., Madri J. A., and Ment L. R. (2002). "Paracrine and autocrine functions of neuronal vascular endothelial growth factor (VEGF) in the central nervous system". In: *Journal of Biological Chemistry* 277.13, pp. 11410–11415.

Oh S. K. W., Fong W. J., Teo Y., Tan H. L., Padmanabhan J., Chin A. C. P., and Choo A. B. H. (2005). "High density cultures of embryonic stem cells". In: *Biotechnology and Bioengineering* 91.5, pp. 523–533.

Ohtaki Y., Ishii G., Hasegawa T., and Nagai K. (2011). "Adult neuroblastoma arising in the superior mediastinum". In: *Interactive Cardiovascular and Thoracic Surgery* 13.2, pp. 220–222.

Oloumi A., MacPhail S. H., Johnston P. J., Banáth J. P., and Olive P. L. (2000). "Changes in subcellular distribution of topoisomerase IIα correlate with etoposide resistance in multicell spheroids and xenograft tumors". In: *Cancer Research* 60.20, pp. 5747–5753.

Orlova V. V., Hil F. E. van den, Petrus-Reurer S., Drabsch Y., Dijke P. ten, and Mummery C. L. (2014). "Generation, expansion and functional analysis of endothelial cells and pericytes derived from human pluripotent stem cells". In: *Nature Protocols* 9.6, pp. 1514–1531.

Ostrovidov S., Jiang J., Sakai Y., and Fujii T. (2004). "Membrane-based PDMS microbioreactor for perfused 3D primary rat hepatocyte cultures". In: *Biomedical Microdevices* 6.4, pp. 279–287.

Palmer T. D., Willhoite A. R., and Gage F. H. (2000). "Vascular niche for adult hippocampal neurogenesis". In: *Journal of Comparative Neurology* 425.4, pp. 479–494.

Pampaloni F., Reynaud E. G., and Stelzer E. H. K. (2007). "The third dimension bridges the gap between cell culture and live tissue". In: *Nature Reviews Molecular Cell Biology* 8.10, pp. 839–845.

Papoutsakis E. T. (1991). "Fluid-mechanical damage of animal cells in bioreactors". In: *Trends in Biotechnology* 9.1, pp. 427–437.

Park J. A., Choi K. S., Kim S. Y., and Kim K. W. (2003). "Coordinated interaction of the vascular and nervous systems: From molecule- to cell-based approaches". In: *Biochemical and Biophysical Research Communications* 311.2, pp. 247–253.

Parks S. K., Chiche J., and Pouyssegur J. (2013). "Disrupting proton dynamics and energy metabolism for cancer therapy". In: *Nature Reviews Cancer* 13.9, pp. 611–623.

Patel M. (1998). "Inhibition of neuronal apoptosis by a metalloporphyrin superoxide dismutase mimic". In: *Journal of Neurochemistry* 71.3, pp. 1068–74.

Pedersen P. L. (1978). "Tumor mitochondria and the bioenergetics of cancer cells". In: *Progress in Experimental Tumor Research* 22.1, pp. 190–274.

Pettersson F., Colston K. W., and Dalgleish A. G. (2001). "Retinoic acid enhances the cytotoxic effects of gemcitabine and cisplatin in pancreatic adenocarcinoma cells". In: *Pancreas* 23.3, pp. 273–279.

Plunkett E. V. E. and Cross M. E. (2014). "Formation and circulation of cerebrospinal fluid". In: *Physics, Pharmacology and Physiology for Anaesthetists: Key Concepts for the FRCA*. 2nd ed. Cambridge: Cambridge University Press, p. 319.

Prescott M. J. and Lidster K. (2017). "Improving quality of science through better animal welfare: The NC3Rs strategy". In: *Lab Animal* 46.4, pp. 152–156.

Putter P. J. (2015). "The development of functional hyaluronan hydrogels for neural tissue engineering". PhD thesis. University of Oxford, pp. 1–250.

Reynolds C. P., Matthay K. K., Villablanca J. G., and Maurer B. J. (2003). "Retinoid therapy of high-risk neuroblastoma". In: *Cancer Letters* 197.1-2, pp. 185–192.

Rich J. N. and Eyler C. E. (2008). "Cancer stem cells in brain tumor biology". In: *Cold Spring Harbor Symposia on Quantitative Biology* 73.1, pp. 411–20.

Rijntjes P. J. M., Moshage H. J., Van Gemert P. J. L., De Waal R., and Yap S. H. (1986). "Cryopreservation of adult human hepatocytes". In: *Journal of Hepatology* 3.1, pp. 7–18.

Rizvanov A. A., Yalvaç M. E., Shafigullina A. K., Salafutdinov I. I., Blatt N. L., Sahin F., Kiyasov A. P., and Palotás A. (2010). "Interaction and self-organization of human mesenchymal stem cells and neuro-blastoma SH-SY5Y cells under co-culture conditions: A novel system for modeling cancer cell micro-environment". In: *European Journal of Pharmaceutics and Biopharmaceutics* 76.2, pp. 253–259.

Russ J. C. (2011). "Correcting imaging defects". In: *The Image Processing Handbook*. 6th. Boca Raton, Florida: CRC Press, pp. 235–244.

Sanfilippo S., Canis M., Ouchchane L., Botchorishvili R., Artonne C., Janny L., and Brugnon F. (2011). "Viability assessment of fresh and frozen/thawed isolated human follicles: reliability of two methods (Trypan blue and Calcein AM/ethidium homodimer-1)". In: *Journal of Assisted Reproduction and Genetics* 28.12, pp. 1151–1156.

Sarkanen J. R., Nykky J., Siikanen J., Selinummi J., Ylikomi T., and Jalonen T. O. (2007). "Cholesterol supports the retinoic acid-induced synaptic vesicle formation in differentiating human SH-SY5Y neuroblastoma cells". In: *Journal of Neurochemistry* 102.6, pp. 1941–1952.

Schleiermacher G., Rubie H., Hartmann O., Bergeron C., Chastagner P., Mechinaud F., and Michon J. (2003). "Treatment of stage 4s neuroblastoma – Report of 10 years' experience of the French Society of Paediatric Oncology (SFOP)". In: *British Journal of Cancer* 89.3, pp. 470–476.

Schmid J. O., Dong M., Haubeiss S., Friedel G., Bode S., Grabner A., Ott G., Mürdter T. E., Oren M., Aulitzky W. E., and Kuip H. van der (2012). "Cancer cells cue the p53 response of cancer-associated fibroblasts to cisplatin". In: *Cancer Research* 72.22, pp. 5824–5832.

Schneider L., Giordano S., Zelickson B. R., Johnson M., Benavides G., Ouyang X., Fineberg N., Darley-Usmar V. M., and Zhang J. (2011). "Differentiation of SH-SY5Y cells to a neuronal phenotype changes cellular bioenergetics and the response to oxidative stress". In: *Free radical biology & medicine* 51.11, pp. 2007–2017.

Semenza G. L. (2010). "HIF-1 : Upstream and downstream of cancer metabolism". In: *Current Opinion in Genetics and Development* 20.1, pp. 51–56.

Shalinsky D. R., Bischoff E. D., Gregory M. L., Lamph W. W., Heyman R. A., Hayes J. S., Thomazy V., and Davies P. J. (1996). "Enhanced antitumor efficacy of cisplatin in combination with ALRT1057 (9-cis retinoic acid) in human oral squamous carcinoma xenografts in nude mice". In: *Clinical Cancer Research* 2.3, pp. 511–520.

Shaloam D. and Tchounwou P. B. (2014). "Cisplatin in cancer therapy: Molecular mechanisms of action". In: *European Journal of Pharmacology* 740.1, pp. 364–378.

Shannon A. M., Bouchier-Hayes D. J., Condron C. M., and Toomey D. (2003). "Tumour hypoxia, chemotherapeutic resistance and hypoxia-related therapies". In: *Cancer Treatment Reviews* 29.4, pp. 297–307.

Shen Q., Goderie S. K., Jin L., Karanth N., Sun Y., Abramova N., Vincent P., Pumiglia K., and Temple S. (2004). "Endothelial cells stimulate self-renewal and expand neurogenesis of neural stem cells". In: *Science* 304.5675, pp. 1338–1340.

Shi Y., Kirwan P., and Livesey F. J. (2012). "Directed differentiation of human pluripotent stem cells to cerebral cortex neurons and neural networks". In: *Nature Protocols* 7.10, pp. 1836–1846.

Shin D., Ahn J., Lee K., Lee Y., and Lee Y. (2004). "Ascorbic acid responsive genes during neuronal differentiation of embryonic stem cells". In: *Neuroreport* 15.12, pp. 1959–1963.

Shu X. Z., Liu Y., Palumbo F. S., Luo Y., and Prestwich G. D. (2004). "In situ crosslinkable hyaluronan hydrogels for tissue engineering". In: *Biomaterials* 25.7–8, pp. 1339–1348.

Siddik Z. H. (2003). "Cisplatin: Mode of cytotoxic action and molecular basis of resistance". In: *Oncogene* 22.47, pp. 7265–7279.

Smith G. M., Liu Y., and Hong J. W. (2013). *Neuronal Cell Culture*. Vol. 1078, pp. 153–161.

Span P. N. and Bussink J. (2015). "Biology of Hypoxia". In: *Seminars in Nuclear Medicine* 45.2, pp. 101–109.

Sun L., Hui A. M., Su Q., Vortmeyer A., Kotliarov Y., Pastorino S., Passaniti A., Menon J., Walling J., Bailey R., Rosenblum M., Mikkelsen T., and Fine H. A. (2006). "Neuronal and glioma-derived stem cell factor induces angiogenesis within the brain". In: *Cancer Cell* 9.4, pp. 287–300.

Szot C. S., Buchanan C. F., Freeman J. W., and Rylander M. N. (2011). "3D in vitro bioengineered tumors based on collagen I hydrogels". In: *Biomaterials* 32.31, pp. 7905–7912.

Tannock I. F. (1989). "Combined modality treatment with radiotherapy and chemotherapy". In: *Journal of the European Society for Therapeutic Radiology and Oncology* 16.2, pp. 83–101.

Thoma C. R., Zimmermann M., Agarkova I., Kelm J. M., and Krek W. (2014). "3D cell culture systems modeling tumor growth determinants in cancer target discovery". In: *Advanced Drug Delivery Reviews* 69-70.1, pp. 29–41.

Thonhoff J. R., Lou D. I., Jordan P. M., Zhao X., and Wu P. (2008). "Compatibility of human fetal neural stem cells with hydrogel biomaterials in vitro". In: *Brain Research* 1187.1, pp. 42–51.

Toole B. P. and Hascall V. C. (2002). "Hyaluronan and tumor growth". In: *The American Journal of Pathology* 161.3, pp. 745–747.

Turaç G., Hindley C. J., Thomas R., Davis J. A., Deleidi M., Gasser T., Karaöz E., and Pruszak J. (2013). "Combined flow cytometric analysis of surface and intracellular antigens reveals surface molecule markers of human neuropoiesis". In: *PLoS ONE* 8.6, pp. 1–14.

Vaira V., Fedele G., Pyne S., Fasoli E., Zadra G., Bailey D., Snyder E., Faversani A., Coggi G., Flavin R., Bosari S., and Loda M. (2010). "Preclinical model of organotypic culture for pharmacodynamic profiling of human tumors". In: *Proceedings of the National Academy of Sciences of the United States of America* 107.18, pp. 8352–8356.

Van der Kuip H., Mürdter T. E., Sonnenberg M., McClellan M., Gutzeit S., Gerteis A., Simon W., Fritz P., and Aulitzky W. E. (Apr. 2006). "Short term culture of breast cancer tissues to study the activity of the anticancer drug taxol in an intact tumor environment". In: *BMC Cancer* 6.1, p. 86.

Vaupel P. and Harrison L. (2004). "Tumor hypoxia: Causative factors, compensatory mechanisms and cellular response". In: *The Oncologist* 9.suppl 5, pp. 4–9.

Villasante A. and Vunjak-Novakovic G. (2015). "Tissue-engineered models of human tumors for cancer research". In: *Expert Opinion on Drug Discovery* 10.3, pp. 257–268.

Wan X., Ball S., Willenbrock F., Yeh S., Vlahov N., Koennig D., Green M., Brown G., Jeyaretna S., Li Z., Cui Z., Ye H., and O'Neill E. (2017). "Perfused three-dimensional organotypic culture of Human cancer cells for therapeutic evaluation". In: *Scientific Reports* 7.1, pp. 94–108.

Wan X., Bovornchutichai P., Cui Z., O'Neill E., and Ye H. (2017). "Morphological analysis of human umbilical vein endothelial cells co-cultured with ovarian cancer cells in 3D: An oncogenic angiogenesis assay". In: *PLoS ONE* 12.7, e0180296.

Wan X., Li Z., Ye H., and Cui Z. (2016). "Three-dimensional perfused tumour spheroid model for anti-cancer drug screening". In: *Biotechnology Letters* 38.8, pp. 1389–1395.

Wang K., Diskin S. J., Zhang H., Attiyeh E. F., Winter C., Hou C., Schnepp R. W., Diamond M., Bosse K., Mayes P. A., Glessner J., Kim C., Frackelton E., Garris M., Wang Q., Glaberson W., Chiavacci R., Le N., Jagannathan J., Saeki N., Sasaki H., Grant S. F. A., Iolascon A., Mosse Y. P., Cole K. A., Li H., Devoto M., McGrady P. W., London W. B., Capasso M., Rahman N., Hakonarson H., and Maris J. M. (2010). "Integrative genomics identifies LMO1 as a neuroblastoma oncogene". In: *Nature* 469.13, pp. 216–220.

Wang L., Luo H., Chen X., Jiang Y., and Huang Q. (2014). "Functional characterization of S100A8 and S100A9 in altering monolayer permeability of human umbilical endothelial cells". In: *PLoS ONE* 9.3, pp. 1–13.

Wang T. Y., Forsythe J. S., Parish C. L., and Nisbet D. R. (2012). "Biofunctionalisation of polymeric scaffolds for neural tissue engineering". In: *Journal of Biomaterials Applications* 27.4, pp. 369–390.

Warburg O. (1956). "On the origin of cancer cells". In: *Science* 123.3191, pp. 309–314.

Watt F. M. and Huck W. T. S. (2013). "Role of the extracellular matrix in regulating stem cell fate". In: *Nature Reviews Molecular Cell Biology* 14.8, pp. 467–473.

Westermark U. K., Wilhelm M., Frenzel A., and Henriksson M. A. (2011). "The MYCN oncogene and differentiation in neuroblastoma". In: *Seminars in Cancer Biology* 21.4, pp. 256–266.

Willerth S. M. and Sakiyama-Elbert S. E. (2007). "Approaches to neural tissue engineering using scaffolds for drug delivery". In: *Advanced Drug Delivery Reviews* 59.4-5, pp. 325–338.

Wu M. H., Huang S. B., Cui Z., Cui Z., and Lee G. B. (2008). "Development of perfusion-based micro 3-D cell culture platform and its application for high throughput drug testing". In: *Sensors and Actuators B: Chemical* 129.1, pp. 231–240.

Wu M. H., Urban J. P. G., Cui Z., and Cui Z. (2006). "Development of PDMS microbioreactor with well-defined and homogenous culture environment for chondrocyte 3-D culture". In: *Biomedical Microdevices* 8.4, pp. 331–340.

Xie H. R., Hu L. S., and Li G. Y. (2010). *SH-SY5Y human neuroblastoma cell line: In vitro cell model of dopaminergic neurons in Parkinson's disease*. Vol. 123, pp. 1086–1092.

Xie Y., Hardouin P., Zhu Z., Tang T., Dai K., and Lu J. (2006). "Three-dimensional flow perfusion culture system for stem cell proliferation inside the critical-size beta-tricalcium phosphate scaffold". In: *Tissue Engineering* 12.12, pp. 3535–3543.

Xu X., Farach-Carson M. C., and Jia X. (2014). "Three-dimensional in vitro tumor models for cancer research and drug evaluation". In: *Biotechnology Advances* 32.7, pp. 1256–1268.

Xu X., Jha A. K., Harrington D. A., Farach-Carson M. C., and Jia X. (2012). "Hyaluronic acid-based hydrogels: From a natural polysaccharide to complex networks". In: *Soft Matter* 8.12, pp. 3280–3294.

Yamada K. M. and Cukierman E. (2007). "Modeling tissue morphogenesis and cancer in 3D". In: *Cell* 130.4, pp. 601–610.

Zeeberg K., Cardone R. A., Greco M. R., Saccomano M., Nøhr-Nielsen A., Alves F., Pedersen S. F., and Reshkin S. J. (2016). "Assessment of different 3D culture systems to study tumor phenotype and chemosensitivity in pancreatic ductal adenocarcinoma". In: *International Journal of Oncology* 49.1, pp. 243–252.

Zhang X., Wang W., Yu W., Xie Y., Zhang X., Zhang Y., and Ma X. (2005). "Development of an in vitro multicellular tumor spheroid model using microencapsulation and its application in anticancer drug screening and testing". In: *Biotechnology Progress* 21.4, pp. 1289–1296.

Zhao F. and Ma T. (2005). "Perfusion bioreactor system for human mesenchymal stem cell tissue engineering: Dynamic cell seeding and construct development". In: *Biotechnology and Bioengineering* 91.4, pp. 482–493.

Zhao L., Au J. L. S., and Wientjes M. G. (2010). "Comparison of methods for evaluating drug-drug interaction". In: *Frontiers in Bioscience (Elite Edition)* 23.2, pp. 241–249.

Zhuang P., Sun A. X., An J., Chua C. K., and Chew S. Y. (2018). "3D neural tissue models: From spheroids to bioprinting". In: *Biomaterials* 154.1, pp. 113–133.